On convected wave structures and spectral transfer in space plasmas – applications to solar corona and solar wind

Von der Fakultät für Elektrotechnik, Informationstechnik, Physik
der Technischen Universität Carolo-Wilhelmina
zu Braunschweig
zur Erlangung des Grades eines
Doktors der Naturwissenschaften
(Dr. rer. nat.)
genehmigte
Dissertation

von Daniel Verscharen
aus Bonn

Bibliografische Information der Deutschen Nationalbibliothek

Die Deutsche Nationalbibliothek verzeichnet diese Publikation in der Deutschen Nationalbibliografie; detaillierte bibliografische Daten sind im Internet über `http://dnb.d-nb.de` abrufbar.

1. Referentin oder Referent: Prof. Dr. Uwe Motschmann
2. Referentin oder Referent: Prof. Dr. Eckart Marsch
eingereicht am: 14. Oktober 2011
mündliche Prüfung (Disputation) am: 11. Januar 2012

ISBN 978-3-942171-64-9

uni-edition GmbH 2012
http://www.uni-edition.de

Printed in Germany

Vorveröffentlichungen der Dissertation

Teilergebnisse aus dieser Arbeit wurden mit Genehmigung der Fakultät für Elektrotechnik, Informationstechnik, Physik, vertreten durch den Mentor der Arbeit, in folgenden Beiträgen vorab veröffentlicht:

Publikationen

- Verscharen, D., Marsch, E., Motschmann, U. und Müller, J: *Kinetic cascade beyond MHD of solar wind turbulence in two-dimensional hybrid simulations*, Physics of Plasmas, eingereicht, 2011

- Verscharen, D: *Schwach kompressive, hochfrequente Wellen im inhomogenen Multifluid-Plasma*, Mitteilungen der Deutschen Geophysikalischen Gesellschaft 3, 5-9, 2011

- Verscharen, D. und Marsch, E.: *Apparent temperature anisotropies due to wave activity in the solar wind*, Annales Geophysicae 29, 909-917, 2011, doi: 10.5194/angeo-29-909-2011

- Verscharen, D. und Marsch, E.: *Compressive high-frequency waves riding on an Alfvén/ion-cyclotron wave in a multi-fluid plasma*, Journal of Plasma Physics 77, 693-707, 2011, doi: 10.1017/S0022377811000080

- Marsch, E. und Verscharen, D.: *On nonlinear Alfvén-cyclotron waves in multi-species plasma*, Journal of Plasma Physics 77, 385-403, 2011, doi: 10.1017/S0022377810000541

Tagungsbeiträge

- Verscharen, D., Marsch, E., Motschmann, U. und Müller, J.: *Compressive wave structures on kinetic scales resulting from a two-dimensional turbulent cascade in the solar wind*, Vortrag, Workshop "Cosmic Rays and the Heliospheric Plasma Environment", Bochum, Deutschland, 12.-16.9.2011

- Verscharen, D. und Marsch, E.: *Apparent temperature anisotropies due to wave activity in the solar wind*, Vortrag, 478. W.&E.-Heraeus-Seminar "Fusion and Astrophysical Plasmas", Bad Honnef, Deutschland, 18.-20.4.2011

- Verscharen, D. und Marsch, E.: *Compressive high-frequency waves riding on an Alfvén-cyclotron wave in a multi-fluid plasma*, Poster, EGU General Assembly, Wien, Österreich, 3.-8.4.2011

- Verscharen, D. und Marsch, E.: *Schwach kompressive, hochfrequente Wellen im inhomogenen Multifluid-Plasma*, Vortrag, 71. Jahrestagung der DGG, Köln, Deutschland, 21.-24.2.2011

- Verscharen, D. und Marsch, E.: *Kinetics of non-Maxwellian distribution functions in the turbulent solar wind*, Vortrag, Workshop “New perspectives on cosmic rays in the heliosphere”, Parys/Potchefstroom, Südafrika, 22.-26.3.2010
- Verscharen, D. und Marsch, E.: *Kinetik nicht-maxwellscher Verteilungsfunktionen des turbulenten Sonnenwindplasmas*, Vortrag, DPG-Frühjahrstagung, Bonn, Deutschland, 15.-19.3.2010

Contents

Summary

Alfvén/ion-cyclotron waves are important normal modes in a plasma. Their existence can explain several observed features in space plasmas such as temperature anisotropies and preferred heating of certain ion species in the solar corona and the solar wind. The properties of this wave mode and different aspects of the spectral transfer of wave energy in wavenumber space are analyzed.

Every plasma wave is a complex interplay between the electromagnetic fields and the plasma particles. The way Alfvén/ion-cyclotron waves shape a particle distribution function is treated with kinetic methods in an analytical model, and an additional observational effect in particle measurements is found. The nature of the important Alfvén/ion-cyclotron mode is discussed in a multi-fluid analysis. Therefore, a system of coupled differential equations is achieved, which describes the linear and nonlinear properties of Alfvén/ion-cyclotron waves in parallel propagation with an arbitrary finite amplitude. This derived system of differential equations is then used to analyze the dispersion properties of weakly-compressive high-frequency waves, which are superposed on a low-frequency Alfvén/ion-cyclotron wave. In a certain parameter range, a wave instability is found, which can be interpreted as a linear spectral transfer process due to the non-uniform background of the low-frequency wave. A particular example for a nonlinear spectral transfer process is the parametric decay of a monochromatic plasma wave. It is treated in a two-dimensional numerical study using a hybrid code. The same code is then used to analyze the spectral transfer from an initially broad turbulent spectrum on low-wavenumber MHD scales into the dispersive kinetic regime, where dissipation of certain wave modes is found. Also here compressive fluctuations grow during the cascade and make a significant contribution to the turbulent spectrum on small scales.

The thesis is completed with a general introduction to waves and turbulence in space plasmas and with a basic presentation of the applied mathematical methods.

Preface

Plasma turbulence is a field with a long and successful history. Yet, many questions remain open, and modern space probes reveal new unsolved problems and so far unknown structures beyond the well established theories. Therefore, it cannot be the focus of a PhD thesis to find something like the concluding answer to wave structures or a conclusive picture of turbulence in space plasmas. It might only contribute to various particular aspects of the field, trying to bring some building blocks into the general picture. This restriction is true for every thesis but maybe even more for a contribution to this special field.

Hence, this work rather tries to approach the problem from various directions than pointing out one single aspect. Analytical kinetic plasma theory is used in the first part to analyze the nature of plasma waves and their influence on measurements of particle velocities. The second part attends to the multi-fluid nature of plasma waves and how their properties are affected by non-uniform plasma conditions. In the third part, hybrid simulations are applied to analyze nonlinear wave–wave interactions and spectral transfer numerically.

This structure of the thesis leads to the fact that individual chapters or groups of two chapters could stand alone and can in parts be read more or less independently from each other. However, they all contribute from different sides to the general common scientific questions regarding the nature of space plasma fluctuations and their generation. A general introduction is given at the beginning. Each chapter has its own short introduction addressing aspects that are important only for the particular chapter. To avoid the necessity of inconvenient thumbing through this thesis, some important relations are repeated if this improves the reading fluency. The results are discussed separately in each chapter. The last chapter draws conclusions from the previous units and provides an outlook.

Throughout this thesis, Gauß' version of the cgs-system of units will be used. The equations take a more symmetric form (electric and magnetic field have the same unit, speed of light occurs in Maxwell's equations etc.), and indeed most of the literature in plasma physics is formulated using this system.

Katlenburg-Lindau and Braunschweig, October 2011

Daniel Verscharen

I Introduction

I.1 Solar corona and solar wind as paradigms for space plasmas

A *plasma* is a gas of free electrically charged particles, which has the following characteristic properties:

- *Quasi-neutrality*: The amount of positive and negative electric charges is equal so that the plasma appears electrically neutral on sufficiently large scales. This does not contradict the existence of local space charge densities.
- The *macroscopic dimension* of the plasma is large compared to the scale on which neighboring charges shield their Coulomb potentials mutually. This length scale is called the *Debye length*. Otherwise, this collective shielding would not occur and the condition of quasi-neutrality would be violated.
- The *number of particles* in a sphere with the radius of the Debye length is large. This requirement guarantees that the direct influence of neighboring particles on each other is negligible compared to collective effects. The kinetic/thermal mean energy of a particle is, therefore, higher than its potential energy in the Coulomb potential of its neighbors.

These properties characterize a plasma at first glance (Baumjohann and Treumann, 1996). More than 99% of the visible matter in the universe is in the plasma state. Also, most mass of the solar system is in this state because the Sun, as the dominating mass, is a plasma ball in itself. Its outer atmosphere above the photospheric surface is called the *solar corona*. It can be seen with the naked eye during a solar eclipse as an extended and structured glow around the occulted Sun. Since the 1940s, it has been already known from spectroscopic analyses (see the review by Kohl *et al.*, 2006) that the temperature of the corona exceeds several million degrees Kelvin, whereas the solar photosphere, the main source of the solar light emission, has a temperature of only 5700 K. The reason for this increase in the plasma temperature with height, coinciding with a strong decrease in density, is still an open question and is known as the *coronal heating problem*. There are many further complications to this problem, which will be discussed later.

The corona expands out further and passes into the so-called *solar wind*. It is a plasma outflow into the heliosphere and carries the interplanetary magnetic field. Due to the radial motion of the solar wind flow and the rotation of the surface of the Sun as the source of the magnetic field lines, the interplanetary magnetic field has a spiral structure, especially

in the ecliptic (Parker, 1958). Close to the corona, its direction is rather radial, while the angle between outflow direction and interplanetary magnetic field increases with distance from Sun. The first ideas about a more or less steady corpuscular outflow from the Sun were confirmed based on observations of the shape of cometary tails (Biermann, 1951). In the meantime, the standard picture consists of three different kinds of solar wind. The first kind is the hot and dilute fast solar wind, which originates in the polar coronal holes and dominates during the solar minimum, coming from solar latitudes down to the border of the heliospheric current sheet. It has quite a constant outflow speed of about 800 km/s. The fast wind shows a broad variety of different wave signatures and is, hence, the main focus of this work. The second type is the dense and cold slow solar wind, which is mainly observed in times of high solar activity. It is believed that its source is connected to the highly-structured coronal magnetic field around magnetic loops. The outflow speed is about 400 km/s and varies more than in the fast wind. The third category of solar wind types are transient events such as coronal mass ejections (CMEs), which are eruptive structures propagating through the background solar wind with speeds in a wide range between 20 to 2000 km/s (see review by Srivastava and Schwenn, 2000).

There are some peculiar plasma properties that are of special interest in space physics. A plasma is called *collisionless* if typical collective effects such as oscillations or waves occur on much shorter time scales than binary Coulomb collisions between the plasma particles. The *collisionality* can be characterized by the collision frequency ν_c compared to the characteristic plasma frequencies, or by the mean free path λ_{mfp} compared to the other scales, respectively. The *electrical conductivity* of a plasma describes the mobility of electrons and ions (the possible carriers of electric currents), which is determined by the rate of collisions that these particles undergo. In a collisionless plasma, therefore, the conductivity is very high and can be assumed as infinite. Most space plasmas can be considered collisionless. A plasma is called *magnetized* if a large-scale (compared to the natural length scales) magnetic field brakes significantly the isotropy in some effects due to deflections of charged particles according to the Lorentz force. Most space plasmas are magnetized because of the ubiquitous magnetic fields in space. One of the various complications in the treatment of a magnetized plasma is the natural anisotropy given by the direction of the magnetic field. In this case, also the conductivity is anisotropic. In the most general case, the conductivity has to be treated as a tensor in the generalized Ohm's law, taking effects such as Pedersen currents, Hall conductivity, and field-parallel conductivities into account (Baumjohann and Treumann, 1996).

Another important parameter for a plasma characterization is the so-called *plasma beta*, which is defined as the ratio of the thermal energy density to the magnetic energy density:

$$\beta \equiv \frac{8\pi n k_B T}{B^2} \tag{I-1.1}$$

with the particle number density n, Boltzmann's constant k_B, temperature T, and magnetic field strength B. It can be defined for single species with the corresponding number density and temperature of this species or as an effective beta with the total number density and the summed up temperature. The border between high and low beta is defined as the limit $\beta = 1$. For lower beta-values, the thermal speed of the particles is smaller than the Alfvén speed; for higher betas, it is larger. This ratio has a significant meaning

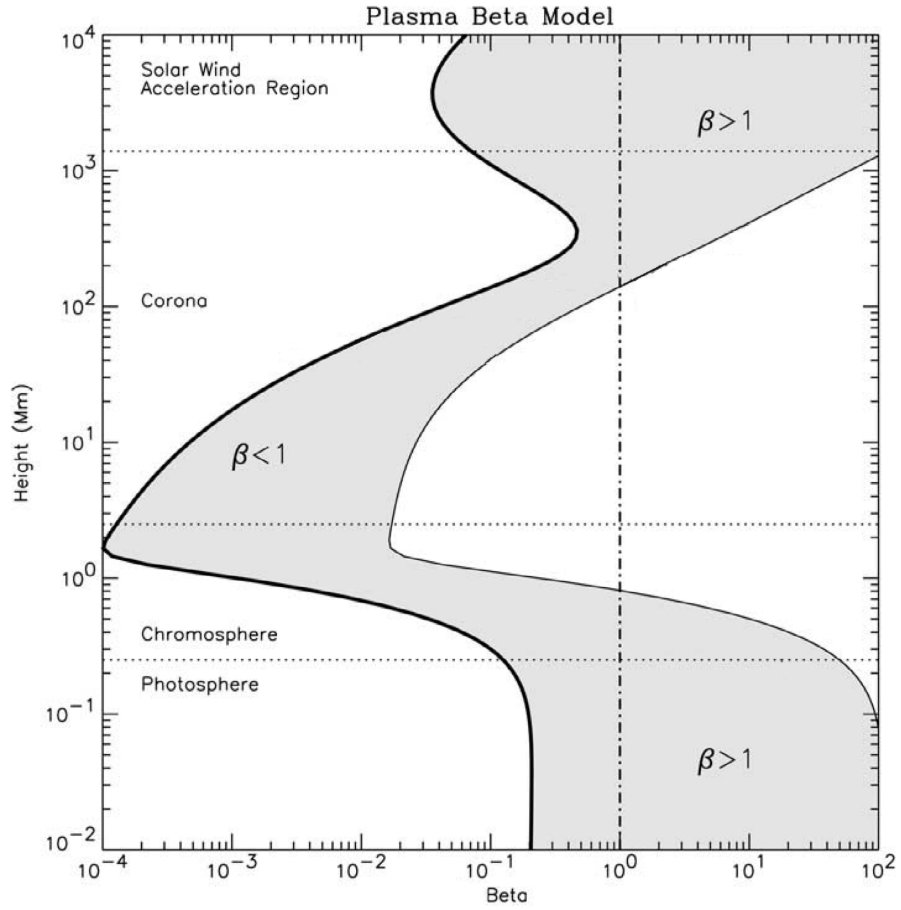

Figure I-1: Plasma beta depending on the height in the solar atmosphere. Adopted from Gary (2001) with kind permission from Springer Science+Business Media: Fig. 3 on page 80 in the original publication.

for damping and resonance processes. Both low- and high-beta plasmas are found in the solar atmosphere as one can see in Fig. I-1. The solar corona is an example for a low-beta plasma, whereas the solar wind can reach the configuration of a high-beta plasma.

Typical parameters for the solar wind at 1 AU are listed in Table I.1. These values show a huge variability in the solar wind. Therefore, the table should be understood as information about the characteristic order of magnitude for these parameters. The complete definition of the parameters is given at the place, where they are used for the first time.

I.2 The heating problem in solar corona and solar wind

In order to describe the heating problem fully, it is not sufficient to reduce it to the fact that the coronal temperature is high. Different particle species show different temperatures, and even the same species can have temperature anisotropies in certain directions with respect to the background magnetic field (Kohl *et al.*, 2006). Some of these features are shown in Fig. I-2.

Table I.1: Typical parameters in the solar wind at 1 AU (SW) and in the corona. The values for the density, temperature, and magnetic field are taken from literature (e.g., Aschwanden, 2005; Borovsky and Gary, 2011), the others are calculated from these. The collision frequency and the mean free path are calculated as described in the NRL Plasma Formulary (2009). All values can scatter a lot around these given estimates.

Symbol	SW	(upper) corona	Definition
$n_\mathrm{p} \sim n_\mathrm{e}$	5 cm^{-3}	10^6 cm^{-3}	proton and electron number density
$T_\mathrm{p} \sim T_\mathrm{e}$	10^5 K	10^6 K	proton and electron temperature
B_0	10^{-4} G	1 G	magnetic field strength
$v_\mathrm{th,p}$	40 km/s	130 km/s	proton thermal speed
$v_\mathrm{th,e}$	1700 km/s	5000 km/s	electron thermal speed
v_A	100 km/s	2000 km/s	proton Alfvén speed
Ω_p	1 s^{-1}	10^4 s^{-1}	proton gyration frequency
Ω_e	1836 s^{-1}	2×10^7 s^{-1}	electron gyration frequency
ω_p	3000 s^{-1}	10^6 s^{-1}	proton plasma frequency
ω_e	10^5 s^{-1}	6×10^7 s^{-1}	electron plasma frequency
ν_c	4×10^{-7} s^{-1}	0.5 s^{-1}	proton collision frequency
ℓ_p	100 km	300 m	proton inertial length
ℓ_e	3 km	5 m	electron inertial length
$\lambda_\mathrm{p} \sim \lambda_\mathrm{e}$	10 m	7 cm	proton and electron Debye length
r_p	40 km	13 m	proton gyration radius
r_e	1 km	25 cm	electron gyration radius
$\lambda_\mathrm{mfp,p}$	10^8 km	250 km	proton collisional mean free path
$\beta_\mathrm{p} \sim \beta_\mathrm{e}$	0.2	0.003	proton and electron beta

Minor ions have higher temperatures and usually higher temperature anisotropies than protons. Ions are observed to have both higher temperature anisotropies parallel and perpendicular to the magnetic field from time to time. In most cases, however, the perpendicular temperature anisotropy dominates (Bourouaine *et al.*, 2010). Observations show that most of the ion species have more or less the same thermal velocity (von Steiger, 2008). Due to the definition of the thermal speed $v_{\mathrm{th}j} \equiv \sqrt{2k_\mathrm{B}T_j/m_j}$ of species j, the temperature ratio of different ion species should be more or less the mass ratio of the species in this case.

Solar wind particle temperatures observed by spacecraft show a non-adiabatic dependence on the distance from Sun, which indicates that an ongoing heating mechanism has to act on the particles during their passage through the heliosphere (Richardson *et al.*, 1995; Totten *et al.*, 1995; Cranmer *et al.*, 2009). Direct in-situ measurements of the proton and electron temperatures are shown in Fig. I-3. It is possible to define an "effective" polytropic index pretending to have an adiabatic behavior for the protons. Observations show that it drops from about 1.5 at 0.3 AU to about 1.3 at 5 AU. In the outer heliosphere, pick-up ions contribute significantly to the total pressure of the solar wind and deliver an important energy input, which can explain the non-adiabatic temperature behavior in this region (Fahr and Chashei, 2002; Smith *et al.*, 2006). In the inner heliosphere, this effect

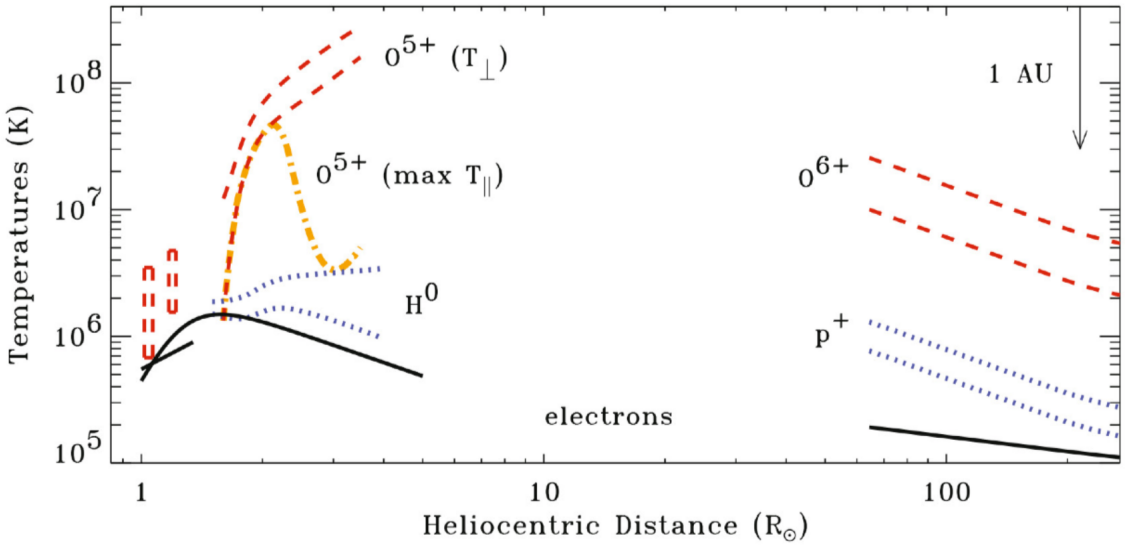

Figure I-2: Different temperatures of coronal and solar wind particle species. The data above a distance of 0.3 AU is taken by in-situ detectors (Helios), the data closer to the Sun by remote-sensing techniques (UV spectro-polarimetry). From Kohl *et al.* (2006) with kind permission from Springer Science+Business Media: Fig. 39 on page 94 in the original publication.

is not dominating and the heating mechanism is unclear.

A correct explanation for coronal heating, solar wind acceleration, and non-adiabatic expansion has to explain all the microphysical properties, which are explicitly observed. The "fine structure" of the heating problem shows already one reason, why a single-fluid description like (magneto)hydrodynamics is insufficient to describe the physical processes appropriately, a point which will be discussed in more detail later.

It is widely accepted that classical Joule heating due to collisions between the plasma particles, which carry electric currents, cannot explain the heating, especially not the structural deviations from thermal equilibrium. In the solar corona, the expected collisional heating rate is too low to explain the observed high temperatures (Cranmer and van Ballegooijen, 2003; Gary *et al.*, 2005a). Yet in the chromosphere, Ohmic dissipation cannot compensate for radiative losses, and therefore another process such as shock heating is assumed to maintain the temperature at lower heights in the solar atmosphere (Ulmschneider and Kalkofen, 2003). The temperature rises even higher in the transition region up to coronal temperatures of more than 10^6 K, whereas the probability for collisions becomes lower and lower due to the decrease in density. Some authors solve this problem in their numerical fluid codes by increasing the resistivity or the viscosity, respectively, to unrealistic values (so-called *anomalous* resistivity/viscosity) and include the microphysics in this way effectively (Silin *et al.*, 2005; Wu *et al.*, 2010; Bingert *et al.*, 2010). However, the aim of this thesis is to shed light on the microphysics of the heating mechanism, while macroscopic and global effects are disregarded. Macroscopic effects due to the stratification of the solar atmosphere or structures in the magnetic field like coronal loops are, therefore, not taken into account in the following. The treated plasma volumes are in most cases very small compared to any of these large-scale inhomogeneities.

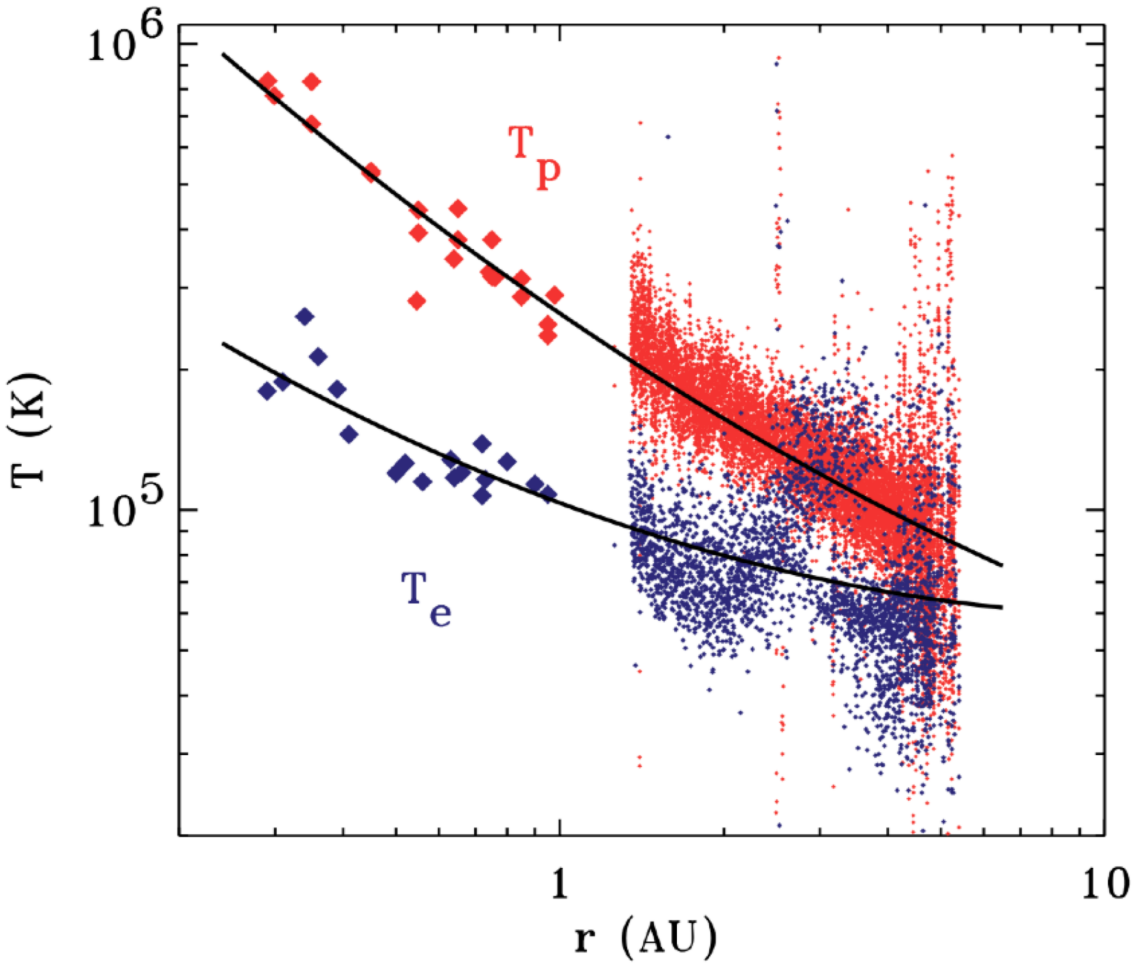

Figure I-3: Measurements of proton and electron temperatures in the fast solar wind ($U \gtrsim$ 600 km/s) by Helios (inner heliosphere, diamonds) and Ulysses (outer heliosphere, small points). The lines show fit results and indicate the non-adiabatic temperature evolution. From Cranmer *et al.* (2009), reproduced by permission of the AAS.

It has been known for a long time that resonant absorption of electrostatic or electromagnetic wave energy can lead to very efficient heating, even in a collisionless plasma (see the review by Marsch, 2006) as will be discussed later. Fusion and other experimental plasma devices make use of exactly this effect to heat the plasma to the desired temperatures. Currents for Ohmic heating would be too strong to keep the plasma in a stable confinement (e.g., O'Brien and Robinson, 1993). The difference to space plasmas, however, is that in laboratory plasma physics the wave generators are known (i.e., the microwave antennae or gyrotrons around the confined plasma), whereas the origin of the space plasma waves is still unclear. Possible generation mechanisms are all kinds of micro-instabilities (Gary, 1993), converting free energy from the particle distribution function to wave energy at the corresponding wavenumbers and frequencies. A broad turbulent spectrum with an active turbulent cascade might also deliver waves with the matching properties (Cranmer and van Ballegooijen, 2003), and even waves with non-matching wavenumbers and frequencies can decay to appropriate, dissipating fluctuations. The acceleration of

the solar wind is also believed to be driven by wave activity. There are several different other models such as ambipolar static acceleration, shock acceleration, micro-flare energization, reconnection (in the corona or the chromosphere), and exospheric models (see reviews by Aschwanden, 2005; Marsch, 2006). Nevertheless, these approaches fail to explain the fine structure of the observed temperatures in detail, and some of them would require very atypical and unobserved conditions. The resonant dissipation of wave energy is, therefore, still a widely accepted scenario for both the heating of the corona and the acceleration of the solar wind. Before the dissipation of wave energy can be treated, the origin and properties of the ubiquitous space plasma fluctuations have to be discussed. These questions are the central objectives of this work.

It is important to state that all of the treated structures are convected with the background plasma flow. In the case of the corona, the bulk flow of the plasma is more or less at rest with respect to the Sun or the observer at Earth (neglecting the Earth's orbital motion of course). In the solar wind, however, all wave structures propagate in the reference frame moving with the solar wind bulk outflow velocity, which typically exceeds both the Alfvén speed and the sound speed in the solar rest frame. They are, therefore, convected structures and usually treated in the bulk rest frame if not stated differently.

I.3 The nature of space plasma turbulence

Besides their origin, also the nature of the observed fluctuations in the interplanetary magnetic field (IMF) are under debate (Bruno and Carbone, 2005). They are observed all over the heliosphere, and it is accepted that they originate mainly from the main energy source in the solar system, namely the Sun. However, also local mechanisms and drivers play a role in the evolution of the plasma.

It is noteworthy that magnetic field fluctuations in a plasma always come along with fluctuations in the particle motions, reflected by fluctuations in the particle distribution function. The solar wind plasma is the carrier of all these fluctuations in the heliosphere. In this sense, the solar wind can be used as a messenger of the coronal conditions. Measurements of solar wind particles, however, have to be treated with care. The coherent motion of particles in electromagnetic wave fields can lead to an apparent temperature after the averaging during the particle measurement process. This effect and its impacts will be discussed in Chapt. III.

In the past, IMF fluctuations were first interpreted as independently propagating and non-interacting MHD waves, which originate in the corona and change their properties only due to gradients in the background parameters such as the background magnetic field or the plasma density. This interpretation has been widely discussed by Belcher and Davis (1971). They showed that fluctuations in the magnetic field are highly correlated (or anti-correlated) with fluctuations in the velocity as shown in Fig. I-4. This is a unique feature of Alfvén waves, which led to the interpretation of the observed fluctuations as superposed waves. There have been mainly two fundamental concepts to explain the solar wind turbulence in the framework of this wave picture. The so-called *slab* model assumes the fluctuations in the solar wind to be a superposition of Alfvén waves, which propagate parallel to the background magnetic field. The other branch of models are the *isotropic* models, which assume that the power spectral density is distributed isotropically

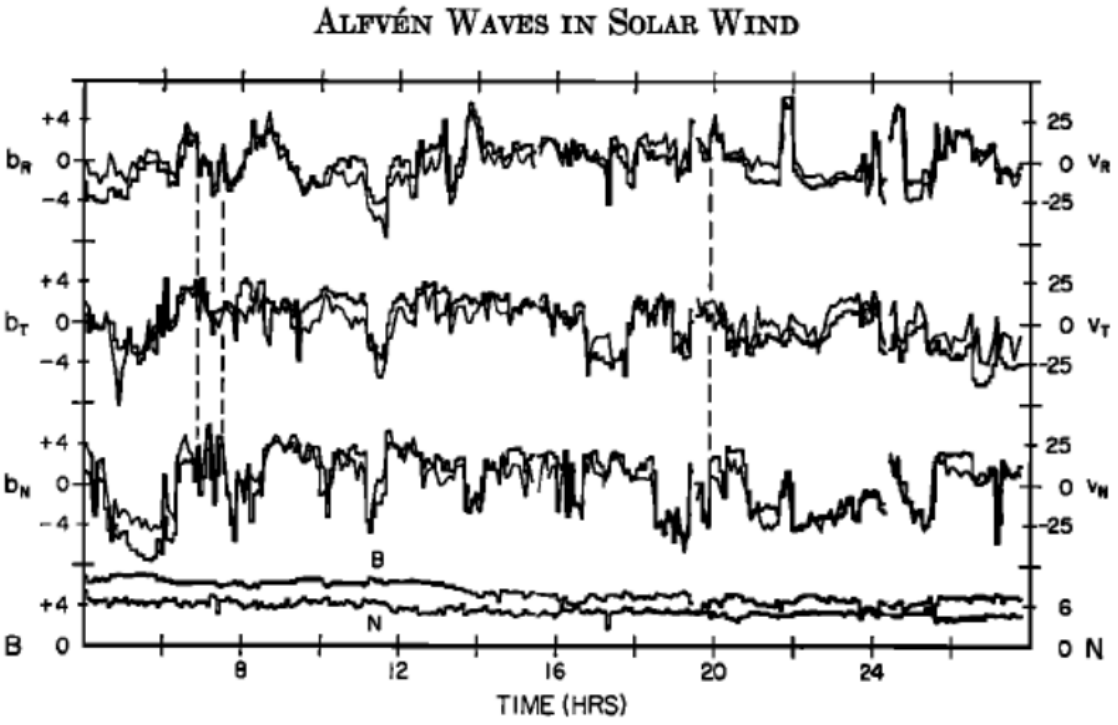

Figure I-4: Measurements from a Mariner spacecraft. A time series of magnetic field and velocity components is shown. The high correlation between magnetic field fluctuations and velocity fluctuations is a clear indication for the presence of Alfvén waves. From Belcher and Davis (1971).

into all directions.

The observed waves show mainly a propagation outward from the Sun, which would contradict a local generation mechanism during their passage through the heliosphere. The measure that indicates the dominating propagation direction is the magnetic cross-helicity, which can be obtained from measurements of the magnetic field and the bulk motion of the particles (Schwenn and Marsch, 1991). On its transit from the Sun into the heliosphere, the solar wind passes a point, where its outflow velocity becomes super-Alfvénic. This point is called the *Alfvén-critical distance*. If a wave with the Alfvén speed as its phase speed is convected beyond this point, it cannot propagate back to the Sun because it had to be faster than the Alfvén speed in this case. This is the reason, why the preference of outward propagation is an indication for a generation mechanism inside the Alfvén-critical distance (Tu and Marsch, 1995).

Observations indicate in many cases, however, that the fluctuations show characteristics of turbulence such as a broad power-law spectrum with the typical breaks in the spectral slope (e.g., Horbury *et al.*, 2005, and references therein). Turbulence is usually characterized as a combination of highly random fluctuations on many different scales. The spectral analysis of an isotropic and homogeneous turbulent fluid leads to three different ranges in the power spectrum. The *driving range* at low frequencies/wavenumbers is the part of the spectrum, into which energy is deposited due to macroscopic effects. The energy is then transported to higher frequencies, corresponding to small-scale fluc-

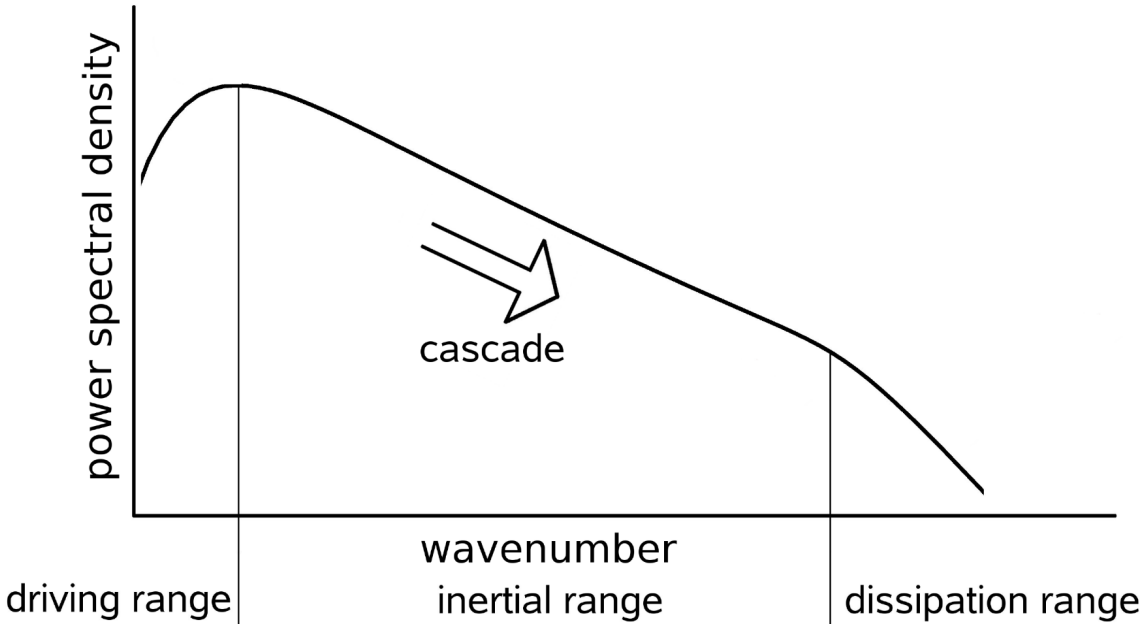

Figure I-5: Schematic understanding of the power spectrum of typical isotropic, homogeneous fluid turbulence. The energy is introduced to the system in the driving range. From these large scales, it is transported through the inertial range down to dissipative scales, where it is dissipated and transformed to heat.

tuations, through nonlinear interactions between eddies of different scales. This happens over the so-called *inertial range*. Eventually the energy is dissipated on small scales in the so-called *dissipation range* (Leslie, 1973). The transfer of energy from one wavenumber/frequency to another is called *spectral transfer*. A schematic spectrum of isotropic fluid turbulence is shown in Fig. I-5. The occurrence of these different ranges—especially the inertial range and a break to the dissipation range—is an indication for an active turbulent cascade with high-order couplings and a nonlinear transport of energy in wavenumber space until the onset of dissipation as it has been suggested by Coleman (1968) for the solar wind. In this interpretation, fluctuations with higher frequencies are generated during the propagation through the heliosphere due to self-organization and the coupling of waves with other waves. These are inherently nonlinear effects. Regarding plasma turbulence, their principles have been described since the early beginnings of plasma fusion research (e.g., Kadomtsev, 1965; Vedenov, 1968; Davidson, 1972). Turbulence might be also generated locally by wave–particle processes such as the already mentioned pick-up process in the outer heliosphere or micro-instabilities in the solar wind (Gary, 1993).

In the classic paper by Matthaeus *et al.* (1990), the authors suggest a new model for the fluctuations in the solar wind. They analyze the two-point correlation function defined as $R(\boldsymbol{r}) \equiv \langle \boldsymbol{B}(\boldsymbol{x}) \cdot \boldsymbol{B}(\boldsymbol{x}+\boldsymbol{r}) \rangle$ for spacecraft measurements of magnetic field fluctuations under the Taylor assumption (explained later), where the brackets indicate averaging. They obtain the famous *Maltese cross* diagram, which is shown in Fig. I-6. In this diagram, fluctuations with high wavenumbers occur at small values for the separation $\boldsymbol{r}$. Fluctuations that propagate parallel to the background magnetic field have a high correlation in the perpendicular separation and vice versa. A simple slab wave superposition would, there-

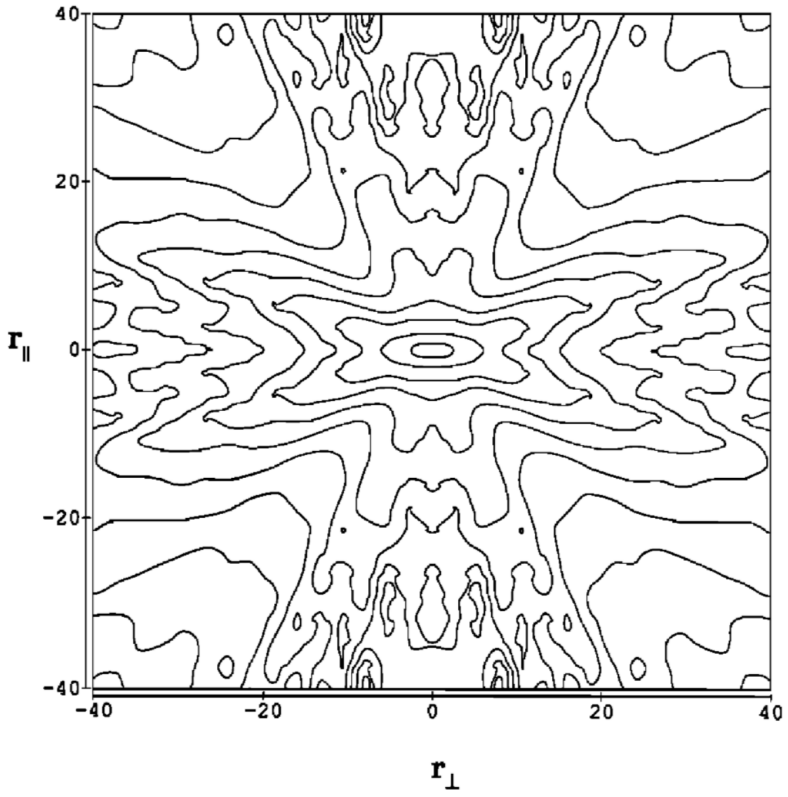

Figure I-6: Contour plot of the two-point correlation function $R(\boldsymbol{r})$ for solar wind fluctuations depending on the separation $(r_\perp, r_\parallel)$ with respect to the background magnetic field. The distances are given in units of 10^{10} cm. The measurements were taken for the first quadrant only and then mirrored to complete this view. From Matthaeus *et al.* (1990).

fore, lead to a correlation only along the axis $r_\parallel = 0$. An isotropic spectrum would lead to circles in this diagram. Both is obviously not the case in the observed spectral range. This finding led Matthaeus, Goldstein, and Roberts to the idea of a *composite model* for solar wind fluctuations. In this picture, the main contributors are two components, a parallel slab one and a perpendicular 2D component. After this discovery, the picture evolved and led to the interpretation that solar wind fluctuations consist of a population of Alfvénic fluctuations (slab component), which do not interact with each other much, and which originate from the solar corona. A second population can be understood as fully developed turbulence (2D component), which rises from the nonlinear evolution of solar wind fluctuations on the way through the heliosphere (Horbury *et al.*, 2005; Alexandrova *et al.*, 2008a). All of these interpretations and models only hold for the inertial range, where the MHD approximation is valid. For the dissipative scales, beginning at about the ion inertial length, these models are not applicable because effects due to the gyromotion of the particles have to be taken into account. He *et al.* (2011b) calculate two-dimensional correlation functions for transversal and longitudinal magnetic field fluctuations and density fluctuations down to scales of about five ion gyroradii based on Cluster measurements. They also find two components in the correlation function (parallel and perpendicular to the background magnetic field), where the field-perpendicular energy cascade seems to dominate. In another analysis, He *et al.* (2011a) find evidence for the coexistence of

left- and right-handed normal mode waves in solar wind turbulence. The interpretation is that the left-handed waves correspond to a superposition of Alfvén/ion-cyclotron (A/IC) waves, whereas the right-handed (and mainly obliquely propagating waves) are a superposition of fast/whistler (F/W) waves or kinetic Alfvén waves (KAWs). The right-handed waves are believed to survive the cyclotron resonance of the ions since the left-handed gyration of the ions cannot pick up the right-handed rotation of the electric field. Therefore, normal mode turbulence is believed to consist of right-handed waves at frequencies higher than the proton gyration frequency, which is in good agreement with previous observations (Goldstein *et al.*, 1994). Effects on these scales are discussed in this work in detail later.

Sophisticated numerical and theoretical treatments of plasma turbulence have recently been applied to space plasmas. Gyrokinetic approaches (Schekochihin *et al.*, 2008; Howes, 2008) allow one to describe small-scale fluctuations in the direction perpendicular to the background magnetic field. Therefore, they are in favor of kinetic Alfvén waves, which obey the anisotropy relation $k_\perp \gg k_\parallel$ (Goldreich and Sridhar, 1995). KAWs are linear compressive plasma waves with different possible polarizations. The right-handed polarization is favored for the most common geometries (Hollweg, 1999). Effects of the cyclotron resonance are suppressed in the gyrokinetic approaches. Therefore, kinetic dissipation can occur only due to the Landau resonance, and thus only parallel heating by the electric wave field can be explained (Bian and Kontar, 2010), which is in conflict with the observations of a preferentially perpendicular heating of both the solar wind and coronal ions (Marsch *et al.*, 2004; Kohl *et al.*, 2006; Bourouaine *et al.*, 2010).

A/IC waves are observed directly in the solar wind (Jian *et al.*, 2009). Effects from the cyclotron resonance of these waves on the plasma particles are also observed (Gary *et al.*, 2005b; Kasper *et al.*, 2008). These and other considerations (e.g., Podesta *et al.*, 2010) challenge the importance and validity of the gyrokinetic approaches and the meaning of kinetic Alfvén waves in space plasma turbulence. One direct consequence of the presence of Alfvén/ion-cyclotron waves is a particular shaping of the velocity distribution function (Heuer and Marsch, 2007). The resonant quasilinear diffusion operator leads to time-asymptotic solutions for the distribution function on circles around the wave phase speed in the solar wind rest frame (Isenberg and Lee, 1996). After a sufficiently long interaction of waves with the distribution function, it should form so-called *plateaus*, i.e., circular shapes around the position of the wave phase speed in a velocity space coordinate system, which is more or less the Alfvén speed in this case (Marsch and Tu, 2001). These structures are indeed observed as shown in Fig. I-7, where the circular contours of the distribution function can be seen. Another observational evidence for the existence of A/IC waves is the surfing effect of alpha particles (Marsch *et al.*, 1981). Drifting Helium particles can fulfill the condition $\omega/k = u_\parallel$ with the drift velocity $u_\parallel$ along the magnetic field, the wave frequency ω, and the wavenumber k. The polarization relation for A/IC waves, which will be used extensively in this work, requires that particles fulfilling this relation have no transversal bulk velocity. Marsch *et al.* (1981) found that alpha particles flow out radially in the solar wind, unaffected by the wave electric field in some cases. These measurements are shown in Fig. I-8.

Most of the above mentioned models for solar wind fluctuations assume the solar wind to be an incompressible fluid. However, the solar wind is clearly *not* an incompressible medium (e.g., Roberts *et al.*, 1987b; Grappin *et al.*, 1991; Tu and Marsch, 1995). It

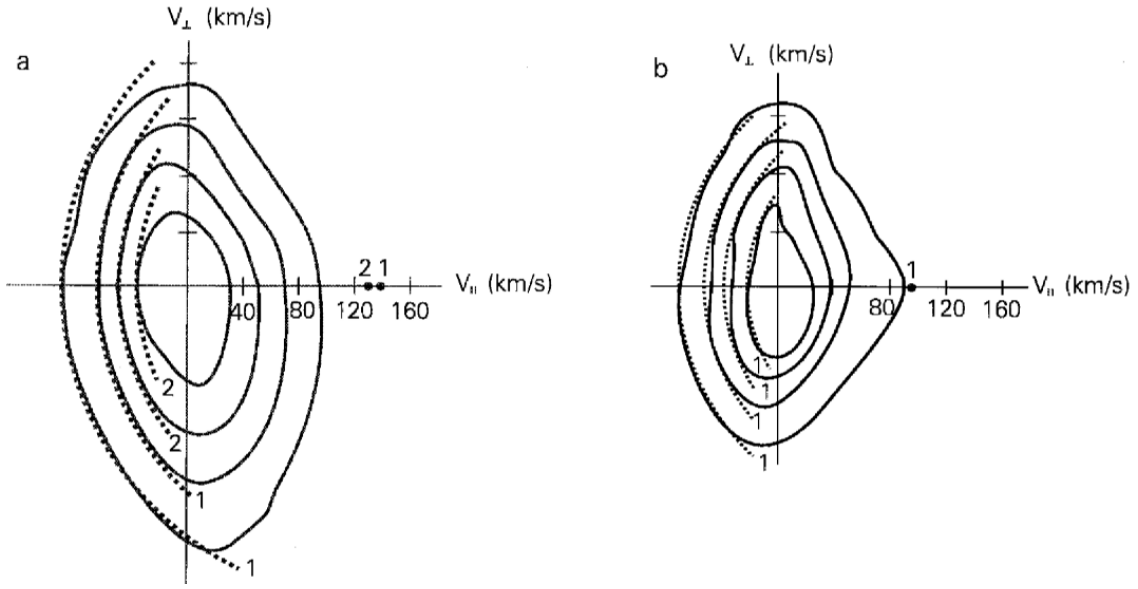

Figure I-7: Measured distribution functions from Helios 2 (bold). The circular arcs indicate diffusion plateaus (dotted). The centers of the arcs are indicated by dots and numbers. a) at 0.3 AU, b) at 0.4 AU. From Marsch and Tu (2001).

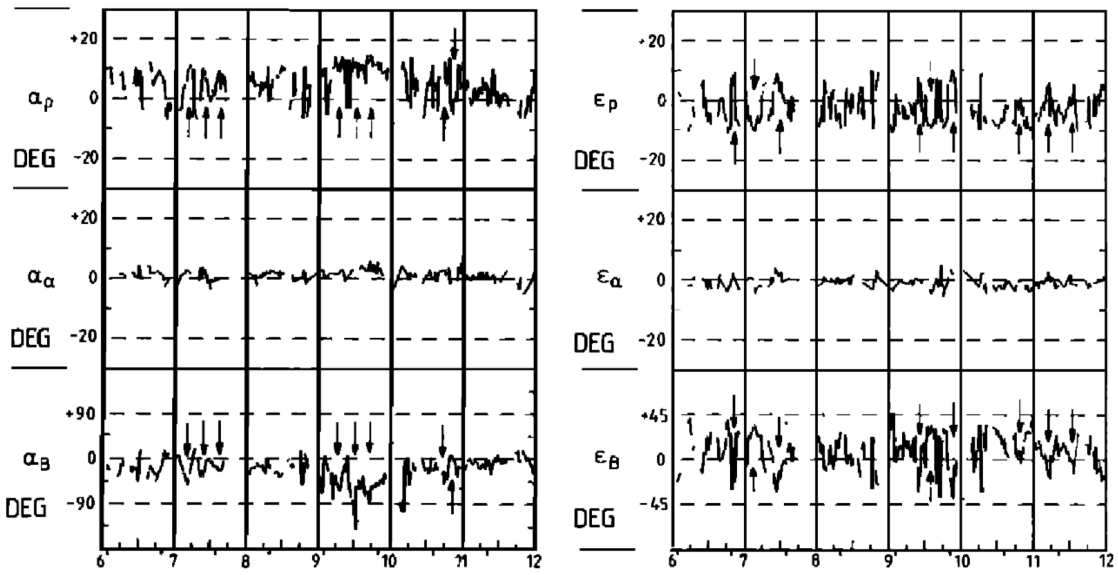

Figure I-8: Azimuthal angle (left) and elevation angle (right) for the bulk velocities of protons and alpha particles depending on time. The lowest line shows the angles for the magnetic field. The alpha particles do not participate in the wave motion and surf on the wave. These results are based on Helios 2 observations from May 1981. From Marsch *et al.* (1981).

shows compressive and electrostatic fluctuations on many scales (Bavassano *et al.*, 1996; Bruno and Carbone, 2005; Kellogg and Horbury, 2005; Yao *et al.*, 2011). The compressive fluctuation power is usually less than the power in the transversal, incompressible

component (Spangler and Spitler, 2004). The little compressibility itself, however, might lead to additional effects that should be investigated in more detail. In the recent past, the improved models take compressive effects more and more into account and investigate their influence. The modern non-MHD codes (hybrid, particle-in-cell, gyrokinetic) allow intrinsically for compressibility. Furthermore, compressible MHD codes have become more and more popular in recent years (Bhattacharjee *et al.*, 1999; Shaikh and Zank, 2010).

I.4 Parametric instability of large-amplitude waves

A complete analytic description of the detailed behavior of fully developed fluid turbulence is impossible because of its complicated nonlinear interactions. Most descriptions rely on phenomenological models for the spectral transfer of energy between different wavenumbers (Zhou and Matthaeus, 1990) as well as on scaling relations like the very successful theories by Kolmogorov or Iroshnikov/Kraichnan (see Chapt. II). Another approach to the evolution of turbulence is the fully nonlinear numerical calculation in the frame of different plasma models (hydrodynamic, magnetohydrodynamic, hybrid, fully kinetic, and some modifications of these). There is, however, another spectral transfer process, the details of which can be understood more easily. It is the so-called *parametric instability* of plasma waves. Under certain conditions, a monochromatic plasma wave is unstable and decays into daughter waves with different wavenumbers and frequencies than the mother (retaining the common nomenclature for the participating waves). The first description of such a process was provided by Galeev and Oraevskii (1963), who studied a linearly polarized MHD Alfvén wave and found that this wave decays into daughter waves with different frequencies, and that the mother cannot propagate infinitely as a stable wave. They discovered the *decay instability*. The authors already discussed the role of compressibility in the plasma. The decay products correspond to a forward propagating magnetosonic wave, a backward propagating Alfvén wave, and another forward propagating magnetic wave (Cohen, 1975; Hollweg *et al.*, 1993).

Later, other authors discussed further scenarios. Lashmore-Davies and Stenflo (1979) describe another instability that can also occur under conditions, when the decay instability is forbidden. A linear MHD Alfvén wave is shown to be unstable in a resistive MHD fluid to purely growing density perturbations and side-band waves if its amplitude exceeds a certain threshold. This instability is directly related to dispersive effects and is called the *modulational instability*. Since the solar wind plasma has a significantly higher beta than assumed in the previous treatments, Goldstein (1978) and Derby (1978) discuss a high-β plasma wave. In their models, they consider circularly-polarized Alfvén waves as exact solutions of the fluid equations and show that these waves are also unstable to two magnetic waves (forward and backward propagating with respect to the mother wave) and one forward propagating density wave. An additional result of parametric instabilities is the *beat mode* (Longtin and Sonnerup, 1986; Wong and Goldstein, 1986). It occurs as the interaction product of the forward and backward propagating side-band waves from the modulational instability. It is a compressive mode with frequencies and wavenumbers around those of the pump wave. It is mainly important for high-beta plasmas (Hollweg, 1994). The possible parametric instabilities depend on several factors: thresholds for the

amplitude, polarization, handedness of the pump wave and, in particular, the plasma beta. It is important to note that, in many cases, the daughter-wave products do not correspond to normal modes of the plasma. In the case of the "cold" decay instability, two products correspond to the ion-acoustic and Alfvén waves. But this is not the case for all parametric instabilities. Analytical treatments yield (exponential) growth rates over certain wavenumber ranges. Of course, the daughter waves cannot grow infinitely and will, thus, result in a saturated nonlinear state, which might look similar to a turbulent plasma, even though the spectral transfer did not begin in form of the classical turbulent cascading. The mother wave delivers free energy, from which the daughter waves are fed. Therefore, the amplitude of the pump wave has to decrease with growing daughter-wave amplitudes. Especially if the fully nonlinear evolution of daughter products is of interest, numerical simulations become necessary. Also in these treatments, different parametric instabilities are found (e.g., Viñas and Goldstein, 1991a,b; Araneda, 1998). The influence of daughter waves on the plasma particles is for example discussed by Araneda *et al.* (2007, 2008).

All these considerations show already that the pure existence of a wave can lead to the excitation of other waves with different frequencies and wavenumbers. The parametric instability is, hence, a spectral transfer process that is believed to play an important role in the generation and evolution of space plasma turbulence. It also shows that a collisionless plasma cannot maintain monochromatic waves under all possible solar wind conditions for an infinite amount of time and evolves towards a kind of turbulent state.

I.5 Dissipation of plasma fluctuations

The interaction of waves with particles in a collisionless plasma has been discussed for a long time. The electric field plays a key role in these interactions. There are mainly two dissipative processes, which will be discussed from the mathematical point of view in Chapt. II. It is important to remember the two fundamental types of wave polarization here. The term *transversal* refers to a situation, when the vector of the fluctuating observable is perpendicular to the direction of propagation. At the *longitudinal* polarization, the vector of the fluctuating quantity is parallel to the direction of propagation. A fluctuating longitudinal electric field can lead to dissipation of wave energy in the direction of propagation because the particles can couple to this field resonantly and be accelerated. This effect is called Landau-resonant wave–particle interaction. In the case of a magnetized plasma, the direction of propagation of longitudinal waves is the same as the direction of the background magnetic field. Transversal fluctuations can fulfill the condition of cyclotron-resonance. In this case, the gyromotion of the particles is in the same plane as the rotating transversal electric field if the wave propagates along the constant magnetic field. The particles' motion can couple to the wave electric field, which then can accelerate particles. This leads to a heating mainly perpendicular to the background magnetic field, which is also observed. The waves with wavevector $\boldsymbol{k}$ and frequency ω have to hold some peculiar properties to undergo these two kinds of resonances. For the Landau resonance, the phase speed of the waves has to be comparable to the thermal speed of the particles. For a particle with speed $\boldsymbol{v}$, the resonance condition is $\boldsymbol{k} \cdot \boldsymbol{v} \approx \omega$. Only if $v_{\mathrm{th}} \approx \omega/k$, a significant part of the distribution function can participate in the resonant interaction. The cyclotron-resonance (with the condition $k_{\parallel} v_{\parallel} - \omega \pm n\Omega_j = 0$ with gy-

rofrequency Ω_j for species j and an integer n with $n = 1$ for parallel propagation, the index $\parallel$ indicates the components parallel to the background field) requires waves with frequencies comparable to the gyration frequency of the particles that fall victim to the wave–particle interaction. This leads to a refinement of the central question that shall be addressed by this work: How can waves with the matching properties for these resonances be generated? Waves with a low wavenumber and a low frequency (like Alfvén waves) are easily generated by foot-point motions of flux tubes in the solar atmosphere and be convected into the solar wind. However, this does not explain the observationally confirmed existence of waves in the cyclotron-resonant spectral range. It is important to understand the different generation mechanisms for fluctuating electric fields. While some wave types exhibit a longitudinal or transversal electric field by nature, other more indirect or hidden mechanisms can provide them. Possible candidates are obliquity in the propagation, ponderomotive effects, and ubiquitous decay products for example. The search for mechanisms that generate longitudinal or transversal electric fields is another formulation of the objective of this thesis.

The onset of dissipation on small scales leads to the observed breaks in turbulence spectra (Alexandrova *et al.*, 2008a,b). These breaks are directly related to the natural scales of the participating particle species. The inertial range reaches down to the first typical ion scale, the proton inertial length ℓ_p, where the first break in the spectrum is usually observed. Then an electron inertial range is expected down to the typical electron scales, where the next break occurs (Alexandrova *et al.*, 2009). The exact position of the breaks, however, is still under debate. It is not completely clear if the observations support a break at the inverse gyroradius, the inverse inertial length scale, or another typical length scale (Perri *et al.*, 2010). A typical spectrum of space plasma turbulence from satellite observations is shown in Fig. I-9.

The theory of the sometimes favored KAWs predicts a spectral slope for the magnetic field fluctuations of the form $\sim k_\perp^{-7/3}$ below the MHD scales (Schekochihin *et al.*, 2008), and in fact observations indicate a spectral index of about -2.8 (Alexandrova *et al.*, 2009), which might be inside the error bars up to the electron scales. The complete interpretation of this part of the spectrum is, however, not yet clear.

I.6 Key questions

From the different problems and open questions that have been stated in the Introduction so far, the central issues treated in this thesis on the nature and generation of waves and turbulence in the solar wind are:

- How can coherent motions due to waves be described, and how can they influence particle measurements from space probes?
- What is the nature of fluctuations below the ion scales?
- How are these waves associated with electric fields that can accelerate/thermalize particles?
- What is the role of compressive effects in solar wind turbulence?

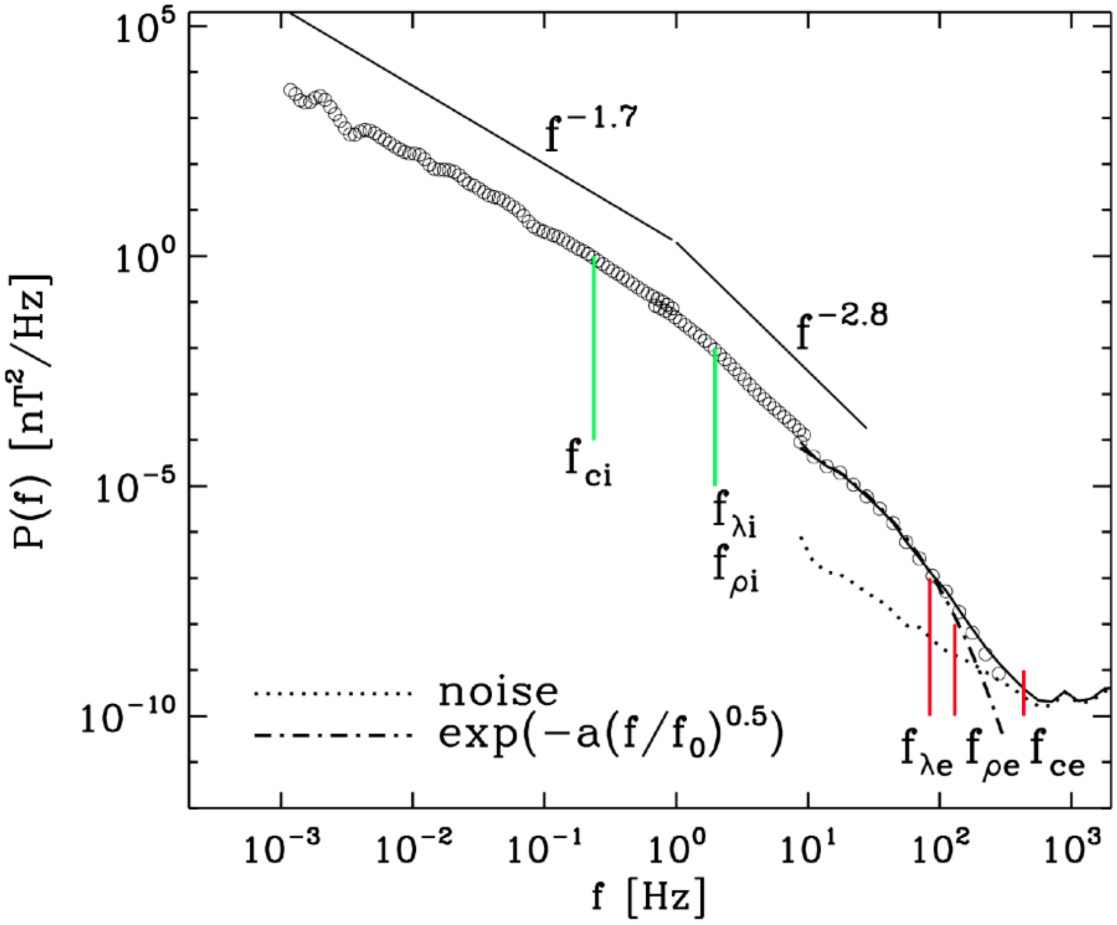

Figure I-9: Measurements of the magnetic power spectrum by Cluster in the free solar wind. The typical frequencies are indicated as the gyrofrequency (f_c), the frequencies associated with the thermal gyroradius (f_ϱ) and the inertial length (f_λ) for protons and electrons. The breaks in the spectra are clearly visible. At frequencies above 10 Hz, the spectrum follows rather an exponential function than a power-law. This might be due to strong dissipation. Reprinted figure with permission from Alexandrova *et al.* (2009). Copyright 2009 by the American Physical Society.

- Are the solar wind fluctuations (at least partly) a non-interacting superposition of waves?
- How does the (anisotropic) spectral transfer work?

These questions, or at least some aspects thereof, shall be addressed in this work in the form of different approaches.

II Basic mathematics for describing plasma waves and wave–particle interactions

II.1 Fundamentals of kinetic plasma theory

Kinetic theory is based on the description of a particle ensemble by the behavior of the particle distribution function f. This function is defined as the differential phase-space density at a given time t, and it is usually normalized to the number of particles in the treated volume. Thus, the total number N of particles in the described ensemble is given by

$$N = \iint f(\boldsymbol{x}, \boldsymbol{p}, t)\, \mathrm{d}^3x\, \mathrm{d}^3p, \tag{II-1.1}$$

where the spatial coordinate is denoted by $\boldsymbol{x}$ and the momentum by $\boldsymbol{p}$. An equation that describes the evolution of the distribution function is called *kinetic equation*. These equations follow from the general consideration of continuity in phase-space, and in this sense kinetic physics is a fluid description, not in 3D position-space but in 6D phase-space. From very fundamental considerations about the conservation of particles, the continuity equation

$$\frac{\partial f}{\partial t} + \frac{\partial}{\partial \boldsymbol{x}} \cdot \left(\frac{\mathrm{d}\boldsymbol{x}}{\mathrm{d}t} f \right) + \frac{\partial}{\partial \boldsymbol{p}} \cdot \left(\frac{\mathrm{d}\boldsymbol{p}}{\mathrm{d}t} f \right) = 0 \tag{II-1.2}$$

is found if particles are not abruptly ejected to other phase-space elements by collisions (e.g., Landau and Lifshitz, 1980). If the motion of each particle can be described by the Hamiltonian $\mathcal{H}$, the trajectories of the particles follow Hamilton's equations of motion in phase-space:

$$\frac{\mathrm{d}\boldsymbol{x}}{\mathrm{d}t} = \frac{\partial \mathcal{H}}{\partial \boldsymbol{p}}, \qquad \frac{\mathrm{d}\boldsymbol{p}}{\mathrm{d}t} = -\frac{\partial \mathcal{H}}{\partial \boldsymbol{x}}. \tag{II-1.3}$$

With these relations, Eq. (II-1.2) can be rewritten as

$$\frac{\partial f}{\partial t} + \frac{\mathrm{d}\boldsymbol{x}}{\mathrm{d}t} \cdot \frac{\partial f}{\partial \boldsymbol{x}} + \frac{\mathrm{d}\boldsymbol{p}}{\mathrm{d}t} \cdot \frac{\partial f}{\partial \boldsymbol{p}} = \frac{\mathrm{d}f}{\mathrm{d}t} = 0, \tag{II-1.4}$$

which means that the total derivative of the phase-space density is zero along the trajectories of the particles that are described by the Hamiltonian $\mathcal{H}$ and the related equations

of motion. This conservation of the particle distribution function is one of the key statements of statistical mechanics and also known as *Liouville's theorem*. As mentioned before, Eq. (II-1.2) can be interpreted as a continuity equation of a phase-space fluid. The transition to Eq. (II-1.4) is analogous to the assumption of incompressibility in classical fluid theory. Therefore, it is appropriate to state that the phase-space fluid is incompressible for a Hamiltonian system, which is an equivalent formulation of Liouville's theorem. Boltzmann generalized Liouville's theorem to the so-called *Boltzmann equation* for the case, when binary particle collisions are taken into account.

In the cases relevant for this work, several particle species are treated with different distribution functions, which are labeled by the index j. Since relativistic processes are not of interest, one can change from the momentum-dependent distribution function to a velocity distribution function $f_j(\boldsymbol{x}, \boldsymbol{v}, t)$ to describe particles of species j with velocity $\boldsymbol{v}$.

A plasma consists of different charged particle species, which are influenced by electric fields $\boldsymbol{E}$ and magnetic fields $\boldsymbol{B}$. These fields are generated by electric currents $\boldsymbol{j}$ and electric charge densities ϱ_c, and therefore the feedback of the particles on themselves must be taken into account in a self-consistent way. The kinetic equation describing particles under the influence of electric and magnetic fields is the *Vlasov equation*, in which the Lorentz force term is used for the temporal momentum change. This equation can be written as

$$\frac{\partial f_j}{\partial t} + \boldsymbol{v} \cdot \frac{\partial f_j}{\partial \boldsymbol{x}} + \frac{q_j}{m_j}\left(\boldsymbol{E} + \frac{1}{c}\boldsymbol{v} \times \boldsymbol{B}\right) \cdot \frac{\partial f_j}{\partial \boldsymbol{v}} = 0. \tag{II-1.5}$$

It is valid for all charged species j in a plasma such as ions or electrons with electric charge q_j and mass m_j, respectively. The speed of light is denoted by c. The characteristics of the Vlasov equation are given by

$$\frac{\mathrm{d}\boldsymbol{v}}{\mathrm{d}t} = \frac{q_j}{m_j}\left(\boldsymbol{E} + \frac{1}{c}\boldsymbol{v} \times \boldsymbol{B}\right), \tag{II-1.6}$$

$$\frac{\mathrm{d}\boldsymbol{x}}{\mathrm{d}t} = \boldsymbol{v} \tag{II-1.7}$$

and correspond to the equations of motion for a single particle under the influence of the fields $\boldsymbol{E}$ and $\boldsymbol{B}$. The particles themselves generate a space charge density

$$\varrho_\mathrm{c} = \sum_j q_j \int f_j(\boldsymbol{x}, \boldsymbol{v}, t)\, \mathrm{d}^3 v \tag{II-1.8}$$

and a current density

$$\boldsymbol{j} = \sum_j q_j \int \boldsymbol{v} f_j(\boldsymbol{x}, \boldsymbol{v}, t)\, \mathrm{d}^3 v, \tag{II-1.9}$$

derived from the zeroth and first velocity moments of the distribution function, which will be discussed in more detail later. With these relations, Maxwell's equations can be written

as

$$\operatorname{div} \boldsymbol{E} = 4\pi \sum_j q_j \int f_j(\boldsymbol{x}, \boldsymbol{v}, t)\, \mathrm{d}^3 v, \tag{II-1.10}$$

$$\operatorname{curl} \boldsymbol{E} = -\frac{1}{c}\frac{\partial \boldsymbol{B}}{\partial t}, \tag{II-1.11}$$

$$\operatorname{div} \boldsymbol{B} = 0, \tag{II-1.12}$$

$$\operatorname{curl} \boldsymbol{B} = \frac{4\pi}{c} \sum_j q_j \int \boldsymbol{v} f_j(\boldsymbol{x}, \boldsymbol{v}, t)\, \mathrm{d}^3 v + \frac{1}{c}\frac{\partial \boldsymbol{E}}{\partial t}. \tag{II-1.13}$$

The influence of charged matter on the fields becomes obvious in this formulation, which is sometimes also called the *Vlasov-Maxwell equations*. Since Maxwell's equations are differential equations, a 'constant offset' in the fields can generally be added, which is then called the *background field*.

All the above remarks show that the Vlasov equation is a profoundly nonlinear equation. The set of Maxwell's equations and the Vlasov equation form a coupled nonlinear system of integro-differential equations. For this reason, a direct analytical solution is in most cases impossible and simplifications become necessary.

II.1.1 Unmagnetized plasma

Linear Vlasov theory for unmagnetized plasmas is discussed in many textbooks (e.g., Akhiezer *et al.*, 1975). The general idea of linear theory is that the distribution function f_j consists of a background function f_{j0} and an added small perturbation δf_j. The ensemble average (which is for ergodic processes the same as the temporal average) is denoted by angle brackets. The background and the perturbation fulfill the relations

$$\langle f_j \rangle = f_{j0}, \qquad \langle \delta f_j \rangle = 0. \tag{II-1.14}$$

The Vlasov equation is linearized, which is a good assumption for small perturbations. It yields

$$\frac{\partial \delta f_j}{\partial t} + \boldsymbol{v} \cdot \frac{\partial \delta f_j}{\partial \boldsymbol{x}} + \frac{q_j}{m_j}\left(\delta \boldsymbol{E} + \frac{1}{c}\boldsymbol{v} \times \delta \boldsymbol{B}\right) \cdot \frac{\partial f_{j0}}{\partial \boldsymbol{v}} = 0. \tag{II-1.15}$$

The disturbances in the distribution function δf_j and in the fields $\delta \boldsymbol{E}$ and $\delta \boldsymbol{B}$ are assumed to be decomposable in Fourier components for each quantity $\delta A(\boldsymbol{x}, t)$ according to

$$\delta A(\boldsymbol{x}, t) = \iint \delta A(\boldsymbol{k}, \omega) e^{i(\boldsymbol{k}\cdot\boldsymbol{x} - \omega t)}\, \mathrm{d}^3 k\, \mathrm{d}\omega \tag{II-1.16}$$

with wavevector $\boldsymbol{k}$ and frequency ω. The argument $(\boldsymbol{k}, \omega)$ of the Fourier amplitude is omitted in the following. Space- and time-dependent quantities should be all understood as the corresponding Fourier components if not stated in a different way. Under this

assumption, Maxwell's equations for the perturbation fields become

$$\boldsymbol{k} \cdot \delta\boldsymbol{E} = -4\pi i \sum_j q_j \int \delta f_j \, \mathrm{d}^3 v, \tag{II-1.17}$$

$$\boldsymbol{k} \times \delta\boldsymbol{E} = \frac{\omega}{c} \delta\boldsymbol{B}, \tag{II-1.18}$$

$$\boldsymbol{k} \cdot \delta\boldsymbol{B} = 0, \tag{II-1.19}$$

$$\boldsymbol{k} \times \delta\boldsymbol{B} = -\frac{4\pi i}{c} \sum_j q_j \int \boldsymbol{v} \delta f_j \, \mathrm{d}^3 v - \frac{\omega}{c} \delta\boldsymbol{E} \tag{II-1.20}$$

under the assumption that the background distribution function f_{j0} does not generate time- or space-dependent fields. The linearized Vlasov equation becomes

$$i\,(\boldsymbol{k} \cdot \boldsymbol{v} - \omega)\, \delta f_j + \frac{q_j}{m_j} \left[\delta\boldsymbol{E} \left(1 - \frac{\boldsymbol{k} \cdot \boldsymbol{v}}{\omega} \right) + \frac{\boldsymbol{k} (\boldsymbol{v} \cdot \delta\boldsymbol{E})}{\omega} \right] \cdot \frac{\partial f_{j0}}{\partial \boldsymbol{v}} = 0, \tag{II-1.21}$$

where Faraday's law was used to express the magnetic field perturbation in terms of the electric field perturbation. This expression allows one to achieve an algebraic solution for the perturbation δf_j in Fourier space. Based on this concept, many different problems of plasma physics can be treated such as the determination of the dielectric tensor and its consequences, the occurrence and conditions for micro-instabilities, or the finding of various dispersion relations for plasma waves (e.g., Stix, 1992; Gary, 1993; Melrose and McPhedran, 2005).

As an example of the applicability, the quasilinear theory of Landau damping will be shown, which is a very important and solely kinetic effect. For the sake of simplicity, the quasilinear diffusion is derived for an isotropic plasma. In this case, the scalar product of $\boldsymbol{v} \times \delta\boldsymbol{B}$ with $\partial f_{j0}/\partial \boldsymbol{v}$ vanishes because f_{j0} only depends on the modulus of the velocity. The perturbation can then be written as

$$\delta f_j = i \frac{q_j}{m_j} \frac{\delta\boldsymbol{E}}{\boldsymbol{k} \cdot \boldsymbol{v} - \omega} \cdot \frac{\partial f_{j0}}{\partial \boldsymbol{v}}. \tag{II-1.22}$$

Now the perturbed quantities in terms of Fourier integrals are taken and used in the Vlasov equation again. Then the equation has to be ensemble averaged, and thus the oscillating terms vanish. For the ensemble averaging of the quadratic electric field terms, the relation

$$\langle \delta E_i(\boldsymbol{k}, \omega) \delta E_\ell^*(\boldsymbol{k}', \omega') \rangle = \left(\delta\boldsymbol{E}^2 \right) \frac{k_i k_\ell}{k^2} \delta(\boldsymbol{k} - \boldsymbol{k}') \delta(\omega - \omega') \tag{II-1.23}$$

is needed, where the asterisk indicates the complex conjugated quantity and δ Dirac's delta distribution (Lifshitz and Pitaevskii, 1981). Only quadratic terms remain, leading to

$$\frac{\partial f_{j0}}{\partial t} = \frac{\partial}{\partial v_i} \left(D_{i,\ell} \frac{\partial f_{j0}}{\partial v_\ell} \right) \tag{II-1.24}$$

with

$$D_{i,\ell} = \frac{q_j^2}{m_j^2} \iint \frac{k_i k_\ell}{k^2} \frac{i(\delta\boldsymbol{E}^2)}{\boldsymbol{k} \cdot \boldsymbol{v} - \omega} \, \mathrm{d}^3 k \, \mathrm{d}\omega. \tag{II-1.25}$$

The interaction of waves with particles leads to a diffusion in velocity space with the non-trivial diffusion coefficient $D_{i,\ell}$. This behavior is known as quasilinear diffusion. For $\boldsymbol{k} \cdot \boldsymbol{v} = \omega$, the interaction becomes resonant, and the so-called Landau-damping occurs. The damping rate can be calculated by taking Gauß' law and using the expression for the perturbation δf_j (Vedenov, 1963).

II.1.2 Magnetized plasma

The effects of a (strong) constant background magnetic field have not been taken into account until now. Most of space and laboratory plasmas, however, are permeated by a magnetic field. For instance, the background magnetic field of the solar corona is responsible for the visible coronal loops. The solar wind is infused by the Parker spiral in first order, and also the confining magnetic field used in certain fusion experiments is a constant background field of this type. The most important difference to the unmagnetized case is the situation that the motion of particles behaves differently depending on their velocity's orientation with respect to the field in the magnetized case. Since the plasma particles are charged ions and electrons, their motion perpendicular to the magnetic field is diverted onto a circular path (i.e., gyration), which is superimposed on the parallel trajectory. The anisotropy due to the background field leads to many additional effects in the collective behavior of the plasma.

This section mainly follows the very clear derivation by Akhiezer *et al.* (1975). These authors provide a clear and general derivation of linear theory, also taking oblique propagation of perturbations into account. Nevertheless, the literature provides a broad variety of calculations for the linear theory in magnetized plasmas (e.g., Davidson, 1972; Lifshitz and Pitaevskii, 1981; Gary, 1993; Gurnett and Bhattacharjee, 2005).

The perturbation of the distribution function is derived in a similar way as in the unmagnetized case. However, now the Lorentz force due to the constant background magnetic field $\boldsymbol{B}_0$ has to be added. It is given in the form

$$\frac{q_j}{m_j c} \left[\boldsymbol{v} \times \boldsymbol{B}_0\right] \cdot \frac{\partial f_j}{\partial \boldsymbol{v}} = -\Omega_j \frac{\partial f_j}{\partial \varphi}, \tag{II-1.26}$$

where the reasonable coordinate system is used in which the z-axis is parallel to $\boldsymbol{B}_0$. The gyration frequency of the species j is defined as

$$\Omega_j \equiv \frac{q_j B_0}{m_j c}. \tag{II-1.27}$$

The azimuthal angle φ between the x-axis and the field-perpendicular velocity component $v_\perp$ is defined by $\cos\varphi \equiv v_x / v_\perp$. The velocity component $v_\parallel$ is the component parallel to $\boldsymbol{B}_0$. In this cylindrical coordinate system, the velocity vector is determined by the components $(v_\perp, v_\parallel, \varphi)$. This coordinate system is depicted in Fig. II-1. The zeroth-order distribution function f_{j0} is supposed to be independent of the azimuthal angle φ in velocity space, which is the symmetry that makes this coordinate system appropriate.

The perturbations are again Fourier decomposed in plane waves, and hence the linearized Vlasov equation reads

$$i\left(\boldsymbol{k} \cdot \boldsymbol{v} - \omega\right) \delta f_j - \Omega_j \frac{\partial \delta f_j}{\partial \varphi} = -\frac{q_j}{m_j} \left[\delta \boldsymbol{E} \left(1 - \frac{\boldsymbol{k} \cdot \boldsymbol{v}}{\omega}\right) + \frac{\boldsymbol{k} (\boldsymbol{v} \cdot \delta \boldsymbol{E})}{\omega}\right] \cdot \frac{\partial f_{j0}}{\partial \boldsymbol{v}}, \tag{II-1.28}$$

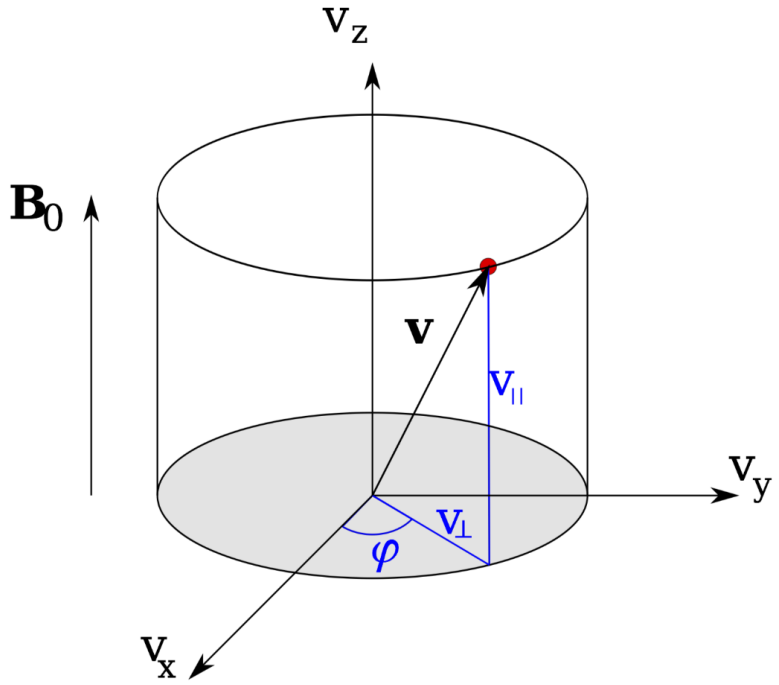

Figure II-1: Geometry of the cylindrical coordinate system for the velocity components. The cylindrical symmetry axis is given by the background magnetic field $\boldsymbol{B}_0$.

where Faraday's law in Fourier space was again used to express $\delta\boldsymbol{B}$ in terms of $\delta\boldsymbol{E}$.

This differential equation in φ can be solved with the method of variation of parameters. The solution can be very generally found as

$$\delta f_j = \frac{q_j}{m_j\Omega_j}\exp\left[\frac{i}{\Omega_j}\int_0^{\varphi}(\boldsymbol{k}\cdot\boldsymbol{v}-\omega)\,\mathrm{d}\varphi'\right]\left\{\int_0^{\varphi}\exp\left[-\int_0^{\varphi'}\frac{i}{\Omega_j}(\boldsymbol{k}\cdot\boldsymbol{v}-\omega)\,\mathrm{d}\varphi''\right]\right.$$
$$\left.\times\left[\delta\boldsymbol{E}\left(1-\frac{\boldsymbol{k}\cdot\boldsymbol{v}}{\omega}\right)+\frac{\boldsymbol{k}(\boldsymbol{v}\cdot\delta\boldsymbol{E})}{\omega}\right]\cdot\frac{\partial f_{j0}}{\partial\boldsymbol{v}}\,\mathrm{d}\varphi'+C\right\}. \quad \text{(II-1.29)}$$

The constant of the integration in the first exponential cancels with itself in the second exponential (with the opposite sign). The remaining constant C is independent of φ and has to satisfy the 2π-periodicity of δf_j, i.e., $\delta f_j(\varphi+2\pi)=\delta f_j(\varphi)$. This means that

$$C = \exp\left[\frac{i}{\Omega_j}\int_0^{2\pi}(\boldsymbol{k}\cdot\boldsymbol{v}-\omega)\,\mathrm{d}\varphi\right]\left\{\int_0^{2\pi}\exp\left[-\int_0^{\varphi}\frac{i}{\Omega_j}(\boldsymbol{k}\cdot\boldsymbol{v}-\omega)\,\mathrm{d}\varphi'\right]\right.$$
$$\left.\times\left[\delta\boldsymbol{E}\left(1-\frac{\boldsymbol{k}\cdot\boldsymbol{v}}{\omega}\right)+\frac{\boldsymbol{k}(\boldsymbol{v}\cdot\delta\boldsymbol{E})}{\omega}\right]\cdot\frac{\partial f_{j0}}{\partial\boldsymbol{v}}\,\mathrm{d}\varphi\right\}. \quad \text{(II-1.30)}$$

The coordinate system is turned around the z-axis in such a way that the y-component of the wavevector is zero, i.e., $\boldsymbol{k}=(k_\perp,0,k_\parallel)$. This choice permits to simplify the above

integration with the relation

$$\int_0^{\varphi} (\boldsymbol{k}\cdot\boldsymbol{v}-\omega)\ \mathrm{d}\varphi' = (k_\parallel v_\parallel - \omega)\,\varphi + k_\perp v_\perp \sin\varphi. \tag{II-1.31}$$

The occurring exponential of $\sin\varphi$ can be expressed as

$$e^{-i\lambda_j \sin\varphi} = \sum_{\ell=-\infty}^{+\infty} J_\ell(\lambda_j) e^{-i\ell\varphi} \tag{II-1.32}$$

with the Bessel functions $J_\ell(\lambda_j)$ with $\lambda_j = k_\perp v_\perp/\Omega_j$ and integer ℓ, which follows from the general series expansion

$$e^{\frac{1}{2}z\left(t-\frac{1}{t}\right)} = \sum_{\ell=-\infty}^{+\infty} t^\ell J_\ell(z), \qquad (t\neq 0) \tag{II-1.33}$$

(e.g., Abramowitz and Stegun, 1972). All trigonometric functions of φ in the Lorentz force term are written in terms of $\exp(\pm i\varphi)$. Since one sums over all ℓ, the index can be shifted appropriately. One finds for the integral in the curly brackets of Eqs. (II-1.29) and (II-1.30)

$$\left\{\dots\right\} = \int_0^{\varphi,2\pi} \sum_{\ell=-\infty}^{+\infty} \boldsymbol{g}_j\cdot\delta\boldsymbol{E}\exp\left[-\frac{i}{\Omega_j}\left(k_\parallel v_\parallel - \omega + \ell\Omega_j\right)\varphi\right]\mathrm{d}\varphi \tag{II-1.34}$$

(n.b., the upper limit at the integral sign has to be chosen correspondingly to the equation) with the vector

$$\begin{aligned}
g_{j1} &= \frac{1}{2}\left[\left(1-\frac{k_\parallel v_\parallel}{\omega}\right)\frac{\partial f_{j0}}{\partial v_\perp} + \frac{k_\parallel v_\perp}{\omega}\frac{\partial f_{j0}}{\partial v_\parallel}\right]\left[J_{\ell+1}(\lambda_j) + J_{\ell-1}(\lambda_j)\right],\\
g_{j2} &= \frac{1}{2i}\left[\left(1-\frac{k_\parallel v_\parallel}{\omega}\right)\frac{\partial f_{j0}}{\partial v_\perp} + \frac{k_\parallel v_\perp}{\omega}\frac{\partial f_{j0}}{\partial v_\parallel}\right]\left[J_{\ell+1}(\lambda_j) - J_{\ell-1}(\lambda_j)\right],\\
g_{j3} &= \frac{\partial f_{j0}}{\partial v_\parallel}J_\ell(\lambda_j) + \frac{1}{2}\left[\frac{k_\perp v_\parallel}{\omega}\frac{\partial f_{j0}}{\partial v_\perp} - \frac{k_\perp v_\perp}{\omega}\frac{\partial f_{j0}}{\partial v_\parallel}\right]\left[J_{\ell+1}(\lambda_j) + J_{\ell-1}(\lambda_j)\right].
\end{aligned} \tag{II-1.35}$$

The Bessel function identities

$$J_{\ell+1}(\lambda_j) + J_{\ell-1}(\lambda_j) = \frac{2\ell}{\lambda_j}J_\ell(\lambda_j), \qquad J_{\ell+1}(\lambda_j) - J_{\ell-1}(\lambda_j) = -2J'_\ell(\lambda_j) \tag{II-1.36}$$

are used to find

$$\begin{aligned}
g_{j1} &= \left[\left(1-\frac{k_\parallel v_\parallel}{\omega}\right)\frac{\partial f_{j0}}{\partial v_\perp} + \frac{k_\parallel v_\perp}{\omega}\frac{\partial f_{j0}}{\partial v_\parallel}\right]\frac{\ell}{\lambda_j}J_\ell(\lambda_j),\\
g_{j2} &= \left[\left(1-\frac{k_\parallel v_\parallel}{\omega}\right)\frac{\partial f_{j0}}{\partial v_\perp} + \frac{k_\parallel v_\perp}{\omega}\frac{\partial f_{j0}}{\partial v_\parallel}\right]iJ'_\ell(\lambda_j),\\
g_{j3} &= \frac{\partial f_{j0}}{\partial v_\parallel}J_\ell(\lambda_j) + \left[\frac{k_\perp v_\parallel}{\omega}\frac{\partial f_{j0}}{\partial v_\perp} - \frac{k_\perp v_\perp}{\omega}\frac{\partial f_{j0}}{\partial v_\parallel}\right]\frac{\ell}{\lambda_j}J_\ell(\lambda_j).
\end{aligned} \tag{II-1.37}$$

The integration can now be carried out and yields

$$\delta f_j = \frac{iq_j}{m_j} e^{i\lambda_j \sin\varphi} \sum_{\ell=-\infty}^{+\infty} \frac{\boldsymbol{g}_j \cdot \delta\boldsymbol{E}}{k_\parallel v_\parallel - \omega + \ell\Omega_j} e^{-i\ell\varphi} \tag{II-1.38}$$

for the perturbation in a magnetized plasma.

The resonance condition has changed from $\boldsymbol{k}\cdot\boldsymbol{v} - \omega = 0$ in the unmagnetized case to

$$k_\parallel v_\parallel - \omega + \ell\Omega_j = 0, \qquad \ell = 0, \pm1, \pm2, \ldots, \tag{II-1.39}$$

and hence a full band of new resonances occurs. Such a resonance is called *cyclotron resonance*, whereas the usual Landau resonance for $\ell = 0$ is just a special case. For the purely field-parallel case (i.e., $\lambda_j = k_\perp = 0$), the divergent part in g_{j1} and g_{j2} has to be expressed again by use of Eq. (II-1.36). Then the x-component of the electric field provides a contribution very symmetric to the y-component, and no further resonances occur than $\ell = 0$ and $\ell = \pm1$.

The quasilinear diffusion in the general magnetized case leads to the so-called *pitch-angle diffusion*. The complete derivation is not shown here, but the result shall be discussed to understand the principal physics of inelastic pitch-angle scattering. The following equations are taken from Marsch (2006) and references therein. The distribution function of species j is modified due to the resonant quasilinear pitch-angle diffusion according to

$$\frac{\delta f_j}{\delta t} = \int \frac{1}{(2\pi)^3} \sum_M \hat{\mathcal{B}}_M(\boldsymbol{k}) \frac{1}{v_\perp} \frac{\partial}{\partial\alpha} \left(v_\perp \nu_{j,M}(\boldsymbol{k},\boldsymbol{v}) \frac{\partial f_{j0}}{\partial\alpha} \right) \mathrm{d}^3k, \tag{II-1.40}$$

where the sum is taken over all (linear) wave modes M. The pitch-angle gradient in the wave reference frame is given by

$$\frac{\partial}{\partial\alpha} = v_\perp \frac{\partial}{\partial v_\parallel} - \left(v_\parallel - \frac{\omega}{k_\parallel} \right) \frac{\partial}{\partial v_\perp}, \tag{II-1.41}$$

and the normalized magnetic field fluctuation spectrum is defined as

$$\hat{\mathcal{B}}_M(\boldsymbol{k}) = \frac{|\boldsymbol{B}_M(\boldsymbol{k})|^2}{VB_0^2} \left(\frac{k_\parallel}{k} \right)^2 \frac{1}{1 - \left| \hat{\boldsymbol{k}} \cdot \boldsymbol{e}_M(\boldsymbol{k}) \right|^2} \tag{II-1.42}$$

with the Fourier amplitude $\boldsymbol{B}_M(\boldsymbol{k})$ of the magnetic field fluctuations and an arbitrarily large integration volume V. The wave polarization vector is denoted by $\boldsymbol{e}_M(\boldsymbol{k})$ with length unity. The circular components are defined as

$$e_M^\pm = e_{Mx} \pm i e_{My}. \tag{II-1.43}$$

In Eq. (II-1.40), the ion–wave relaxation rate $\nu_{j,M}$ has been introduced. It can be represented by

$$\nu_{j,M}(\boldsymbol{k},\boldsymbol{v}) = \pi \frac{\Omega_j^2}{|k_\parallel|} \sum_{\ell=-\infty}^{+\infty} \delta\left(v_{\mathrm{R}\ell} - v_\parallel\right) \left| \frac{1}{2} \left(J_{\ell-1}(\lambda_j) e_M^+ + J_{\ell+1}(\lambda_j) e_M^- \right) + \frac{v_\parallel}{v_\perp} J_\ell(\lambda_j) e_{Mz} \right|^2. \tag{II-1.44}$$

The resonance speed is defined as

$$v_{\mathrm{R}\ell} \equiv \frac{\omega - \ell\Omega_j}{k_\parallel}. \tag{II-1.45}$$

The pitch-angle diffusion is not discussed quantitatively in this work because of the huge variety of possible effects. However, a qualitative discussion of some aspects seems to be helpful for understanding particular features of wave–particle interactions. The diffusion equation in Eq. (II-1.40) describes a change of the distribution function over time. It leads to an isotropization of the particle motion around the reference frame centered on the parallel wave phase speed $\omega/k_\parallel$ if the diffusion operator (esp., the scattering rate $\nu_{j,M}$) is non-zero. There are several restrictions to this condition. The first trivial requirement is the non-vanishing amplitude $\boldsymbol{B}_M(\boldsymbol{k})$ at the corresponding wavenumber. Second, the delta function in Eq. (II-1.44) has to contribute. This means that the parallel particle velocity $v_\parallel$ has to fit the resonance speed $v_{\mathrm{R}\ell}$, which is an important constraint on the width of the distribution function and the dispersion of the considered wave mode. The Bessel functions on the right-hand side of Eq. (II-1.44) only contribute if either $k_\perp \neq 0$ or the evaluated order of the Bessel function is zero because $J_\ell(0) = \delta_{\ell,0}$. This shows directly that only the two cyclotron resonances with $\ell = \pm 1$ and the Landau resonance with $\ell = 0$ occur for parallel propagation, which means that oblique propagation is indispensable for higher harmonic resonances. Multiplication with the polarization vectors shows that the cyclotron resonance only occurs for wave modes with a circularly polarized component, while the Landau resonance only occurs for wave modes with a longitudinally polarized component.

II.2 Multi-fluid description

II.2.1 Momenta and bulk description

In many cases, the full kinetic or even the simplified quasilinear description is not reasonable. The degree of complexity of the description can be drastically reduced by taking the moments of the distribution function or the Vlasov equation, respectively (e.g., Chen, 1985; Schindler, 2006). The infinite set of moments describes the distribution function completely. However, in most cases the development of the moment equations can be broken at a certain degree, and the set of equations can be closed by external conditions without loss of accuracy. The n-th moment of the velocity distribution function $f_j(\boldsymbol{x}, \boldsymbol{v}, t)$ is defined as

$$M_j^{(n)}(\boldsymbol{x}, t) \equiv \int \boldsymbol{v}^n f_j(\boldsymbol{x}, \boldsymbol{v}, t)\, \mathrm{d}^3 v. \tag{II-2.46}$$

The first momenta are frequently used and therefore particularly named. These are

$$n_j(\boldsymbol{x},t) = \int f_j(\boldsymbol{x},\boldsymbol{v},t)\,\mathrm{d}^3v, \tag{II-2.47}$$

$$\boldsymbol{U}_j(\boldsymbol{x},t) = \frac{1}{n_j}\int \boldsymbol{v} f_j(\boldsymbol{x},\boldsymbol{v},t)\,\mathrm{d}^3v, \tag{II-2.48}$$

$$P_j(\boldsymbol{x},t) = m_j\int (\boldsymbol{v}-\boldsymbol{U}_j)(\boldsymbol{v}-\boldsymbol{U}_j) f_j(\boldsymbol{x},\boldsymbol{v},t)\,\mathrm{d}^3v, \tag{II-2.49}$$

$$\boldsymbol{Q}_j(\boldsymbol{x},t) = \frac{1}{2}\int (\boldsymbol{v}-\boldsymbol{U}_j)^2(\boldsymbol{v}-\boldsymbol{U}_j) f_j(\boldsymbol{x},\boldsymbol{v},t)\,\mathrm{d}^3v, \tag{II-2.50}$$

called the number density, the bulk velocity, the pressure tensor (using the dyadic product), and the heat flux vector of the particle species j. The thermal pressure p_j is related to the pressure tensor by

$$p_j = nk_\mathrm{B}T = \frac{1}{3}\mathrm{Tr}P_j \tag{II-2.51}$$

with the kinetic temperature T (Marsch, 2006). In the following, pressure anisotropies are neglected and only the scalar thermal pressure is used. These parameters describe the typical properties of a fluid for each particle species. Therefore, this approach is denoted as the *multi-fluid description* of a plasma.

It is also possible to take the momenta of the full collisionless Vlasov equation (II-1.5) for the particle species j by applying the integral operation in Eq. (II-2.46) to the full equation instead of the function f_j and using then the definition of the momenta above. The 0-th moment of the Vlasov equation is the so-called continuity equation

$$\frac{\partial n_j}{\partial t} + \mathrm{div}\,(n_j\boldsymbol{U}_j) = 0, \tag{II-2.52}$$

which describes the conservation of particles of species j. The first moment describes the evolution of the bulk velocity and contains the conservation of momentum:

$$m_j n_j \frac{\partial \boldsymbol{U}_j}{\partial t} + m_j n_j \left(\boldsymbol{U}_j\cdot\nabla\right)\boldsymbol{U}_j = -\mathrm{grad}\,p_j + n_j q_j\left[\boldsymbol{E} + \frac{1}{c}\boldsymbol{U}_j\times\boldsymbol{B}\right]. \tag{II-2.53}$$

Furthermore, also the energy equation can be found as the next moment. All these operations are extensively described by Marsch (2006).

With the relations from Eqs. (II-1.8) through (II-1.13), Maxwell's equations are given by

$$\mathrm{div}\,\boldsymbol{E} = 4\pi\sum_j n_j q_j, \tag{II-2.54}$$

$$\mathrm{curl}\,\boldsymbol{E} = -\frac{1}{c}\frac{\partial \boldsymbol{B}}{\partial t}, \tag{II-2.55}$$

$$\mathrm{div}\,\boldsymbol{B} = 0, \tag{II-2.56}$$

$$\mathrm{curl}\,\boldsymbol{B} = \frac{4\pi}{c}\sum_j n_j q_j \boldsymbol{U}_j + \frac{1}{c}\frac{\partial \boldsymbol{E}}{\partial t} = \frac{1}{c}\frac{\partial \boldsymbol{D}}{\partial t}, \tag{II-2.57}$$

where $\boldsymbol{D}$ denotes the electric displacement field, which is connected to the electric field through the dielectric tensor ε according to $\boldsymbol{D} = \varepsilon \boldsymbol{E}$.

A disadvantage of the multi-fluid description is that kinetic resonances, such as the Landau or the cyclotron resonance, cannot be described self-consistently. Furthermore, all non-equilibrium effects are not treatable because the structure of non-trivial distribution functions cannot be represented by the first few moments. The equation for $M_j^{(n)}$ always contains already the moment $M_j^{(n+1)}$. Therefore, an infinite number of moment equations is needed to describe the evolution completely. A finite set of moment equations can be closed by relations that connect a higher moment with an already known one. For example, pressure and density can be related by the adiabatic law $p_j \propto n_j^{\gamma_j}$ with the adiabatic index γ_j to finish the moment development after the first moment equation. An early closure of the equations means that a few moments are sufficient to describe the distribution function properly, which in turn means that the distribution is close to a Maxwellian equilibrium distribution. Thus, collisions are implicitly taken into account to maintain the Maxwellian distribution if a closure relation is applied. This is an important disadvantage for all fluid descriptions (of course not if an infinite set of equations for all fluid moments was taken into account). The more moments are accessible, however, the higher is the accuracy of the structural description of the plasma. On the other hand, all natural length scales and frequencies are available in the multi-fluid description, which will be used later in Chapts. IV and V. This makes the multi-fluid approach in many cases—especially in dilute space plasmas—by far more appropriate than the one-fluid picture of magnetohydrodynamics (MHD). Classical MHD does not contain any scale of the plasma and is, therefore, limited to very low frequencies and very large length scales compared to all plasma scales. An improvement of MHD can be obtained by the inclusion of the first-order ion motion in form of an additional Hall term. This leads to the Hall-MHD description (Krauss-Varban *et al.*, 1994; Vocks *et al.*, 1999). These equations are not completely scale-free. The ion gyrofrequency is a natural scale of this system, and effects due to the finite gyration frequency of the ions can be taken into account. The Hall-MHD approach will be used and described later in this work since the hybrid equations, which are used in the numerical analyses in Chapts. VI and VII, reduce to Hall-MHD at the limit of very low temperatures.

II.2.2 Cold plasma dispersion relation

The most simple description of waves in a plasma, which takes the multi-species nature into account, is based on the considerations by Appleton (1932) together with contributions by Douglas Hartree. For a cold and homogeneous plasma, they describe the dispersion relation, which is the relation between wavevector $\boldsymbol{k}$ and frequency ω for different wave modes. Because of their discoverers, a particular form of it is also sometimes called the *Appleton-Hartree dispersion relation*. The following considerations are based on the textbooks by Stix (1992) and Swanson (2003).

A plasma is considered to be *cold* if the pressure is zero, or at least negligible. This means that the momentum equation for the plasma takes the same form as the equation of

motion for a single particle. From Eq. (II-2.53), this assumption leads to

$$\frac{\mathrm{d}\boldsymbol{U}_j}{\mathrm{d}t} = \frac{q_j}{m_j}\left[\boldsymbol{E} + \frac{1}{c}\boldsymbol{U}_j \times \boldsymbol{B}\right]. \tag{II-2.58}$$

After linearization and Fourier decomposition, the differential equation becomes an algebraic equation for the velocity and the fields:

$$-i\omega\boldsymbol{U}_j = \frac{q_j}{m_j}\left[\boldsymbol{E} + \frac{1}{c}\boldsymbol{U}_j \times \boldsymbol{B}_0\right] \tag{II-2.59}$$

with the constant background magnetic field $\boldsymbol{B}_0$. Combining Faraday's law and Ampère's law in Fourier space allows one to write the general wave equation

$$\boldsymbol{k} \times \boldsymbol{k} \times \boldsymbol{E} = -\frac{4\pi i\omega}{c^2}\boldsymbol{j} - \frac{\omega^2}{c^2}\boldsymbol{E}, \tag{II-2.60}$$

or with the definition of the dielectric tensor:

$$\boldsymbol{k} \times \boldsymbol{k} \times \boldsymbol{E} + \frac{\omega^2}{c^2}\varepsilon\boldsymbol{E} = 0. \tag{II-2.61}$$

The dielectric tensor itself can be found by combining the definition of the current density in the multi-fluid description with the relation

$$\boldsymbol{D} = \varepsilon\boldsymbol{E} = \boldsymbol{E} + \frac{4\pi i}{\omega}\boldsymbol{j} \tag{II-2.62}$$

in Fourier space. This leads to the following form of the dielectric tensor:

$$\varepsilon = \begin{pmatrix} S & -iD & 0 \\ iD & S & 0 \\ 0 & 0 & P \end{pmatrix} \tag{II-2.63}$$

with

$$S \equiv \frac{1}{2}(R + L), \qquad D \equiv \frac{1}{2}(R - L), \tag{II-2.64}$$

$$R \equiv 1 - \sum_j \frac{\omega_j^2}{\omega(\omega + \Omega_j)}, \qquad L \equiv 1 - \sum_j \frac{\omega_j^2}{\omega(\omega - \Omega_j)}, \tag{II-2.65}$$

$$P \equiv 1 - \sum_j \frac{\omega_j^2}{\omega^2}, \tag{II-2.66}$$

following the usual nomenclature in plasma physics. The plasma frequency of species j is denoted by

$$\omega_j \equiv \sqrt{\frac{4\pi n_j q_j^2}{m_j}}. \tag{II-2.67}$$

The wave equation (II-2.61) together with these definitions leads to the dispersion relation of a cold plasma in the general form:

$$\begin{pmatrix} \frac{\omega^2}{c^2}S - k^2 & -i\frac{\omega^2}{c^2}D & 0 \\ i\frac{\omega^2}{c^2}D & \frac{\omega^2}{c^2}S - k^2\cos^2\vartheta & k^2\cos\vartheta\sin\vartheta \\ 0 & k^2\cos\vartheta\sin\vartheta & \frac{\omega^2}{c^2}P - k^2\sin^2\vartheta \end{pmatrix} \begin{pmatrix} E_x \\ E_y \\ E_z \end{pmatrix} = 0, \tag{II-2.68}$$

where the coordinate system is set in such a way that the wavevector lays in the $y-z$-plane. The angle ϑ is the angle between $\boldsymbol{k}$ and $\boldsymbol{B}_0 = B_0\hat{\boldsymbol{e}}_z$. The non-trivial dispersion relation now requires that the determinant of the matrix in Eq. (II-2.68) is zero. The solutions of this requirement are:

$$Ak^4 - Bk^2 + C = 0 \tag{II-2.69}$$

with

$$A = S\sin^2\vartheta + P\cos^2\vartheta, \tag{II-2.70}$$

$$B = \frac{\omega^2}{c^2}\left[SP\left(1+\cos^2\vartheta\right) + RL\sin^2\vartheta\right], \tag{II-2.71}$$

$$C = \frac{\omega^4}{c^4}RLP. \tag{II-2.72}$$

The two important extreme cases are the parallel ($\vartheta = 0°$) and perpendicular ($\vartheta = 90°$) propagation. The solutions are then simply given by

$$\vartheta = 0° : \qquad P = 0, \qquad k^2 = \frac{\omega^2}{c^2}R, \qquad k^2 = \frac{\omega^2}{c^2}L. \tag{II-2.73}$$

$$\vartheta = 90° : \qquad k^2 = \frac{\omega^2}{c^2}P, \qquad k^2 = \frac{\omega^2}{c^2}\frac{RL}{S}. \tag{II-2.74}$$

These waves represent from the upper left to the lower right the following normal modes: the free plasma oscillation (also called *Langmuir wave*), the R-mode (also called *fast wave* at lower frequencies or *whistler wave* at higher frequencies), the L-mode (also called *ion-cyclotron wave*), the ordinary wave (also called *O-mode* corresponding to an electromagnetic light wave in the plasma), and the extraordinary wave (also called *X-mode*) together with the upper and lower hybrid oscillations.

The L-mode is of special interest for this work for reasons that will become clear later. Therefore, its dispersion is discussed in more detail. The L-mode is also called ion-cyclotron wave, or—due to its behavior at low frequencies, where it becomes the usual MHD Alfvén mode—it is also called Alfvén/ion-cyclotron (A/IC) mode. The dispersion relation $k^2c^2 = \omega^2 L$ can be expressed in two ways. The direct way is

$$k^2 = \frac{\omega^2}{c^2} - \sum_j \frac{\omega_j^2}{c^2}\frac{\omega}{\omega - \Omega_j} \tag{II-2.75}$$

for the exact parallel propagation. The first term on the left-hand side arises from Maxwell's displacement current and is, hence, often neglected for all processes that are slow

compared to the propagation of light in vacuo. In the low-frequency limit, the ordering $\omega \ll \Omega_\mathrm{p} \ll \Omega_\mathrm{e}$ can be applied, and Taylor expansion in $(\omega/\Omega_\mathrm{p})^2$ yields

$$k^2 = \frac{\omega_\mathrm{p}^2}{\Omega_\mathrm{p}^2 c^2}\omega^2 \qquad \Rightarrow \qquad \frac{\omega}{k} = \pm v_\mathrm{Ap} \tag{II-2.76}$$

with the proton Alfvén speed

$$v_\mathrm{Ap} \equiv \frac{B_0}{\sqrt{4\pi n_\mathrm{p} m_\mathrm{p}}}. \tag{II-2.77}$$

This constant phase-speed of the wave reflects the well known linear dispersion relation for the classical MHD Alfvén wave that will be discussed in Sect. II.2.3.2 in more detail.

A good approximation for the A/IC wave at smaller frequencies compared to the electron gyration frequency and for moderate values of ϑ can be obtained from Eq. (II-2.69) with the assumptions $\omega \ll \Omega_\mathrm{e}$ and $m_\mathrm{e} \ll m_\mathrm{p}$. This means that the contribution to P comes mainly from the electrons, while contributions to R and L come from the protons. The polynomial coefficients are then given by

$$A \simeq -\frac{\omega_\mathrm{e}^2}{\omega^2}\cos^2\vartheta, \qquad B \simeq -\frac{\omega_\mathrm{e}^2}{2c^2}(R+L)(1+\cos^2\vartheta), \qquad C \simeq -\frac{\omega_\mathrm{e}^2\omega^2}{c^4}RL, \tag{II-2.78}$$

$$R \simeq \frac{c^2}{v_\mathrm{Ap}^2}\frac{\Omega_\mathrm{p}}{\Omega_\mathrm{p}+\omega}, \qquad L \simeq \frac{c^2}{v_\mathrm{Ap}^2}\frac{\Omega_\mathrm{p}}{\Omega_\mathrm{p}-\omega}. \tag{II-2.79}$$

Therewith, Eq. (II-2.69) becomes

$$(\ell_\mathrm{p}k)^4\cos^2\vartheta - \frac{\omega^2}{\Omega_\mathrm{p}^2-\omega^2}\left(1+\cos^2\vartheta\right)(\ell_\mathrm{p}k)^2 + \frac{1}{\Omega_\mathrm{p}^2}\frac{\omega^4}{\Omega_\mathrm{p}^2-\omega^2} = 0, \tag{II-2.80}$$

where the proton inertial length

$$\ell_\mathrm{p} \equiv \frac{c}{\omega_\mathrm{p}}, \tag{II-2.81}$$

which is also called *skin depth*, is introduced. One root of Eq. (II-2.80) is given by

$$\left(\frac{\omega}{\Omega_\mathrm{p}}\right)^2 = \frac{1}{2}\Big[\left(1+\cos^2\vartheta\right)(\ell_\mathrm{p}k)^2 + \cos^2\vartheta(\ell_\mathrm{p}k)^4 - (\ell_\mathrm{p}k)^2\sqrt{\left(1-\cos^2\vartheta\right)^2 + 2\left(\cos^2\vartheta+\cos^4\vartheta\right)(\ell_\mathrm{p}k)^2 + \cos^4\vartheta(\ell_\mathrm{p}k)^4}\Big], \tag{II-2.82}$$

which is another useful representation for the A/IC dispersion relation that will be used later.

The R-mode wave is also called the fast/whistler (F/W) wave. Its dispersion for low frequencies compared to the electron gyrofrequency can be approximated with the expansion of the electron contribution in terms of $\omega/\Omega_\mathrm{e} \ll 1$ and using the relation $\ell_\mathrm{p}\Omega_\mathrm{p} = -\ell_\mathrm{e}\Omega_\mathrm{e}$ for an electron-proton plasma. The number one on the right-hand side of the definition of R is again rooted in Maxwell's displacement current. Therefore, it can

be disregarded in the case considered here. The parallel dispersion relation $k^2c^2 = \omega^2 R$ can then be written as

$$\frac{\omega}{\Omega_\mathrm{p}} = \frac{k^2\ell_\mathrm{p}^2}{2}\left[1 + \sqrt{1 + \frac{4}{k^2\ell_\mathrm{p}^2}}\right]. \tag{II-2.83}$$

This relation will be also used in the following chapters several times. At higher frequencies, the ion contribution in the square-root term of Eq. (II-2.83) becomes negligible, and the dispersion then reads

$$\frac{\omega}{\Omega_\mathrm{p}} \approx k^2\ell_\mathrm{p}^2, \tag{II-2.84}$$

which is the classical cold electron whistler wave dispersion relation (Baumjohann and Treumann, 1996).

So far, the treated wave modes are only normal modes for a cold plasma. Including effects of variable pressure leads to further wave modes, which belong then to the large family of compressive wave modes. Only some cases are discussed in this work, for example in Chapt. V. For a description of finite temperature effects, either the fluid or the Vlasov picture is an appropriate formulation. They are described extensively in the literature (e.g., Gary, 1993; Stix, 1992; Swanson, 2003). An example for the complexity of the dispersion of plasma waves in a warm plasma is shown in Fig. II-2. In this diagram, the ion-acoustic speed occurs, which is defined by

$$c_\mathrm{s} \equiv \sqrt{\frac{\gamma_\mathrm{e}k_\mathrm{B}T_\mathrm{e} + \gamma_\mathrm{p}k_\mathrm{B}T_\mathrm{p}}{m_\mathrm{e} + m_\mathrm{p}}}, \tag{II-2.85}$$

where T_j is the temperature of species j and k_B the Boltzmann constant. The different wave branches are defined as follows, starting the description of the diagram at the low-frequency side. The fast MHD mode branch begins at O_1 and reaches with its linear dispersion until A, where it turns into the R-mode and later to the characteristic whistler dispersion ($\omega \propto k^2$). It shows the electron cyclotron-resonance at C. The MHD torsional Alfvén wave is the low, linear part from O_2 to F. Then it approaches as the ion-cyclotron wave the cyclotron resonance of the protons at G. For the chosen parameters, it continues on the other side of the resonance and couples with the ion-acoustic wave at I. The slow MHD mode begins at O_3. Its phase speed is the ion sound speed with a factor for the obliquity in propagation. It turns into a resonance with the protons at P. The detailed mode couplings at high wavenumbers and frequencies around the points D and K are discussed in the textbook by Swanson (2003).

The solutions of the corresponding dispersion relation alone do not describe all details of a plasma wave. Further characteristic informations about the wave properties are given by the polarization relation, which describes how the electromagnetic field vectors and the velocity vectors of the wave are oriented and related with respect to each other. Together with the dispersion relation, the polarization relation allows one to describe the full space- and time-dependent behavior of all oscillating quantities (electric field, magnetic field, and velocities of the plasma particles) for the particular wave type. The polarization relations are usually determined from the equations of motion together with Maxwell's

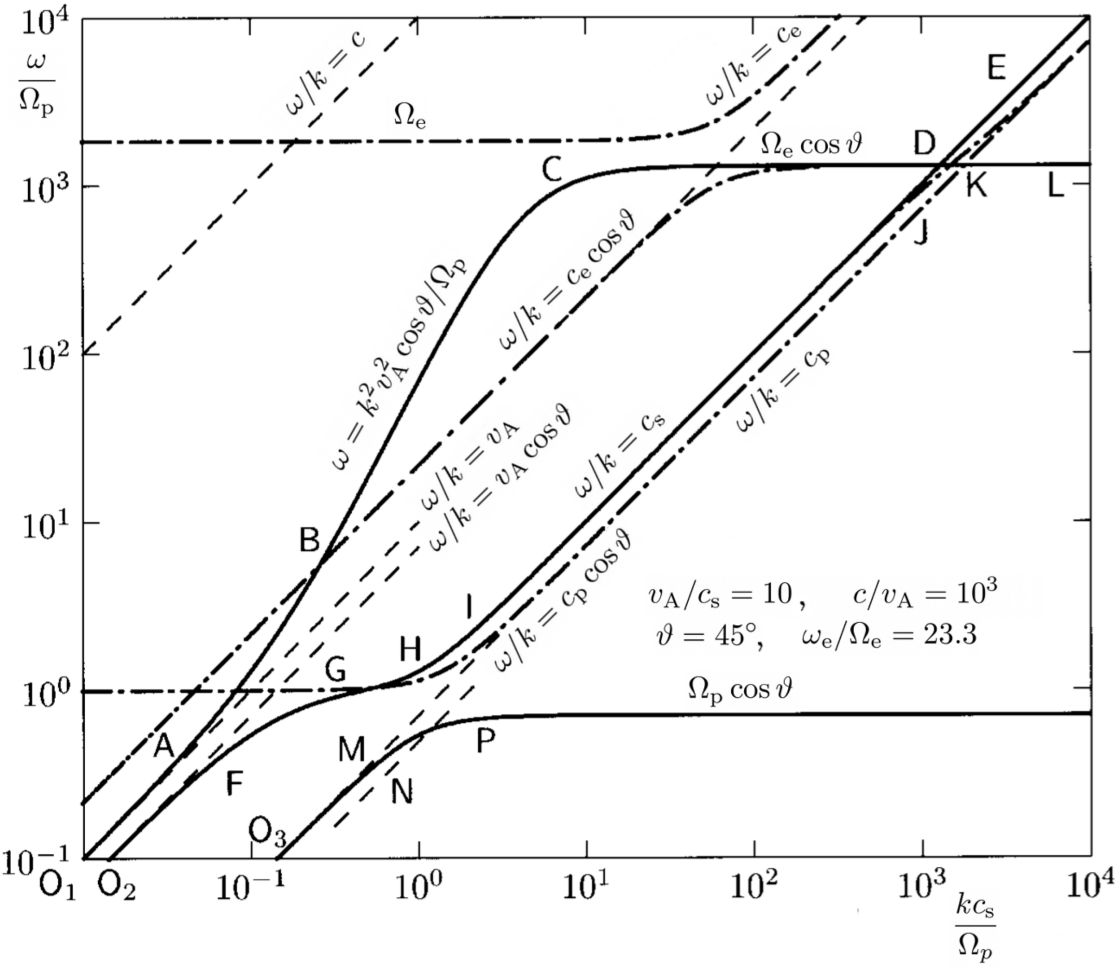

Figure II-2: Dispersion relation for a warm and overdense ($\omega_e > \Omega_e$) electron-proton plasma for a propagation angle of $\vartheta = 45°$. The full lines come from a fluid dispersion approximation at low frequencies, while the dash-dotted lines represent a warm dispersion approximation that neglects the ion-momentum. The different branches are described in the text. Reproduced with permission of Taylor and Francis Group LLC-Books from Swanson (2003); permission conveyed through Copyright Clearance Center, Inc.

equations, once the dispersion is known. There is no general, concise form of it. Therefore, the polarization relation is stated in the following work explicitly only at the places, where a certain wave mode polarization is of interest.

II.2.3 MHD approximation

II.2.3.1 The single-species magnetofluid

In some special cases, a plasma can be described as a highly conducting single-species fluid. This approximation is called the ideal magnetohydrodynamic (MHD) description (e.g., Akhiezer *et al.*, 1975). This approximation is only valid if all time-dependent effects are slow compared to the gyration period or other characteristic time scales of all

plasma species. Like in other low-moment fluid theories, also MHD assumes a distribution function close to Maxwellian equilibrium implicitly. In viscous MHD, the expression for the viscous stress (and therefore dissipative effects) is also based on the assumption of Maxwellian background distribution functions with small deviations from equilibrium. To explain the observed dissipation in space plasmas, the viscous dissipation often requires a higher collisionality than typically found in the solar corona and the solar wind. This is a central problem of the applicability of MHD in space physics. Kinetic and scale-dependent effects, which are not accessible by MHD, appear to play a more important role than viscous dissipation due to collisions. Electrostatic effects on small scales are completely neglected by MHD. In the following, viscous effects shall be neglected in first order. The MHD fluid is described by a continuity equation and a momentum equation similar to the multi-fluid equations:

$$\frac{\partial \varrho}{\partial t} + \operatorname{div}(\varrho \boldsymbol{U}) = 0, \tag{II-2.86}$$

$$\varrho \frac{\partial \boldsymbol{U}}{\partial t} + \varrho(\boldsymbol{U} \cdot \nabla)\boldsymbol{U} = -\operatorname{grad} p + \frac{1}{c}\boldsymbol{j} \times \boldsymbol{B}, \tag{II-2.87}$$

where the mass density of the magnetofluid is denoted by ϱ. The species index can be omitted because the plasma is assumed to consist of one species only. Additionally Ohm's law is given with the (isotropic for low magnetic fields) conductivity σ as

$$\boldsymbol{j} = \sigma\left(\boldsymbol{E} + \frac{1}{c}\boldsymbol{U} \times \boldsymbol{B}\right). \tag{II-2.88}$$

It contains the conductive current, which stems from the Lorentz transformation into the reference frame that is fixed to the moving plasma element. It can be assumed in many cases that the conductivity of the MHD fluid tends to infinity so that the electric field has to fulfill the condition

$$\boldsymbol{E} = -\frac{1}{c}\boldsymbol{U} \times \boldsymbol{B}. \tag{II-2.89}$$

With this expression for the electric field, the magnetic field follows the induction equation in the form

$$\frac{\partial \boldsymbol{B}}{\partial t} = \operatorname{curl}\left[\boldsymbol{U} \times \boldsymbol{B}\right]. \tag{II-2.90}$$

Ampère's law does not contain the displacement current and permits a direct representation of the current density in terms of the curl of the magnetic field. The system of MHD equations permits three kinds of waves to propagate (at low frequencies), which shall be discussed in the following section.

II.2.3.2 MHD waves

An adiabatic relation is assumed for the pressure with $p \propto \varrho^{\gamma}$. The set of MHD equations can now be linearized and written in its Fourier components. Combining the adiabatic

pressure gradient with the continuity equation allows one to write the momentum equation and the induction equation as

$$-\omega \boldsymbol{U} + v_\mathrm{s}^2 \boldsymbol{k} \frac{\boldsymbol{k}\cdot\boldsymbol{U}}{\omega} = \frac{1}{4\pi\varrho_0}(\boldsymbol{k}\times\boldsymbol{B})\times\boldsymbol{B}_0, \tag{II-2.91}$$

$$-\omega \boldsymbol{B} = \boldsymbol{k}\times(\boldsymbol{U}\times\boldsymbol{B}_0), \tag{II-2.92}$$

where the definition of the fluid sound speed

$$v_\mathrm{s} \equiv \sqrt{\frac{\gamma p_0}{\varrho_0}} \tag{II-2.93}$$

was used. The two equations can be combined to find the dispersion relation for MHD waves. The angle ϑ between the vectors $\boldsymbol{k}$ and $\boldsymbol{B}_0$ can again be used to simplify the vector identities. Then the vector relation

$$\begin{pmatrix} k^2 v_\mathrm{A}^2 \cos^2\vartheta - \omega^2 & 0 & 0 \\ 0 & k^2(v_\mathrm{A}^2 + v_\mathrm{s}^2\sin^2\vartheta) - \omega^2 & k^2 v_\mathrm{s}^2 \cos\vartheta\sin\vartheta \\ 0 & k^2 v_\mathrm{s}^2\cos\vartheta\sin\vartheta & k^2 v_\mathrm{s}^2\cos^2\vartheta - \omega^2 \end{pmatrix} \boldsymbol{U} = 0 \tag{II-2.94}$$

is found with the MHD Alfvén speed $v_\mathrm{A} \equiv B_0/\sqrt{4\pi\varrho}$. The determinant of the matrix has to vanish for non-trivial solutions. This leads to three possible solutions for the wave phase speed, being able to propagate in different directions with respect to the background magnetic field:

$$\frac{\omega}{k} = \pm v_\mathrm{A}\cos\vartheta, \tag{II-2.95}$$

$$\frac{\omega}{k} = \pm\frac{1}{\sqrt{2}}\sqrt{v_\mathrm{A}^2 + v_\mathrm{s}^2 \pm \sqrt{\left(v_\mathrm{A}^2 + v_\mathrm{s}^2\right)^2 - 4v_\mathrm{A}^2 v_\mathrm{s}^2\cos^2\vartheta}}, \tag{II-2.96}$$

which are the classical (shear) Alfvén wave and the two magnetosonic waves. These two are characterized according to their phase speed as the slow and the fast mode.

The polarization of Alfvén waves is an important property that can be used for identifying fluctuations as Alfvénic or not (Belcher and Davis, 1971). It can be obtained from the induction equation, assuming the simple dispersion relation $\omega = \pm k v_\mathrm{A}\cos\vartheta$. This yields

$$\mp\frac{\boldsymbol{B}}{B_0} = \frac{\boldsymbol{U}}{v_\mathrm{A}} - \frac{\boldsymbol{k}\cdot\boldsymbol{U}}{k v_\mathrm{A}\cos\vartheta}\hat{\boldsymbol{e}}_z. \tag{II-2.97}$$

In the incompressible case ($\operatorname{div}\boldsymbol{U} = 0$) as well as in the parallel case (due to $\operatorname{div}\boldsymbol{B} = 0$), this relation becomes

$$\mp\frac{\boldsymbol{B}}{B_0} = \frac{\boldsymbol{U}}{v_\mathrm{A}}. \tag{II-2.98}$$

Effects of compressibility due to nonlinear effects will be discussed later in Chapt. V. This polarization relation means that the magnetic field and the velocity are either parallel or anti-parallel for the classical shear Alfvén wave.

II.2.3.3 Spectral transfer in (magneto)hydrodynamics

Homogeneous, isotropic fluid turbulence shows an ubiquitous spectral power-law dependence of the power spectral density $\mathcal{P}_k$ of the fluctuations on the wavenumber k following $\mathcal{P}_k \sim k^{-5/3}$. This famous hydrodynamic scaling relation was found by Kolmogorov (1941). However, its applicability to MHD turbulence is under debate (e.g., Podesta, 2011). Hydrodynamic turbulence is a nonlinear effect rising from the advection term in the momentum equation. Fourier transformation of nonlinearities leads to expressions that contain convolution terms in wavenumber and frequency according to the convolution theorem (Leslie, 1973). It was Kolmogorov (1941) who developed a simple scaling law for the behavior of eddies on different scales, which appears to be applicable for many cases in fluid turbulence and is confirmed in many experiments, too (McComb, 1990).

His considerations are based on the assumption that the transfer of energy in Fourier space is a local process, and the transfer over a large range in wavenumber is negligible. He divided the turbulence spectrum into three ranges: the driving range at large scales, the dissipation range at small scales, and the inertial range in between these two, in which the energy is shifted to higher wavenumbers without significant dissipation or production. The famous Kolmogorov turbulence scaling law is valid for the inertial range only. The turbulence is, furthermore, assumed to be homogeneous and isotropic. For a stationary turbulent situation, the production rate of turbulent energy is equal to the dissipation rate ε. The spectrum $\mathcal{P}_k$ is defined in a way that $\mathcal{P}_k \, \mathrm{d}k$ corresponds to the energy that is contained in the modes between the scalar wavenumbers k and $k + \mathrm{d}k$. Now this spectrum $\mathcal{P}_k$ has to be related to the dissipation rate ε, which has been done in form of a dimensional analysis by Kolmogorov. The energy transfer can be written as $\varepsilon \sim v^2/t$ with the typical turbulent eddy velocity v and the so-called eddy-turnover time t, which is approximately given by $1/kv$. The spectrum has the dimension of energy per wavenumber and can be written as $\mathcal{P}_k \sim v^2/k$. Expressing the velocity in terms of ε and t allows one to write

$$\mathcal{P}_k \sim \varepsilon^{2/3} k^{-5/3}, \tag{II-2.99}$$

which is the famous Kolmogorov spectral scaling for the inertial range.

For MHD turbulence, Iroshnikov (1963) and Kraichnan (1965) found independently a different scaling law, which leads to a power-law behavior of $\mathcal{P}_k \sim k^{-3/2}$. The observed solar wind turbulence spectra, however, show in many cases a steeper power index, which would be in favor of the classical hydrodynamic Kolmogorov picture (see e.g., Horbury *et al.*, 2005). The spectra indicate an even higher power index for the field-parallel propagation, whereas it seems to be Kolmogorov-like in the perpendicular direction (Wicks *et al.*, 2010). The reason for this behavior is still unclear.

III Apparent temperature anisotropies due to wave activity

The following chapter has been published in wide parts before submission of this thesis. The publication can be found under the following reference:

Daniel Verscharen and Eckart Marsch: *Apparent temperature anisotropies due to wave activity in the solar wind*, Ann. Geophys. 29, 909-917, 2011, doi:10.5194/angeo-29-909-2011.

III.1 Temperature anisotropies and non-resonant wave–particle interactions

As mentioned before, the fast solar wind plasma is permeated by plasma fluctuations on many scales. Of course, any plasma wave has to fulfill the Vlasov-Maxwell equations presented in Chapt. II and can, therefore, be understood as the space- and time-dependent self-consistent interplay between the periodic variations of the electromagnetic field and related motions of the particles, being represented by their velocity distribution function (VDF).

In the recent literature, the shaping of distribution functions due to wave activity has been widely discussed (Wang *et al.*, 2006; Wu and Yoon, 2007; Wu *et al.*, 2009; Wang and Wu, 2009). Obviously the presence of wave forces (or their spectra) will lead to a deformation of the distribution function with respect to a Maxwellian shape and cause a velocity spreading after appropriate averaging over the wave effects. The plasma-physics definition of temperature is based on a statistical particle ensemble and usually defined in terms of the random kinetic energy (via the mean square of the particle velocity) in the particles' mean-velocity frame. This definition of temperature is not necessarily equal to the thermodynamic temperature, which may be called the *intrinsic temperature* of the particle ensemble. The fluctuation of the mean square velocity owing to wave activity is able to cause an effective broadening of the distribution function similar to real heating and thus may mimic genuine heating. Therefore, some authors have referred to this process as "apparent heating" (Wang *et al.*, 2006), others as "non-resonant wave–particle interactions". The common ground of these wave effects is that they are reversible and therefore not dissipative and do not represent real heating. Collisions, however, might be able to dissipate coherent wave motion efficiently and thus will lead to a real heating and an increase in the intrinsic temperature (Schekochihin *et al.*, 2008; Howes, 2008). In the following, collisions are still excluded from the treatment of the VDFs, in order to

demonstrate the collisionless effects of waves and reveal the apparent heating due to wave activity.

As mentioned in the Introduction, substantial ion temperature anisotropies have been observed in the solar wind and discussed by different authors (Marsch *et al.*, 1981, 2004; Bale *et al.*, 2009; Bourouaine *et al.*, 2010). Typically the proton temperature is higher perpendicular to the magnetic field than parallel to it. These anisotropies have mostly been discussed as being the result of the cyclotron-resonant interaction with circularly polarized waves, a process which can be quantified by means of quasilinear theory. On the other hand, such anisotropic distribution functions can become unstable if the anisotropy exceeds a certain threshold that depends on the plasma beta (Gary *et al.*, 2000, 2001). For a typical solar wind beta of about 1, the beta dependence is not severe and the distribution function becomes unstable for $T_\perp/T_\parallel \gtrsim 2$. This instability can in turn excite and radiate ion-cyclotron waves. In this way, wave excitation can reduce the ion temperature anisotropy efficiently and yield moderate and stable values (Gary, 1993; Bale *et al.*, 2009).

The general theory of this wave–particle interaction is well established, and in fact many traits of it were confirmed by observations (Marsch, 2006). However, the apparent heating effects are not well understood and have not yet been discussed in the context of ion–wave interactions below and near the ion inertial scale. Yet, they should be included in an appropriate description of space plasmas that are subjected to strong Alfvén/ion-cyclotron (A/IC) wave activity such as it is typical for the solar wind in the inner heliosphere. To study possible physical causes of apparent wave heating is the aim of this chapter. Firstly, the effect of a strong plasma wave on an intrinsically Maxwellian distribution function is discussed. Secondly, a concise form of the resulting model VDF is constructed, and then it is discussed how such a distribution function would look like in a real plasma measurement made on a space probe.

III.2 Model distribution functions

III.2.1 Wave effects on the distribution function

To study the effects that waves have on the shape of a velocity distribution function, the constants of individual particle motion in a given wave field have to be determined, and then the fact can be exploited that any function of these constants of motion is a solution of the Vlasov equation (Davidson, 1983; Stix, 1992). Here the influence of a single monochromatic wave is discussed only. It is supposed here to be transversal and left-hand circularly polarized and its magnetic field can be assumed to have the form

$$\boldsymbol{B} = \begin{pmatrix} b\cos(kz - \omega t) \\ b\sin(kz - \omega t) \\ B_0 \end{pmatrix} \tag{III-2.1}$$

with the constant field component B_0 along the z-axis and a constant wave amplitude b. The wave frequency is ω and the parallel wavenumber k. Its magnetic field is associated with an electric field, which according to Faraday's law is given by

$$\operatorname{curl} \boldsymbol{E} = -\frac{1}{c}\frac{\partial \boldsymbol{B}}{\partial t}. \tag{III-2.2}$$

The equation of motion for a single particle with charge q_j and mass m_j in this electromagnetic field is determined by the Lorentz force:

$$\frac{\mathrm{d}\boldsymbol{v}}{\mathrm{d}t} = \frac{q_j}{m_j}\left(\boldsymbol{E} + \frac{1}{c}\boldsymbol{v}\times\boldsymbol{B}\right). \tag{III-2.3}$$

It is useful and transparent to write this equation in the components of the cylindrical coordinate system, which has been introduced in Chapt. II, as follows:

$$\frac{\mathrm{d}v_\perp}{\mathrm{d}t} = \Omega_j\left(\frac{\omega}{k} - v_\parallel\right)\frac{b}{B_0}\sin\left(\phi-\varphi\right), \tag{III-2.4}$$

$$\frac{\mathrm{d}v_\parallel}{\mathrm{d}t} = \Omega_j v_\perp \frac{b}{B_0}\sin\left(\phi-\varphi\right), \tag{III-2.5}$$

$$\frac{\mathrm{d}\varphi}{\mathrm{d}t} = -\Omega_j\left[1 + \left(\frac{\omega}{k} - v_\parallel\right)\frac{1}{v_\perp}\frac{b}{B_0}\cos\left(\phi-\varphi\right)\right], \qquad v_\perp \neq 0, \tag{III-2.6}$$

where the abbreviation $\phi \equiv kz - \omega t$ is used for the wave phase. The gyrofrequency is again denoted by Ω_j. A similar set of equations has already been used in a test-particle description to describe the nonlinear behavior of particles that are trapped in the wave fields (Matsumoto, 1979). Also non-resonant heating effects have been treated with similar equations under the assumption of low plasma betas both in the monochromatic parallel case and for a spectrum of oblique MHD waves (Hamza *et al.*, 2006; Lu and Li, 2007; Li *et al.*, 2007; Lu and Chen, 2009). However, the initial conditions in these cases break the condition of the coherent particle motion, which is necessary to maintain the wave in a self-consistent way. Neglecting the coherence and violating the self-consistency may be an appropriate description for a minor particle species in the sense of a test-particle approach. But the description is insufficient for the dominating main species that carry the currents and charges maintaining the wave itself. Li *et al.* (2007) also consider consistent initial conditions that do reflect the coherent wave motion and find that these particles do not experience the non-resonant heating because they are not picked-up by the wave fields. A model for the coherent particle motion of the dominating species in a wave field at high plasma betas should be based on a Vlasov description to take the finite thermal width of the distribution into account. Numerical self-consistent simulations are another approach to this problem (e.g., Li and Habbal, 2005; Araneda *et al.*, 2008, 2009; Maneva *et al.*, 2010). In order to determine an adequate model distribution function, one first can determine two constants of motion for the kinematic system from Eqs. (III-2.4) through (III-2.6). These are the generalized momentum of the particle and its total kinetic energy in the wave frame:

$$M_j = v_\perp\cos\left(\phi-\varphi\right) + \frac{B_0}{b}v_\parallel\left[1 - \frac{\omega}{\Omega_j} + \frac{kv_\parallel}{2\Omega_j}\right], \tag{III-2.7}$$

$$P = v_\perp^2 + \left(v_\parallel - \frac{\omega}{k}\right)^2. \tag{III-2.8}$$

Both M_j and P can be shown to be constant, simply by taking the derivatives with respect to t and using the equations of motion in Eqs. (III-2.4) through (III-2.6). It is known (Akhiezer *et al.*, 1975) that any distribution function, which is a function of these con-

stants of motion, always fulfills the Vlasov equation. Therefore, the ansatz

$$f_j = N_j \exp\left(-\frac{P}{v_{\mathrm{th}j}^2}\right)\exp\left(\frac{2V_{\mathrm{w}j}M_j}{v_{\mathrm{th}j}^2}\right) \tag{III-2.9}$$

can be made with the normalization factor N_j and constant coefficients $v_{\mathrm{th}j}$ and $V_{\mathrm{w}j}$, which can essentially be defined as the density, thermal velocity of the VDF, and mean fluid-velocity amplitude of the particles in association with the wave motion.

The right second term in the expression for M_j compensates the frame-shift of $v_\parallel$ by ω/k in the definition of P if the condition

$$V_{\mathrm{w}j} = -\frac{b}{B_0}\frac{\omega/k}{1-\omega/\Omega_j} \tag{III-2.10}$$

is fulfilled, and if one can ignore the weak effects due to a small spread in the parallel direction ($kv_\parallel \ll \Omega_j$). Interestingly enough, this relation then corresponds to the wave polarization relation found by Sonnerup and Su (1967) for a circularly polarized wave with a vanishing parallel bulk drift. In their classical solution, they showed that the transversal velocity is determined by

$$\boldsymbol{V}_{j\mathrm{t}} = -\frac{\omega/k}{1-\omega/\Omega_j}\frac{\boldsymbol{B}_\mathrm{t}}{B_0} \tag{III-2.11}$$

for vanishing drifts in the z-direction. The transversal magnetic field vector is defined as $\boldsymbol{B}_\mathrm{t} = (B_x, B_y, 0)$ with the first two components as obtained from Eq. (III-2.1). The dispersion relation of the waves was given in Chapt. II. It can be written as

$$k^2 + \sum_j \frac{1}{\ell_j^2}\frac{\omega}{\omega-\Omega_j} = 0, \tag{III-2.12}$$

whereby the small displacement current in Maxwell's equations was neglected. The index j numbers all participating species (in the case considered later only protons and electrons).

After normalization, the non-gyrotropic model VDF of the particles in response to the wave forces reads

$$f_{\mathrm{w}j}(v_\perp, v_\parallel, \varphi) = \frac{n_{j0}}{\pi^{3/2}v_{\mathrm{th}j}^3}\exp\left(-\frac{V_{\mathrm{w}j}^2+\omega^2/k^2}{v_{\mathrm{th}j}^2}\right)\exp\left(-\frac{v_\perp^2+v_\parallel^2}{v_{\mathrm{th}j}^2}\right) \times \exp\left(\frac{2v_\perp V_{\mathrm{w}j}}{v_{\mathrm{th}j}^2}\cos(\phi-\varphi)\right). \tag{III-2.13}$$

The first exponential stems from the normalization, and does not change the structure of the distribution function but depends on the particles sloshing velocity amplitude $V_{\mathrm{w}j}$ and wave phase speed ω/k. It is interesting to note that this model distribution function is equal to a Maxwellian distribution in cylindrical coordinates, yet which is shifted by $\boldsymbol{V}_{j\mathrm{t}}$ in the transversal direction and can be written in this shifted Maxwellian form as

$$f_j \sim \exp\left(-\frac{(v_x-V_{jx})^2+(v_y-V_{jy})^2}{v_{\mathrm{th}j}^2}\right) \tag{III-2.14}$$

with the cartesian speed components V_{jx} and V_{jy}, reflecting the rigid displacement of the whole VDF in the wave field. This is an ansatz commonly used to initialize consistently numerical simulations (Araneda *et al.*, 2008) and represents the sloshing motion of particles in the wave field (e.g., Markovskii *et al.*, 2009). A thermodynamical derivation of an equivalent distribution function from arguments on the entropy have been published parallel to this work by Nariyuki (2011a).

A VDF that has an additional intrinsic temperature anisotropy is supposed to be represented by a modified bi-Maxwellian distribution. The appropriate choice for a VDF in a wave field including an intrinsic temperature anisotropy is given by

$$f_{\mathrm{a}j} \sim \exp\left(-\frac{V_{\mathrm{w}j}^2}{v_{\mathrm{th}j\perp}^2} - \frac{\omega^2/k^2}{v_{\mathrm{th}j\parallel}^2}\right)\exp\left(-\frac{v_\perp^2}{v_{\mathrm{th}j\perp}^2} - \frac{v_\parallel^2}{v_{\mathrm{th}j\parallel}^2}\right)\exp\left(\frac{2v_\perp V_{\mathrm{w}j}}{v_{\mathrm{th}j\perp}^2}\cos\left(\phi-\varphi\right)\right), \quad \text{(III-2.15)}$$

where different thermal speeds in the perpendicular and parallel direction are chosen to account for the intrinsic anisotropy. It is important to note, however, that this distribution function is not an exact solution of the Vlasov equation anymore. Without wave activity, this distribution function obtains the usual bi-Maxwellian form. This modified bi-Maxwellian VDF is not applied in the following since the considerations are focussed on the role of apparent temperature anisotropies only.

III.2.2 Wave effects on particle measurements

The solar wind is permeated by magnetic field fluctuations and waves (Tu and Marsch, 1995) of all kind. A particle detector that is able to determine the velocity distribution function of particles (e.g., such as flown aboard the Helios spacecraft) counts particles in different energy and direction channels and thereby integrates the net particle fluxes into the various single channels over the so-called sampling time T. In a first approximation, one may interpret this time as kind of an exposure time (like in photography) and thereby neglect time-dependent sampling effects on the instrument's pointing direction (to different solid looking angles) or on the accessibility of the particles to the different energy channels during the measurement cycle. Effects of the proper motion of the detector with respect to the solar wind flow are also neglected for the first estimation. A possibility to handle the effects arising from this relative motion would be to treat the waves as frozen in the solar wind and being with the fixed spatial structure convected over the space probe. This assumption is called Taylor hypothesis and is valid only for $\boldsymbol{k}\cdot\boldsymbol{V}_{\mathrm{SW}} \gg \omega$, where $\boldsymbol{V}_{\mathrm{SW}}$ denotes the solar wind flow velocity. Since the Alfvén speed is typically about a factor of 10 less than the flow speed of the solar wind in the spacecraft reference frame, this Doppler effect would even increase the sampling problem because waves with lower wavenumbers appear at higher frequencies for the detector. These lower wavenumber structures typically have a higher power than waves at higher wavenumbers. Therefore, the relative motion of the solar wind with respect to the spacecraft amplifies the wave effect on the measured distribution function additionally.

Such a model instrument would not be able to take snapshots of the VDF but integrate the sloshing distribution over time T and would therefore obtain a spread in the VDF due to the wave activity. In the following, the influence of this final integration time on the actual measurement is determined theoretically.

The relevant spectral range is limited to frequencies that are higher than the sampling frequency $2\pi/T$ because slower motions would be more or less resolved. They would merely lead to a rigid shift of the full distribution function without deformation. The analysis software of a plasma instrument would set the origin of the reference frame to the shifted center of the VDF so that no change would be detectable. On the upper frequency side, the acting part of the wave spectrum should be limited by the gyrofrequency because the waves are supposed to be strongly damped in the case of A/IC waves at this scale, and thus beyond it the observed spectral energy goes down significantly. The slope of the spectral energy density follows Kolmogorov's law at lower frequencies (Tu and Marsch, 1995). Numerical simulations show that at wave numbers around $k \approx 0.8/\ell_\mathrm{p}$ the A/IC spectral slope usually breaks because of the onset of dissipation at these scales (Ofman *et al.*, 2005). Here only a monochromatic wave with $\omega = 2\pi/T$ is assumed.

Given all these assumptions, the time-averaging process of the VDF under the influence of waves may be expressed mathematically as

$$\bar{f}_j = \frac{1}{T}\int_0^T f_{\mathrm{w}j}\mathrm{d}t. \tag{III-2.16}$$

One can now insert the model function of Eq. (III-2.13), in which the last exponential factor can be expanded (Abramowitz and Stegun, 1972) and represented by a sum over modified Bessel functions I_m according to the relation:

$$e^{a\cos b} = I_0(a) + 2\sum_{m=1}^{\infty} I_m(a)\cos(mb). \tag{III-2.17}$$

The time dependence of the averaged distribution function $\bar{f}_j$ is hidden in the wave phase $\phi(t)$. The coordinates of the distribution function (i.e., z, $v_\perp$, and $v_\parallel$) have no time dependence in this context. The expression for $f_{\mathrm{w}j}$ in Eq. (III-2.13) delivers a value of the VDF at each position in phase space and at each time. Without any restriction, the spatial position can be taken $z = 0$. Then the time-averaged distribution function can be written as

$$\bar{f}_j = N_j \exp\left(-\frac{v_\perp^2 + v_\parallel^2}{v_{\mathrm{th}j}^2}\right)\left[I_0\left(\frac{2v_\perp V_{\mathrm{w}j}}{v_{\mathrm{th}j}^2}\right) + \frac{2}{T}\sum_{m=1}^{\infty} I_m\left(\frac{2v_\perp V_{\mathrm{w}j}}{v_{\mathrm{th}j}^2}\right)\frac{\sin(m\omega T + m\varphi) - \sin(m\varphi)}{m\omega}\right]. \tag{III-2.18}$$

The sum is always zero for all possible positions in φ if $\omega = 2\pi/T$. So the above formula can be simplified and written as

$$\bar{f}_{1j} = N_j \exp\left(-\frac{v_\perp^2 + v_\parallel^2}{v_{\mathrm{th}j}^2}\right) I_0\left(\frac{2v_\perp V_{\mathrm{w}j}}{v_{\mathrm{th}j}^2}\right). \tag{III-2.19}$$

Thus, the intrinsically non-gyrotropic distribution function appears to become gyrotropic again after this kind of averaging process. Still, a wider spectrum of waves could lead to a

deformation of the distribution function in the coordinate φ, but as stated above the higher frequencies on shorter time scales than the sampling time T are not expected to change the result much.

Next, an A/IC wave is assumed. This wave has to fulfill a dispersion relation, which can be taken from the cold plasma limit in Eq. (II-2.82), yielding the parallel dispersion relation as

$$\left(\frac{\omega}{\Omega_\mathrm{p}}\right)^2 = (k\ell_\mathrm{p})^2 + \frac{1}{2}(k\ell_\mathrm{p})^4 - \frac{1}{2}(k\ell_\mathrm{p})^3\sqrt{(k\ell_\mathrm{p})^2+4}. \tag{III-2.20}$$

For high values of k, the dispersion shows the asymptotic behavior $\omega \to \Omega_\mathrm{p}$, which can be seen by expanding the function $\sqrt{1+x}$ with $x = 4/(k\ell_\mathrm{p})^2$ to second order. Typical solar wind parameters are used for a distance between spacecraft and Sun of about 0.5 AU, which is where strongly non-Maxwellian distributions and high wave activity were usually observed in fast solar wind by the Helios spacecraft. The wave activity is observed to be higher at smaller distances to the Sun, which is demonstrated in Fig. III-1. The plasma beta is set to 0.1 and the sampling time to 10 s, which is the real sampling time of the Helios spacecraft. The constant background magnetic field B_0 is assumed to be 5×10^{-4} G and the proton density to be $n = 10$ cm^{-3}. The relative wave amplitude is set to $b/B_0 = 0.25$. The distribution function at $\varphi = \pi$ is plotted at negative values for $v_\perp$, in order to make plots that can more easily be compared with the observations. The calculated distribution function is shown in Fig. III-2.

Heavy ions with mass m_i, which are also present in the solar wind (von Steiger, 2008), react on the wave field in a slightly different way. The dependence of $V_{\mathrm{w}j}$ on the charge-to-mass ratio in Eq. (III-2.10) is small for lower frequencies. The thermal speed, however, is significantly lower than the proton thermal speed by a factor of $\sqrt{m_\mathrm{p}/m_\mathrm{i}}$. Therefore, the distribution function of heavy ions is more narrow than the proton distribution function but shifted by the same amount due to the wave motion as can be seen in Eq. (III-2.13). This can lead to a more severe deformation of the distribution function after the averaging process, which might also lead to ring-like apparent VDFs for heavy ions in strong wave fields.

The apparent temperature anisotropy can now be calculated by taking the second moment of the distribution function according to the formula

$$A \equiv \frac{T_\perp}{T_\parallel} = \frac{\int_{-\infty}^{+\infty}\int_{0}^{+\infty} \bar{f}_{1j} v_\perp^3 \,\mathrm{d}v_\perp \mathrm{d}v_\parallel}{2\int_{-\infty}^{+\infty}\int_{0}^{+\infty} \bar{f}_{1j} v_\parallel^2 v_\perp \,\mathrm{d}v_\perp \mathrm{d}v_\parallel}. \tag{III-2.21}$$

The integration over φ leads to the factor 2 in the denominator. The above distribution function of Fig. III-2 has an apparent temperature anisotropy of $A = 1.64$.

By varying the wave parameters and the particle thermal speed, correspondingly varying forms of the distribution function can be created. The dependence of the resulting apparent temperature anisotropy on the plasma beta and the wave amplitude b is shown in Fig. III-3.

The obtained distribution function looks from the first point of view very similar to a

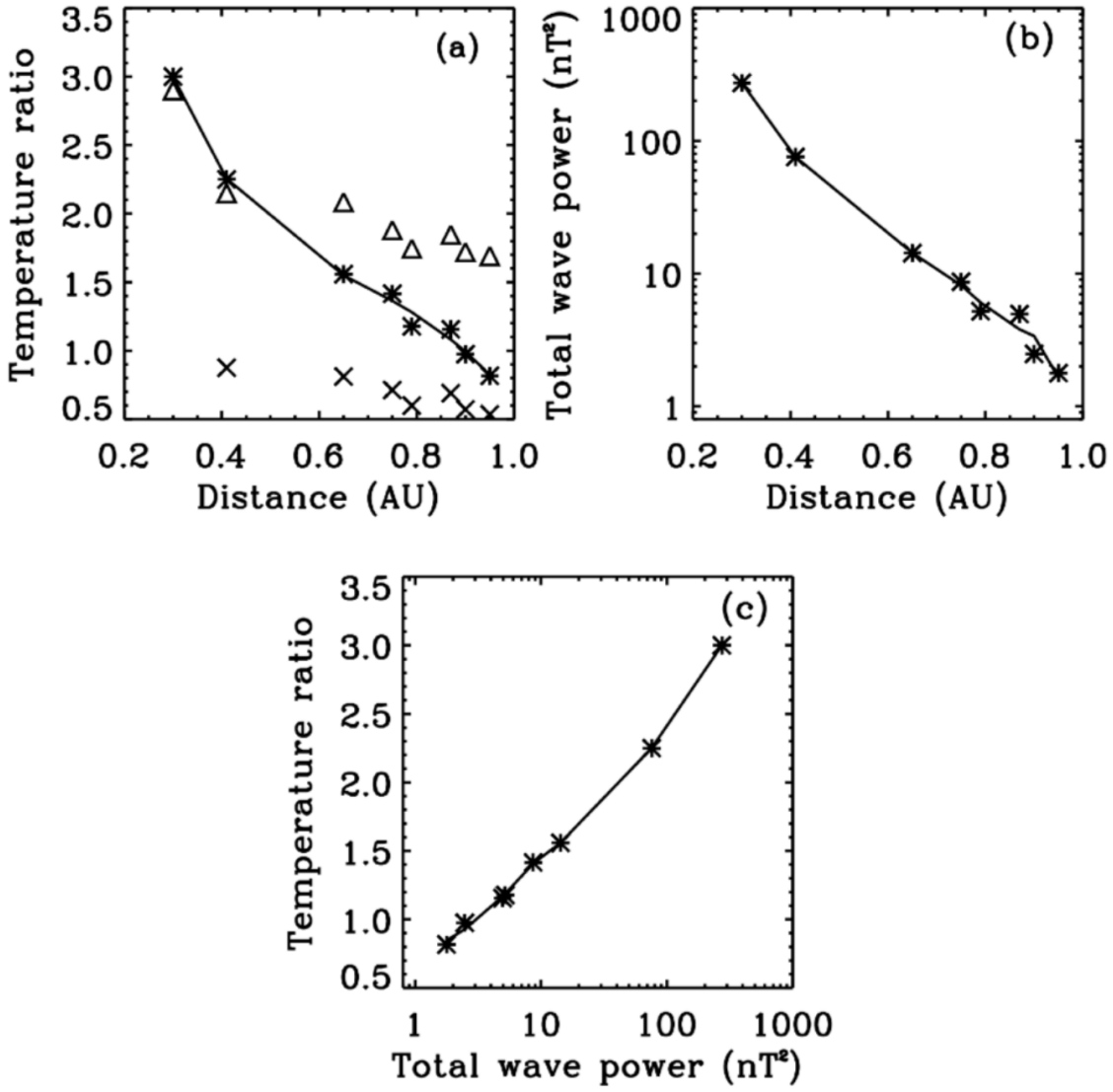

Figure III-1: Dependence of fluctuation power, temperature anisotropy, and distance from the Sun on each other. The lines show polynomial fits to the data. a) triangles: thresholds for ion-cyclotron instability, crosses: thresholds for firehose instability. From Bourouaine *et al.* (2010).

classical bi-Maxwellian distribution function of the form

$$f_{\mathrm{bm}j} \sim \exp\left(-\frac{v_\perp^2}{v_{\mathrm{th}j\perp}^2} - \frac{v_\parallel^2}{v_{\mathrm{th}j\parallel}^2}\right). \tag{III-2.22}$$

In Fig. III-4, a bi-Maxwellian VDF is shown for an (intrinsic) anisotropy of $v_{\mathrm{th}\perp}^2/v_{\mathrm{th}\parallel}^2 = 2$. The general form of the VDF in Fig. III-2 can also be approximated by this mathematical representation, which underlines the difficulties arising from the correct definition of the observed temperature. Interpreting the wave-broadened distribution function $\bar{f}_j$ as a bi-Maxwellian leads to an apparent difference in the two thermal velocities of the bi-Maxwellian VDF. Therefore, the wave-broadening can also be expressed in terms of a cor-

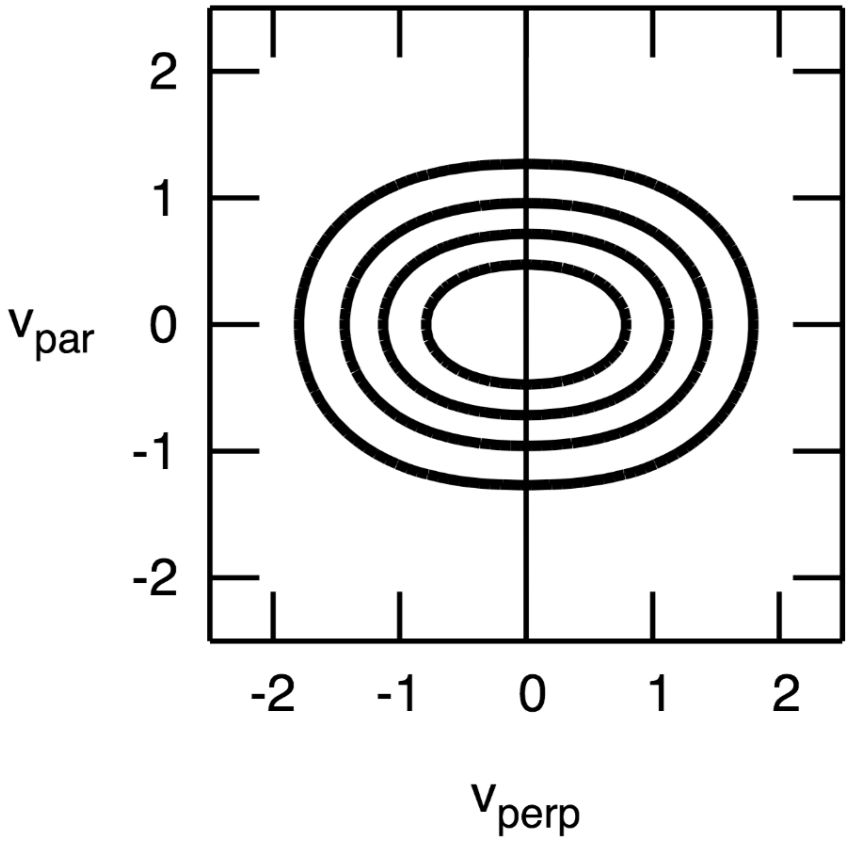

Figure III-2: Distribution function in the presence of a large-amplitude wave. The solid line represents the background magnetic field direction. Velocities are given in units of the thermal speed. The broadening in the perpendicular direction is clearly visible.

responding apparent thermal velocity anisotropy. Applying the second moment relation from Eq. (III-2.21) to a bi-Maxwellian distribution function yields the ratio $A = v_{\mathrm{th}j\perp}^2 / v_{\mathrm{th}j\parallel}^2$. This means that the anisotropy in the apparent thermal speeds is given directly by $\sqrt{A}$.

Considering waves with higher frequencies, one must admit that the approximation $kv_\parallel \ll \Omega_j$ is not valid anymore. Then further modifications of the VDF have to be accepted in the wave field, and a non-Maxwellian dependence also on the parallel speed coordinate $v_\parallel$ is found. Accordingly the distribution is

$$f_{\mathrm{h}j} = f_{\mathrm{w}j} \exp\left(\frac{2v_\parallel}{v_{\mathrm{th}j}^2} \left[\frac{\omega}{k} + \frac{B_0}{b} V_{\mathrm{w}j} \left(1 - \frac{\omega}{\Omega_j} + \frac{kv_\parallel}{2\Omega_j} \right) \right] \right). \tag{III-2.23}$$

If the time-averaging process is applied to this distribution function, the results change significantly. The additional term makes the distribution function more prolate already at lower wave amplitude and for higher beta values. Thus it becomes even more similar to a bi-Maxwellian distribution function as it is shown in Fig. III-4. An example for this situation is shown in Fig. III-5, where the parameters $\omega = 10\pi/T$, $b = 0.1$, and $\beta = 0.5$ have been assumed.

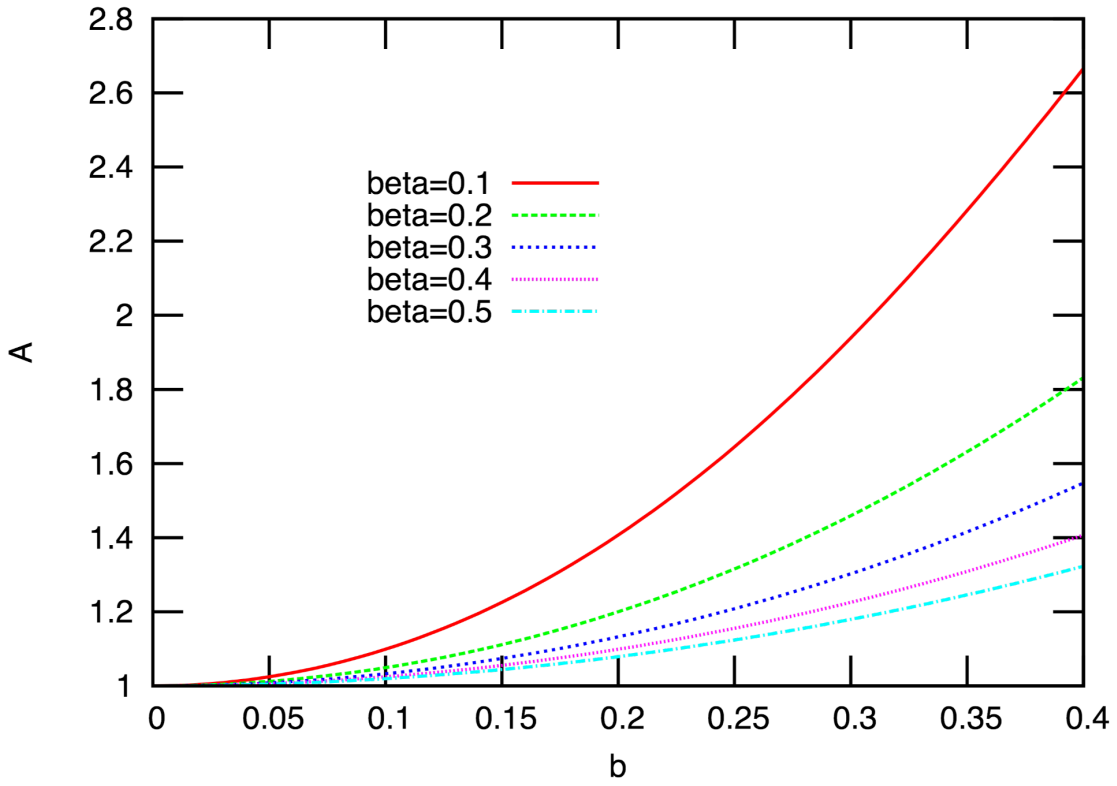

Figure III-3: Apparent temperature anisotropy in dependence on the normalized amplitude b of a wave with $\omega = 2\pi/T$. The evaluation of the anisotropy according to Eq. (III-2.21) is shown for different values of the plasma beta.

For comparison, also a typical measurement by the Helios 2 spacecraft from 1976 is shown. The anisotropy of the observed distribution function is comparable to the calculated apparent anisotropy, whereas other effects such as the formed beam along the background field is not reproduced by the above calculations. The model distribution function fits the observed distribution function well. This shows that the broadening effect and the detailed shaping mainly depend on the frequency of the waves and the plasma beta. The measured distribution function is better represented by the corrected distribution function for higher frequencies. This distribution is not simply a shifted Maxwellian but has a further non-Maxwellian dependence on $v_{\parallel}$, which can represent the observations better.

III.3 Discussion

This study could show how the VDF is shaped by the presence of a large-amplitude wave. In the case of transversal wave activity, the distribution function obtains a shift in the direction perpendicular to the background magnetic field. If the distribution function is averaged over time, this shift will lead to a smearing in the perpendicular velocity component, which in turn would be interpreted as a temperature anisotropy in favor of the perpendicular direction. Every real measured distribution function can only be determined by sampling within a certain time period, and this implies averaging. Thus, the resulting

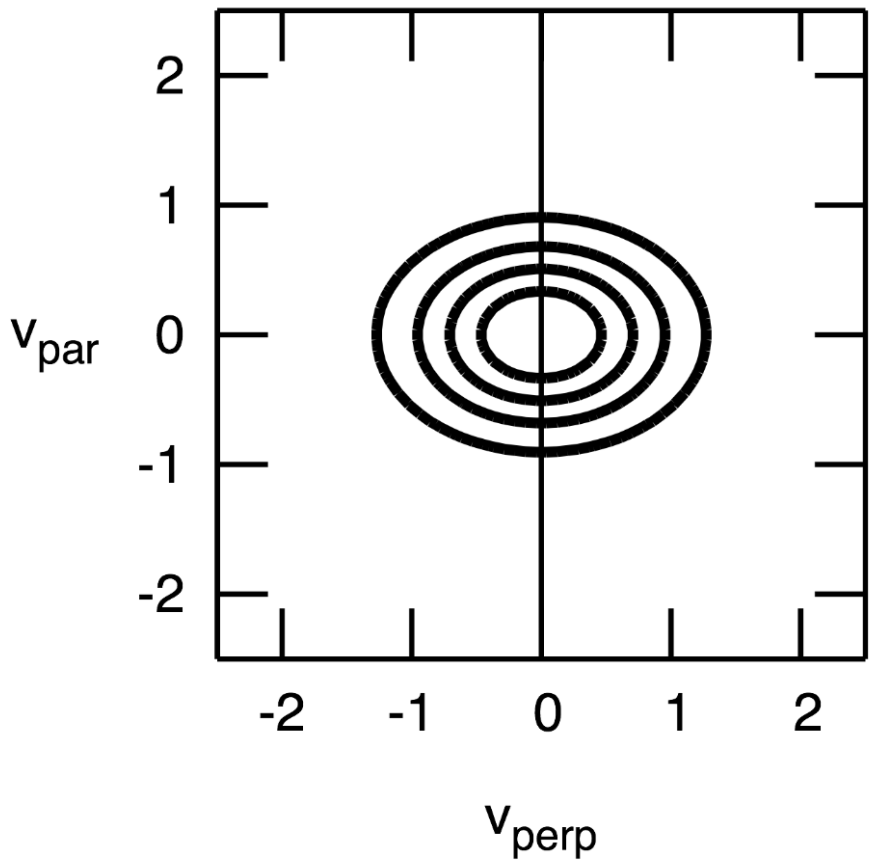

Figure III-4: Bi-Maxwellian velocity distribution function for a temperature anisotropy of 2.

temperature as the second moment of the VDF reflects this procedure.

It was possible to demonstrate, using a simplified model, how this effect can lead to a significant change in the observed distribution functions as plasma measurements are always done by counting particles over a certain sampling time T. This sampling period corresponds again to time averaging. The broadening of particle distributions due to microturbulence is a well known fact, which is exploited in spectroscopy to determine remotely, for example, the turbulence level in the solar corona (e.g., Kohl *et al.*, 2006) from ultraviolet emission line broadenings. In the context of measurements of plasma VDFs in the solar wind, however, this was not taken into account before to the author's knowledge.

Also compressive fluctuations can be treated in a similar way. However, then broadening would be observed mostly in the parallel direction. Consistently with the present emphasis on perpendicular broadening, most recent observations show a higher transversal wave activity in almost all cases in the fast solar wind (Horbury *et al.*, 2005; Alexandrova *et al.*, 2008b).

The meaning of intrinsic temperature anisotropies should be further discussed in the future. As mentioned before, a severe limitation to $T_\perp/T_\parallel$ is observed in the solar wind

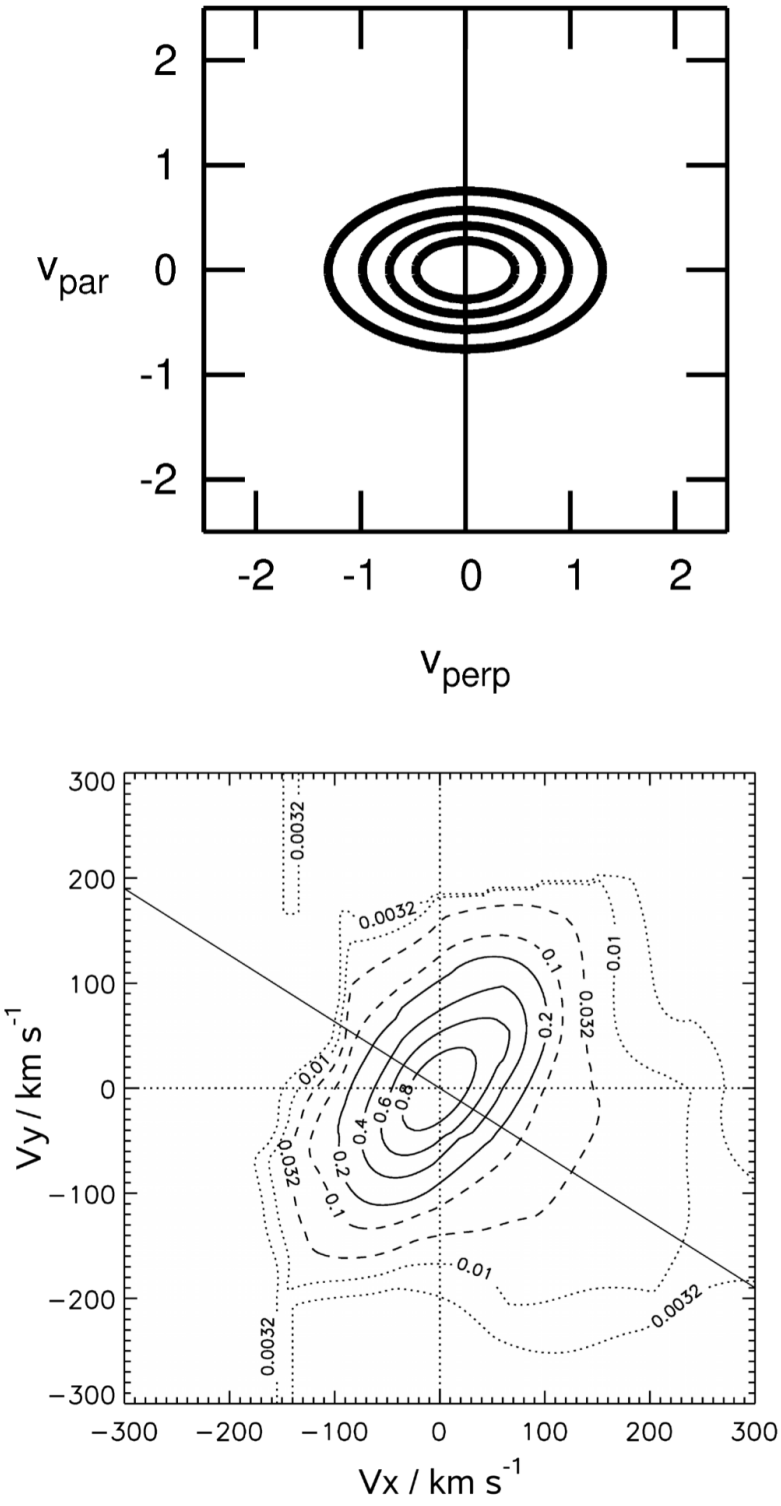

Figure III-5: Top: Like in Fig. III-2 but including higher-order corrections. Bottom: Typical proton distribution function measured by the Helios 2 spacecraft in 1976. The black line indicates the direction of the background magnetic field.

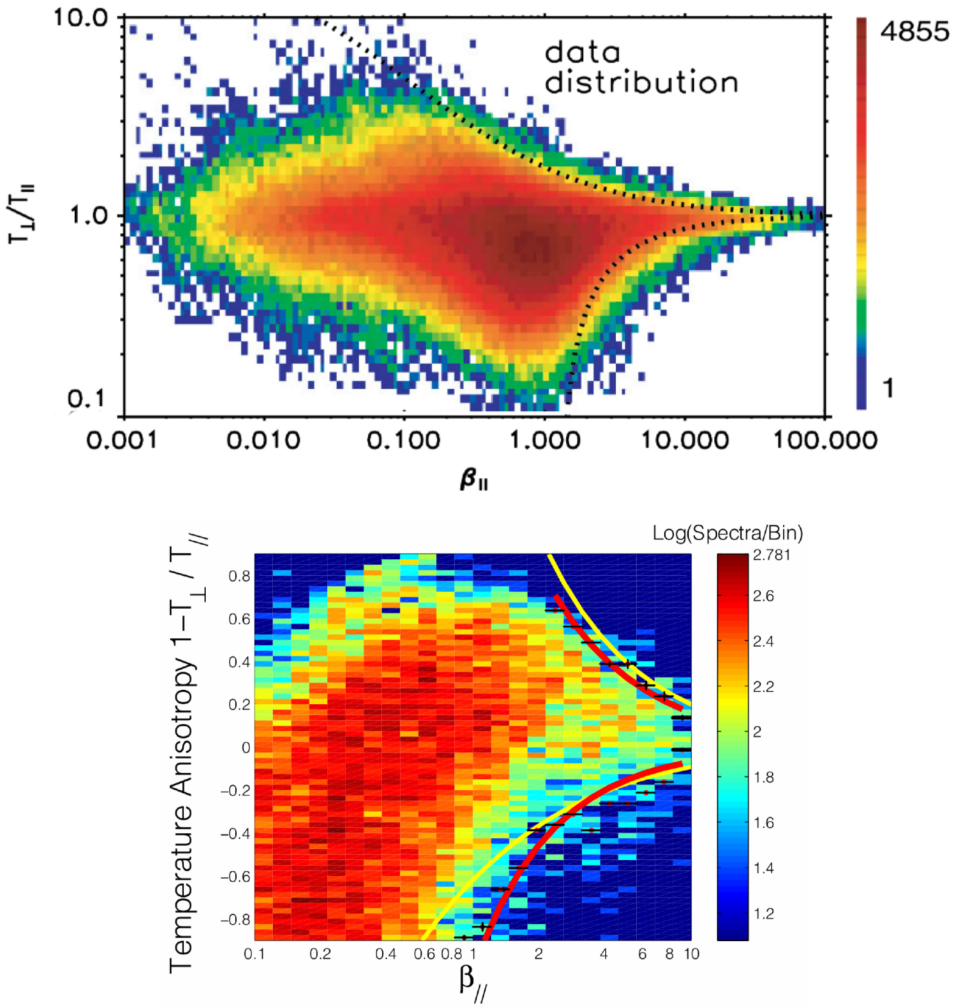

Figure III-6: Top: Number of solar wind measurements of temperature anisotropies depending on the plasma beta by the Wind spacecraft at about 1 AU. The lines indicate the thresholds for mirror mode and firehose instability. The measurements seem to be well constrained by the theoretical thresholds. Reprinted figure with permission from Bale *et al.* (2009). Copyright by the American Physical Society. Bottom: The same but from the Helios spacecraft at about 0.3 AU. From Marsch *et al.* (2006).

(Marsch *et al.*, 2006; Bale *et al.*, 2009; Marsch *et al.*, 2009) in relation with plasma microinstabilities, which reveal a sensitive beta dependence. The statistics of this effect is shown in Fig. III-6, where the measured temperature anisotropies are shown depending on the plasma beta. This finding gives a clear indication that the observed temperature anisotropies are largely intrinsic. This finding even more underlines the importance of an adequate definition and treatment of the measured plasma temperatures. The apparent higher temperature, which has been found in the model VDFs, is not the result of resonant heating processes such as Landau damping or cyclotron-resonant wave–particle interactions. Hence, this wave-related mechanism is reversible, and for a vanishing wave field also the apparent anisotropy would disappear.

Non-resonant wave–particle interactions have been studied in the framework of quasilinear theory by Bourouaine *et al.* (2008). They demonstrate that the non-resonant heating is more effective for lower plasma betas since the efficiency of the quasilinear diffusion is mainly proportional to $v_A - v_\parallel$. The beta dependence is confirmed, and the dependence of the parallel particle velocity in the wave frame is also found in the above considerations as in Eq. (III-2.8) for example. However, it was possible to show that the dispersion of A/IC waves can compensate for the reference frame shift in the Vlasov picture. Furthermore, Bourouaine *et al.* (2008) found a stronger effect of the non-resonant heating on heavy ion species, which is also consistent with this model.

In the context of the measurement effect according to Eq. (III-2.16), the determination of temperature is not an ergodic measurement anymore if wave fields lead to a coherent particle motion as it is the case in the solar wind. This leads to the problem that the assumption of Markovian statistics is violated since the particle motion is additionally affected by the deterministically time-dependent wave motion during the averaging. Non-ergodicity in this case means that the temperature based on time averaging is different from the temperature based on ensemble averaging. But all real temperature measurements in dilute plasmas have to be done by averaging over time leading to the apparent deformations in the distribution function shown above. An appropriate ensemble average, however, is not accessible on the required scales in the solar wind due to the low particle number density. Recently Hizanidis *et al.* (2010) found that the applicability of classical quasilinear diffusion is not guaranteed in a coherent electromagnetic wave field. They developed a new kinetic theory for wave–particle interactions and find time-dependent diffusion tensors describing the velocity evolution of the VDF. This is a manifestation of the non-ergodicity of the measurement process. Maybe a completely different description of the microphysical behavior should be applied to these coherent cases as it is proposed and discussed in the textbook by Elskens and Escande (2003). The wave broadening effect could be excluded locally if, at the position and time where the measurement is taken, enough particles are present with the local coherent speed additional to their thermal speed. In all accessible solar wind plasma cases however, the number of particles, which can be counted under constant conditions compared to $\phi = kz - \omega t$, is practically always too small.

A shorter sampling time would bring the observation closer to a "snapshot" of the real distribution function. A faster measurement would help avoiding heavy smearing in velocity space due to wave activity. The comparatively small number density of particles in the solar wind, however, requires long sampling times or larger geometry factors, which are not affordable. The Solar Orbiter mission should provide new insights because the improved instruments to be flown on board this spacecraft and the higher particle densities expected closer to the Sun will permit much shorter sampling times down to 100 ms.

In this work, a monochromatic wave is assumed that leads to smearing out of the VDF by the time-averaging process. A more realistic assumption would be a broad spectrum of waves, which the particles have to follow and the VDF to respond to. Nariyuki (2011b) presented such a generalization under certain constraints. Furthermore, the particle flux will not be steady in all directions during the sampling time T. Also, a realistic spacecraft model should be applied, including the detailed time dependence of the sampling method as well as the relative velocity of the spacecraft with respect to the solar wind. If such appropriate models were available, the analysis of the distribution function could in

turn provide new information about the waves such as their polarization or propagation direction. Up to now, only waves propagating parallel to the background magnetic field have been dealt with in the above model. To complete the analysis, also oblique wave propagation should be taken into account.

IV Nonlinear Alfvén/ion-cyclotron waves in a multi-fluid plasma description

The following chapter has been published in wide parts before submission of the thesis. It is mainly dedicated as the basis for Chapt. V. The discussion in Sect. IV.4.4 reveals a new aspect, which is separated from the following chapters. The reference for the pre-published article is:

Eckart Marsch and Daniel Verscharen: *On nonlinear Alfvén-cyclotron waves in multi-species plasma*, J. Plasma. Phys. 77, 385-403, 2011, doi:10.1017/S0022377810000541.

IV.1 Nonlinear Alfvén waves and their side-effects

Not only the previously discussed turbulent low-amplitude fluctuations but also large-amplitude Alfvén waves are ubiquitous in space plasmas and particularly prominent in the solar wind (Tu and Marsch, 1995; Bruno and Carbone, 2005). They are an essential component of magnetohydrodynamic (MHD) turbulence in the heliosphere and known to originate mainly in the solar coronal holes (Cranmer, 2009). As has been shown in the ample literature and mentioned in Chapt. I, an Alfvén mother (pump) wave is prone to parametric instability (Stenflo, 1976; Derby, 1978; Goldstein, 1978; Longtin and Sonnerup, 1986; Brodin and Stenflo, 1988; Hollweg, 1994; Wong and Goldstein, 1986; Viñas and Goldstein, 1991b,a; Stenflo and Shukla, 2000; Ruderman and Simpson, 2004; Stenflo and Shukla, 2007), by which it can generate cyclotron and acoustic daughter waves that may undergo kinetic effects (Araneda, 1998) and collisionless Landau damping (Inhester, 1990; Araneda *et al.*, 2007). The continuous and wide interest in these waves also comes from their astounding properties, namely that Alfveń/ion-cyclotron (A/IC) waves, like parallel fast/whistler (F/W) waves, are nonlinear eigenmodes (Sonnerup and Su, 1967; Stenflo, 1976) of the MHD and multi-fluid equations as shown below for propagation along the mean magnetic field.

Nonlinearly excited (Spangler, 1989) acoustic waves appear to be common in space plasmas as well, and density fluctuations (Tu and Marsch, 1995; Bruno and Carbone, 2005) are observed everywhere in the solar wind, although at a comparatively low fluctuation level of merely a few percent. However, since compressive fluctuations can be damped through kinetic effects like Landau damping on the thermal ions and electrons, they can provide an effective dissipation mechanism for the nonlinear damping

(Medvedev *et al.*, 1997) of Alfvén waves. Consequently the understanding of the coupling between Alfvénic wave activity and density or charge-density fluctuations is of paramount interest and importance in basic plasma physics but alike in its applications to nonlinear processes in space (Stenflo and Shukla, 2007) and astrophysical plasmas.

As will be shown in this chapter, a coupled set of nonlinear second-order wave equations for the transverse magnetic field, the transverse gyromotion of any particle species in the multicomponent plasma considered, and the related longitudinal electric field can be derived, which together describe the wave–wave interactions and their mutual forcing. These equations provide a physically and intuitively clear picture of the field and particle/plasma dynamics and allow one to understand the results of recent hybrid simulations of the parametric decay of Alfvén waves and their effects on the plasma particles better. The main aim of this chapter is to provide algebraic derivations and physical explanations. A numerical treatment of the full equations to be derived subsequently appears promising, yet is beyond the scope of this work.

In analytical (Araneda *et al.*, 2007), hybrid simulation, and other numerical simulation (Araneda *et al.*, 2008) studies of the parametric instabilities of A/IC waves, it became obvious that ion trapping (Araneda *et al.*, 2008, 2009) in the nonlinearly driven ion-acoustic waves and pitch-angle scattering by the transverse daughter waves were found to cause anisotropic heating of the proton core velocity distribution and simultaneously to create a proton beam along the mean field (Araneda *et al.*, 2008; Valentini and Veltri, 2009). These numerical results are in close agreement with observed kinetic features in the solar wind and support the observation that pitch-angle scattering (Heuer and Marsch, 2007; Marsch and Tu, 2001) is the key to understand the kinetic characteristics of thermal solar wind protons. But only recently convincing evidence has been found for convected A/IC waves to exist in the solar wind as discussed in the Introduction. Also simulations of electric field spectra (Valentini *et al.*, 2008) have shown that the short-scale termination of solar wind turbulence is characterized by the occurrence of longitudinal electrostatic fluctuations. The spectra thus obtained seem to be consistent with the electrostatic waves actually measured in the solar wind (Bale *et al.*, 2005) close to the Earth's bow shock and, in particular, in the ion-cyclotron range (Kellogg *et al.*, 2006).

The present study will provide the foundation for insight into and further study of the processes occurring at macroscopic and microscopic scales in solar wind turbulence and thus will throw light on the related dissipation processes through kinetic cascades and wave–particle interactions (Marsch, 2006). The nonlinear equations derived here are used to describe an elliptically polarized Alfvén wave as a simple but non-trivial example of their application at the end of this chapter. They form the basis for the considerations about the dispersion relations derived in Chapt. V.

IV.2 The multi-fluid equations in conservation form

IV.2.1 Fluid equations in the wave frame

In this section, the basic multi-fluid equations (Goossens, 2003) for a plasma consisting of electrons and various ionic species shall be recapitulated for the appropriate geometry. The starting point are the fundamental conservation laws, and then no approximations

with respect to the field amplitudes shall be made in order to be able to discuss and analyze nonlinear waves and convected wave-like structures. It is advantageous to use coordinates in the frame of reference moving with the wave, which has a normal to its front denoted by $\hat{\boldsymbol{n}}$ and a propagation speed $\boldsymbol{V} = V\hat{\boldsymbol{n}}$ in the inertial frame or center of momentum frame that is defined below. This unit vector obeys the relation $\hat{\boldsymbol{n}}^2 = 1$. The coordinate in this moving frame is $\boldsymbol{\xi} \equiv \boldsymbol{x} - \boldsymbol{V}t$ and all variables are assumed to depend on space and time only through $\boldsymbol{\xi}$. Thus, spatial and temporal derivatives in the wave frame are reduced to derivatives with respect to $\boldsymbol{\xi}$. Such a coordinate transformation has been used by many authors, for example to study solitary waves in multi-ion plasmas (Hackenberg *et al.*, 1998) or their stability properties (McKenzie *et al.*, 1993). Therefore, by using co-moving coordinates, Maxwell's partial differential equations in space and time and similarly the fluid equations for the different species can be reduced to simpler differential equations in terms of $\boldsymbol{\xi}$. The continuity equation from Eq. (II-2.52), thus, reads

$$\frac{\partial}{\partial \boldsymbol{\xi}} \cdot \left(n_j \boldsymbol{V}_j \right) = 0 \tag{IV-2.1}$$

with $\boldsymbol{V}_j$ being the flow velocity of species j in the moving frame $\boldsymbol{V}_j \equiv \boldsymbol{U}_j - \boldsymbol{V}$, and n_j is its number density. With the charge denoted as q_j, the total charge density is given by

$$\varrho_\mathrm{c} = \sum_j \varrho_{\mathrm{c}j} = \sum_j q_j n_j, \tag{IV-2.2}$$

which must obey Gauß' law:

$$4\pi\varrho_\mathrm{c} = \frac{\partial}{\partial \boldsymbol{\xi}} \cdot \boldsymbol{E}. \tag{IV-2.3}$$

Similarly the total current density is given by

$$\boldsymbol{J} = \sum_j q_j n_j \boldsymbol{U}_j, \tag{IV-2.4}$$

which has to obey Ampère's law:

$$\boldsymbol{J} = \frac{c}{4\pi} \frac{\partial}{\partial \boldsymbol{\xi}} \times \boldsymbol{B} + \frac{1}{4\pi} \frac{\partial}{\partial \boldsymbol{\xi}} \cdot (\boldsymbol{VE}). \tag{IV-2.5}$$

The second term of Eq. (IV-2.5) is the displacement current. The conduction minus convection current density may be written as

$$\boldsymbol{j} \equiv \boldsymbol{J} - \varrho_\mathrm{c} \boldsymbol{V} = \sum_j \varrho_{\mathrm{c}j} \boldsymbol{V}_j. \tag{IV-2.6}$$

To complete the set of Maxwell's equations, the magnetic field must be divergence free:

$$\frac{\partial}{\partial \boldsymbol{\xi}} \cdot \boldsymbol{B}' = 0. \tag{IV-2.7}$$

Faraday's induction equation requires the curl of the electric field in the wave frame to vanish:

$$\frac{\partial}{\partial \boldsymbol{\xi}} \times \boldsymbol{E}' = 0 \tag{IV-2.8}$$

with the primed variables being defined in the wave frame. The Lorentz transformation has been used to derive Eq. (IV-2.8) since it gives the connection between the electromagnetic fields in the plasma's center of momentum frame and the moving wave frame through the relation

$$\boldsymbol{E}' = \boldsymbol{E} + \frac{1}{c}\boldsymbol{V} \times \boldsymbol{B}. \tag{IV-2.9}$$

Of course, the magnetic field remains invariant to lowest order in V/c, and thus $\boldsymbol{B}' = \boldsymbol{B}$. For later purposes, the mass density of particle kind j is defined here as $\varrho_j \equiv n_j m_j$ with the total mass density

$$\varrho = \sum_j \varrho_j. \tag{IV-2.10}$$

The center of momentum velocity (for which one is free to choose $\boldsymbol{U} = 0$) is defined as follows:

$$\varrho \boldsymbol{U} = \sum_j \varrho_j \boldsymbol{U}_j. \tag{IV-2.11}$$

Since the individual ion and electron dynamics are of special interest, their momentum equations are not summed up like in MHD, but instead the separate multi-fluid equations are used. The individual momentum equation of species j from Eq. (II-2.53) can conveniently be quoted in conservation form in the moving frame, reading

$$\frac{\partial}{\partial \boldsymbol{\xi}} \cdot \left(m_j n_j \boldsymbol{V}_j \boldsymbol{V}_j + p_j \mathbf{1} \right) = q_j n_j \left(\boldsymbol{E}' + \frac{1}{c} \boldsymbol{V}_j \times \boldsymbol{B}' \right). \tag{IV-2.12}$$

The expression $\boldsymbol{V}_j \boldsymbol{V}_j$ means a tensor in dyadic notation and $\mathbf{1}$ the unit dyade. For the equation of the partial pressure, one may take a simple polytropic equation of state for the purpose of closure and thus write

$$p_j = p_{j0} \left(\frac{n_j}{n_{j0}} \right)^{\gamma_j} \tag{IV-2.13}$$

with some constant reference density n_{j0} and pressure p_{j0}. Equivalently one may consider the (polytropic, with index γ_j) entropy equation

$$\boldsymbol{V}_j \cdot \frac{\partial}{\partial \boldsymbol{\xi}} \ln \left(p_j \varrho_j^{-\gamma_j} \right) = 0. \tag{IV-2.14}$$

The set of Eqs. (IV-2.1), (IV-2.3), (IV-2.5), (IV-2.7), (IV-2.8), (IV-2.9), (IV-2.12), and (IV-2.13) is closed and sufficient to calculate all the independent but coupled variables. In what follows, a reduced geometry shall be assumed.

IV.2.2 Reduced multi-fluid equations in one-dimensional geometry

A one-dimensional spatial setup, i.e., a dependence on only one spatial coordinate and components with respect to $\hat{\boldsymbol{n}}$ are considered, where the unit vector may correspond to the unit wavevector $\hat{\boldsymbol{k}}$ in Fourier variables. Thus, the components are generally defined as

$$\xi = \hat{\boldsymbol{n}} \cdot (\boldsymbol{x} - \boldsymbol{V}t), \tag{IV-2.15}$$

$$\boldsymbol{V}_j = V_{j\mathrm{n}}\hat{\boldsymbol{n}} + \boldsymbol{V}_{j\mathrm{t}}, \tag{IV-2.16}$$

$$\boldsymbol{V}_{j\mathrm{t}} = (\mathbf{1} - \hat{\boldsymbol{n}}\hat{\boldsymbol{n}}) \cdot \boldsymbol{V}_j. \tag{IV-2.17}$$

Transverse components are obtained by projection perpendicular to the longitudinal direction. The corresponding magnetic field components are defined as $B_\mathrm{n} = \hat{\boldsymbol{n}} \cdot \boldsymbol{B}$ and $\boldsymbol{B}_\mathrm{t} = (\mathbf{1} - \hat{\boldsymbol{n}}\hat{\boldsymbol{n}}) \cdot \boldsymbol{B}$, from which it follows that $\hat{\boldsymbol{n}} \times \boldsymbol{B}_\mathrm{t} = \hat{\boldsymbol{n}} \times \boldsymbol{B}$ and that $\boldsymbol{B}_\mathrm{t} \cdot \hat{\boldsymbol{n}} = 0$. The fluid equations then read as follows. For the longitudinal momentum conservation, one has

$$\frac{\mathrm{d}}{\mathrm{d}\xi}\left(n_j V_{j\mathrm{n}} V_{j\mathrm{n}} + \frac{p_j}{m_j}\right) = \frac{q_j n_j}{m_j}\left(E'_\mathrm{n} + \frac{1}{c}\left(\boldsymbol{V}_j \times \boldsymbol{B}'\right) \cdot \hat{\boldsymbol{n}}\right), \tag{IV-2.18}$$

and for transverse momentum conservation one obtains the equation

$$\frac{\mathrm{d}}{\mathrm{d}\xi}\left(n_j V_{j\mathrm{n}} \boldsymbol{V}_{j\mathrm{t}}\right) = \frac{q_j n_j}{m_j}\left(\boldsymbol{E}'_\mathrm{t} + \frac{1}{c}\left(\boldsymbol{V}_j \times \boldsymbol{B}'\right)_\mathrm{t}\right). \tag{IV-2.19}$$

The longitudinal magnetic field is strictly conserved and thus constant:

$$\frac{\mathrm{d}B'_\mathrm{n}}{\mathrm{d}\xi} = 0, \tag{IV-2.20}$$

and the charge density obeys Gauß' law

$$\frac{\mathrm{d}E'_\mathrm{n}}{\mathrm{d}\xi} = 4\pi \sum_j q_j n_j. \tag{IV-2.21}$$

Taking the curl of $\boldsymbol{E}'$ after Eq. (IV-2.8) in the wave frame, one finds

$$\hat{\boldsymbol{n}}\frac{\mathrm{d}}{\mathrm{d}\xi} \times \boldsymbol{E}' = \hat{\boldsymbol{n}} \times \frac{\mathrm{d}\boldsymbol{E}'_\mathrm{t}}{\mathrm{d}\xi} = 0 = \hat{\boldsymbol{n}} \times \frac{\mathrm{d}\boldsymbol{E}_\mathrm{t}}{\mathrm{d}\xi} + \hat{\boldsymbol{n}} \times \left(\frac{1}{c} V \hat{\boldsymbol{n}} \times \frac{\mathrm{d}\boldsymbol{B}_\mathrm{t}}{\mathrm{d}\xi}\right), \tag{IV-2.22}$$

where the last part of the equation follows from the previous Eq. (IV-2.9). In conclusion, $\boldsymbol{E}'_\mathrm{t}$ is constant and can be set equal to zero. Using this result, the transverse electric field is obtained through Eq. (IV-2.9), which is equivalent to writing

$$\boldsymbol{E}_\mathrm{t} = -\frac{1}{c} V (\hat{\boldsymbol{n}} \times \boldsymbol{B}_\mathrm{t}) \tag{IV-2.23}$$

and makes the transverse electric field a dependent auxiliary variable being fully determined by the transverse magnetic field. For the longitudinal electric field component in the wave frame, one has

$$E'_\mathrm{n} = E_\mathrm{n} + \frac{1}{c}\hat{\boldsymbol{n}} \cdot (V\hat{\boldsymbol{n}} \times \boldsymbol{B}), \tag{IV-2.24}$$

which yields $E'_\mathrm{n} = E_\mathrm{n}$, which is to be used in Gauß' law (IV-2.21). For the one-dimensional spatial geometry chosen here, the longitudinal current density can be written as

$$J_\mathrm{n} = \frac{c}{4\pi}\hat{\boldsymbol{n}} \cdot \left(\hat{\boldsymbol{n}} \times \frac{\mathrm{d}\boldsymbol{B}}{\mathrm{d}\xi}\right) + \frac{1}{4\pi}\frac{\mathrm{d}}{\mathrm{d}\xi}(VE_\mathrm{n}). \tag{IV-2.25}$$

Since the curl of $\boldsymbol{B}$ has only transverse components, one obtains from Eq. (IV-2.25) that the longitudinal current density in the wave frame must be strictly constant, which is given by

$$j_\mathrm{n} = \sum_j q_j n_j V_{j\mathrm{n}} = \sum_j \varrho_{\mathrm{c}j} V_{j\mathrm{n}} = \sum_j q_j F_{j\mathrm{n}}. \tag{IV-2.26}$$

The individual particles fluxes $F_{j\mathrm{n}}$ are conserved according to the longitudinal continuity equation, which expresses flux conservation in the form

$$\frac{\mathrm{d}}{\mathrm{d}\xi}\left(n_j V_{j\mathrm{n}}\right) = \frac{\mathrm{d}F_{j\mathrm{n}}}{\mathrm{d}\xi} = 0. \tag{IV-2.27}$$

The transverse component of Ampère's law including the induction current can be cast in the form

$$\boldsymbol{j}_\mathrm{t} = \frac{c}{4\pi}\left(\hat{\boldsymbol{n}} \times \frac{\mathrm{d}\boldsymbol{B}_\mathrm{t}}{\mathrm{d}\xi}\right) + \frac{1}{4\pi}V\frac{\mathrm{d}\boldsymbol{E}_\mathrm{t}}{\mathrm{d}\xi} = \sum_j q_j n_j \boldsymbol{V}_{j\mathrm{t}}, \tag{IV-2.28}$$

whereby $\boldsymbol{V}_{j\mathrm{t}} = \boldsymbol{U}_{j\mathrm{t}}$ since $\boldsymbol{V}$ has no transverse component, but $\boldsymbol{V}_{j\mathrm{n}} = \boldsymbol{U}_{j\mathrm{n}} - \boldsymbol{V}$. The right-hand side of Eq. (IV-2.22) gives an expression for the gradient of the transverse electric field component. It can be inserted in Ampère's law, which thus can be written as

$$\frac{1}{4\pi}V\frac{\mathrm{d}\boldsymbol{E}_\mathrm{t}}{\mathrm{d}\xi} = -\frac{1}{4\pi c}V^2\left(\hat{\boldsymbol{n}} \times \frac{\mathrm{d}\boldsymbol{B}_\mathrm{t}}{\mathrm{d}\xi}\right) = \sum_j n_j q_j \boldsymbol{V}_{j\mathrm{t}} - \frac{c}{4\pi}\left(\hat{\boldsymbol{n}} \times \frac{\mathrm{d}\boldsymbol{B}_\mathrm{t}}{\mathrm{d}\xi}\right). \tag{IV-2.29}$$

If $(V/c)^2 \ll 1$, which will be assumed in the remainder, then the displacement current term can be safely neglected. It is certainly needed if one wants to make the transition to free electromagnetic waves correctly, which is not of special interest here. Therefore, this term will not be kept anymore. The basic equation for the magnetic field, which is Ampère's law for the transverse component, then reads

$$\frac{4\pi}{c}\sum_j n_j q_j \boldsymbol{V}_{j\mathrm{t}} = \frac{\mathrm{d}}{\mathrm{d}\xi}\left(\hat{\boldsymbol{n}} \times \boldsymbol{B}_\mathrm{t}\right). \tag{IV-2.30}$$

The magnetic field is free of divergence, which means in the used geometry and variables that Eq. (IV-2.20) is fulfilled with $B_\mathrm{n} = B'_\mathrm{n}$. The last two equations together fully determine the vector magnetic field, given the current density is provided. The transverse electric field is obtained from Eq. (IV-2.23) and the longitudinal one from Gauß' law (IV-2.21) with $E_\mathrm{n} = E'_\mathrm{n}$.

Quoted again, the transverse momentum equation for each species reads

$$\frac{\mathrm{d}}{\mathrm{d}\xi}\left(n_j V_{j\mathrm{n}} \boldsymbol{V}_{j\mathrm{t}}\right) = \frac{q_j}{m_j c} n_j \left(\boldsymbol{V}_j \times \boldsymbol{B}\right)_\mathrm{t} = \frac{q_j n_j}{m_j c}\left(V_{j\mathrm{n}}\hat{\boldsymbol{n}} \times \boldsymbol{B}_\mathrm{t} + \boldsymbol{V}_{j\mathrm{t}} \times \hat{\boldsymbol{n}} B_\mathrm{n}\right), \tag{IV-2.31}$$

whereby the electric field term has been written out in detail. Similarly, the longitudinal momentum equation reads

$$\frac{\mathrm{d}}{\mathrm{d}\xi}\left(n_j V_{j\mathrm{n}}^2 + \frac{p_j}{m_j}\right) = \frac{q_j n_j}{m_j}\left(E_\mathrm{n} + \frac{1}{c}(\boldsymbol{V}_j \times \boldsymbol{B})\cdot\hat{\boldsymbol{n}}\right), \tag{IV-2.32}$$

which must be supplemented, to obtain closure, by the entropy or pressure equation

$$\frac{\mathrm{d}}{\mathrm{d}\xi}\ln\left(p_j \varrho_j^{-\gamma_j}\right) = 0. \tag{IV-2.33}$$

In what follows, it turns out to be convenient to use the natural spatial and temporal scales of the multicomponent plasma, which depend on the various fluid and field parameters. A longitudinal gyration length for the species j is defined as

$$r_j \equiv \frac{V_{j\mathrm{n}}}{\Omega_j} = \frac{F_{j\mathrm{n}}}{\Omega_j}\frac{1}{n_j}, \tag{IV-2.34}$$

which corresponds to the gyroradius calculated with the longitudinal velocity instead of the perpendicular one. It is implicitly dependent on n_j via the drift speed and Eq. (IV-2.27). Another interesting length is given by the strictly constant quantity

$$L_j \equiv \frac{B_\mathrm{n} c}{4\pi q_j F_{j\mathrm{n}}} = r_j\left(\frac{V_{\mathrm{A}j}}{V_{j\mathrm{n}}}\right)^2 = \frac{1}{r_j}\left(\frac{c}{\omega_j}\right)^2. \tag{IV-2.35}$$

Here the Alfvén speed $V_{\mathrm{A}j}^2 \equiv B_\mathrm{n}^2/(4\pi n_j m_j)$ based on the mass density ϱ_j of species j only, the respective plasma frequency ω_j, and the gyrofrequency Ω_j carrying the sign of the charge q_j are introduced. Note that L_j is strictly constant and its inverse sums over all species up to zero, i.e., $\sum_j 1/L_j = 0$ because of the condition of zero longitudinal total current: $j_\mathrm{n} - \varrho_\mathrm{c} V = \sum_j q_j n_j V_{j\mathrm{n}} = 0$. The inverse standard Alfvén speed based on B_n is obtained by the summation

$$\frac{1}{V_\mathrm{A}^2} \equiv \sum_j \frac{1}{V_{\mathrm{A}j}^2}. \tag{IV-2.36}$$

Concerning the compressive dynamics, it is important to note that longitudinal and transverse motions are coupled through p_j and $r_j = V_{j\mathrm{n}}/\Omega_j$, i.e., through the particle number density, when the mass continuity equation (IV-2.27) and entropy equation (IV-2.33) are exploited.

IV.3 Wave equations

In this section, the basic equations for the fields and plasma multi-fluid parameters are recast into the form of coupled wave equations. For that purpose, they shall not straightforwardly be Fourier transformed but rather rewritten by use of multiple differentiation, in such a form that one finally obtains single "wave equations" for the electric field and magnetic field components. Remember that in the moving frame all variables depend

solely on the coordinate $\xi = \boldsymbol{x} \cdot \hat{\boldsymbol{n}} - Vt$. The pressure equation is considered first again. One may use for the species' sound speed the standard definition

$$c_j^2 \equiv \frac{\partial p_j}{\partial \varrho_j} \tag{IV-3.37}$$

and can then re-evaluate the momentum equation by use of

$$\frac{\mathrm{d}}{\mathrm{d}\xi}\left(\frac{p_j}{m_j}\right) = c_j^2 \frac{\mathrm{d}n_j}{\mathrm{d}\xi}, \tag{IV-3.38}$$

which together with Eq. (IV-2.27) permits to quote the longitudinal momentum equation in the form

$$\left(c_j^2 - V_{j\mathrm{n}}^2\right)\frac{\mathrm{d}n_j}{\mathrm{d}\xi} = \frac{q_j n_j}{m_j}\left(E_\mathrm{n} + \frac{1}{c}(\boldsymbol{V}_{j\mathrm{t}} \times \boldsymbol{B}_\mathrm{t}) \cdot \hat{\boldsymbol{n}}\right). \tag{IV-3.39}$$

It is convenient to introduce the effective Debye length λ_j of species j as follows:

$$\frac{1}{\lambda_j^2} \equiv \frac{\omega_j^2}{c_j^2 - V_{j\mathrm{n}}^2}, \tag{IV-3.40}$$

the sum of which gives the total Debye length still including the differential drifts:

$$\frac{1}{\lambda_\mathrm{D}^2} \equiv \sum_j \frac{1}{\lambda_j^2}. \tag{IV-3.41}$$

Both λ_j and λ_D are not necessarily real quantities. Each species brings in its own length scale λ_j. It is also convenient to introduce the second-order wave operator (which still parametrically depends on V via the $V_{j\mathrm{n}}$):

$$\mathcal{D}_E \equiv \frac{\mathrm{d}^2}{\mathrm{d}\xi^2} - \frac{1}{\lambda_\mathrm{D}^2}. \tag{IV-3.42}$$

Finally, one obtains a driven wave equation for the longitudinal electric field

$$\mathcal{D}_E E_\mathrm{n} = \frac{1}{c}\sum_j \frac{1}{\lambda_j^2}(\boldsymbol{V}_{j\mathrm{t}} \times \boldsymbol{B}_\mathrm{t}) \cdot \hat{\boldsymbol{n}}, \tag{IV-3.43}$$

in which the transverse particle motions and electromagnetic fields show up through a nonlinear electromotive force, which is the summed contribution of the longitudinal components of the Lorentz forces acting on each species. This driving force acting on E_n resembles a *convection* electric field. When being decoupled from the transverse plasma and field dynamics, the longitudinal electric field equation just describes free electrostatic oscillations, such as Langmuir and acoustic waves, as will be shown later.

It is useful to return to the transverse momentum equation and rewrite it by exploiting the mass continuity equation. Then it is straightforward to derive

$$\frac{\mathrm{d}\boldsymbol{V}_{j\mathrm{t}}}{\mathrm{d}\xi} = \frac{1}{r_j}\left(\frac{V_{j\mathrm{n}}}{B_\mathrm{n}}\hat{\boldsymbol{n}} \times \boldsymbol{B}_\mathrm{t} - \hat{\boldsymbol{n}} \times \boldsymbol{V}_{j\mathrm{t}}\right). \tag{IV-3.44}$$

Using this equation, one can rewrite the normal component of the convection electric field, which occurs in Eqs. (IV-3.39) and (IV-3.43), as follows:

$$E_{j\mathrm{n}} \equiv \frac{1}{c}\left(\boldsymbol{V}_{j\mathrm{t}} \times \boldsymbol{B}_{\mathrm{t}}\right) \cdot \hat{\boldsymbol{n}} = -\frac{B_{\mathrm{n}}}{V_{j\mathrm{n}}}\frac{r_j}{c}\frac{\mathrm{d}}{\mathrm{d}\xi}\left(\frac{1}{2}\boldsymbol{V}_{j\mathrm{t}}^2\right) = -\frac{m_j}{q_j}\frac{\mathrm{d}}{\mathrm{d}\xi}\left(\frac{1}{2}\boldsymbol{V}_{j\mathrm{t}}^2\right), \tag{IV-3.45}$$

a relation which is going to be used later. If the module of the transverse plasma velocity of species j is constant, then its convection electric field $E_{j\mathrm{n}}$ vanishes. Using Ampère's law from Eq. (IV-2.30) and the previous Eq. (IV-3.45), one can derive by vector cross multiplication of Eq. (IV-2.30) with $\hat{\boldsymbol{n}}$ and subsequent scalar multiplication with $\boldsymbol{B}_{\mathrm{t}}$ another conservation law:

$$\frac{\mathrm{d}}{\mathrm{d}\xi}\left(\sum_j \varrho_j \boldsymbol{V}_{j\mathrm{t}}^2 - \frac{1}{4\pi}\boldsymbol{B}_{\mathrm{t}}^2\right) = 0. \tag{IV-3.46}$$

If the integration constant is zero, this equation expresses equipartition between the transverse total particle kinetic energy and the transverse magnetic energy, like it is the case in a classical MHD Alfvén wave.

Now the equation for the transverse magnetic field is considered. By differentiation of Ampère's law, one can obtain a second-order nonlinear wave equation for the transverse magnetic field:

$$\frac{\mathrm{d}^2}{\mathrm{d}\xi^2}\hat{\boldsymbol{n}} \times \boldsymbol{B}_{\mathrm{t}} = \frac{4\pi}{c}\sum_j q_j\left(n_j\frac{\mathrm{d}\boldsymbol{V}_{j\mathrm{t}}}{\mathrm{d}\xi} + \boldsymbol{V}_{j\mathrm{t}}\frac{\mathrm{d}n_j}{\mathrm{d}\xi}\right). \tag{IV-3.47}$$

Here the skin depth or inertial length $\ell_j = c/\omega_j$ can be used again, the sum of which gives the total skin depth

$$\frac{1}{\ell_{\mathrm{S}}^2} \equiv \sum_j \frac{1}{\ell_j^2}, \tag{IV-3.48}$$

where each species brings in its own length scale ℓ_j. It is again convenient to introduce a second-order wave operator

$$\mathcal{D}_B \equiv \frac{\mathrm{d}^2}{\mathrm{d}\xi^2} - \frac{1}{\ell_{\mathrm{S}}^2}. \tag{IV-3.49}$$

Using this, one finally obtains a driven wave equation for the transverse magnetic field:

$$\mathcal{D}_B\boldsymbol{B}_{\mathrm{t}} = -\sum_j\left(\frac{B_{\mathrm{n}}}{V_{j\mathrm{n}}}\frac{1}{\ell_j^2}\boldsymbol{V}_{j\mathrm{t}} + \frac{1}{\lambda_j^2 c}(\hat{\boldsymbol{n}} \times \boldsymbol{V}_{j\mathrm{t}})\left[E_{\mathrm{n}} + \frac{1}{c}(\boldsymbol{V}_{j\mathrm{t}} \times \boldsymbol{B}_{\mathrm{t}}) \cdot \hat{\boldsymbol{n}}\right]\right). \tag{IV-3.50}$$

On the right-hand side, the transverse currents appear, and the longitudinal charge density variations and related electrostatic effects show up through the nonlinear electromotive force, which involves the longitudinal electric field. Note that this nonlinear driver contains the natural length scales (density dependent) of all the species involved. Of course, this wave equation seems, without further approximation, quite formal but elucidates the nature of the coupling of the unforced transverse magnetic field (dynamics described by

the operator $\mathcal{D}_B$) with the compressive electrostatic fluctuations and transverse plasma motions. When being decoupled from the plasma currents and electric-field (no charges) dynamics, this transverse magnetic field equation just describes the finite penetration of the magnetic field into the skin layer of the plasma and results in its exponential decline on the length scale ℓ_S. To gain better insight into the terms contributing to Eq. (IV-3.50), it may be rewritten also in the form

$$\mathcal{D}_B \boldsymbol{B}_t = -\sum_j \frac{1}{\ell_j^2}\left(\frac{B_n}{V_{jn}}\boldsymbol{V}_{jt} + \frac{c(E_n + E_{jn})}{c_j^2 - V_{jn}^2}(\hat{\boldsymbol{n}} \times \boldsymbol{V}_{jt})\right). \tag{IV-3.51}$$

Similarly one can also rewrite the driven wave equation for the longitudinal electric field in the concise form

$$\mathcal{D}_E E_n = \sum_j \frac{1}{\lambda_j^2} E_{jn}, \tag{IV-3.52}$$

reminding that E_{jn} can be derived after Eq. (IV-3.45) from a potential that is given by the transverse kinetic energy of species j. These two coupled nonlinear equations are completed and closed by Eq. (IV-3.39) for the density and Eq. (IV-3.44) for the transverse velocity of each species.

So far, neither any approximation nor linearization was made, but just the original momentum equations (IV-3.39) and (IV-3.44) have been inserted into the differentiated Ampère's and Gauß' laws. Therefore, the above equations still depend in a highly nonlinear manner on the different number densities n_j. Yet, the transition in Eqs. (IV-3.44) and (IV-3.51) to the incompressible limit is simple because then the electrostatic nonlinear forcing terms E_n and E_{jn} vanish, and the plasma frequency ω_j and the inertial length ℓ_j, respectively, become constants as defined by the fixed background density of species j. This is discussed in the section after the next one.

IV.4 Eigenmodes and driven waves

IV.4.1 Nonlinear Alfvén/ion-cyclotron waves

In order to maintain the linear form of the original equations, it is convenient to introduce new variables relating to left- and right-hand polarized fields, which are defined as follows:

$$\boldsymbol{B}_t^{\pm} = \boldsymbol{B}_t \pm (\hat{\boldsymbol{n}} \times \boldsymbol{B}_t)\,, \tag{IV-4.53}$$

$$\boldsymbol{V}_{jt}^{\pm} = \boldsymbol{V}_{jt} \pm \left(\hat{\boldsymbol{n}} \times \boldsymbol{V}_{jt}\right). \tag{IV-4.54}$$

These field variables are orthogonal, i.e., $\boldsymbol{B}_t^{\pm} \cdot \boldsymbol{B}_t^{\mp} = 0$ and $\boldsymbol{V}_{jt}^{\pm} \cdot \boldsymbol{V}_{jt}^{\mp} = 0$. By taking the cross product of Eqs. (IV-2.30) and (IV-3.44) with the unit vector $\hat{\boldsymbol{n}}$, one obtains after some algebra the equations of motion for the circular transverse variables:

$$\frac{\mathrm{d}\boldsymbol{B}_t^{\pm}}{\mathrm{d}\xi} = \pm\frac{4\pi}{c}\sum_j \varrho_{cj} \boldsymbol{V}_{jt}^{\mp}, \tag{IV-4.55}$$

$$\frac{\mathrm{d}\boldsymbol{V}_{j\mathrm{t}}^{\pm}}{\mathrm{d}\xi} = \mp\frac{1}{r_j}\left(\frac{V_{j\mathrm{n}}}{B_\mathrm{n}}\boldsymbol{B}_\mathrm{t}^{\mp} - \boldsymbol{V}_{j\mathrm{t}}^{\mp}\right). \tag{IV-4.56}$$

First, nonlinear incompressible solutions are considered now. Since $E_\mathrm{n} = 0$, consequently quasineutrality strictly holds, $\sum_j q_j n_j = 0$. The velocity fields and magnetic field must have constant modules and be aligned so that after Eq. (IV-3.45) their respective vector cross product, and thus also $E_{j\mathrm{n}}$ vanishes. As n_j, r_j, $V_{j\mathrm{n}}$, c_j, and ω_j then all are constant, one can solve the resulting linear set Eqs. (IV-4.55) and (IV-4.56) by Fourier transformation, here indicated by the tilde sign, without putting any limitations on the amplitudes of $\boldsymbol{B}_\mathrm{t}^{\pm}$ or $\boldsymbol{V}_{j\mathrm{t}}^{\pm}$ other than from Eq. (IV-3.46), which implies that the magnetic field amplitude is also constant. As usually, Fourier transform means that $\mathrm{d}/\mathrm{d}\xi \to ik$, and thus one can invert the transverse momentum equation (IV-3.44), which yields with the normalized wavevector $\kappa_j \equiv kV_{j\mathrm{n}}/\Omega_j$ the complex vector relation

$$\tilde{\boldsymbol{V}}_{j\mathrm{t}}(k) = \frac{V_{j\mathrm{n}}}{B_\mathrm{n}\left(1-\kappa_j^2\right)}\left(\tilde{\boldsymbol{B}}_\mathrm{t}(k) + i\kappa_j\hat{\boldsymbol{n}}\times\tilde{\boldsymbol{B}}_\mathrm{t}(k)\right). \tag{IV-4.57}$$

This result can be inserted into the Fourier transform of Eq. (IV-3.51) to obtain the algebraic wave equation

$$\left(k^2 + \frac{1}{\ell_\mathrm{S}^2}\right)\tilde{\boldsymbol{B}}_\mathrm{t}(k) = \sum_j \frac{1}{\ell_j^2}\frac{1}{1-\kappa_j^2}\left(\tilde{\boldsymbol{B}}_\mathrm{t}(k) + i\kappa_j(\hat{\boldsymbol{n}}\times\tilde{\boldsymbol{B}}_\mathrm{t}(k))\right), \tag{IV-4.58}$$

which may also be written as

$$\left(k^2 - \sum_j \frac{1}{\ell_j^2}\frac{\kappa_j^2}{1-\kappa_j^2}\right)\tilde{\boldsymbol{B}}_\mathrm{t}(k) = i\left(\sum_j \frac{1}{\ell_j^2}\frac{\kappa_j}{1-\kappa_j^2}\right)(\hat{\boldsymbol{n}}\times\tilde{\boldsymbol{B}}_\mathrm{t}(k)), \tag{IV-4.59}$$

and which yields, by taking the vector cross product of Eq. (IV-4.59) with $\hat{\boldsymbol{n}}$ and by resolving the resulting two equations, the two dispersion relations describing left- and right-hand polarized waves as follows:

$$k^2 = \sum_j \left(\frac{\omega_j}{c}\right)^2 \frac{\pm\kappa_j}{1\mp\kappa_j} = \sum_j \hat{\varrho}_j\left(\frac{\Omega_j}{V_\mathrm{A}}\right)^2 \frac{\pm\kappa_j}{1\mp\kappa_j} \tag{IV-4.60}$$

with the fractional mass density $\hat{\varrho}_j = \varrho_j/\varrho$. Eq. (IV-4.60) is nothing else but the standard dispersion relation for the Alfvén/ion-cyclotron (and fast/whistler) waves in a multicomponent plasma with the differential drifts contained in $V_{j\mathrm{n}}$ and for parallel propagation (see e.g., Davidson, 1983), yet which applies here to arbitrarily large wave amplitudes. Apparently the wave frequency is obtained by the Doppler shift formula $\omega = kV$, where V is hidden in $V_{j\mathrm{n}} = U_{j\mathrm{n}} - V$, i.e., in $\kappa_j \equiv kV_{j\mathrm{n}}/\Omega_j$. Once the wavevector $k = k(V)$ is known, the wave frequency is obtained as a function of the phase speed V.

The long-wavelength limit of Eq. (IV-4.60) is considered, which when being expanded to second order in κ_j reads

$$1 = \sum_j \hat{\varrho}_j\left(\frac{\Omega_j}{kV_\mathrm{A}}\right)^2\left(\pm\kappa_j\right)\left(1\pm\kappa_j\right), \tag{IV-4.61}$$

where the first term of the sum vanishes since $\sum_j \left(\omega_j^2/\Omega_j\right) V_{j\mathrm{n}} = 0$ because of the quasi-neutrality condition, i.e., $\varrho_\mathrm{c} = 0$ in Eq. (IV-2.2) and the zero-longitudinal-current constraint (IV-2.26). The second term then yields

$$1 = \sum_j \hat{\varrho}_j \frac{(U_{j\mathrm{n}}^2 - 2U_{j\mathrm{n}}V + V^2)}{V_\mathrm{A}^2}. \tag{IV-4.62}$$

As a vanishing bulk speed $\boldsymbol{U} = 0$ may be assumed, the center-of-momentum condition means that $\sum_j \hat{\varrho}_j U_{j\mathrm{n}} = 0$, and thus one can solve for the phase speed in the center of momentum frame and obtains

$$V = \pm V_\mathrm{A} \sqrt{1 - \sum_j \hat{\varrho}_j \left(\frac{U_{j\mathrm{n}}}{V_\mathrm{A}}\right)^2}. \tag{IV-4.63}$$

This is the phase speed of an Alfvén wave in a multi-component plasma including field-aligned drift motions leading to a slowing down of the phase speed.

Now the incompressible A/IC wave shall be derived without resort to the Fourier transformation but instead recoursing on Eq. (IV-3.45). Since $E_{j\mathrm{n}} = 0$, each velocity vector and magnetic field must be aligned, which generally implies that $\boldsymbol{V}_{j\mathrm{t}} = a_j \boldsymbol{B}_\mathrm{t}$. This can be inserted in Eq. (IV-3.44) to obtain

$$\frac{\mathrm{d}\boldsymbol{V}_{j\mathrm{t}}}{\mathrm{d}\xi} = \frac{1}{r_j}\left(\frac{V_{j\mathrm{n}}}{B_\mathrm{n} a_j} - 1\right) \hat{\boldsymbol{n}} \times \boldsymbol{V}_{j\mathrm{t}}. \tag{IV-4.64}$$

Twofold differentiation yields the simple harmonic oscillator equation for the gyromotion:

$$\left(\frac{\mathrm{d}^2}{\mathrm{d}\xi^2} + k_j^2\right) \boldsymbol{V}_{j\mathrm{t}} = 0 \tag{IV-4.65}$$

with the squared wavevector defined as

$$k_j^2 = \frac{1}{r_j^2}\left(\frac{V_{j\mathrm{n}}}{B_\mathrm{n} a_j} - 1\right)^2. \tag{IV-4.66}$$

Since all species must spatially oscillate in the same way, the wavevector must not depend on the index j, i.e., one can put $k_j = \pm k$, which yields with $\kappa_j = k r_j$ two possible solutions for the desired proportionality coefficient:

$$a_j = \frac{V_{j\mathrm{n}}}{B_\mathrm{n}} \frac{1}{1 \pm \kappa_j}. \tag{IV-4.67}$$

Knowing the coefficient a_j, it can be used in the wave equation (IV-3.51) without electric fields yielding another harmonic oscillator equation:

$$\left(\frac{\mathrm{d}^2}{\mathrm{d}\xi^2} + q^2\right) \boldsymbol{B}_\mathrm{t} = 0, \tag{IV-4.68}$$

where the squared wavevector q^2 is an abbreviation for exactly the same sum as appearing on the right hand side of Eq. (IV-4.60). Since all velocities and the magnetic field

are aligned, the wavevector q must be equal to k, and thus one again obtains the same dispersion relation as in the previous Fourier analysis. Finally, the polarization relation (with the plus sign for incompressible A/IC and minus for F/W waves) reads

$$\boldsymbol{V}_{j\mathrm{t}} = \frac{V_{j\mathrm{n}}}{B_\mathrm{n}} \frac{1}{1 \pm \kappa_j} \boldsymbol{B}_\mathrm{t}. \tag{IV-4.69}$$

With this result, the conservation law (IV-3.46) can be evaluated further, and after some algebra the result is obtained that

$$\frac{\mathrm{d}}{\mathrm{d}\xi} \left(\sum_j \hat{\varrho}_j V_{j\mathrm{n}}^2 \frac{1}{\left(1 \pm \kappa_j\right)^2} - V_\mathrm{A}^2 \right) = 0. \tag{IV-4.70}$$

Note that the dispersion relation (IV-4.60) can also be cast into the form

$$V_\mathrm{A}^2 = \sum_j \hat{\varrho}_j V_{j\mathrm{n}}^2 \frac{\mp \kappa_j}{\kappa_j^2 \left(1 \pm \kappa_j\right)}, \tag{IV-4.71}$$

which facilitates a comparison with the previous equation. Expansion of Eqs. (IV-4.70) and (IV-4.71) to lowest order in $\kappa_j = k r_j$ yields the MHD dispersion relation (IV-4.62), i.e., in this case, the conservation equation (IV-4.70) has a zero integration constant and simply expresses equipartition between kinetic and magnetic energy densities. This is not true any more if effects due to the finite gyromotion are considered.

IV.4.2 Linear electrostatic waves

Pure linear electrostatic waves are discussed now, which are obtained by taking the trivial solutions $\boldsymbol{V}_{j\mathrm{t}} = \boldsymbol{B}_\mathrm{t} = 0$ of the wave equation (IV-3.51), which also implies that $E_{j\mathrm{n}} = 0$. Then the linearized electrostatic wave equation (IV-3.52) simply reads $\mathcal{D}_E E_\mathrm{n} = 0$. After Fourier transformation, one obtains that $(k^2 + \lambda_\mathrm{D}^{-2}) \tilde{E}_\mathrm{n}(k) = 0$, which explicitly yields the dispersion relation

$$k^2 = \sum_j \frac{\omega_j^2}{\left(U_{j\mathrm{n}} - V\right)^2 - c_j^2}. \tag{IV-4.72}$$

Only the case of zero drifts may be considered here, i.e., $U_{j\mathrm{n}} = 0$ and a simple electron-proton plasma. Then one always finds two solutions for V^2 from the equation

$$k^2 = \frac{\omega_\mathrm{e}^2}{V^2 - c_\mathrm{e}^2} + \frac{\omega_\mathrm{p}^2}{V^2 - c_\mathrm{p}^2}. \tag{IV-4.73}$$

In the long-wavelength limit ($k \to 0$), the diverging phase speed $V_\mathrm{L}(k) = \omega_\mathrm{P}/k$ corresponds to the Langmuir wave with the total plasma frequency being defined by $\omega_\mathrm{P}^2 \equiv \omega_\mathrm{e}^2 + \omega_\mathrm{p}^2$. For the ion-acoustic or sound wave, the constant speed is found as

$$V_\mathrm{S} = \sqrt{\frac{\omega_\mathrm{e}^2 c_\mathrm{p}^2 + \omega_\mathrm{p}^2 c_\mathrm{e}^2}{\omega_\mathrm{P}^2}} = \sqrt{\frac{k_\mathrm{B}(\gamma_\mathrm{e} T_\mathrm{e} + \gamma_\mathrm{p} T_\mathrm{p})}{m_\mathrm{e} + m_\mathrm{p}}}. \tag{IV-4.74}$$

The general solution in terms of frequency follows from the biquadratic equation

$$\omega^4 - \omega^2\left(\omega_\mathrm{e}^2 + \omega_\mathrm{p}^2 + (c_\mathrm{e}k)^2 + (c_\mathrm{p}k)^2\right) + (c_\mathrm{e}k)^2(c_\mathrm{p}k)^2 + \omega_\mathrm{e}^2(c_\mathrm{p}k)^2 + \omega_\mathrm{p}^2(c_\mathrm{e}k)^2 = 0. \quad \text{(IV-4.75)}$$

In the short-wavelength limit ($k \to \infty$), two solutions are obtained corresponding to the proton-acoustic wave with $\omega \approx kc_\mathrm{p}$ or electron-acoustic wave with $\omega \approx kc_\mathrm{e}$. Both modes are usually strongly Landau damped if a thermal Vlasov description of the plasma is used. The sound wave, however, can exist since $m_\mathrm{e} \ll m_\mathrm{p}$ and thus $V_\mathrm{S} \approx \sqrt{k_\mathrm{B}\gamma_\mathrm{e}T_\mathrm{e}/m_\mathrm{p}}$ for $T_\mathrm{e} > T_\mathrm{p}$ so that strong proton Landau damping can be avoided.

For a multi-component plasma with drifts, the structure of the eigenmodes becomes correspondingly richer as each species contributes its own plasma frequency and thermal speed as well as drift speed. In the presence of a compressive transverse wave, these modes all become coupled and are driven by the nonlinear ponderomotive electric fields $E_{j\mathrm{n}}$ according to Eq. (IV-3.52). Similarly the transverse eigenmodes defined by Eq. (IV-4.60) are driven according to Eq. (IV-3.51) by the longitudinal electric field E_n and the combined action of the various $E_{j\mathrm{n}}$.

IV.4.3 Compressive Alfvén/ion-cyclotron–acoustic waves

In this section, the coupling between the nonlinear electromagnetic A/IC waves and the electrostatic modes is considered. It is important to recall that no assumptions, such as incompressibility, had to be made as to derive the wave equations (IV-3.51) and (IV-3.52). Also the transverse momentum equation (IV-3.44) shall be rewritten, which describes the gyromotion as a second-order wave equation. Since the longitudinal gyration scale r_j depends on the density according to Eq. (IV-2.34), its differentiation has to be considered. If the magnetic field is neglected for a moment, then one gets for the transverse motion an equation in the form

$$\left(\frac{\mathrm{d}^2}{\mathrm{d}\xi^2} + \frac{1}{r_j^2} - \frac{\mathrm{d}\ln n_j}{\mathrm{d}\xi}\frac{\mathrm{d}}{\mathrm{d}\xi}\right)\boldsymbol{V}_{j\mathrm{t}} = 0. \quad \text{(IV-4.76)}$$

Mathematically speaking, this is the well known equation for a harmonic oscillator with an amplitude that may vary exponentially in ξ at a scale set by the density gradient length. For the differential operator yielding harmonic oscillations (first two terms of Eq. (IV-4.76)), the symbol $\mathcal{D}_{V_j}$ is introduced to be used below. For the density gradient term, one may approximately write

$$\frac{\mathrm{d}}{\mathrm{d}\xi}\ln n_j = \frac{\mathrm{d}}{\mathrm{d}\xi}\ln(\bar{n}_j + \delta n_j) \approx \frac{1}{\bar{n}_j}\frac{\mathrm{d}}{\mathrm{d}\xi}\delta n_j = \frac{\delta n_j}{\bar{n}_j}\frac{\mathrm{d}\ln\delta n_j}{\mathrm{d}\xi} \quad \text{(IV-4.77)}$$

with the averaged constant background density $\bar{n}_j$. If the gradient is positive (negative), and therefore the density increases (decreases), the longitudinal scale, and thus the amplitude of $\boldsymbol{V}_{j\mathrm{t}}$ will decrease (increase) correspondingly. However, as long as the relative density variation remains small, a few percent say, this change will occur on a much larger scale than r_j, namely $\bar{L}_j \equiv r_j\bar{n}_j/\delta n_j$. If the density fluctuates about zero, the net effect of the density modulation on $\boldsymbol{V}_{j\mathrm{t}}$ will remain comparatively small.

For the sake of consistency in the remainder of this section, this density-induced possible amplitude variation of $\boldsymbol{V}_{j\mathrm{t}}$ according to Eq. (IV-4.76) will be fully retained, but later

on the density variations will be neglected and all density-dependent parameters considered to be fixed at their background values without denoting them explicitly by a barred symbol. Yet, remember that the essential and lowest-order variations of the densities of all species have been considered and already taken care of in Gauß' law and the dynamics of E_n, which indeed is of order unity as the background electric field is zero and similarly in Ampère's law through the appearance of the electric fields E_n and $E_{j\mathrm{n}}$.

By using conserved or constant quantities, normalized variables are introduced now such that $\boldsymbol{v}_{j\mathrm{t}} \equiv \boldsymbol{V}_{j\mathrm{t}}/V$ and $\boldsymbol{b}_\mathrm{t} \equiv \boldsymbol{B}_\mathrm{t}/B_\mathrm{n}$. Similarly normalized electric fields are introduced as follows:

$$e_{j\mathrm{n}} \equiv \frac{cE_{j\mathrm{n}}}{B_\mathrm{n}V}, \qquad e_\mathrm{n} \equiv \frac{cE_\mathrm{n}}{B_\mathrm{n}V}. \tag{IV-4.78}$$

According to Eq. (IV-3.51), the field $e_{j\mathrm{n}}$ is just an abbreviation for the gradient of a potential given by the transverse kinetic energy, for which one has the normalized form

$$e_{j\mathrm{n}} = -\frac{V}{\Omega_j}\frac{\mathrm{d}}{\mathrm{d}\xi}\left(\frac{1}{2}\boldsymbol{v}_{j\mathrm{t}}^2\right). \tag{IV-4.79}$$

Using the same normalization for the transverse electric field from Eq. (IV-2.23), one simply obtains that

$$\boldsymbol{e}_\mathrm{t} = -(\hat{\boldsymbol{n}} \times \boldsymbol{b}_\mathrm{t}), \tag{IV-4.80}$$

which is fully determined by the solution for $\boldsymbol{b}_\mathrm{t}$. Like $\boldsymbol{e}_\mathrm{t}$, the charge densities $\varrho_{\mathrm{c}j}$ are now merely auxiliary quantities and obtained from an integration of the previous equation (IV-3.39), which in the new variables can be written as

$$r_j\frac{\mathrm{d}}{\mathrm{d}\xi}\ln\varrho_{\mathrm{c}j} = (e_\mathrm{n} + e_{j\mathrm{n}})\frac{VV_{j\mathrm{n}}}{c_j^2 - V_{j\mathrm{n}}^2} \tag{IV-4.81}$$

and then be formally integrated with the result

$$\varrho_{\mathrm{c}j}(\xi) = q_j\bar{n}_j\exp\left(V\Omega_j\int_{\bar{\xi}}^{\xi}\mathrm{d}\xi'\,\frac{e_\mathrm{n}(\xi') + e_{j\mathrm{n}}(\xi')}{c_j^2(\xi') - V_{j\mathrm{n}}^2(\xi')}\right). \tag{IV-4.82}$$

As an outcome of all the above considerations, the resulting set of fluid wave equations can now be summarized. Firstly, for each species' transverse motion, a forced and amplitude-modulated harmonic oscillator equation is obtained reading

$$\mathcal{D}_{V_j}\boldsymbol{v}_{j\mathrm{t}} = \left(\frac{V^2}{c_j^2 - V_{j\mathrm{n}}^2}(e_\mathrm{n} + e_{j\mathrm{n}})\frac{\mathrm{d}\boldsymbol{v}_{j\mathrm{t}}}{\mathrm{d}\xi} + \frac{1}{r_j}\boldsymbol{b}_\mathrm{t} + \frac{\mathrm{d}}{\mathrm{d}\xi}\hat{\boldsymbol{n}} \times \boldsymbol{b}_\mathrm{t}\right)\frac{\Omega_j}{V}. \tag{IV-4.83}$$

Secondly, one can rewrite the mutually driven and coupled wave equations for the longitudinal electric field and transverse magnetic field in the concise forms

$$\mathcal{D}_E e_\mathrm{n} = \sum_j \frac{1}{\lambda_j^2}e_{j\mathrm{n}}, \tag{IV-4.84}$$

$$\mathcal{D}_B \boldsymbol{b}_\mathrm{t} = -\sum_j \frac{1}{\ell_j^2}\left(\frac{V}{V_{j\mathrm{n}}}\boldsymbol{v}_{j\mathrm{t}} + \frac{V^2}{c_j^2 - V_{j\mathrm{n}}^2}(e_\mathrm{n} + e_{j\mathrm{n}})(\hat{\boldsymbol{n}} \times \boldsymbol{v}_{j\mathrm{t}})\right). \tag{IV-4.85}$$

It is worth to remember that, up to this point of the algebraic derivations, no linearization has been made, and the density variations have been entirely accounted for. Eqs. (IV-4.81) or (IV-4.82) permit to calculate the density of species j completely through the line integral over the electric fields that appear in the exponential Boltzmann factor in Eq. (IV-4.82). So the density is a functional of the electric potentials. However, this dependence of n_j on ξ may now, without loss of essential physics, be neglected if the density fluctuations can be assumed to remain small (i.e., MHD shocks (Goossens, 2003) or electrostatic shocks and double layers are not considered here). Thus, all scales and parameters such as $V_{j\mathrm{n}}, c_j, \omega_j, \lambda_j, \ell_j$, and r_j, which have non-vanishing mean values, will from here on be calculated by use of the background number density $\bar{n}_j$ as well as the conditions for quasi-neutrality and zero longitudinal current and the center-of-momentum condition. All compressive effects are described by the longitudinal electric field e_n in this approximation. Consequently the nonlinear equations (IV-4.83), (IV-4.84), and (IV-4.85) form a closed set, which yet will generally require a numerical treatment to obtain solutions.

Note that, in each of these equations, the spatial variations are determined by the natural scales of the dynamics of the involved field variables, i.e., by the longitudinal scale r_j for the transverse motions of the particles, their Debye lengths λ_j for the charge fluctuations, respectively, and their skin depths ℓ_j for the magnetic field penetration into the plasma driven by the transverse currents. Differential motion of the species j might be important and is therefore included in its drift speed $V_{j\mathrm{n}}$. Its effect on the parametric instabilities has been studied, addressing the modulational and decay instability of Alfvén waves by considering streaming of alpha particles in the solar wind (Hollweg *et al.*, 1993). If there are no differential motions along the mean field in the background plasma, i.e., if for all j the normal velocity $U_{j\mathrm{n}} = 0$, then $V_{j\mathrm{n}} = -V$, and thus the longitudinal gyration scale simply becomes $r_j = -V/\Omega_j$, which by its definition is not for each species a positive definite quantity as the gyrofrequency carries the sign of the charge of the species considered. The factor in front of the electric field term in the above Eqs. (IV-4.83) and (IV-4.85) thus changes in the drift-free case to $1/(1-(c_j/V)^2)$, which becomes $1/(1-\beta_j)$ for $V = V_\mathrm{A}$ with the species plasma beta being here defined as $\beta_j = (c_j/V_\mathrm{A})^2$. For the parallel propagation considered here, only this factor contains the thermal speed, and therefore this factor simply becomes unity for a cold multi-species plasma without drifts.

IV.4.4 Electric field fluctuations driven by an elliptically polarized Alfvén wave

In this section, electrostatic waves are considered, which can be generated by an elliptically polarized Alfvén wave, which for the sake of simplicity is assumed to be given. Then the effect, this wave has in generating compressive fluctuations driven by the spatial variation of the kinetic energy of the particles moving coherently in the same wave magnetic field, shall be studied. The starting point is Eq. (IV-4.84), which can with the help of

Eq. (IV-4.79) be written as a driven oscillator equation for the longitudinal electric field:

$$\mathcal{D}_E e_\mathrm{n} = -\sum_j \frac{V}{2\Omega_j}\frac{1}{\lambda_j^2}\frac{\mathrm{d}v_{j\mathrm{t}}^2}{\mathrm{d}\xi}. \tag{IV-4.86}$$

Before the wave fields are written down, a proper coordinate system shall be defined. For the right-handed orthogonal system, the unit vectors $\hat{\boldsymbol{n}} = \boldsymbol{e}_3 = \boldsymbol{e}_1 \times \boldsymbol{e}_2$, $\boldsymbol{e}_1 = \boldsymbol{e}_2 \times \hat{\boldsymbol{n}}$, and $\boldsymbol{e}_2 = \hat{\boldsymbol{n}} \times \boldsymbol{e}_1$ are chosen. The wave may have a wavenumber k, and its normalized (dimensionless) magnetic field reads

$$\boldsymbol{b}_\mathrm{t} = b_1\boldsymbol{e}_1\cos(k\xi) + b_2\boldsymbol{e}_2\sin(k\xi). \tag{IV-4.87}$$

Similarly the related flow velocity of species j is given by

$$\boldsymbol{v}_{j\mathrm{t}} = v_{j1}\boldsymbol{e}_1\cos(k\xi) + v_{j2}\boldsymbol{e}_2\sin(k\xi). \tag{IV-4.88}$$

The associated electric field according to Eq. (IV-4.86) reads

$$e_{j\mathrm{n}} = \frac{kV}{\Omega_j}\cos(k\xi)\sin(k\xi)\left(v_{j1}^2 - v_{j2}^2\right). \tag{IV-4.89}$$

On the other hand, using the original definition (IV-3.45) of this field, the result

$$e_{j\mathrm{n}} = \cos(k\xi)\sin(k\xi)(b_2 v_{j1} - b_1 v_{j2}) \tag{IV-4.90}$$

is obtained, which, by comparison of the last two equations, determines the particle velocity components as $v_{j1,2} = b_{2,1}\Omega_j/(kV)$. Finally, one has

$$e_{j\mathrm{n}} = \frac{\Omega_j}{2kV}\sin(2k\xi)\left(b_1^2 - b_2^2\right), \tag{IV-4.91}$$

which can be inserted in Eq. (IV-4.84). The forced oscillator equation

$$\frac{\mathrm{d}^2 e_\mathrm{n}}{\mathrm{d}\xi^2} + q^2 e_\mathrm{n} = \varepsilon\frac{\sin(2k\xi)}{2k} \tag{IV-4.92}$$

is obtained. The Debye length λ_D was defined in Eq. (IV-3.41). As an abbreviation, the complex wavevector $q \equiv i/\lambda_\mathrm{D}$ is used, and furthermore the forcing amplitude is introduced as

$$\varepsilon = \sum_j \frac{1}{\lambda_j^2}\frac{\Omega_j}{V}(b_1^2 - b_2^2), \tag{IV-4.93}$$

which vanishes for a circularly polarized wave with $b_1 = b_2$ but is non-zero otherwise. The solution of Eq. (IV-4.92) can be obtained by using the Green's function method and Fourier transformation. The Green's function $G(\xi)$ for the differential operator in Eq. (IV-4.92) has to fulfill the general condition

$$\frac{\mathrm{d}^2 G}{\mathrm{d}\xi^2} + q^2 G = \delta(\xi). \tag{IV-4.94}$$

In Fourier space, it is given by

$$G = \frac{1}{\sqrt{2\pi}} \frac{1}{q^2 - k^2}. \tag{IV-4.95}$$

This function can be back-transformed to real space according to

$$G(\xi) = \frac{1}{2\pi} \int \frac{e^{ik\xi}}{q^2 - k^2} \mathrm{d}k = \frac{1}{q} \left[\frac{e^{iq\xi} - e^{-iq\xi}}{2i} \right] = \frac{\sin(q\xi)}{q}, \tag{IV-4.96}$$

where the Cauchy integration according to the residue theorem is used at the two poles of the integrand at $k = \pm q$.

The convolution integral of the forcing term with the Green's function then yields the solution depending upon ξ in the form of another convolution integral, which can be calculated analytically with the (in q symmetric) result

$$\begin{aligned} e_\mathrm{n}(\xi) = G(\xi) * \varepsilon \frac{\sin(2k\xi)}{2k} &= \frac{\varepsilon}{2kq} \int_0^\xi \sin\left(q(\xi - \xi')\right) \sin(2k\xi') \mathrm{d}\xi' \\ &= \frac{\varepsilon}{4kq} \left(\frac{\sin(2k\xi) + \sin(q\xi)}{2k + q} - \frac{\sin(2k\xi) - \sin(q\xi)}{2k - q} \right). \end{aligned} \tag{IV-4.97}$$

Eq. (IV-4.97) solves the original Eq. (IV-4.92), which can easily be shown by straightforward differentiation. By definition, the square of the wavevector $q = q(V)$ is given by the right-hand side of the electrostatic dispersion relation (IV-4.72). Therefore, q is a real number for an appropriate choice of V. The solution is then related naturally with the electrostatic eigenmodes, i.e., the sound, ion-acoustic, and Langmuir waves, which was already discussed in a previous section. The overall solution (IV-4.97) apparently describes forced compressive (charge) waves occurring as electrostatic eigenmodes and a superposed electric wave at the second harmonic of the transverse Alfvén pump wave, the anisotropy (due to its elliptic polarization) of which determines the amplitude of these driven longitudinal electric field oscillations. L'Hôpital's rule allows one to determine the behavior in the resonant cases. For the resonances ($q \to \pm 2k$), one finds

$$e_\mathrm{n}(\xi) = -\frac{\varepsilon}{2q^2} \left[\xi \cos(q\xi) - \frac{\sin(q\xi)}{q} \right], \tag{IV-4.98}$$

which corresponds to the amplitude of the compressible oscillation growing or decaying with ξ, i.e., an instability in space. The spatial evolution of e_n for the resonant and the non-resonant case is shown in Fig. IV-1.

IV.5 Discussion

Starting from the multi-fluid equations of a warm plasma, the coupled wave equations for the particles' gyromotions about the mean field, for the transverse magnetic field, and for the longitudinal electric field have been derived and investigated. The nonlinear coupling is a natural outcome of the electromotive forces arising from compressive A/IC

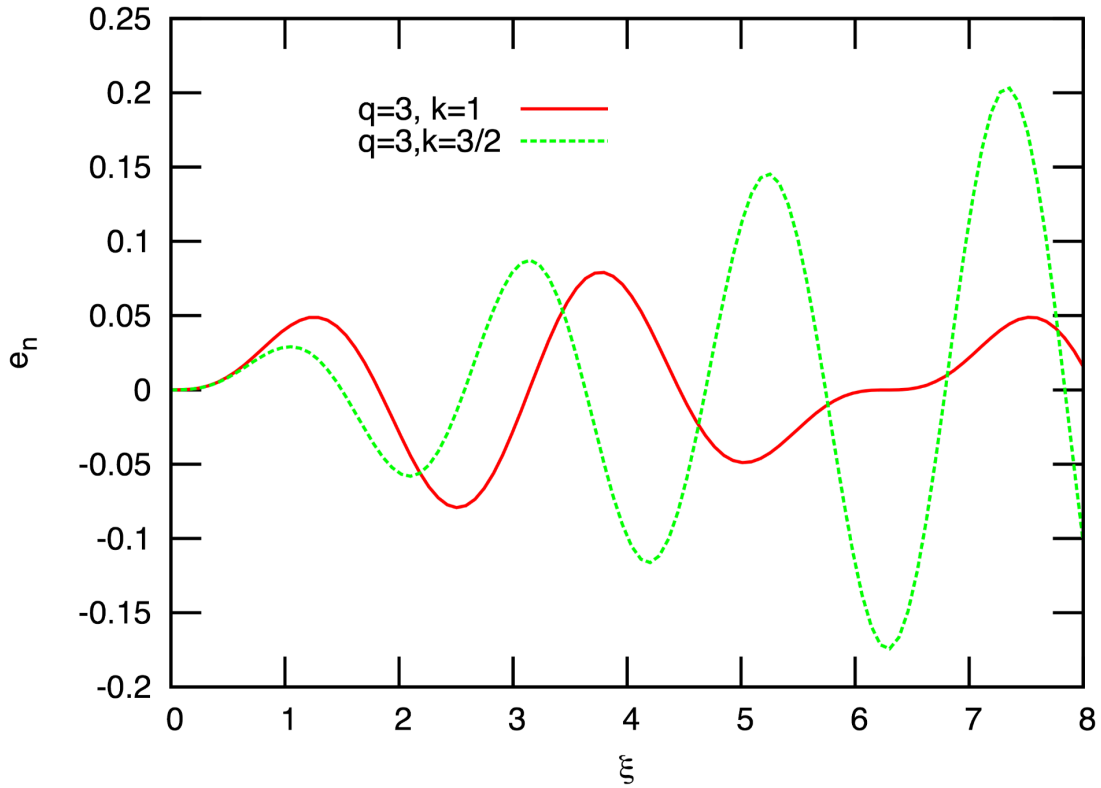

Figure IV-1: Non-resonant and resonant evolution of e_{n} in an elliptically polarized wave field. The parameters are $\varepsilon = 0.3$ and $q = 3$. In the non-resonant case, the wavenumber of the background wave is set to $k = 1$, in the resonant case to $k = q/2 = 3/2$. The linear growth of the amplitude is visible. The non-resonant wave does not grow.

waves and can be derived from a potential that is just the kinetic energy associated with the gyromotion in the electromagnetic wave. Electric waves are, thus, excited, which can react back on the pump wave by nonlinear effects through terms in its own wave equation, which contains the electric field explicitly. Known limiting cases are reproduced such as the standard linear electric waves like the ion-acoustic or Langmuir waves of course and for the transverse magnetic field the usual two branches of A/IC and F/W waves in case of a two-component electron-proton plasma or many similar related branches in the case of a multi-ion plasma. The main result of this chapter is the closed set of second-order wave equations (IV-4.83), (IV-4.84), and (IV-4.85), from solutions of which the transverse electric field and charge densities of each species can be derived as auxiliary quantities. To find their nonlinear solutions is left as a future task, which will presumably require a numerical treatment. The equations are studied in Chapt. V in the frame of a perturbation analysis.

The structure of the equations already permits to derive some qualitative conclusions and to treat some simple applications (like the effect of elliptical polarization) analytically. Further study is certainly required to corroborate them quantitatively. Apparently the weakly-compressive large-amplitude A/IC waves can drive electric fluctuations along the mean field, essentially of the ion-acoustic type, and thus will naturally produce an electric

field that can accelerate particles and will lead to heating via Landau damping in a kinetic Vlasov description. By excitation of acoustic waves, the amplitude of the driver wave will be diminished until a dynamic wave–wave equilibrium is reached. Similar processes are clearly found in direct numerical simulations (Araneda *et al.*, 2008, 2009; Valentini *et al.*, 2008; Valentini and Veltri, 2009). The third-order coupling terms in Eqs. (IV-4.83) and (IV-4.85) correspond to such three-wave processes in Fourier space and therefore will lead to cascading of spectral energy and broadening of the original spectrum of the pump wave, which is not necessarily monochromatic. This way, a new path towards micro- and macro-turbulence could be opened, and a non-MHD cascade is rendered possible by these compressive A/IC–acoustic wave interactions.

V Compressive high-frequency waves riding on an Alfvén/ion-cyclotron wave in a multi-fluid plasma

The following chapter has been published in wide parts before submission of the thesis. The copyright holder of the pre-publication is Cambridge University Press, and the cited parts are reprinted with permission. The reference of the published article is:

Daniel Verscharen and Eckart Marsch: *Compressive high-frequency waves riding on an Alfvén/ion-cyclotron wave in a multi-fluid plasma*, J. Plasma Phys. 77, 693-707, 2011, doi:10.1017/S0022377811000080.

V.1 Resonances, compressibility, and parametric decay of nonlinear Alfvén waves

The plasma waves in the solar wind can be understood as riding on a varying background due to the broad spectrum of different wave modes. Here weakly-compressive high-frequency plasma waves are studied, which are superposed on a large-amplitude Alfvén wave in a multi-fluid plasma consisting of protons, electrons, and alpha particles like in the solar wind. The term 'high-frequency wave' refers to the wavenumber regime around the inverse ion inertial length ℓ_p in contrast to the non-dispersive low-frequency MHD limit.

It is worth to repeat from Chapt. II that there are two important kinetic resonances that can lead to dissipative heating of a plasma by wave–particle interactions with waves that propagate parallel to the background magnetic field. The first is Landau resonance, requiring a parallel wave electric field, and the second is cyclotron resonance (e.g., Akhiezer *et al.*, 1975; Hollweg and Isenberg, 2002), which couples to the perpendicular wave electric field. The condition for Landau resonance is given by $kv_\parallel - \omega = 0$, where k denotes the parallel wave number, $v_\parallel$ the particle velocity in the direction parallel to the background magnetic field, and ω the wave frequency. This effect can lead to parallel heating of the particles (Lehe *et al.*, 2009). In a low-beta plasma such as the solar corona, it is difficult to fulfill this condition if the wave phase speed is close to the Alfvén speed because $v_\mathrm{th} \ll V_\mathrm{A}$ (Chandran *et al.*, 2010a).

The cyclotron resonance is connected with the transverse electromagnetic field, and the resonance condition is given by $kv_\parallel - \omega - n\Omega_j = 0$, where n is an integer and Ω_j is the particle gyrofrequency (only $n = \pm 1$ is allowed in the case of parallel propagation).

This resonance can lead to pitch-angle diffusion, which is indeed observed in solar wind protons (see Chapt. I). The perpendicular fluctuations must have high wavenumbers in the range of the inverse gyroradius to fulfill the resonance condition. Alfvén/ion-cyclotron (A/IC) waves are possible candidates for waves that can undergo this kind of interaction. However, their origin and evolution are not fully understood, even though their existence in the solar wind was recently proven. Indirect evidence for Alfvén-cyclotron heating was already referred to by several authors beforehand from simulations (Gary *et al.*, 2005b) and proton in-situ observations (Marsch and Tu, 2001; Kasper *et al.*, 2008).

The role of weakly-compressive waves in the different phenomena of plasma heating is currently under wide discussion (Tu and Marsch, 1994; Chandran, 2005; Bale *et al.*, 2005; Kellogg *et al.*, 2006; Chandran *et al.*, 2009; Verdini *et al.*, 2010). Especially, kinetic Alfvén waves (KAWs) have come into the focus of the debate because they are both transverse and compressive. However, several problems also arise from this interpretation of solar wind fluctuations, especially at high wavenumbers (Podesta *et al.*, 2010).

It has also been known for a long time that compressibility plays a major role in the context of the parametric instabilities of large-amplitude waves (Galeev and Oraevskii, 1963; Goldstein, 1978; Lashmore-Davies and Stenflo, 1979; Stenflo and Shukla, 2007). These instabilities are always connected with compressive components of the daughter-wave products. The subsequent analysis is based on the previous derivations in Chapt. IV, which treat the density fluctuations in terms of the longitudinal electrostatic field and a ponderomotive electric field. The relation between density fluctuations and ponderomotive forces in the context of parametric instabilities was discussed before by Sharma and Shukla (1983) for many different wave modes. However, the work of those authors was focused on frequencies around the upper-hybrid frequency, which is much higher than the frequencies considered here and hence beyond the scope of this work. Electromagnetic circularly polarized waves can also be generated from the high-frequency side. For example, Murtaza and Shukla (1984) discussed how an upper-hybrid wave can generate such waves in a two-fluid model. For this purpose, electrostatic effects and ponderomotive forces had to be included in the model describing the high-frequency pump wave. The importance of electrons in the decay of compressional Alfvén waves was discussed more recently by Brodin *et al.* (2008) in terms of the Hall-MHD description. These authors found a new decay channel for oblique daughter waves and discovered that the wave decay products could grow on scales around the ion inertial length. They also discussed the role of kinetic Alfvén waves as decay products and their possible ability to heat the plasma.

The present chapter concentrates on purely parallel wave propagation, but the role of both electrostatic and electromagnetic components of the wave modes in a multi-fluid plasma are considered. The nonlinear coupling of the longitudinal electrostatic field and of the ponderomotive electric fields with the transversal electromagnetic wave fields is the main reason for the significant changes that are found in the mode structure and polarization. However, the modified wave modes and the possible decay products are, due to the given geometry, forced to propagate along the mean field which is determined by the constant longitudinal magnetic field component. Hence, genuine oblique wave propagation is not considered.

The multi-fluid wave equations are solved by using an eigenvalue and eigenvector method that opens a new and unusual way of analyzing the pump-wave decay and disper-

sion properties of the resulting plasma waves. This approach also provides the dispersion and polarization properties of these waves in a comprehensible and direct way.

As mentioned before, it is known for a long time that the solar wind is permeated by waves and structures on many different scales. But also in the solar corona, low-frequency waves in the magnetic field were recently observed by remote-sensing techniques (De Pontieu *et al.*, 2007; McIntosh *et al.*, 2011). Therefore, it is obviously necessary to assume an inhomogeneous background magnetic field in theory and modeling. The natural choice for such a field might be one consisting of low-frequency Alfvén waves.

Consequently the scenario assumed for the present theoretical treatment is the following. A low-frequency Alfvén/ion-cyclotron (A/IC) wave is assumed to provide the non-uniform background magnetic field and corresponding background velocity field according to the wave polarization relation. In the flank of this wave, a linear dispersion and stability analysis is performed for a three-component plasma consisting of protons, electrons, and alpha particles, whereby drifts among these species with respect to each other can also be included. The situation is sketched in Fig. V-1. The applied multi-fluid model allows one to consider transverse waves with an intrinsic weakly-compressive component. If transverse dispersion branches at wavenumbers close to the inverse ion gyroradius are found, then these can be made responsible for possible perpendicular ion heating. Their compressive electrostatic components can, in turn, explain parallel heating. Since the observations indicate large perpendicular temperature anisotropies in the corona (Antonucci *et al.*, 2000; Kohl *et al.*, 2006) as well as in fast solar wind (Marsch, 2006), the assumption of weak compressibility seems to be justified empirically and is also consistent with the measured density fluctuation level (Tu and Marsch, 1995).

V.2 Theoretical approach and numerical treatment

V.2.1 The multi-fluid model

Following the detailed derivations in Chapt. IV, the subsequent set of second-order ordinary coupled differential equations of the relevant fields for parallel propagation is obtained, in which case B_n is a conserved quantity, and hence the fields can be made dimensionless as follows: $\boldsymbol{v}_{j\mathrm{t}} \equiv \boldsymbol{V}_{j\mathrm{t}}/V_\mathrm{A}$ and $\boldsymbol{b}_\mathrm{t} \equiv \boldsymbol{B}_\mathrm{t}/B_\mathrm{n}$. Similarly the normalized longitudinal electric fields are defined as follows:

$$e_{j\mathrm{n}} \equiv \frac{cE_{j\mathrm{n}}}{B_\mathrm{n}V_\mathrm{A}}, \qquad e_\mathrm{n} \equiv \frac{cE_\mathrm{n}}{B_\mathrm{n}V_\mathrm{A}}. \tag{V-2.1}$$

Length scales can all be normalized in units of the proton inertial length scale $\ell_\mathrm{p} = c/\omega_\mathrm{p}$. In the following, all velocities are normalized to the proton Alfvén speed $V_\mathrm{A} = B_\mathrm{n}/\sqrt{4\pi n_\mathrm{p} m_\mathrm{p}}$ and then denoted by lower case letters. This choice is different than the normalization in Chapt. IV, but it is more appropriate here because the wave phase speed V will be used as a free parameter for different evaluations of the wave equations. Therefore, it is better to normalize with a fixed velocity. The natural choice for such a velocity is the proton Alfvén speed. In this normalization system, frequencies are normalized to the proton gyration frequency Ω_p, which is equal to $V_\mathrm{A}/\ell_\mathrm{p}$. In the subsequent chapter, Ω_j

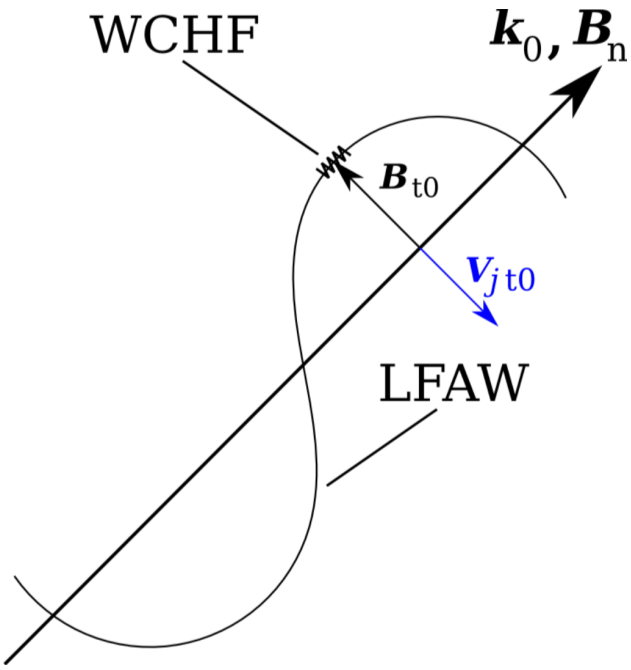

Figure V-1: Geometry of the scenario. On a constant magnetic field $\boldsymbol{B}_\mathrm{n}$ along the axis of propagation $\boldsymbol{k}_0$, a low-frequency Alfvén wave (LFAW) propagates and generates the transverse background fields $\boldsymbol{B}_{\mathrm{t}0}$ and $\boldsymbol{V}_{j\mathrm{t}0} = -\zeta \boldsymbol{B}_{\mathrm{t}0}$ with $\zeta = \text{const.} > 0$. Weakly-compressive high-frequency waves (WCHF) are superposed in the flank of the Alfvén wave.

is used as the *normalized* gyration frequency of species j. Also the original definition

$$e_{j\mathrm{n}} = \frac{1}{c}\left(\boldsymbol{v}_{j\mathrm{t}} \times \boldsymbol{b}_\mathrm{t}\right) \cdot \hat{\boldsymbol{n}} \tag{V-2.2}$$

is recalled. Using the same normalization for the transverse electric field, one obtains

$$\boldsymbol{e}_\mathrm{t} = -v(\hat{\boldsymbol{n}} \times \boldsymbol{b}_\mathrm{t}), \tag{V-2.3}$$

which is fully determined by the solution found for $\boldsymbol{b}_\mathrm{t}$, which means it is a dependent auxiliary field. Completing the required definitions, the differential operator

$$\mathcal{D}_{V_j} \equiv \frac{\mathrm{d}^2}{\mathrm{d}\xi^2} + \frac{1}{r_j^2} \tag{V-2.4}$$

shall be quoted, where the spatial coordinate along B_n is defined as $\xi_\mathrm{n} = \xi$, which will be used continuously in the subsequent chapter. After these preparations, one can state the differential equations as derived from the equations for parallel wave propagation. Firstly, for each particle species with respect to its transverse motion, the forced harmonic oscillator equation is given by

$$\mathcal{D}_{V_j} \boldsymbol{v}_{j\mathrm{t}} = \left(\frac{e_\mathrm{n} + e_{j\mathrm{n}}}{c_j^2 - v_{j\mathrm{n}}^2} \frac{\mathrm{d}\boldsymbol{v}_{j\mathrm{t}}}{\mathrm{d}\xi} + \frac{\boldsymbol{b}_\mathrm{t}}{r_j} + \hat{\boldsymbol{n}} \times \frac{\mathrm{d}\boldsymbol{b}_\mathrm{t}}{\mathrm{d}\xi} \right) \Omega_j \tag{V-2.5}$$

in this normalization. Secondly, one can rewrite the mutually coupled and driven wave equations for the transverse magnetic field as

$$\mathcal{D}_B \boldsymbol{b}_\mathrm{t} = -\sum_j \frac{1}{\ell_j^2}\left(\frac{\boldsymbol{v}_{j\mathrm{t}}}{v_{j\mathrm{n}}} + \frac{(e_\mathrm{n} + e_{j\mathrm{n}})}{c_j^2 - v_{j\mathrm{n}}^2}(\hat{\boldsymbol{n}} \times \boldsymbol{v}_{j\mathrm{t}})\right) \tag{V-2.6}$$

and the longitudinal electric field

$$\mathcal{D}_E e_\mathrm{n} = \sum_j \frac{e_{j\mathrm{n}}}{\lambda_j^2}. \tag{V-2.7}$$

All involved parameters such as $v_{j\mathrm{n}}, c_j, \lambda_j, \ell_j$, and r_j have non-vanishing mean values as the density n_j is always non-zero, and its fluctuations throughout are assumed to be small. Note that Ω_j is strictly constant as it depends on the conserved quantity B_n. The other parameters can be calculated by use of the background number density $\bar{n}_j$ as well as by exploiting the conditions for quasi-neutrality, zero longitudinal current, and zero center-of-momentum velocity (see Chapt. IV). Compression is accounted for solely by the longitudinal electric field in this approximation. This is the major advantage of this multi-fluid system.

Furthermore, the multi-fluid approach incorporates the natural scales of the plasma and therefore permits the treatment of dispersive waves in the high-frequency range, which is not accessible by MHD considerations. The compressibility can be accounted for in a comparably lucid way through the electric field variables e_n and $e_{j\mathrm{n}}$. The nonlinear equations (V-2.5) through (V-2.7) form a closed set of differential equations, which describe the leading-order compressive effects via $e_\mathrm{n}(\xi)$. Before these field equations are written down in their respective components, an appropriate coordinate system is chosen, which is the same as in Sect. IV.4.4. The normalized (dimensionless) transverse magnetic field is

$$\boldsymbol{b}_\mathrm{t} = b_1(\xi)\boldsymbol{e}_1 + b_2(\xi)\boldsymbol{e}_2. \tag{V-2.8}$$

Similarly the transverse flow velocity of any species j is given by

$$\boldsymbol{v}_{j\mathrm{t}} = v_{j1}(\xi)\boldsymbol{e}_1 + v_{j2}(\xi)\boldsymbol{e}_2. \tag{V-2.9}$$

The dimensionless particle speed along the direction of propagation in the fixed coordinate system (not in the co-moving frame) is denoted by $u_{j\mathrm{n}}$. If there are no differential drift motions along the mean magnetic field in the background plasma, i.e., if for all j one has $u_{j\mathrm{n}} = 0$, then $v_{j\mathrm{n}} = -v$, and hence the longitudinal gyration length becomes $r_j = -v/\Omega_j$, which by definition is not a positive-definite quantity as the gyrofrequency carries the sign of the charge of the species considered. Using Eq. (V-2.8) and Eq. (V-2.9), the longitudinal electric field associated with species j simply reads

$$e_{j\mathrm{n}} = v_{j1}b_2 - v_{j2}b_1. \tag{V-2.10}$$

It is known from Chapt. IV that $e_{j\mathrm{n}}$ can also be expressed as the gradient of a potential, which is given by the transverse kinetic energy of species j and then has the form

$$e_{j\mathrm{n}} = -\frac{1}{\Omega_j}\frac{\mathrm{d}}{\mathrm{d}\xi}\left(\frac{1}{2}\boldsymbol{v}_{j\mathrm{t}}^2\right) \tag{V-2.11}$$

in this normalization. In terms of components, the relation

$$-\frac{1}{\Omega_j}\frac{\mathrm{d}v_{j1,2}}{\mathrm{d}\xi} = \pm b_{2,1} \tag{V-2.12}$$

can be found from a comparison of Eq. (V-2.10) with Eq. (V-2.11), which can be used to replace the first derivative of the transverse velocity by the magnetic field. Written out explicitly, the set of differential equations in the new dimensionless normalization finally reads as follows:

$$\frac{\mathrm{d}^2 v_{j1,2}}{\mathrm{d}\xi^2} + \frac{v_{j1,2}}{r_j^2} = \left[\frac{b_{1,2}}{r_j} \mp \frac{\mathrm{d}b_{2,1}}{\mathrm{d}\xi} \mp \frac{e_n + e_{j\mathrm{n}}}{c_j^2 - v_{j\mathrm{n}}^2} b_{2,1}\right]\Omega_j, \tag{V-2.13}$$

$$\frac{\mathrm{d}^2 b_{1,2}}{\mathrm{d}\xi^2} - \frac{b_{1,2}}{\ell_\mathrm{S}^2} = -\sum_j \frac{1}{\ell_j^2}\left[\frac{v_{j1,2}}{v_{j\mathrm{n}}} \mp \frac{e_n + e_{j\mathrm{n}}}{c_j^2 - v_{j\mathrm{n}}^2} v_{j2,1}\right], \tag{V-2.14}$$

$$\frac{\mathrm{d}^2 e_\mathrm{n}}{\mathrm{d}\xi^2} - \frac{e_\mathrm{n}}{\lambda_\mathrm{D}^2} = \sum_j \frac{1}{\lambda_j^2}(v_{j1} b_2 - v_{j2} b_1). \tag{V-2.15}$$

The operators on the left-hand sides of Eqs. (V-2.13) through (V-2.15) describe the dynamics of the uncoupled free fields and have a simple physical interpretation. After Fourier transformation (yielding $\mathrm{d}/\mathrm{d}\xi \to ik$), the solution of Eq. (V-2.13) gives a helical gyration in space of the transverse velocity about the mean field B_n with wavenumber $k = \pm 1/r_j$. The solution of Eq. (V-2.14) corresponds to diamagnetism, i.e., the static penetration of the transverse field into the plasma by the skin depth $\ell_\mathrm{S} = c/\omega_\mathrm{P}$. Eq. (V-2.15) gives for $v = 0$ the static screening by the Debye length λ_D or for finite speed v the electrostatic wave dispersion relation $(k\lambda_\mathrm{D})^2 + 1 = 0$. This, for zero drifts, transforms into the electrostatic dispersion relation

$$k^2 = \sum_j \frac{\omega_j^2}{v^2 - c_j^2}, \tag{V-2.16}$$

the zeros of which yield the Langmuir and ion-acoustic waves as it is presented in detail in Chapt. IV. For finite right-hand sides of the above differential equations, the fields are coupled (note that the abbreviation from Eq. (V-2.10) has to be included). The incompressible limit (with $e_\mathrm{n} = e_{j\mathrm{n}} = 0$) then gives the monochromatic (only a single $k = k(V)$ is permitted from the dispersion relation) electromagnetic A/IC wave, which has a constant but arbitrarily large amplitude. When considering compressibility, the electric and electromagnetic waves are linked and interact through the nonlinear rightmost terms in the above wave equations. Considering compressibility may require either a perturbative approach or numerical treatment.

V.2.2 Perturbative approach and linearization

The above equations are a system of second-order wave equations. To simplify it, the system is reduced to a system of first-order equations. Therefore, the quantities $e'_\mathrm{n} \equiv \mathrm{d}e_\mathrm{n}/\mathrm{d}\xi$, $b'_{1,2} \equiv \mathrm{d}b_{1,2}/\mathrm{d}\xi$, and $v'_{j1,2} \equiv \mathrm{d}v_{j1,2}/\mathrm{d}\xi$ are introduced. With this substitution, the system corresponds to a set of 14 coupled nonlinear first-order ordinary differential equations

in ξ for an electron–proton plasma. For each additional particle species, four coupled equations are added.

In the next step, the system (V-2.13) through (V-2.15) is linearized around a background given by the wave amplitude vectors $\boldsymbol{v}_{jt0}$ and $\boldsymbol{b}_{jt0}$ to determine the wave dispersion. A suitable choice of the background values is given in Sect. V.2.3.

Nonlinear couplings of low-frequency waves with fluctuations at high frequencies cannot be described by a linearized system. The low-frequency wave with wavenumber k_0, however, may be treated as a constant inhomogeneous background if the high-frequency waves with wavenumbers k fulfill the condition $k_0 \ll k$. The high-frequency waves are then treated in the flank of this low-frequency wave that does not change its fields significantly over several periods of the high-frequency waves. The particle velocities, the electromagnetic field, and their derivatives are combined in a state vector

$$\boldsymbol{y} \equiv (v'_{\mathrm{p}1}, v'_{\mathrm{p}2}, \ldots, v_{\mathrm{p}1}, v_{\mathrm{p}2}, \ldots, b'_1, b'_2, b_1, b_2, e'_{\mathrm{n}}, e_{\mathrm{n}}), \tag{V-2.17}$$

and therewith one can write the linearized equation as

$$\frac{\mathrm{d}}{\mathrm{d}\xi}\delta\boldsymbol{y} = \mathcal{A}\delta\boldsymbol{y} \tag{V-2.18}$$

with the quadratic matrix $\mathcal{A} = (a_{i,j}) \in M(n)$ with $n = 4s + 6$, where s is the total number of species. The solution of Eq. (V-2.18) is in general given by

$$\delta\boldsymbol{y} = \sum_{i=1}^{4s+6} \alpha_i \delta\boldsymbol{y}_i e^{\lambda_i \xi} \tag{V-2.19}$$

with the eigenvalues λ_i and the corresponding eigenvectors $\delta\boldsymbol{y}_i$. Since $\mathcal{A}$ is a real matrix, the complex-conjugated eigenvalues and eigenvectors are also solutions once a complex eigenvalue and eigenvector pair is found. The coefficients α_i are arbitrary. However, they must be equal for the pairwise complex-conjugated eigenvalues to construct a real solution.

An imaginary part of an eigenvalue λ_i always indicates a periodic fluctuation. Due to the rule of pairwise complex-conjugated eigenvalues, they are represented by real sine or cosine functions. Real parts of λ_i correspond to growth or damping. The imaginary part is denoted as k and the real part as $\varkappa$. If the eigenvalues are pairwise symmetric in the real part, the growth is described by hyperbolic sine or cosine functions, which is the symmetric solution for the instabilities growing in positive and in negative ξ-direction.

The eigenvalues can be calculated numerically with the QR-method after transforming $\mathcal{A}$ to an upper Hessenberg matrix (Press *et al.*, 1992). The existence of the complex-conjugated eigenvalues means that, for wave-like daughter products, two solutions always exist, one forward and one backward propagating with the same frequencies.

V.2.3 Background wave

An adequate background to calculate the dispersion is the flank of a circularly polarized Alfvén wave since these waves are exact eigenmodes of a plasma and obey Eqs. (V-2.13) and (V-2.14) in the incompressible limit with arbitrary amplitudes. The phase speed of

this wave is denoted by v_0. It is left-hand polarized and has a magnetic field of the structure

$$\boldsymbol{b}_{\mathrm{t}0} = b\begin{pmatrix}\cos(k_0\xi)\\ \sin(k_0\xi)\end{pmatrix}, \tag{V-2.20}$$

as it has already been used in Chapt. III. Without loss of generality, this field is evaluated at the point $\xi = 0$. For sufficiently low k_0-values, this field appears as a constant magnetic background field of the magnitude $\boldsymbol{b}_{\mathrm{t}0} = (b, 0)$ as stated above. Therefore, this background describes analogous conditions as used to treat oblique propagation of linear modes. However, the wave is additionally associated with a transversal velocity for each species. Corresponding to this magnetic field, a background velocity field occurs that is determined by the polarization relation of circularly polarized Alfvén waves

$$\boldsymbol{v}_{j\mathrm{t}0} = \frac{v_{j\mathrm{n}0}}{1 + k_0 v_{j\mathrm{n}0}/\Omega_j}\boldsymbol{b}_{\mathrm{t}0} \tag{V-2.21}$$

as derived by Sonnerup and Su (1967) for example. The normal velocity component of the particle species j in the reference frame moving with v_0 is denoted by $v_{j\mathrm{n}0}$. The polarization relation is also in agreement with the results from the previous chapter on nonlinear A/IC waves. For a sufficiently small wavenumber k_0, the wave fulfills the Alfvénic dispersion relation $v_0 \simeq v_{\mathrm{A}}$.

The transformation of the transverse velocity to the co-moving reference frame does not change the value for $\boldsymbol{v}_{j\mathrm{t}0}$. Therefore, the polarization relation provides the necessary (constant) value for $\boldsymbol{v}_{j\mathrm{t}0}$ depending on a given (small) k_0 and the wave amplitude b. To evaluate the polarization relation exactly, the dispersion relation for the circularly polarized Alfvén waves is used. It is given by

$$k_0^2 + \sum_{j=1}\frac{\omega_j^2}{c^2}\frac{k_0 v_{j\mathrm{n}0}}{k_0 v_{j\mathrm{n}0} + \Omega_j} = 0 \tag{V-2.22}$$

in the non-relativistic limit as used in Chapts. II and IV.

V.3 Dispersion of high-frequency waves

In this section, the wave dispersion relation of high-frequency waves propagating on the non-uniform background Alfvén wave is studied. The most important free parameter of the system of equations (V-2.13) through (V-2.15) is the disposable wave phase speed v. For a fixed v, the eigenvalue/eigenvector method provides the corresponding wavenumber values $k(v)$. The relation $\omega = kv$ then delivers the corresponding ω, and hence, by scanning through all relevant values of v, the full dispersion relation can be determined. The growth rate γ can be determined similarly by evaluating $\gamma = \varkappa v$ with the spatial growth rate $\varkappa$ from the eigenvalue determination. The very high-frequency branches, which are dominated by the electron dynamics, are not treated in detail since the ions carry the main momentum and their wave-induced motion is, therefore, more important for the heating and acceleration processes. The electron density and relative velocity with respect to the protons and the other ionic species are determined by the requirement of vanishing charge

density (quasi-neutrality) and vanishing constant longitudinal currents of the background, such that

$$\sum_{j=1} n_j q_j = 0, \tag{V-3.23}$$

$$\sum_{j=1} n_j q_j v_{j\mathrm{n}} = 0. \tag{V-3.24}$$

The specific heat ratio is set to its adiabatic value of $\gamma_j = 5/3$ for all species.

V.3.1 Homogeneous background

Before the case of an inhomogeneous plasma is discussed, the system of equations and the linearization is applied to an electron–proton plasma for a homogeneous background and with $\beta_j = 0$. The background field is set to $B_\mathrm{n} = 5 \times 10^{-5}$ G and the particle number densities to $n_\mathrm{p} = n_\mathrm{e} = 5$ cm^{-3}. The ratio $B_\mathrm{n}^2/n_\mathrm{p}$ must be parameterized even in the dimensionless normalization of the system in order to fix the normalized plasma frequency $\omega_j/\Omega_\mathrm{p}$ for electrostatic processes. The result of the calculation is shown in Fig. V-2. The three incompressible branches correspond to the transverse particle motions. One of them represents a free motion with the gyration frequency for the protons at $\omega = 1$, their normalized gyrofrequency. The branch approaching the gyrofrequency asymptotically corresponds to the A/IC wave. The cold dispersion relation for parallel A/IC waves from Chapt. II,

$$\omega^2 = k^2 + \frac{k^4}{2} - \frac{k^3}{2}\sqrt{k^2+4}, \tag{V-3.25}$$

is additionally plotted as a green dotted line. The branch at low k-values with high phase speed v corresponds to the fast/whistler (F/W) mode shown as a red dashed line. The corrected low-frequency dispersion for the multi-fluid R-mode wave (i.e., the fast/whistler wave including ionic effects) is given analytically by

$$\frac{\omega}{\Omega_\mathrm{p}} = \frac{k^2\ell_\mathrm{p}^2}{2}\left[1 + \sqrt{1 + \frac{4}{k^2\ell_\mathrm{p}^2}}\right] \tag{V-3.26}$$

as shown in Eq. (II-2.83) of Chapt. II. Both relations show a perfect agreement with the numerical calculations made with the eigenvalue method. This confirms the validity of this approach.

In Fig. V-3, the dispersion relation is shown for a plasma consisting of electrons, protons, and alpha particles without any relative drifts and without a background wave field. The particle species have a beta of 0.01. The proton number density is set to $n_\mathrm{p} = 5$ cm^{-3}, the alpha particle number density to $n_\alpha = 0.04 n_\mathrm{p}$, and the electron number density according to Eq. (V-3.23). The alpha-particle cyclotron branch approaches asymptotically the frequency $\omega = 1/2$ as expected. This value corresponds to the alpha-particle gyrofrequency in normalized units. The cyclotron branch of the protons is slightly deformed in the low-k range in comparison to the cold plasma dispersion relation. Also the F/W wave mode is slightly shifted. The presence of the alpha particles is responsible for this deviation. Further correction terms would be needed to represent the dispersion relation in this three-fluid plasma analytically.

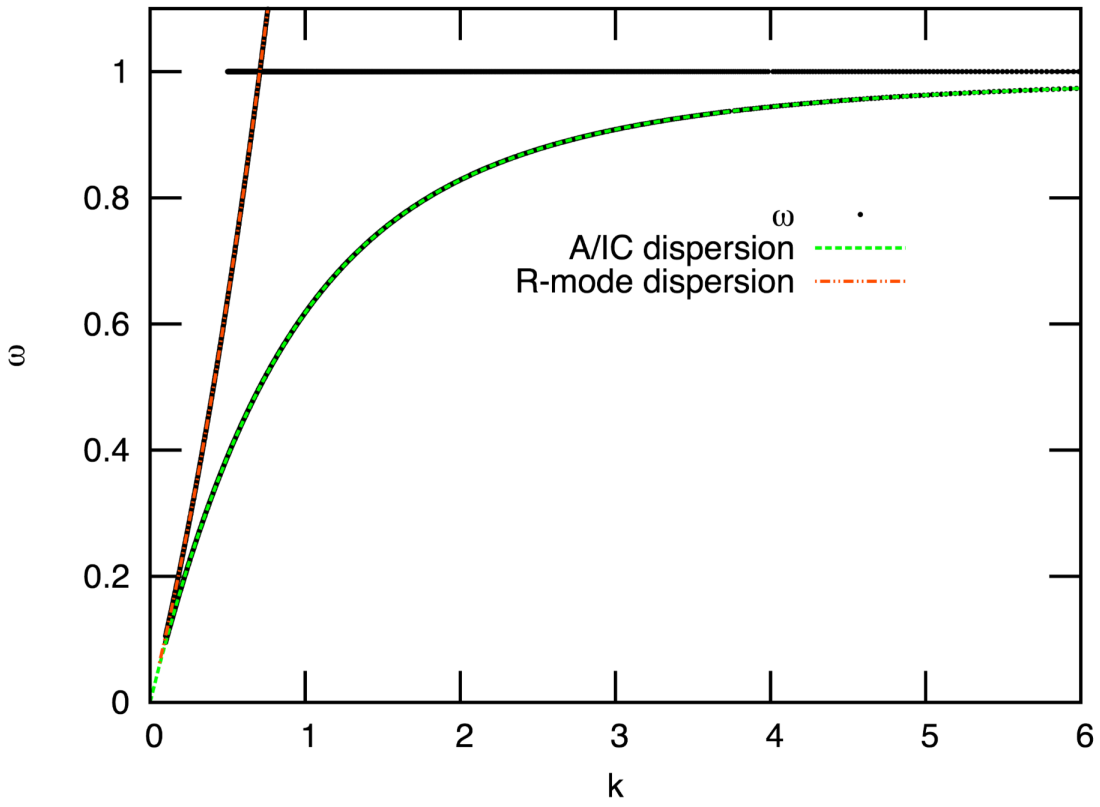

Figure V-2: Dispersion relation for an electron–proton plasma in a homogeneous background with $\beta_j = 0$. The cold dispersion relation for Alfvén/ion-cyclotron waves and for ion-corrected R-mode waves are additionally plotted.

This model also allows one to include relative drifts of the particles along the wave-normal direction. The relative drift speed between protons and alpha particles is defined as $v_\mathrm{d} \equiv v_\mathrm{pn} - v_{\alpha\mathrm{n}}$. In Fig. V-4, the dispersion relation for $v_\mathrm{d} = 0.2$ is shown. The alpha-particle branch starting at $\omega = \Omega_\alpha$ is turned into the so-called beam-mode branch (line inclined to the left) derived from the resonance condition

$$\omega = \Omega_\alpha + k u_{\alpha\mathrm{n}}, \tag{V-3.27}$$

where $u_{\alpha\mathrm{n}} = v - v_{\alpha\mathrm{n}}$ denotes again the alpha-particle bulk speed component along the wave-normal direction in the proton rest frame. For a vanishing drift $u_{\alpha\mathrm{n}}$, this mode is flattened back to the horizontal line $\omega = \Omega_\alpha = 1/2$.

V.3.2 Inhomogeneous background

Next, the above system of coupled wave equations can be applied to an inhomogeneous background plasma, which corresponds to realistic solar wind conditions. The plasma consists of three species: protons, electrons, and alpha particles. The relative drift between protons and alphas is set to $v_\mathrm{d} = v_\mathrm{pn} - v_{\alpha\mathrm{n}} = 0.2$ and the plasma beta to $\beta_j = 0.01$ for each species. The background wave is assumed to have a normalized wavenumber of

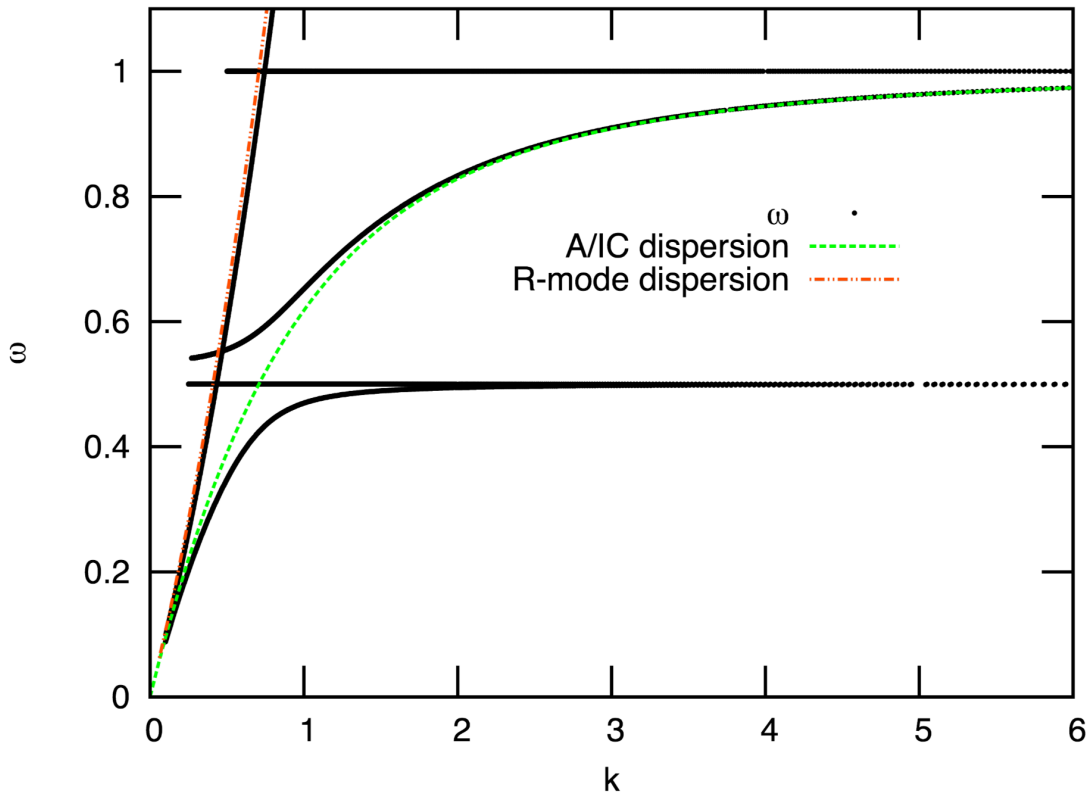

Figure V-3: The same as Fig. V-2 for a plasma consisting of electrons, protons, and alpha particles with $\beta_j = 0.01$.

$k_0 = 0.01$ and an amplitude of $b = 0.1$. Such a wave has a phase speed of almost the local proton Alfvén speed. The wavenumber is small enough to neglect any direct nonlinear couplings between the background wave and the high-frequency waves. For the latter, the background wave appears as a quasi-constant field, with respect to which the system can be linearized. The results are shown in Fig. V-5.

The dispersion branches are deformed for several reasons. The proton A/IC branch at lower wavenumbers is not further deformed as compared to Fig. V-3. Some branches turn at some bifurcation positions into completely different dispersion branches. These transitions correspond to mode couplings. For example, the faster sound wave (alpha-particle mode) couples with the A/IC wave of the protons at high wavenumbers, whereas the ion-acoustic wave couples with the drift-deformed A/IC wave of the alpha particles. The R-mode couples with the ion gyration at $\omega = 1$ but, interestingly enough, not with the alpha-particle beam mode. It shows a break at $\omega = 1$ and then continues above that frequency.

Two additional linear branches occur with merely constant phase speeds of $v \approx 0.13$ and $v \approx 0.03$. Such linear acoustic modes as these two were also found by Mann *et al.* (1997) for a warm plasma. The wave phase speed of these modes is usually determined

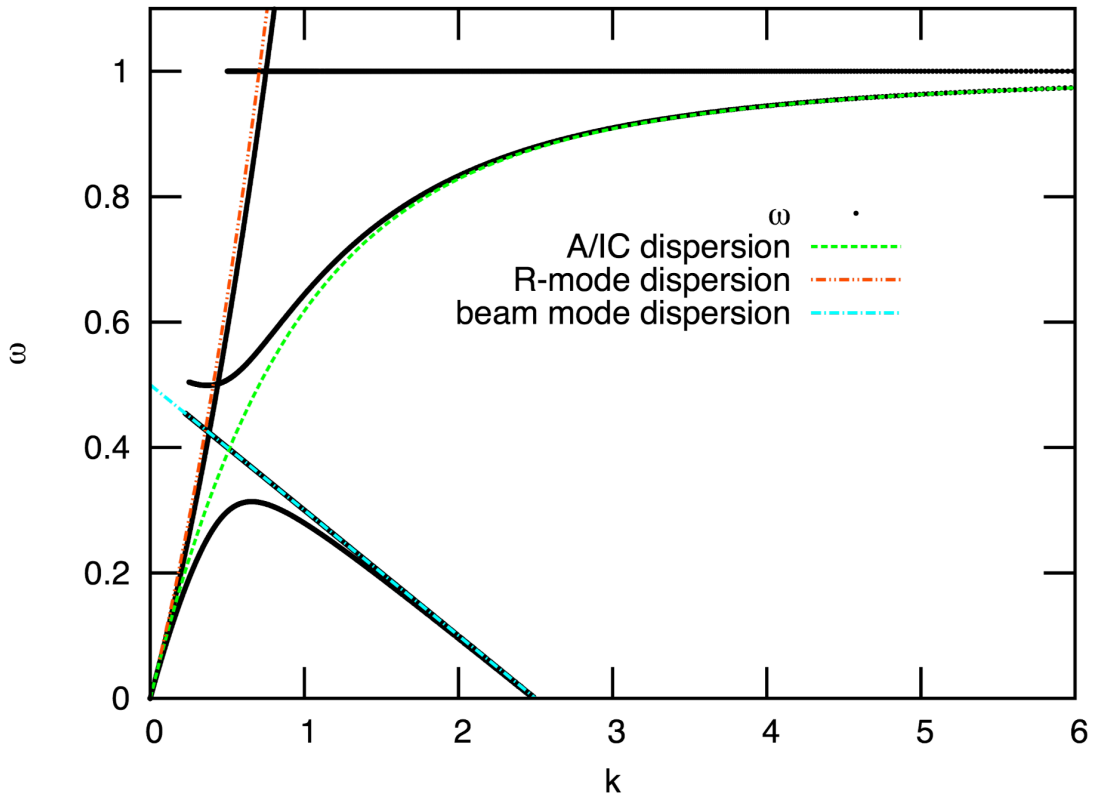

Figure V-4: Dispersion relation for a plasma consisting of protons, electrons, and drifting alpha particles with $v_\mathrm{d} = 0.2$. The beam mode occurs for drifting alpha particles.

by

$$v_{\mathrm{Ph1}} = \frac{\gamma_\mathrm{p} k_\mathrm{B} T_\mathrm{p} + \gamma_\mathrm{e} k_\mathrm{B} T_\mathrm{e}}{m_\mathrm{p}}, \tag{V-3.28}$$

$$v_{\mathrm{Ph2}} = \frac{\gamma_\alpha k_\mathrm{B} T_\alpha}{m_\alpha} \tag{V-3.29}$$

for a plasma with $n_\alpha \ll n_\mathrm{p}$. The first is the so-called ion-acoustic speed, the second is the sound speed of the alpha-particle component. In the present case, these velocities are given by $v_{\mathrm{Ph1}} = 0.13$ and $v_{\mathrm{Ph2}} = 0.23$ in normalized units. The first one corresponds perfectly with the fast (steeper line) sound wave that has been found here. The drift velocity v_d of the alpha particles is the reason for the deviation of the second linear mode. In the non-drifting reference case, the two velocities match ($v_{\mathrm{Ph2}} - v_\mathrm{d} = 0.03$). If the numerical dispersion code is applied to a plasma without drift, the second sound-wave branch is directly found at $v = v_{\mathrm{Ph2}}$ (not shown here).

The two sound-wave modes do not appear in the homogeneous plasma. Remember that the phase speed v is a free parameter in the calculation, and a wavenumber is given by the eigenvalues obtained for each v. If a wave is not dispersive and therefore has a constant phase speed, it is not possible to calculate the full set of possible k-values that belong to this v. The sound waves exist already in the homogeneous case; however, they

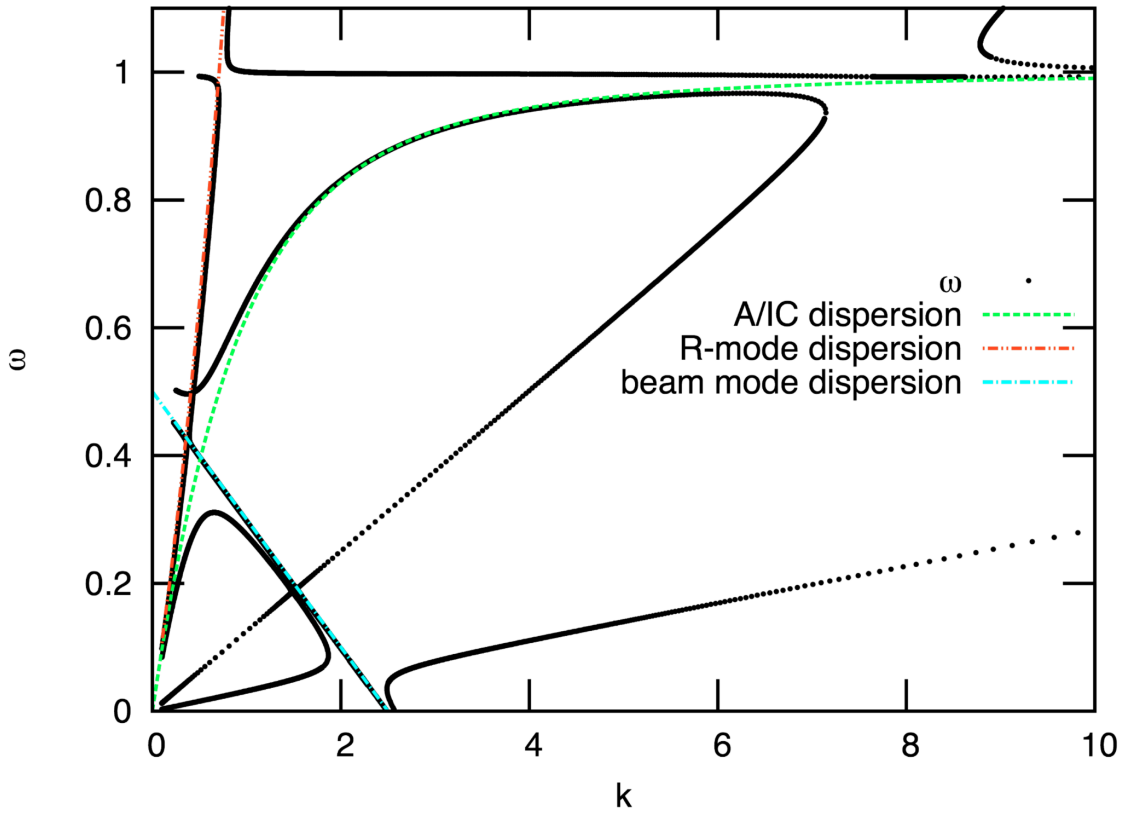

Figure V-5: Dispersion relation for a plasma consisting of protons, electrons, and drifting alpha particles. The frequency ω is shown in dependence on the wavenumber k in dimensionless units. The derived A/IC branch deviates from the cold dispersion branch at low and high wavenumbers. Mode coupling between the various branches occurs as discussed in the text.

become visible only after becoming dispersive due to mode coupling. This type of wave becomes only dispersive for non-zero beta and in the presence of the background wave. Also above the corresponding gyrofrequencies $\omega = 1$ and $\omega = 1/2$, the branches continue with their constant phase speed.

The waves on all branches have a compressive component, owing to the non-vanishing electric fields e_{n} and $e_{j\mathrm{n}}$. The real part of the eigenvalues λ_i is always zero, i.e., none of the compressive modes is unstable in this case.

Note that it is the amplitude of the background wave which mainly determines the strength of the mode coupling and hence the position and shape of the deformation of the ion-cyclotron branch. For higher amplitudes, the branch turns earlier away from the A/IC dispersion branch, and hence the phase speed of the linear mode increases already at lower k-values. The plasma beta determines the phase speeds of the linear branches. Higher betas lead to higher phase speeds of these modes. The phase speeds can be adjusted relative to each other by choosing different betas for the individual species. However, the overall topology of the dispersion branches is not significantly changed by assigning different beta values to different species.

However, if beta is chosen to be greater than 1, then the situation changes tremen-

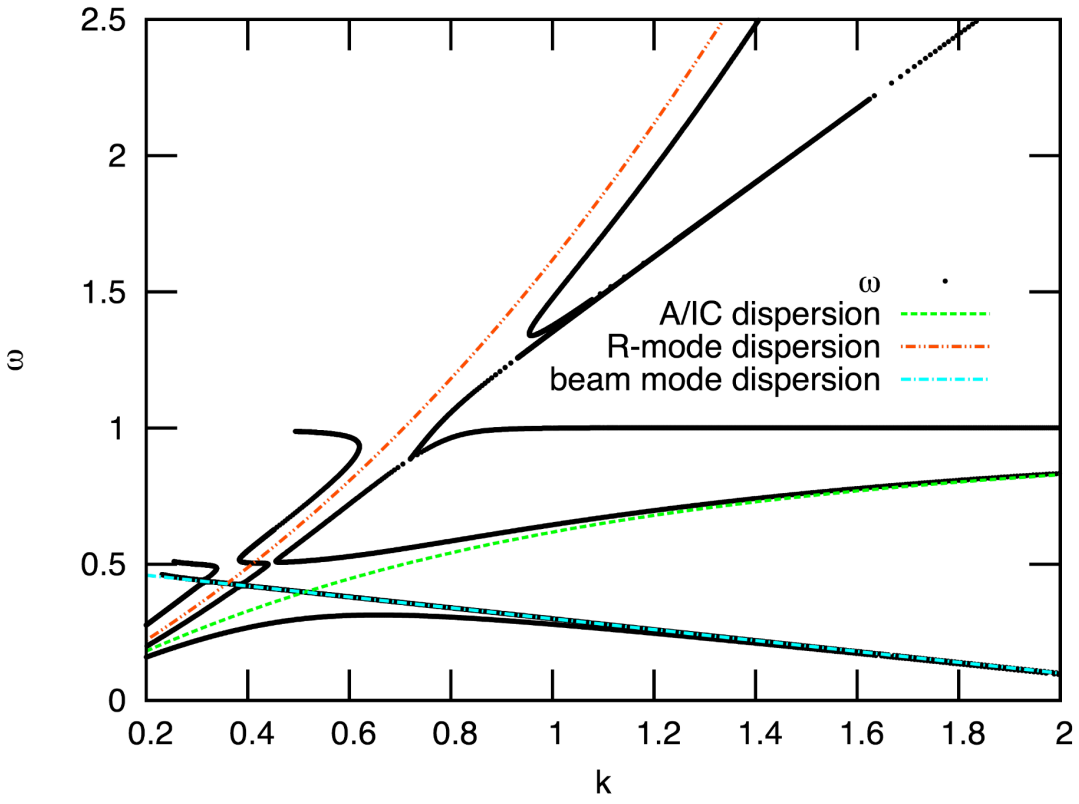

Figure V-6: Dispersion relation for a plasma with $\beta = 1.2$.

dously. The sound waves become unstable. In Fig. V-6, the dispersion is shown for a situation with $\beta_j = 1.2$. The corresponding growth rates $\gamma = \varkappa v$ of the modes are shown in Fig. V-7.

Mode coupling between the sound wave and the F/W wave mode leads to an instability that occurs at $k \approx 0.8 \ldots 1.6$. Interestingly enough, this range is the ion gyroradius scale for moderate plasma betas close to 1. This growing instability can, therefore, provide wave energy to the dissipative regime by means of Landau resonance since the particle distribution has a significant number of particles at the corresponding wave speed of about $v \approx 1.36$ for a plasma with $\beta_j \gtrsim 1$. This instability vanishes if the background wave is absent, i.e., in the homogeneous case. For higher beta values, the position of the instability is shifted to higher wavenumbers.

V.4 Discussion

As expected, the inhomogeneity of the background wave field leads to a deformation of the standard normal modes in the plasma. All of the discovered waves have a compressive component. Compressibility and inhomogeneity of the background plasma are the causes for the new effects in the dispersion properties. The initially non-compressive A/IC waves become slightly compressive due to the inhomogeneous background and are therefore able to interact with the protons via their electrostatic field components in addition to the

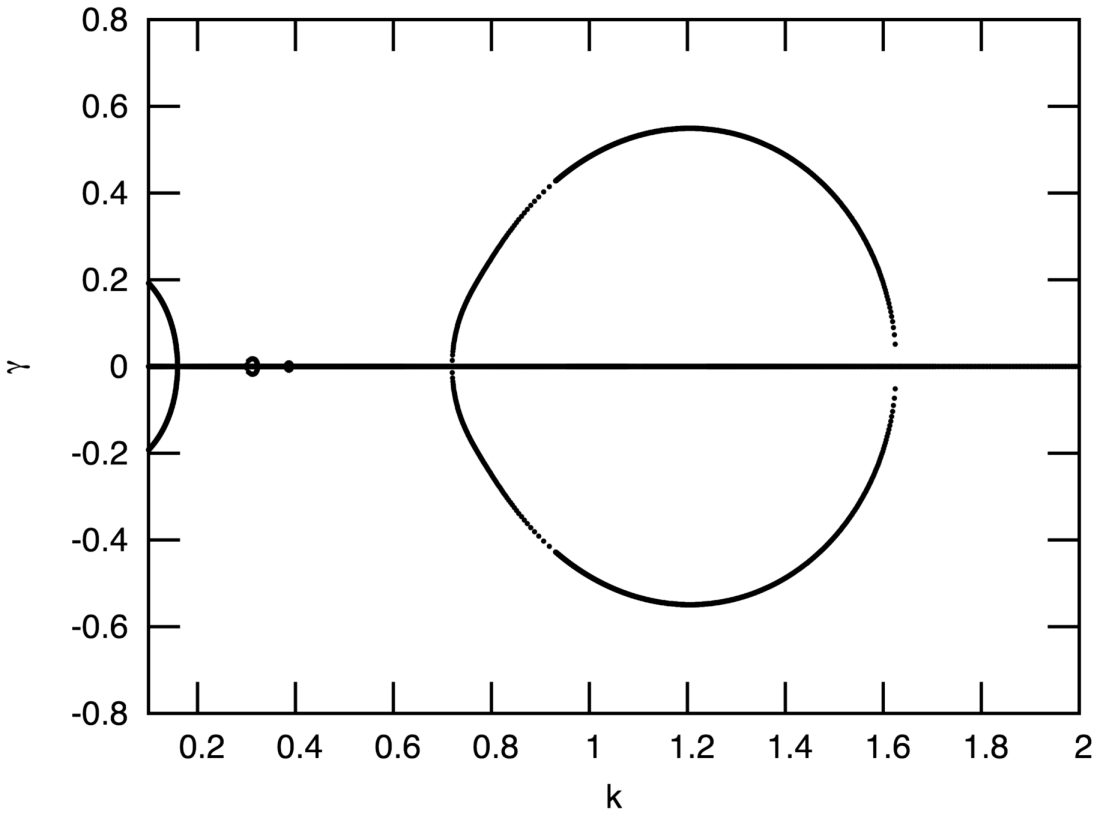

Figure V-7: Imaginary part of the frequency depending on k.

cyclotron resonance enabled by their transverse components. The quantitative details of these wave–particle interactions cannot be treated in the fluid description since they are purely kinetic processes. They require a kinetic Vlasov treatment, at least in the frame of quasilinear theory and are therefore beyond the scope of this work. The kinetic refinement of the dispersion analysis of circularly polarized waves of the same type was described by Stenflo (1976), who also showed how relativistic effects and compressibility can modify the dispersion of large-amplitude waves in multi-fluid theory.

The non-constant (due to the presence of the pump wave) background leads to nonlinear mode couplings between some of the linear wave modes. It also leads to the excitation of initially non-dispersive modes such as the ion-acoustic wave or the alpha-particle sound wave, yet now with k-dependent wave speeds.

The acoustic modes can grow at wavenumbers around the ion gyration scale under certain conditions and for adequate parameters. Thus, they are good candidates for a longitudinal electrostatic wave field, with which particles can undergo Landau-resonant wave–particle interactions. Kinetic Alfvén waves (KAWs) have recently been discussed as another possible reason for this kind of interaction. KAWs owe their compressibility to the oblique geometry of their propagation with respect to a constant background field. In this study, it was possible to show that also waves with purely parallel propagation can grow nonlinearly at the corresponding resonant wavenumbers, provided that the background has a non-trivial—but quite reasonable—magnetic field configuration. These two

mechanisms are quite different in nature and should be further investigated and compared with each other.

The instability of ion-acoustic modes coupled to transverse modes were also discussed in studies of the parametric decay of large-amplitude pump waves and evaluated by numerical simulations (Araneda *et al.*, 2007; Valentini and Veltri, 2009). Also in these studies, instabilities of longitudinal waves at high wavenumbers were found, however, at different background parameters. These waves are usually interpreted as results of nonlinear wave–wave interactions. The linearized wave equations, however, can explain a similar growth of daughter waves at higher frequencies than the initial pump-wave frequency as a consequence of compressibility and a non-uniform background. This mechanism can, thus, be understood as a new spectral transfer process of plasma fluctuations. It is very similar to the decay instability, which is found with the characteristic $k \gg k_0$.

The eigenvector analysis still keeps the freedom to choose the amplitudes α_i in Eq. (V-2.19). This means that a wave can, in general, only occur if its amplitude is finite. It is beyond the scope of this work to investigate how the discovered wave branches can be excited in a real plasma. The linear dispersion analysis can only show possible normal modes. The discovered instability leads to growth in the initial phase only until nonlinear couplings and perhaps saturation occur. Yet, unstable modes can grow from the thermal noise (that is constrained as a finite eigenvector of the system of equations) with a certain finite amplitude. In the presence of a large-amplitude wave, this thermal noise can lead to growth according to the calculated growth rate γ at the gyroradius scale range for $\beta_j \gtrsim 1$. Maybe, full nonlinear calculations can investigate the further evolution and possible nonlinear excitations of such modes. The linear approximation appears to reflect the basic situation well (Lehe *et al.*, 2009).

In the future, other background conditions should also be inquired. The above chosen background is one of the simplest inhomogeneous conditions. It is important to note that, in this approach, the background has to change slowly in dependence upon the position ξ. Otherwise, the use of a fixed phase speed v is not possible anymore, and then the present approximation needs to be changed. The original set of coupled wave equations remains valid, yet another mathematical treatment is required to cope with their nonlinearity.

VI Parametric decay of parallel and oblique Alfvén/ion-cyclotron waves in hybrid simulations

VI.1 Parametric decay in numerical simulations

Monochromatic plasma waves with certain properties are known to be parametrically unstable and decay to daughter waves in a multiple-wave interaction process (Galeev and Oraevskii, 1963; Derby, 1978; Goldstein, 1978; Lashmore-Davies and Stenflo, 1979; Wong and Goldstein, 1986; Inhester, 1990; Ruderman and Simpson, 2004). Ubiquitous small thermal fluctuations in the plasma are the seed for growing daughter waves in the presence of a large-amplitude wave if it obeys the necessary unstable characteristics.

Following the early analytical descriptions, numerical simulations have become capable of modeling the parametric decay (Viñas and Goldstein, 1991a; Araneda, 1998). Kinetic simulations allow one to investigate the interaction between particles and the participating waves and show resultant particle heating under typical coronal conditions (Araneda *et al.*, 2008). This observation has brought the parametric decay process into the focus of coronal heating research. Large-amplitude plasma waves are directly observed in the solar chromosphere and corona, which seem to be mainly Alfvénic and strong enough to deliver sufficient energy for the coronal heating (De Pontieu *et al.*, 2007; McIntosh *et al.*, 2011). This makes them promising energy sources also for the acceleration of the fast solar wind, even though the details of the dissipation and the spectral transfer are not well understood.

Most models, however, use a simplified basis such as a one-dimensional geometry. Recently the higher computational resources have paved the way for two-dimensional analyses including the possibility of oblique propagation of mother and daughter waves (Viñas and Goldstein, 1991b; Matteini *et al.*, 2010). There are, however, still many open questions in this context. The compressive component of the fluctuations, for example, is known to be important for the parametric decay. In the oblique case, it is not well understood yet. Also the direction of propagation of the daughter-wave products and their ability for resonant wave–particle heating are still unclear. This work tries to address some of these aspects with the aid of the numerical hybrid code A.I.K.E.F. First, some one-dimensional test runs are presented, before results of the two-dimensional oblique simulation are shown.

VI.2 The hybrid code A.I.K.E.F.

The A.I.K.E.F. (adaptive ion-kinetic electron-fluid) code is based on the work by Bagdonat and Motschmann (2002). The basics of the code were extensively described by Bagdonat (2005). It has been completely revised, and the possibility for adaptive refinement has been included by Müller *et al.* (2011). It is a so-called *hybrid code*, which means that ions are treated as particles, whereas electrons are treated as a massless charge-neutralizing fluid. This description is reliable as long as gyration effects of the electrons can be neglected. Strong electrostatic effects due to local space charge differences are not treatable in this model because the massless electron fluid would immediately fill up a local space charge and neutralize it. Therefore, a numerical investigation of the results from Chapt. V is not possible with a hybrid code. Electrostatic waves can partly be treated in the frame of the plasma approximation, applying the concept of quasi-neutrality, which is discussed in Sect. VI.2.2.

VI.2.1 The hybrid equations

The basic equations are Maxwell's equations without displacement current, the ion equations of motion, and the momentum equation for the electron fluid. The above cited descriptions of the code are all given in SI-units. For the reason of consistency, they are written in cgs-units hereafter. The code allows for finite resistivity, drag due to neutral particles, and adaptive mesh refinement. All of these additional possibilities have no meaning for this work and are therefore omitted in the following description.

Firstly, the equations of motion for the ions are given by

$$\frac{\mathrm{d}\boldsymbol{v}_j}{\mathrm{d}t} = \frac{q_j}{m_j}\left(\boldsymbol{E} + \frac{1}{c}\boldsymbol{v}_j \times \boldsymbol{B}\right), \tag{VI-2.1}$$

$$\frac{\mathrm{d}\boldsymbol{x}_j}{\mathrm{d}t} = \boldsymbol{v}_j \tag{VI-2.2}$$

as the characteristics of the collisionless Vlasov equation for the ions. The particle position is denoted by $\boldsymbol{x}_j$ and its velocity by $\boldsymbol{v}_j$.

The massless electron fluid has to fulfill the momentum conservation according to

$$m_\mathrm{e}\frac{\mathrm{d}(n_\mathrm{e}\boldsymbol{u}_\mathrm{e})}{\mathrm{d}t} = 0 = -en_\mathrm{e}\left(\boldsymbol{E} + \frac{1}{c}\boldsymbol{u}_\mathrm{e} \times \boldsymbol{B}\right) - \operatorname{grad} p_\mathrm{e}, \tag{VI-2.3}$$

where $\boldsymbol{u}_\mathrm{e}$ stands for the electron bulk velocity and p_e for the pressure of the electron fluid. From the momentum equation, the electric field can be derived as

$$\boldsymbol{E} = -\frac{1}{c}\boldsymbol{u}_\mathrm{e} \times \boldsymbol{B} - \frac{1}{n_\mathrm{e}e}\operatorname{grad} p_\mathrm{e}. \tag{VI-2.4}$$

The weighted ion bulk velocity is defined as $\boldsymbol{u}_\mathrm{i} = \boldsymbol{j}_\mathrm{i}/\varrho_\mathrm{c}$ with the ion current density $\boldsymbol{j}_\mathrm{i}$ and the charge density ϱ_c, which are both calculated from the moments of all ion species' distribution functions. By using quasi-neutrality ($n_\mathrm{i} = n_\mathrm{e} = n$) and $\boldsymbol{j} = \boldsymbol{j}_\mathrm{e} + \boldsymbol{j}_\mathrm{i} = -en_\mathrm{e}\boldsymbol{u}_\mathrm{e} + q_\mathrm{i}n_\mathrm{i}\boldsymbol{u}_\mathrm{i}$, the electric field is given by

$$\boldsymbol{E} = -\frac{1}{c}\boldsymbol{u}_\mathrm{i} \times \boldsymbol{B} + \frac{\operatorname{curl}\boldsymbol{B} \times \boldsymbol{B}}{4\pi\varrho_\mathrm{c}} - \frac{1}{\varrho_\mathrm{c}}\operatorname{grad} p_\mathrm{e} \tag{VI-2.5}$$

with the charge density $\varrho_c = \sum_j n_j q_j$ summed over all ion species. The number density n_j can be determined from the zeroth moment of the ion distribution functions. The polytropic relation

$$p_e = p_{e0}\left(\frac{\varrho_c}{\varrho_{c0}}\right)^{\gamma} \tag{VI-2.6}$$

with the polytropic index γ is assumed for the electron pressure as a closure relation.

The magnetic field is determined by use of the induction equation, following from Faraday's law. With Eq. (VI-2.5), the temporal evolution of the magnetic field can be written as

$$\frac{\partial \boldsymbol{B}}{\partial t} = \text{curl}\ (\boldsymbol{u}_i \times \boldsymbol{B}) - \text{curl}\left(\frac{c}{4\pi\varrho_c}\text{curl}\,\boldsymbol{B} \times \boldsymbol{B}\right). \tag{VI-2.7}$$

The pressure gradient vanishes due to Eq. (VI-2.6) and the vector identity curl grad $= 0$. The set of equations is closed. Even for runs with lower spatial dimensions, the code evaluates the full 3D vector components of all vector quantities. In the following, the boundary conditions are always set to be periodic.

The plasma ions are not treated as single particles but as so-called *superparticles*. This means that always a bunch of ions is treated like one particle with corresponding mass and charge. This strategy helps to save calculation time. The number of superparticles per cell is a free parameter and should be chosen carefully. The particles are initialized with a Maxwellian distribution, shifted to the given initial values for the velocity. The width of the Maxwellian distribution is determined by the species' beta, which is a free parameter as well. A divergence-cleaning algorithm is applied to keep possible unphysical magnetic field errors low and to increase the numerical stability of the system.

VI.2.2 The plasma approximation

In the framework of the so-called *plasma approximation*, quasi-neutrality ($n_p \approx n_e$ for an electron-proton plasma) is assumed, but a non-vanishing divergence of the electric field is allowed (Chen, 1985). The hybrid equations fulfill this approximation. To avoid a misunderstanding, especially regarding the influence of electrostatic effects, the plasma approximation should be discussed here in more detail.

It can be understood as a perturbation expansion with respect to the relative density contrast

$$\mu \equiv \frac{n_e - n_p}{n_p} \ll 1. \tag{VI-2.8}$$

The electron density is, thus, given by

$$n_e = n_p + \mu n_p, \tag{VI-2.9}$$

which is a complete representation of n_e. The electron number density is used in the derivation of only one of the hybrid equations, namely the equation of motion for the electrons. The electron bulk velocity can be written as

$$\boldsymbol{u}_e = \frac{1}{1+\mu}\left[\boldsymbol{u}_p - \frac{c}{4\pi e n_p}\text{curl}\,\boldsymbol{B}\right]. \tag{VI-2.10}$$

The factor before the bracket is obviously close to unity for small μ. In a similar way, the pressure gradient term is dominated by the gradient of n_p as long as μ does not have a large spatial gradient, which is another implicit assumption of the plasma approximation.

The divergence of the electric field has the form

$$\operatorname{div} \boldsymbol{E} = -4\pi e \mu n_\mathrm{p} \tag{VI-2.11}$$

in this system. It is, therefore, small but yet one order lower in the perturbation hierarchy, taking into account that small values of div $\boldsymbol{E}$ may be cumulated and lead to a significant effect.

An interesting special case in wave studies is the electrostatic limit of fluctuations, in which the electric field is assumed to have the form

$$\boldsymbol{E} = -\operatorname{grad} \Phi \tag{VI-2.12}$$

with the electric potential Φ. The Poisson equation takes the form

$$\operatorname{div} \operatorname{grad} \Phi = 4\pi e \mu n_\mathrm{p}. \tag{VI-2.13}$$

Neglecting magnetic couplings with the plasma dynamics, the electron equation of motion (see Eq. (VI-2.4)) yields

$$e n_\mathrm{e} \operatorname{grad} \Phi = \operatorname{grad} p_\mathrm{e} = k_\mathrm{B} T_\mathrm{e} \operatorname{grad} n_\mathrm{e} \tag{VI-2.14}$$

after a corresponding definition of the constant electron temperature T_e from the isothermal ($\gamma = 1$) equation of state. The direct use of the Poisson equation in this balance relation is not applicable because it would be based on higher-order effects again, which are not treatable in this way. The solution of Eq. (VI-2.14) is given by

$$n_\mathrm{e} = n_{\mathrm{e}0} \exp\left(\frac{e\Phi}{k_\mathrm{B} T_\mathrm{e}}\right) \tag{VI-2.15}$$

with the familiar exponential Boltzmann factor.

The electric potential and the electron density are now supposed to vary on a typical scale L. The hydrodynamic change in the electron density is assumed to be significant. Combining the linearized relation from Eq. (VI-2.14), in this case meaning $e\Phi \sim k_\mathrm{B} T_\mathrm{e}$, with the approximated Laplace operator div grad $\sim 1/L^2$ permits then to estimate the value of μ as

$$\mu \sim \frac{\lambda_\mathrm{D}^2}{L^2} \tag{VI-2.16}$$

with the electron Debye length

$$\lambda_\mathrm{D} \equiv \sqrt{\frac{k_\mathrm{B} T_\mathrm{e}}{4\pi n_{\mathrm{e}0} e^2}} \tag{VI-2.17}$$

for a significant gradient in n_e. As long as the changes in Φ occur on long scales compared to the Debye length, the parameter μ is small and quasi-neutrality is a good assumption. This means that the density contrast μ has to be almost constant on small scales of the

order of the Debye length. However, the cumulative effect on larger scales may still be important for electrostatic waves on larger scales. To inquire this effect in more detail, a scale analysis should be applied to the electric field. The change in the electron density n_e is supposed to occur on the typical outer scale L, say, of the order of the ion inertial length. Typically this scale is several orders of magnitude larger than the Debye length, meaning that $\mu \sim 10^{-6}$ for example. This small density contrast justifies the assumption $n_p \approx n_e$ because the densities are almost equal but not exactly equal at each position. The total quasi-neutrality on even larger scales might still be justified because the gradient in n_e should be also of a periodic form for a wave. The integrated electric field on the outer scale is given according to Gauß' law by

$$E \sim -4\pi e \mu n_p L. \tag{VI-2.18}$$

The electric field expressed by the equation of motion in Eq. (VI-2.14) has the form

$$E \sim -\frac{k_B T_e}{eL}. \tag{VI-2.19}$$

Using the relation $\mu \sim \lambda_D^2/L^2$ and the definition of the Debye length from Eq. (VI-2.17) shows that both expressions for E are of the same order of magnitude.

The divergence of the electric field turns out to be of order one in dimensionless units in the typical normalization system. The charge density, however, is by a factor of v_A^2/c^2 smaller than div $\boldsymbol{E}$ in these units, whereas the ion and electron densities are again of order unity. This shows that the divergence of the electric field is non-zero and an important quantity, while the density contrast is unimportant in this approximation.

So the hybrid equations are able to treat electrostatic waves on large scales (limited by the quasi-neutrality) and at low frequencies (limited by the vanishing electron mass). The role of the electron pressure in this balance is crucial as it compensates for all changes in the electrostatic potential Φ according to Eq. (VI-2.14). Without the pressure gradient term, the potential would have to be constant to fulfill the electron equation of motion. The situation is illustrated in Fig. VI-1. If the charge density would be exactly zero over the density gradient initially, the electrons would diffuse due to their high mobility and thermal speed into a configuration, which is consistent with the small space charge difference again and in which the protons pull them back against their drift in a figurative sense. This situation is similar to the classical ambipolar diffusion (Chen, 1985).

It is interesting to consider the meaning of Maxwell's displacement current and the continuity equation in this context. Taking the divergence of the complete Ampère's law yields the classical charge continuity equation

$$\frac{\partial \mu n_p}{\partial t} = \text{div}\left[n_p \boldsymbol{u}_p - (1+\mu) n_p \boldsymbol{u}_e\right]. \tag{VI-2.20}$$

The local temporal derivative and the correction due to density differences in the current are of order μ, while the divergence of $\boldsymbol{j}_{app} = e n_p \left(\boldsymbol{u}_p - \boldsymbol{u}_e\right)$ is of order one in the perturbation hierarchy. Therefore, the assumption div $\boldsymbol{j} \approx$ div $\boldsymbol{j}_{app} \approx 0$ is valid.

These considerations show that the hydrodynamic pressure gradient term in the hybrid equations is able to represent cumulative electrostatic effects, even though the local density difference between electrons and protons may be assumed at most places to be equal. *Local* corrections due to $\mu \neq 0$ have to be taken into account only if spatial changes occur on the scale of the plasma Debye length, which is beyond the treated cases here.

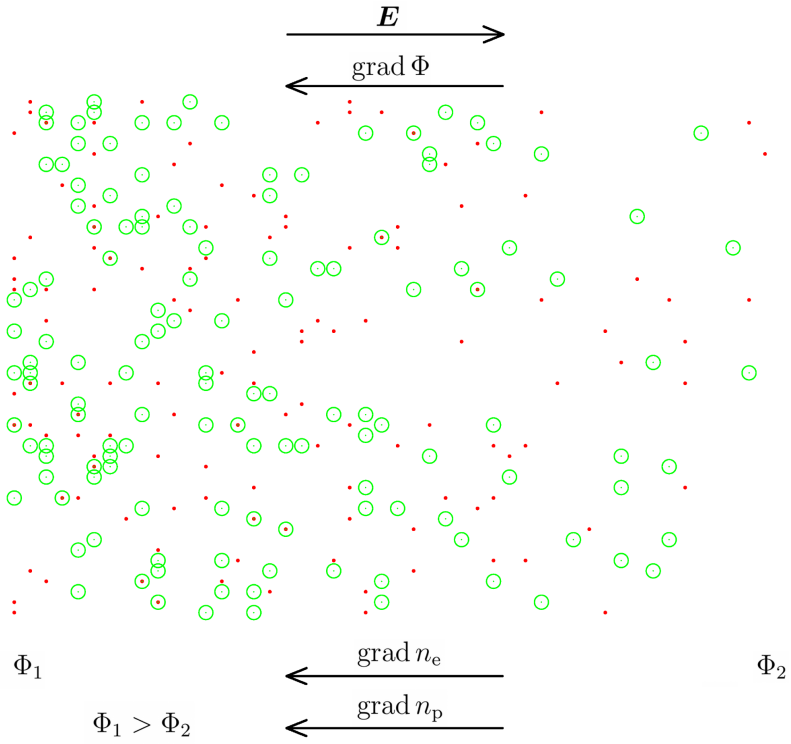

Figure VI-1: Illustration of pressure gradients and the electrostatic field. The different dots represent protons or electrons, respectively. Both obey a density gradient on large scales compared to the Debye length.

VI.3 Parallel propagation

VI.3.1 Parallel Alfvén/ion-cyclotron waves

Alfvén/ion-cyclotron (A/IC) waves can be parameterized by

$$\boldsymbol{B} = \begin{pmatrix} B_\mathrm{t}\cos(k_0 z - \omega_0 t) \\ B_\mathrm{t}\sin(k_0 z - \omega_0 t) \\ B_\mathrm{n} \end{pmatrix} \tag{VI-3.21}$$

as already used in Chapts. III through V.

The transversal components of each quantity are combined in a two-component vector, denoted by the index t. With a constant z-velocity $U_{j\mathrm{n}}$ for the species j, the transversal velocity is given by

$$\boldsymbol{V}_{j\mathrm{t}} = -\frac{\omega_0/k_0 - U_{j\mathrm{n}}}{1 - \omega_0/\Omega_j + k_0 U_{j\mathrm{n}}/\Omega_j}\frac{\boldsymbol{B}_\mathrm{t}}{B_\mathrm{n}}, \tag{VI-3.22}$$

which is the known polarization relation for A/IC waves. The dispersion relation, connecting the frequency ω_0 with a (given) wavenumber k_0, is given by

$$k_0^2 - \frac{\omega_0^2}{c^2} + \sum_{j=1}^{s}\frac{1}{\ell_j^2}\frac{\omega_0 - k_0 U_{jn}}{\omega_0 - k_0 U_{jn} - \Omega_j} = 0. \tag{VI-3.23}$$

The total number of species is denoted by s. The second term in the dispersion relation comes from Maxwell's displacement current and can be safely neglected in the non-relativistic limit. The electrons are massless, so their contribution to the dispersion relation is given by the last term on the left-hand side of

$$k_0^2 + \sum_{j=1}^{s_\mathrm{i}} \frac{1}{\ell_j^2} \frac{\omega_0 - k_0 U_{j\mathrm{n}}}{\omega_0 - k_0 U_{j\mathrm{n}} - \Omega_j} + \frac{1}{\ell_\mathrm{p}^2} \frac{\omega_0 - k_0 U_{e\mathrm{n}}}{\Omega_\mathrm{p}} = 0, \tag{VI-3.24}$$

where s_i is the total number of ionic species. Note that in the electron term the ionic skin depth and the ionic gyration frequency are used, which is useful for reasons of normalization. For a two-component plasma without any drifts, this equation reduces to

$$k_0^2 + \frac{1}{\ell_\mathrm{p}^2} \frac{\omega_0}{\omega_0 - \Omega_\mathrm{p}} + \frac{1}{\ell_\mathrm{p}^2} \frac{\omega_0}{\Omega_\mathrm{p}} = 0. \tag{VI-3.25}$$

The wavenumber k_0 is chosen in a way that an integer number of maxima fits into the simulation box:

$$k_0 = \frac{2\pi n}{L_z} \tag{VI-3.26}$$

with integer n and box size L_z. The code is initialized with a magnetic field of the form

$$\boldsymbol{b} = \frac{1}{|\boldsymbol{b}|} \begin{pmatrix} b \cos k_0 z \\ b \sin k_0 z \\ 1 \end{pmatrix} \tag{VI-3.27}$$

and with a velocity field following Eq. (VI-3.22) with $U_{j\mathrm{n}} = 0$. The initial conditions have to be chosen carefully because the total space charge density and current density have to be zero. This is especially crucial if further species with a beam structure along the magnetic field are considered.

VI.3.2 Results

The parametric decay of a circularly polarized wave is treated with the following parameter set. The initial wave has a wavenumber of $k_0 = 64\pi/L_z$ and an amplitude of $b = 0.25 B_\mathrm{n}$ as described above. The configuration is one-dimensional with a grid in z-direction consisting of 2048 grid points spread over a length of $L_z = 500\ell_\mathrm{p}$. The proton inertial length ℓ_p is the normalization unit for all length scales. The betas are chosen as $\beta_\mathrm{p} = 0.08$ and $\beta_\mathrm{e} = 0.5$. The electrons are supposed to be isothermal ($\gamma = 1$). Each cell contains 800 superparticles. 150 000 time steps are applied with a step width of $\Delta t = 0.01$. The proton gyrofrequency Ω_p is the normalization unit for all frequencies and its inverse value for the time dimension. The magnetic field in all components and the particle density are recorded every 300 time steps along the z-axis, which allows one to perform a Fourier transformation of these fields to determine the decay result and the spectral spread of the wave energy in wavenumber space.

The initial conditions for the magnetic field, the electric field, and the ion velocity are shown in Fig. VI-2. The wave propagates out of the drawing plane, and the vector set rotates in the clockwise direction at each fixed position z.

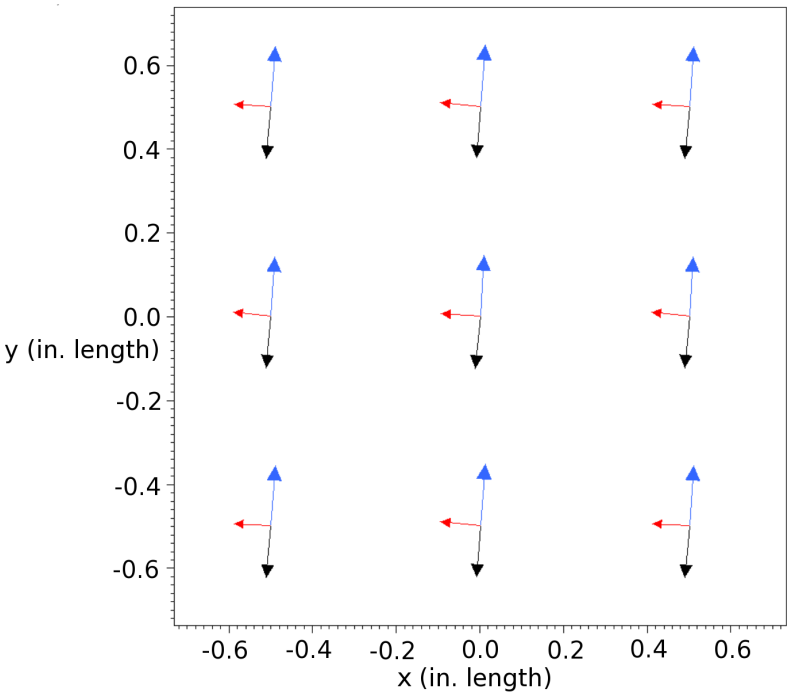

Figure VI-2: Vector fields of an Alfvén/ion-cyclotron wave. Black: tangential magnetic field, red: tangential electric field, blue: tangential proton bulk velocity field. The wave propagates out of the drawing plane.

After a while, the wave decays due to nonlinear couplings with other minor (thermal) fluctuations. This noise is ubiquitous in every numerical simulation due to rounding errors and field approximations of derivatives. Also a natural plasma contains these fluctuations due to thermal noise. To analyze the nature of the daughter-wave products, a Fourier transformation can be applied to the magnetic field or the density, respectively. The fast-Fourier transform (FFT) procedure is used for this purpose. Afterwards the real power spectral density of the Fourier transformed magnetic field $\boldsymbol{B}(k)$ is calculated as

$$\mathcal{P}_k = \boldsymbol{B}(k) \cdot \boldsymbol{B}^*(k), \tag{VI-3.28}$$

where the asterisk indicates complex conjugation. Usually the power is then divided by the spatial length over which the transformation was carried out. In a finite integration domain of the discrete Fourier transform, this just leads to a constant, which is omitted here.

The lowest and highest accessible wavenumbers are constrained by the sampling of the discretized function. The highest accessible (normalized) wavenumber is given by

$$k_{\max} = \frac{\pi(N_x - 1)}{N_x \Delta x} \approx \frac{\pi}{\Delta x}, \tag{VI-3.29}$$

where N_x is the number of spatial steps, and Δx is the interval between each step in the sampling. The lowest wavenumber (apart from the constant value at $k = 0$) is determined by the step width in discrete x-space as

$$k_{\min} = \frac{\pi}{N_x \Delta x} \approx \frac{k_{\max}}{N_x}. \tag{VI-3.30}$$

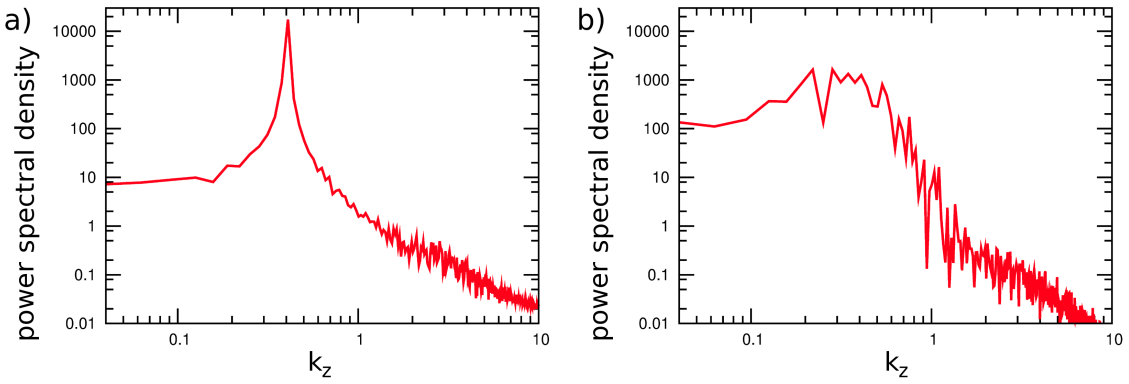

Figure VI-3: Transversal power spectral density of daughter waves after parametric decay of an Alfvén/ion-cyclotron wave in arbitrary units. a) at $t = 180$. b) at $t = 700$.

The dispersion of the waves can be determined by applying the FFT algorithm twice, first in space and then in time. Therefore, a short temporal period has to be selected, over which the temporal Fourier transformation is applied. It must not be too long because then the evolution of the spectrum could mitigate the accuracy of the transformation. On the other hand, one needs quite some periods to apply the Fourier transform in the time domain because otherwise only a small frequency band is accessible. The definition of the highest accessible (normalized) frequency is similar to the above definition of the highest wavenumber:

$$\omega_{\max} = \frac{\pi(N_t - 1)}{N_t \Delta t} \approx \frac{\pi}{\Delta t}, \tag{VI-3.31}$$

where N_t is the number of recorded timesteps and Δt the interval between each saved timestep. The lowest frequency (apart from the constant value at $\omega = 0$) is

$$\omega_{\min} = \frac{\pi}{N_t \Delta t} \approx \frac{\omega_{\max}}{N_t}. \tag{VI-3.32}$$

The total time between the beginning (at $t = 0$) and the end of the transformed interval is given by $t = N_t \Delta t$.

A typical spectrum of transverse magnetic field power for two different times is shown in Fig. VI-3. In Fig. VI-3a, the strong pump wave is visible at $k \approx 0.4$. It has spread already to lower and higher wavenumbers. With the later evolution, this effect continues as can be seen in Fig. VI-3b. After a longer duration, also compressive fluctuations grow, which have not been present at the initialization. The compressive spectra for the same two time steps are shown in Fig. VI-4. In Fig. VI-4b, it is visible how efficiently energy is transformed into low-frequency pressure fluctuations. This is the typical behavior of the parametric decay of such a wave. The total energy in the magnetic field has to be less than the total initial energy in the magnetic field.

A common effect of the modulational instability is the occurrence of some local peaks both in magnetic field and in density in configuration space. After a certain time, these peaks are also observed in the spatial distribution of the magnetic field from this simulation. The field components can exceed values of more than $0.3 B_n$, whereas at other positions it becomes very small. The solely random distribution of wave phases adds up to high values at these positions.

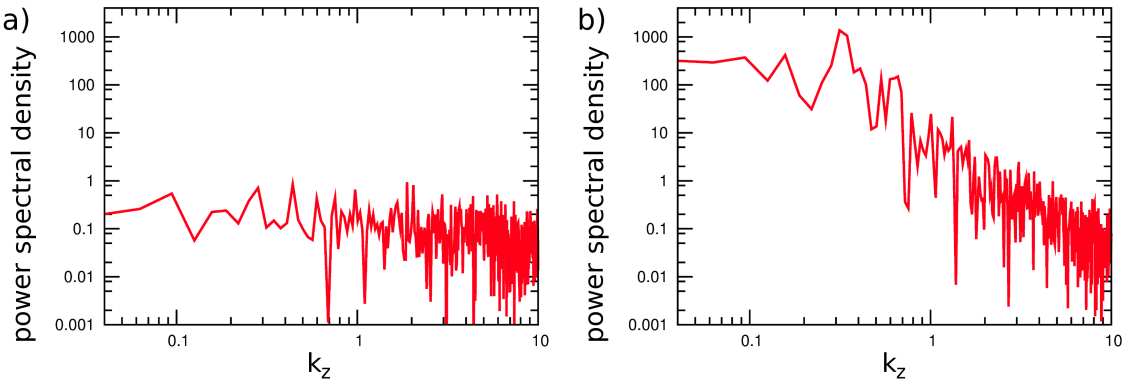

Figure VI-4: Compressional power spectral density of daughter waves after parametric decay of an Alfvén-cyclotron wave. a) at $t = 180$. b) at $t = 700$.

VI.4 Oblique propagation

A wave propagating obliquely with respect to the background magnetic field provides automatically a fluctuation in the longitudinal electric field (e.g., Stix, 1992; Hamza *et al.*, 2006). Some waves are intrinsically oblique like the kinetic Alfvén wave. Therefore, this wave type always exhibits a parallel electric field component (Goldreich and Sridhar, 1995; Hollweg, 1999; Marsch, 2006). This generally different nature of oblique waves can also lead to different wave–particle phenomena compared to the parallel cases. The Alfvén/ion-cyclotron wave mode is again an interesting candidate to achieve efficient plasma heating, also in the oblique propagation. Therefore, this work continues to focus on this normal mode.

VI.4.1 Oblique Alfvén/ion-cyclotron waves

It is also possible to use the A.I.K.E.F. code in more than one dimension. The oblique propagation of A/IC waves and their spectral evolution is studied in this section for an electron-proton plasma. It is known and observed that A/IC waves are damped more if they propagate obliquely with respect to the background magnetic field direction (Jian *et al.*, 2010). The dispersion relation of A/IC waves changes for oblique propagation. The angle between the wavevector $\boldsymbol{k}$ and the constant magnetic field component $\boldsymbol{B}_\mathrm{n}$ is denoted by ϑ.

Sonnerup's solution cannot be used for an oblique initialization since it describes the exact solution of the kinetic equations only for parallel propagation. The cold plasma dispersion for obliquely propagating A/IC waves appears as a good choice for the initialization of the simulation. It is given by

$$\frac{k^4 \cos^2\vartheta}{\omega^4} - \frac{k^2\left(1+\cos^2\vartheta\right)}{\omega^2\left(1-\omega^2\right)} + \frac{1}{1-\omega^2} = 0 \qquad \text{(VI-4.33)}$$

in the applied normalization (Stix, 1992; Chandran *et al.*, 2010b). The A/IC root of this

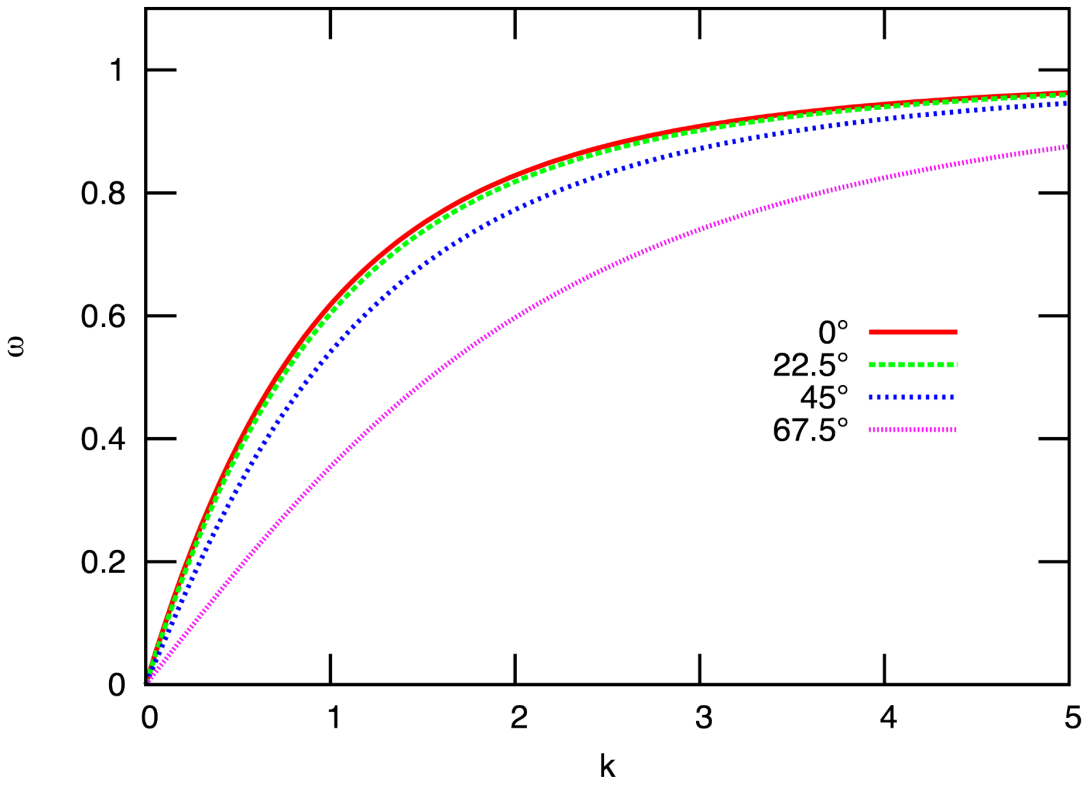

Figure VI-5: Cold dispersion relation for Alfvén/ion-cyclotron waves depending on the angle ϑ between $\boldsymbol{k}$ and $\boldsymbol{B}_0$. The dispersion deviates from the classical branch significantly only for quite oblique propagation angles.

equation can also be written as

$$\omega^2 = \frac{1}{2}\Big[k^4\cos^2\vartheta + k^2(1+\cos^2\vartheta) - k^2\sqrt{k^4\cos^4\vartheta + 2k^2(\cos^4\vartheta+\cos^2\vartheta) + (1-\cos^2\vartheta)^2}\Big]. \quad \text{(VI-4.34)}$$

The dispersion relation depending on the angle ϑ is shown in Fig. VI-5.

The coordinate system of the simulation box is chosen in a way that the z-direction is parallel to the background magnetic field. The orientation of the other axes is set up in such a way that the wavevector has no component along the x-axis. Thus, its component in the y-direction corresponds to the perpendicular component.

An appropriate initialization is a wave from the cold dispersion relation. Therefore, the distribution function can be assumed to have the shape of a delta function, and the ion fluid velocity $\boldsymbol{u}_\mathrm{i}$ becomes equal to the particular ion velocity $\boldsymbol{v}_\mathrm{i}$ for an electron-proton plasma. The above given hybrid equations then correspond to the equations known from Hall-MHD (e.g., Krauss-Varban *et al.*, 1994; Vocks *et al.*, 1999). The approximations in the frame of Hall-MHD suppress some typical wave features that are only present in the kinetic picture as discussed by Krauss-Varban *et al.* (1994). All kinetic effects discussed by these authors do not arise from the multi-fluid nature and the finite electron mass but

from effects of spread distribution functions, which are due to finite β-values. All of these effects, however, are covered in the hybrid description, and therefore this ansatz is appropriate.

The wave is given to be left-hand elliptically polarized with

$$\boldsymbol{B} = \begin{pmatrix} B_x \\ B_y \\ B_z \end{pmatrix} = \begin{pmatrix} 0 \\ 0 \\ B_0 \end{pmatrix} + \begin{pmatrix} B_1 \cos(\boldsymbol{k}\cdot\boldsymbol{r} - \omega t) \\ B_2 \sin(\boldsymbol{k}\cdot\boldsymbol{r} - \omega t) \\ B_3 \sin(\boldsymbol{k}\cdot\boldsymbol{r} - \omega t) \end{pmatrix}. \tag{VI-4.35}$$

The linearized characteristics of the Vlasov equation from Eq. (VI-2.1) and the generalized Ohm's law from Eq. (VI-2.5) lead to an equation of motion, taking the form

$$\frac{\mathrm{d}\boldsymbol{v}_\mathrm{p}}{\mathrm{d}t} = \frac{\operatorname{curl}\boldsymbol{B}\times\boldsymbol{B}_0}{4\pi m_j n_0} - \frac{c_\mathrm{e}^2}{n_0}\operatorname{grad} n_\mathrm{e}. \tag{VI-4.36}$$

The electron sound speed is defined as $c_\mathrm{e} \equiv \sqrt{\gamma p_\mathrm{e}/\varrho_\mathrm{m}} = v_\mathrm{A}\sqrt{\beta_\mathrm{e}}$ with the proton mass density ϱ_m and the electron beta β_e. The density is supposed to behave as $n_\mathrm{e} = n_0 + \hat{n}_\mathrm{e}\sin(\boldsymbol{k}\cdot\boldsymbol{r} - \omega t)$. Its phase (i.e., the fact that it is a sine function and not a cosine for example) is the result of trying to find a consistent solution with the fields $\boldsymbol{B}$, $\boldsymbol{E}$, and $\boldsymbol{v}_\mathrm{p}$. The z-component phase of $\boldsymbol{B}$ and $\boldsymbol{E}$ are found in the same way. The y-component of the term $\operatorname{curl}\boldsymbol{B}\times\boldsymbol{B}_0$ contains B_y and B_z, which shows that these two components must have the same phase. The pressure gradient term, however, has only a non-vanishing component in y and z. Since the gradient has to have the same phase in all components, this phase has to be the same as the phase of the y- and z-components of the magnetic field. With Ampère's law, the full phase relations are determined. These definitions lead to the proton velocity

$$\begin{aligned} v_{\mathrm{p}x} &= -\frac{k_z}{\omega}v_\mathrm{A}^2\frac{B_1}{B_0}\cos(\boldsymbol{k}\cdot\boldsymbol{r} - \omega t), \\ v_{\mathrm{p}y} &= \left(\frac{k_y}{\omega}v_\mathrm{A}^2\frac{B_3}{B_0} - \frac{k_z}{\omega}v_\mathrm{A}^2\frac{B_2}{B_0} + \frac{k_y}{\omega}c_\mathrm{e}^2\frac{\hat{n}_\mathrm{e}}{n_0}\right)\sin(\boldsymbol{k}\cdot\boldsymbol{r} - \omega t), \\ v_{\mathrm{p}z} &= \frac{k_z}{\omega}c_\mathrm{e}^2\frac{\hat{n}_\mathrm{e}}{n_0}\sin(\boldsymbol{k}\cdot\boldsymbol{r} - \omega t). \end{aligned} \tag{VI-4.37}$$

The electric field is given after linearization of the generalized Ohm's law according to Eq. (VI-2.5) as

$$\begin{aligned} E_x &= \frac{1}{c}\left(\frac{k_z}{\omega}v_\mathrm{A}^2 B_2 - \frac{k_y}{\omega}v_\mathrm{A}^2 B_3 - \frac{k_y}{\omega}c_\mathrm{e}^2\frac{\hat{n}_\mathrm{e}}{n_0}B_0 - \ell_\mathrm{p}^2\Omega_\mathrm{p}k_z B_1\right)\sin(\boldsymbol{k}\cdot\boldsymbol{r} - \omega t), \\ E_y &= \frac{1}{c}\left(-\frac{k_z}{\omega}v_\mathrm{A}^2 B_1 + \ell_\mathrm{p}^2\Omega_\mathrm{p}(k_z B_2 - k_y B_3) - c_\mathrm{e}^2\frac{\hat{n}_\mathrm{e}}{n_0}\frac{k_y}{\Omega_\mathrm{p}}B_0\right)\cos(\boldsymbol{k}\cdot\boldsymbol{r} - \omega t), \\ E_z &= -\frac{1}{c}c_\mathrm{e}^2\frac{\hat{n}_\mathrm{e}}{n_0}\frac{k_z}{\Omega_\mathrm{p}}B_0\cos(\boldsymbol{k}\cdot\boldsymbol{r} - \omega t). \end{aligned} \tag{VI-4.38}$$

The polarization relation for the magnetic field components can be calculated from Faraday's law in the form

$$-\frac{1}{c}\frac{\partial\boldsymbol{B}}{\partial t} = \operatorname{curl}\boldsymbol{E} \tag{VI-4.39}$$

and yields

$$\begin{aligned}
\left(1-\frac{k_z^2 v_\mathrm{A}^2}{\omega^2}\right) B_1 &= -\frac{k_z \Omega_\mathrm{p} \ell_\mathrm{p}^2}{\omega}(k_z B_2 - k_y B_3),\\
\left(1-\frac{k_z^2 v_\mathrm{A}^2}{\omega^2}\right) B_2 &= -\frac{k_z k_y v_\mathrm{A}^2}{\omega^2} B_3 - \frac{k_z k_y c_\mathrm{e}^2}{\omega^2}\frac{\hat{n}_\mathrm{e}}{n_0} B_0 - \frac{k_z^2 \Omega_\mathrm{p} \ell_\mathrm{p}^2}{\omega} B_1,\\
\left(1-\frac{k_y^2 v_\mathrm{A}^2}{\omega^2}\right) B_3 &= -\frac{k_z k_y v_\mathrm{A}^2}{\omega^2} B_2 + \frac{k_y^2 c_\mathrm{e}^2}{\omega^2}\frac{\hat{n}_\mathrm{e}}{n_0} B_0 + \frac{k_z k_y \Omega_\mathrm{p} \ell_\mathrm{p}^2}{\omega} B_1.
\end{aligned} \tag{VI-4.40}$$

The latter two relations can be combined to find

$$k_y B_2 + k_z B_3 = 0, \tag{VI-4.41}$$

which means that the divergence of $\boldsymbol{B}$ is always zero for all solutions. In the classical parallel case, these relations lead directly to $B_3 = 0$ and

$$\left(\frac{\omega}{\Omega_\mathrm{p}}\right)^2 = \frac{1}{2}\left[2k_z^2\ell_\mathrm{p}^2 + k_z^4\ell_\mathrm{p}^4 - k_z^3\ell_\mathrm{p}^3\sqrt{k_z^2\ell_\mathrm{p}^2+4}\right], \tag{VI-4.42}$$

which is one representation of the dispersion relation of classical A/IC waves, which has already been used before in Chapt. V (e.g., Stix, 1992; Chandran *et al.*, 2010b). This means, in turn, that the waves are circularly polarized if they fulfill this dispersion relation. To close the system in the general case, the density fluctutations of electrons have to be expressed in terms of known quantities. The linearized continuity equation can infer informations about the density fluctuation amplitude $\hat{n}_\mathrm{e}$:

$$\hat{n}_\mathrm{e} = n_0 \frac{k_y}{k_z}\frac{k^2 v_\mathrm{A}^2}{k^2 c_\mathrm{e}^2 - \omega^2}\frac{B_2}{B_0}. \tag{VI-4.43}$$

This compressibility amplitude is zero for the parallel propagation. After all, the system can be written as

$$B_3 = -\frac{k_y}{k_z} B_2, \tag{VI-4.44}$$

$$B_1 = \Omega_\mathrm{p}\ell_\mathrm{p}^2 \frac{k^2\omega}{k_z^2 v_\mathrm{A}^2 - \omega^2} B_2, \tag{VI-4.45}$$

$$\frac{\hat{n}_\mathrm{e}}{n_0} = \frac{k_y}{k_z}\frac{k^2 v_\mathrm{A}^2}{k^2 c_\mathrm{e}^2 - \omega^2}\frac{B_2}{B_0}. \tag{VI-4.46}$$

It is important to guarantee that the latter expression for the relative density is much smaller than one so that the density does not take 'negative' values and that the linearized continuity equation is still an adequate description for the compressive effects. It is a common phenomenon for oblique waves that the amplitude is limited due to the compressive contribution (Yoon, 2011). Nonlinear waves, however, might have a very different structure than the above assumed planar wave nature. Then also the density modulation can have a different shape than the found sinusoidal dependence on the phase, and the condition for a non-negative density would look differently. But the examination of this is beyond the scope of this work.

The method is the following: Firstly, values for k_y and k_z are chosen. The dispersion relation in Eq. (VI-4.33) then delivers the adequate value for ω. The amplitude of the wave is determined by choosing a value for B_2. With the upper set of equations, the polarization of the magnetic field and the density amplitude are fully determined. The velocity field can then be calculated by Eq. (VI-4.37) in the form

$$\begin{aligned} v_{\mathrm{p}x} &= -\frac{k_z}{\omega} v_{\mathrm{A}}^2 \frac{B_1}{B_0} \cos(\boldsymbol{k}\cdot\boldsymbol{r} - \omega t), \\ v_{\mathrm{p}y} &= \left(-\frac{k^2 v_{\mathrm{A}}^2}{k_z \omega} \frac{B_2}{B_0} + \frac{k_y}{\omega} c_{\mathrm{e}}^2 \frac{\hat{n}_{\mathrm{e}}}{n_0} \right) \sin(\boldsymbol{k}\cdot\boldsymbol{r} - \omega t), \\ v_{\mathrm{p}z} &= \frac{k_z}{\omega} c_{\mathrm{e}}^2 \frac{\hat{n}_{\mathrm{e}}}{n_0} \sin(\boldsymbol{k}\cdot\boldsymbol{r} - \omega t). \end{aligned} \tag{VI-4.47}$$

VI.4.2 Results

The numerical costs are higher in the two-dimensional case. Therefore, the spatial resolution has to be reduced. A grid size of $2\times1024\times1024$ cells is chosen. The minimum in the x-direction is given by 2 for internal programming reasons. The number of superparticles per cell is set to 500 and the time step is 0.01 in units of the inverse proton gyrofrequency. The parametric decay is studied for a monochromatic wave with the amplitude $B_2 = 0.2|\boldsymbol{B}_0|$. The plasma betas are set to $\beta_{\mathrm{p}} = \beta_{\mathrm{e}} = 0.1$.

The boundary conditions are a bit more sophisticated in the case of oblique propagation. The size of the simulation box has to be chosen carefully to make the periodic boundary conditions useful. If the oblique wave does not connect correctly on the upper and lower boundaries and on the left and right boundaries, the boundary itself will lead to wave deformation and undesired side effects such as a non-vanishing divergence of the magnetic field on the boundaries. The number of wave maxima n_z in the z-direction is a useful input parameter. The number of wave maxima in the y-direction is denoted by n_y. It is required that the phases of the wave correspond to each other on the opposite boundaries, which can be written as

$$k_y y + k_z \cdot 0 = k_y y + k_z L_z - 2\pi n_z, \tag{VI-4.48}$$

$$k_y \cdot 0 + k_z z = k_y L_y + k_z z - 2\pi n_y. \tag{VI-4.49}$$

Then the wavenumber $k = \sqrt{k_y^2 + k_z^2}$ is chosen as

$$k = \frac{2\pi n_z}{L_z \cos\vartheta} \tag{VI-4.50}$$

with the size L_z of the box in z-direction. Under this condition, the upper and lower boundaries have the same values for all arbitrary y. The size L_y in the perpendicular direction should be fixed by

$$L_y = \frac{L_z}{\tan\vartheta} \frac{n_y}{n_z} \tag{VI-4.51}$$

to fulfill the condition of equal connection on the left-hand and right-hand side of the box. It is a suitable idea to make the simulation box as close to the quadratic box as possible

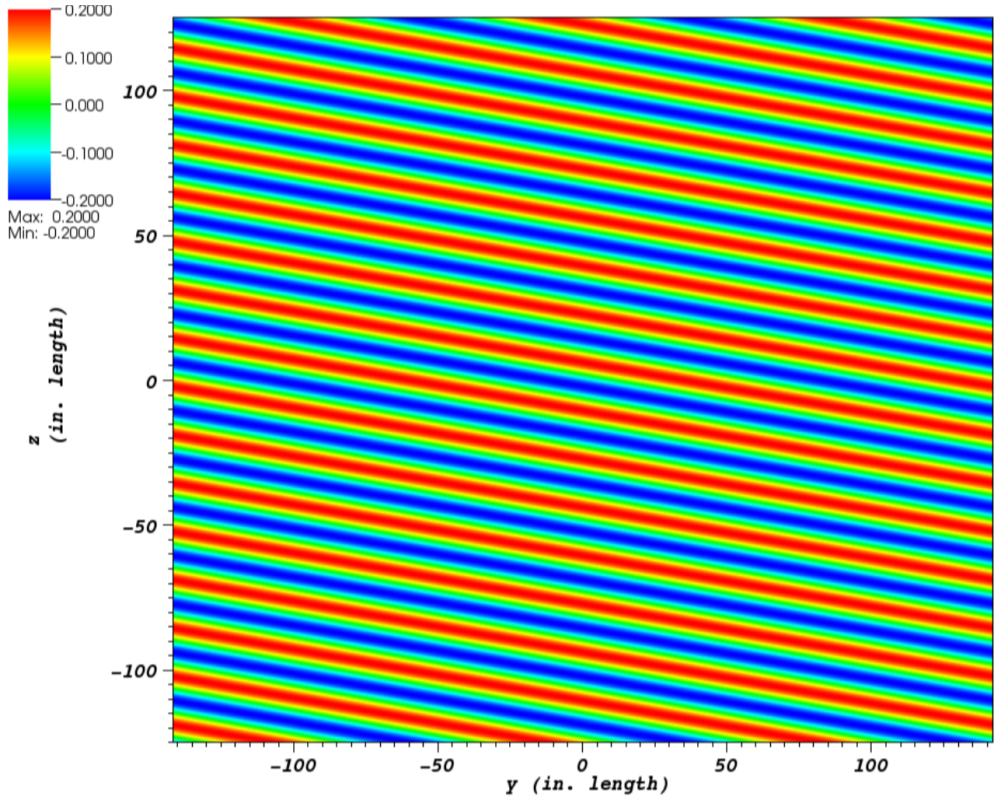

Figure VI-6: Component B_y in the y/z-plane. It is the initial setup for the simulation of obliquely propagating Alfvén/ion-cyclotron waves with $\vartheta = 10°$.

(i.e., $L_y \approx L_z$). This condition and the correct connection lead to the number of maxima n_y in the form

$$n_y = \mathrm{int}\,(n_z \tan\vartheta) + 1. \tag{VI-4.52}$$

The number one is added to keep the box size in y-direction non-zero in the limit of small values for n_z and ϑ. The number of wave trains n_z is chosen in a way that the wavenumber keeps more or less the same value, independent of the angle ϑ. Little deviations in k might occur since the number n_z has to be an integer, too. The wavenumber is fixed to $k \approx 0.39$ in normalized units for the first run.

A typical initial setup for the magnetic field is shown in Fig. VI-6. The condition for the periodic boundaries is clearly visible in this plot. The values of B_y are equal on the upper and the lower boundaries for the same value of y. The values of B_y are equal on the left and the right boundaries for the same values of z. Due to the plane wave ansatz, this condition is fulfilled for all oscillating quantities. Only in this case, the condition $\mathrm{div}\,\boldsymbol{B} = 0$ is guaranteed since otherwise the boundaries generate a source of magnetic field simply due to the jump on these surfaces.

After 50 000 time steps, corresponding to the time $t = 500$, the wave has decayed already. The two-dimensional spectrum is shown in Fig. VI-7. The initial oblique pump wave is visible as a dot at $k_y \approx 0.06$ and $k_z \approx 0.38$. Energy is mainly transported along the initial direction of the wave. It seems to have a higher power until $k_z = 1$ in normalized

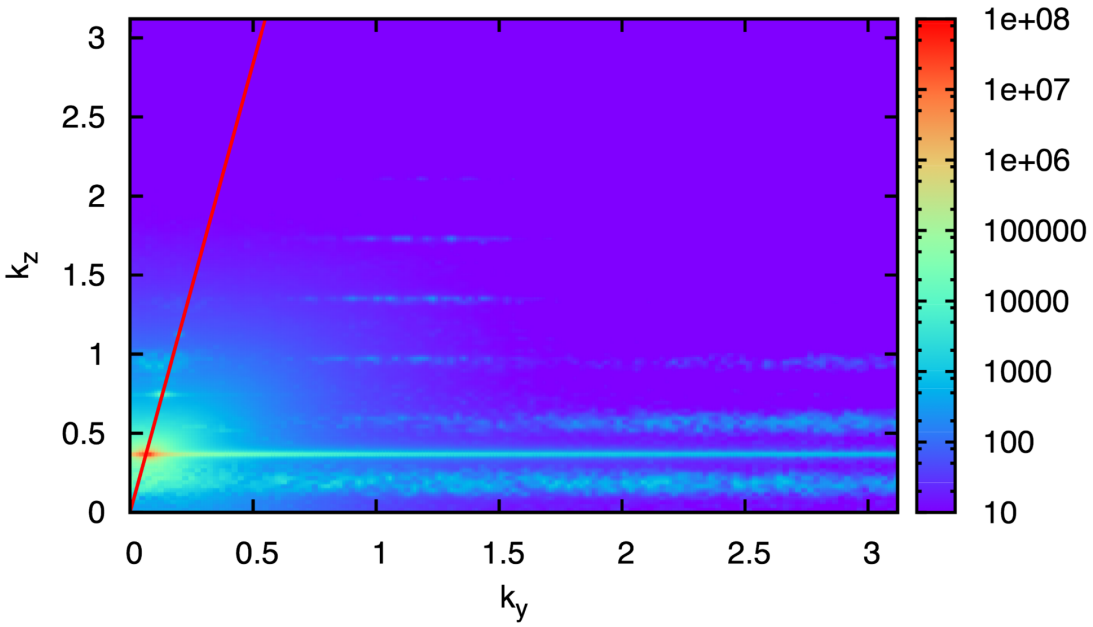

Figure VI-7: Two-dimensional power spectral density of magnetic field fluctuations after $t = 500$. The red line indicates the initial propagation direction with $\vartheta = 10°$. The color coding represents the power spectral density in arbitrary units.

units, which means that also here a spectral break should be expected. There is an increase in wave activity at higher k_y, and significant power is distributed there additionally. At very low values for k_z, a broader perpendicular pattern is visible.

Also the density fluctuation spectrum in two dimensions can be calculated from the simulated data. It is shown in Fig. VI-8. It indicates that the main features visible in the magnetic fluctuation spectrum also possess a compressive component. This is especially true for all components having a non-zero k_y. The lower total level of these fluctuations permits to show some filamentary intermediate structures, which are not as clearly visible in the magnetic field spectrum. These should be understood as a broad-band compressive component of the daughter products.

To study the power distribution in more detail, the 2D Fourier transform can be cut along the direction of the initial propagation. It corresponds to a cut along the red line in Figs. VI-7 and VI-8. The one-dimensional power spectra are shown in Figs. VI-9 and VI-10. The initial wave is still visible in both the magnetic field fluctuations and the density fluctuations. Remember that the initial wave is compressive already due to its obliquity. The initial wave looses some energy compared to the beginning. Energy is first given to different wavenumbers and then dissipated at the small dissipative scales. The wave decays to daughter waves with higher and lower wavenumbers compared to the initial wavenumber.

The dispersion of the daughter waves can in general be determined along any direction in the (k_y, k_z)-plane. Since an enhancement of energy is seen along the initial direction of propagation (i.e., along the red line in Fig. VI-7), it is appropriate to calculate the dispersion along this line. Therefore, the two-dimensional spatial Fourier transform is applied, and a cut is taken along the direction $\vartheta = 10°$ for 60 different time steps, which are sep-

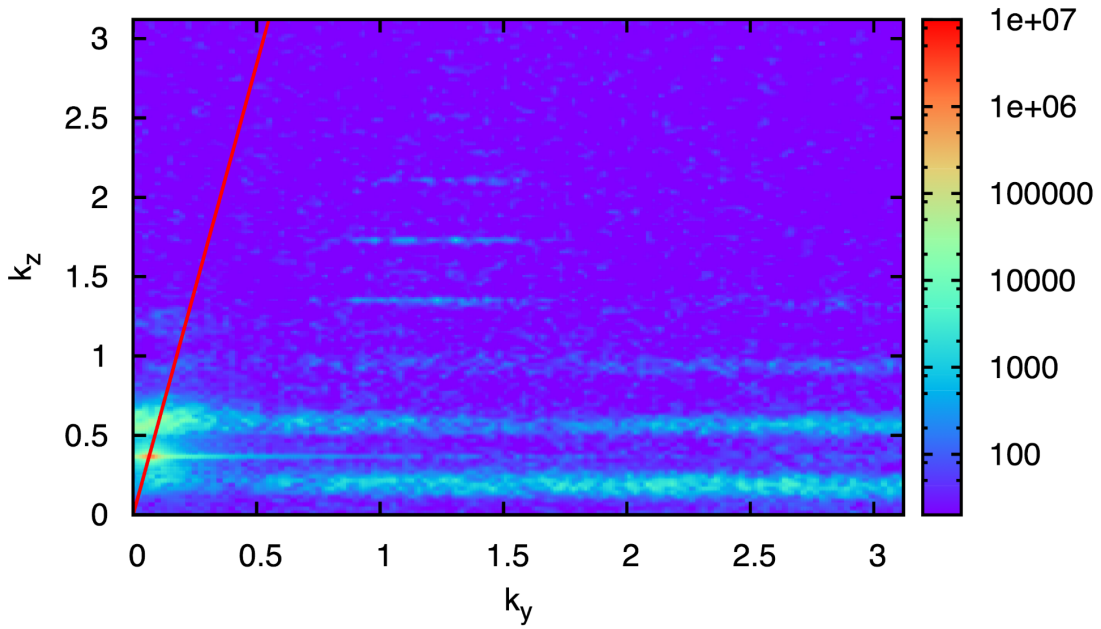

Figure VI-8: Two-dimensional power spectral density of density fluctuations after $t = 500$. The red line indicates the initial propagation direction with $\vartheta = 10°$. The color coding represents the power spectral density in arbitrary units.

arated by a time difference of $1/\Omega_p$. The result is shown in Fig. VI-11. The enhanced power in the (k_y, k_z)-analysis is also very well located in the (ω, k)-plane at $k \approx 0.75$ and $\omega \approx 0.6$. Comparing this point with the theoretical cold dispersion analysis of oblique A/IC waves, shown as a red curve (or in Fig. VI-5, respectively), reveals that this point is located very close to the branch of this wave mode. The pump wave has a significant amplitude compared to the background magnetic field. Therefore, the polarization field has to be added to the background and thus modifies the field, around which the daughter waves propagate. The guiding field is not anymore strictly parallel to the z-axis. This effect leads to a small broadening and shift in the dispersion analysis.

Calculations with further, moderately oblique propagation angles show comparable results, especially the preferred direction of daughter wave propagation along the initial direction. The obliquity is, however, not arbitrarily high for A/IC waves as stated before.

VI.5 Discussion

The one-dimensional parallel simulation allows one to calculate the evolution of the plasma over a long time interval and with a high spatial resolution. Decay products with lower and higher wavenumbers compared to the initial wavenumber of the pump wave are found. The waves become compressive, which is not the initial situation in the parallel case.

In the two-dimensional simulation, the computational limitations are more severe. The daughter waves, which are generated already after quite a short time of evolution,

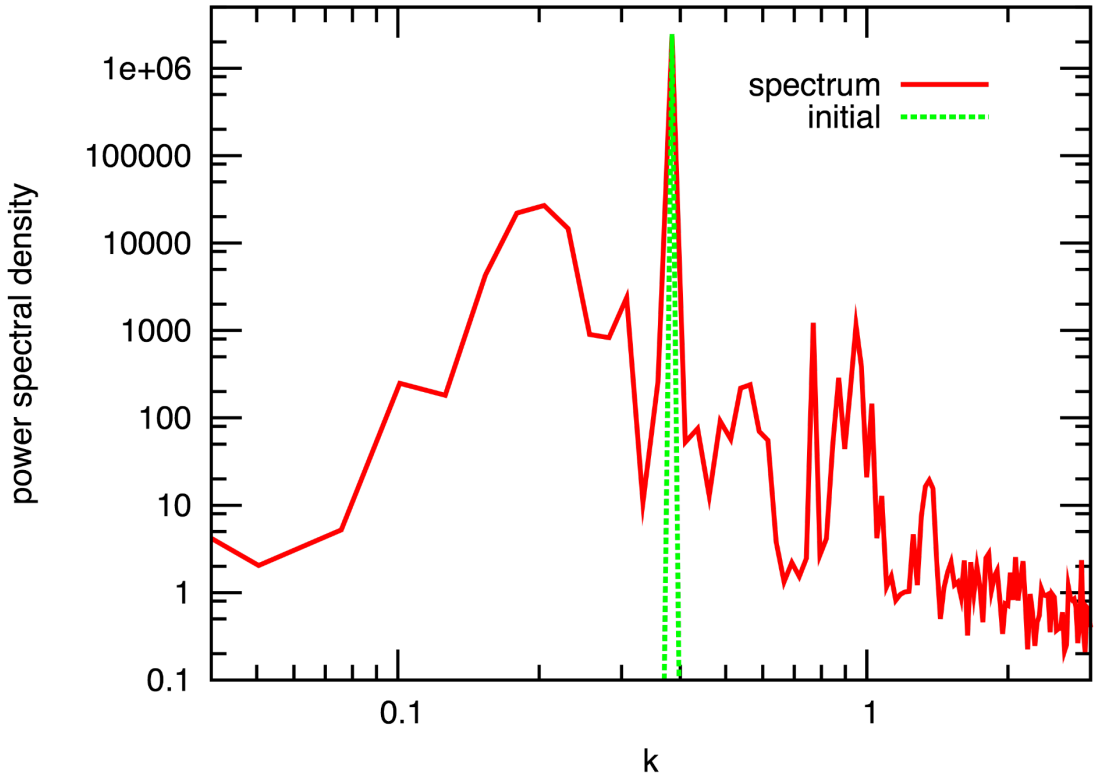

Figure VI-9: One-dimensional power spectral density for magnetic field fluctuations after $t = 500$ along the initial direction of propagation. Additionally the initial spectrum is shown.

are mainly aligned along the initial direction of propagation. This can be understood as a consequence of the conservation of momentum. In general, the wavevectors of the pump wave and the two daughter waves have to form a triangle to fulfill this conservation in a three-wave process. Other arbitrary combinations would be possible for an interaction between four or even more waves (Davidson, 1972). However, it seems that the background magnetic field is not the most important guiding structure, but rather the initial propagation direction forces the geometry of the daughter-wave system at the present parameter set. The oblique hybrid simulations by Matteini *et al.* (2010) can also be interpreted in this sense, even though the authors favor the interpretation of a field-parallel spectral transfer. However, the difference to their setup is the more realistic initialization in the above case apart from the higher numerical resolution. The daughter waves with lower wavenumbers seem to orient themselves more perpendicular to the background field. The modulational instability is the generation mechanism here and seems to favor this direction of propagation.

The role of compressive effects becomes clear in both the one-dimensional and the two-dimensional analysis. The parallel wave is intrinsically incompressive, but the decay generates compressive fluctuations very efficiently. The oblique wave is intrinsically compressive due to its polarization. During its evolution and decay, it also generates a broad spectrum of compressive fluctuations. It is known from other treatments that com-

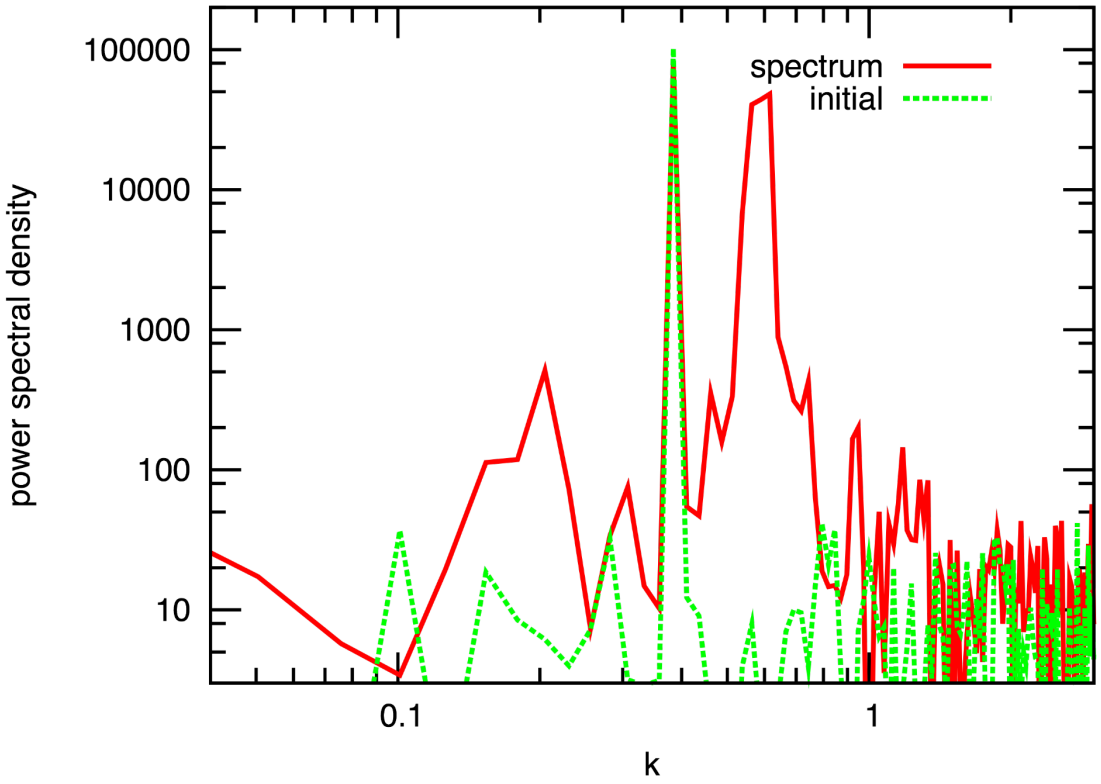

Figure VI-10: One-dimensional power spectral density for density fluctuations after t = 500 along the initial direction of propagation. Additionally the initial spectrum is shown.

pressive waves steepen eventually and can lead to a situation, which the numerical solver cannot handle. Therefore, it is important to choose the evaluation time properly and stay far enough from these steepened end points of the integration. The above results (esp., the normal mode structure and the still dominating pump-wave amplitude), however, underline that the critical time has not yet been reached in this case. It is important to remember that the amplitude of oblique waves is in any case not arbitrary. Its intrinsic compressive effects give an upper limit because negative density values have to be forbidden (Yoon, 2011). This is irrelevant for the parallel propagation.

The dispersion relation of the decay products from the oblique two-dimensional simulation shows that these daughter waves are still A/IC waves, yet with higher wavenumber and frequency. Other wave modes such as the fast/whistler branch for example are not visible. This result is in agreement with previous treatments of the parametric decay, which have shown that the A/IC wave is a typical daughter product of the decay (Araneda *et al.*, 2007). The interpretation is the following: The initial oblique A/IC wave with wavenumber k_0 is prone to the decay instability with $k > k_0$ and the modulational instability with $k < k_0$. Dispersive effects let the decay instability generate A/IC waves (Hollweg, 1994). Obviously this effect occurs very efficiently for $k \gtrsim 0.6$. Daughter waves are only excited in certain ranges and not on a broad wavenumber range. The A/IC waves, however, can easily fulfill the condition of cyclotron resonance for sufficiently high frequencies/wavenumbers. Thus, there is an upper limit for the occurring A/IC waves due

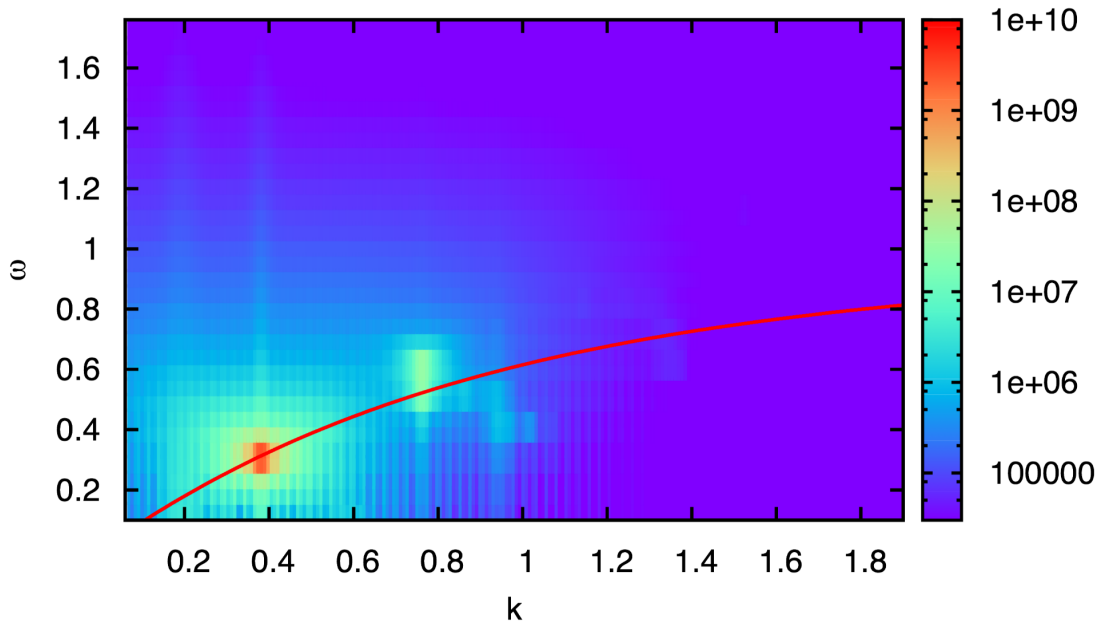

Figure VI-11: One-dimensional dispersion analysis of magnetic field fluctuations along the direction $\vartheta = 10°$. The color coding represents the power spectral density. The enhancement in power corresponds to A/IC waves propagating obliquely to the background magnetic field. The red line shows the cold dispersion relation for oblique A/IC waves with $\vartheta = 10°$.

to the onset of cyclotron damping. This leads to a quite sudden cut in the spectrum at $k \approx 0.9$. The dispersion diagram together with this typical onset of damping underlines the A/IC nature of the daughter waves.

The temperature of the particles does not increase significantly over the integration time. This may be due to the comparably low intensity of the daughter waves and the limited simulation time. One-dimensional simulations show an increase and saturation of particle temperatures due to resonant wave–particle interactions (Araneda *et al.*, 2009). The temperature in the above simulations does, however, increase if no divergence-cleaning or smoothing algorithm is applied to the electromagnetic fields. So maybe a possible heating is suppressed by these schemes, or the observed heating in the previous simulations is only a numerical artifact. This question cannot be answered conclusively here.

VII Spectral transfer of weak turbulence from MHD scales into the kinetic regime

Parts of this chapter have been submitted to a journal before submission of the thesis. The reference of the article is:

Verscharen, D., Marsch, E., Motschmann, U., and Müller, J: *Kinetic cascade beyond MHD of solar wind turbulence in two-dimensional hybrid simulations*, Phys. Plasmas, accepted, 2012

VII.1 The nature and origin of turbulence on kinetic scales

The solar wind is a dilute plasma and known to be in a highly-turbulent state. It exhibits fluctuations in the electromagnetic field, the plasma density, and bulk flow velocity over a wide range of scales (see Chapt. I). However, the nature of solar wind turbulence in the intermediate wavenumber regime situated between the large inertial MHD scales and the small dissipative electron scales is not well understood. Especially the role of oblique wave propagation with respect to the background Parker field is currently under debate. Some authors favor a more or less independent behavior of the so-called slab component (parallel with respect to the background magnetic field) and 2D turbulence (perpendicular) (Montgomery and Turner, 1981; Bieber *et al.*, 1996; Oughton *et al.*, 1998). While in this picture the highly-oblique 2D turbulence is believed to be an example of a strongly-turbulent plasma state with high-order correlations between the fluctuating quantities, the slab component is assumed to be describable within the framework of weak turbulence theory, i.e., as a superposition of normal modes. Other authors interpret the observed anisotropy as being the result of a kinetic Alfvén wave (KAW) cascade (Howes, 2008; Schekochihin *et al.*, 2008), which would suggest a preference of fluctuations with $k_\perp \gg k_\parallel$.

Measurements made by the four Cluster spacecraft have provided further insights into the nature of solar wind turbulence since multi-spacecraft detections of magnetic fluctuations even permit the analysis of their three-dimensional dispersion properties. However, these measurements support different interpretations. A fully evolved nonlinear turbulent state with a preferred 2D component beyond the MHD range was found by Alexandrova *et al.* (2008a). The dispersion relation of this mainly perpendicularly structured component might reflect a nonlinear cascade that also occurs at small scales. However, an interpretation on the basis of normal modes, such as the right-hand circularly polarized

fast/whistler (F/W) waves, is still possible (Narita *et al.*, 2011).

There is strong evidence that the field-parallel component consists at least partly of Alfvén/ion-cyclotron (A/IC) waves, which are dispersive left-hand circularly polarized electromagnetic normal modes of a plasma. The temperature anisotropies and beam structures observed in the solar wind proton distribution functions were explained as resulting from cyclotron-resonant interactions of the ions with these waves (see Chapts. I and II; Marsch *et al.*, 2004; Heuer and Marsch, 2007; Bourouaine *et al.*, 2010). Recently direct wave measurements have confirmed the existence of A/IC waves in the solar wind (Jian *et al.*, 2009). Yet, due to cyclotron-resonant wave–particle interactions, they are strongly damped at wavenumbers corresponding to the inverse inertial length of the resonant ions (Ofman *et al.*, 2005), and thus they are not expected to exist at higher wavenumbers. A coexistence of left-handed and right-handed modes has been recently supported by measurements of the angle distribution of the magnetic helicity in the solar wind (He *et al.*, 2011a). Possible candidates for normal modes beyond the resonant wavenumber range are the F/W modes, which may remain after the dissipation of the A/IC waves (Stawicki *et al.*, 2001), or an ongoing cascade of dispersive KAWs (Howes, 2008). Both these wave modes show right-handed polarization under the conditions prevailing in the solar wind. It is observed that the right-hand polarized waves survive the spectral break, which indicates the transition from the inertial range to the ion dissipative scales, and that they can exist at higher wavenumbers without damping until the resonant electron scales are finally reached (Goldstein *et al.*, 1994).

The following numerical simulation work is focused on studying the transition of isotropic MHD turbulence to non-isotropic kinetic fluctuations on intermediate scales. For this purpose, at least two-dimensional numerical simulations are necessary, with which one can analyze the evolution of turbulence in different directions with respect to the constant background magnetic field. The model system is initialized by a superposition of linear MHD waves. No further external or ongoing driving force is applied, and thus the system will evolve freely from its initial state. The A.I.K.E.F. code has been described already in Chapt. VI. In the following, the boundary conditions are always set to be periodic. The normalization is the same as in Chapt. VI.

VII.2 One-dimensional analysis

VII.2.1 Numerical setup

Turbulence always shows a broad spectrum of waves. It is still unclear how wave energy is transported to higher wavenumbers in the dispersive range of the spectrum, where effects due to the finite ion gyroradius play a role. Furthermore, dissipation of waves by ions begins in the same wavenumber range. Thus, it is interesting to study the evolution of a broad wave spectrum in this wavenumber range. At the beginning, it is done in one spatial dimension parallel to the background magnetic field. The simulation can be initialized with a spectrum of waves. So Alfvén/ion-cyclotron (A/IC) waves are add up according to

$$\boldsymbol{B}_\mathrm{t} = \sum_{n=1}^{n_\mathrm{max}} b_n \begin{pmatrix} \cos(k_n z + p_n) \\ \sin(k_n z + p_n) \end{pmatrix} \tag{VII-2.1}$$

for the transverse magnetic field vector $\boldsymbol{B}_\mathrm{t}$ with $k_n = k_0 + n\Delta k$. The values k_0 and Δk are chosen in an appropriate way to cover the spectrum between k_0 and a maximum value k_max equidistantly in k-space. A random phase between zero and 2π is generated for each wave and is denoted by p_n. This guarantees that, at certain positions like $z = 0$, the field does not pile up. The amplitudes b_n are fixed in such a way that the power spectrum $\mathcal{P}_k$ follows the typical Kolmogorov power-law with a power-index of $-5/3$. This implies $b_n \propto k_n^{-5/6}$. The amplitude is fixed in such a way that the integrated averaged transversal energy density corresponds to the transversal energy density of a monochromatic wave of the amplitude A. Such a monochromatic wave has a transversal energy density

$$\mathcal{E} = \frac{A^2}{8\pi}. \tag{VII-2.2}$$

For the spectrum, the averaged energy density is defined as

$$\bar{\mathcal{E}} \equiv \frac{1}{8\pi T}\int_0^T |\boldsymbol{B}_\mathrm{t}|^2 \mathrm{d}t. \tag{VII-2.3}$$

Parseval's theorem states that the total power in Fourier space has to be the same as the total power in configuration space. For finite time series, it reads

$$\frac{1}{T}\int_0^T |\boldsymbol{B}(t)|^2 \mathrm{d}t = \sum_{n=-\infty}^{\infty} |\boldsymbol{B}(\omega_n)|^2, \tag{VII-2.4}$$

where the Fourier coefficients are defined as

$$\boldsymbol{B}(\omega_n) \equiv \frac{1}{T}\int_0^T \boldsymbol{B}(t) e^{i\omega_n t}\mathrm{d}t \tag{VII-2.5}$$

with $\omega_n = 2\pi n/T$. For a real signal $\boldsymbol{B}(t)$, one can write

$$\frac{1}{T}\int_0^T |\boldsymbol{B}(t)|^2 \mathrm{d}t = \boldsymbol{B}_0^2 + 2\sum_{n=1}^{\infty} |\boldsymbol{B}(\omega_n)|^2 \tag{VII-2.6}$$

(Båth, 1974; Eriksson, 1998). The power spectral density is defined as

$$\mathcal{P}_n = 2T|\boldsymbol{B}(\omega_n)|^2. \tag{VII-2.7}$$

This leads to Parsevals's theorem in the form

$$\frac{1}{T}\int_0^T |\boldsymbol{B}(t)|^2 \mathrm{d}t = \mathcal{P}_0\frac{\Delta\omega}{2} + \sum_{n=1}^{\infty}\mathcal{P}_n\Delta\omega \tag{VII-2.8}$$

with $\Delta\omega = (2\pi T)^{-1}$.

In this case, the total energy density can now be connected with the wave amplitudes b_n by

$$A^2 = \sum_{n=1}^{n_{\max}} b_n^2, \tag{VII-2.9}$$

which leads to

$$b_n = \frac{A k_n^{-5/6}}{\sqrt{\sum_{n=1}^{n_{\max}} k_n^{-5/3}}}. \tag{VII-2.10}$$

For each wave component, the dispersion relation is evaluated according to Eq. (VI-3.24) and the transversal wave velocity field by

$$\boldsymbol{V}_{j\mathrm{t}} = \sum_{n=1}^{n_{\max}} v_n \begin{pmatrix} \cos(k_n z + p_n) \\ \sin(k_n z + p_n) \end{pmatrix} \tag{VII-2.11}$$

with v_n following from the polarization relation in Eq. (VI-3.22) for each wave component. This superposition is not an exact solution anymore because the superposition leads to net ponderomotive fields. However, since the contribution of each wave is only small, this choice of the initial polarization is still adequate. The system itself will find the real polarization after a few steps autonomously and self-consistently. An example for the initial power spectrum is shown in Fig. VII-1.

VII.2.2 Results

Case A In the first case, the evolution of a spectrum, which passes already over the dissipative scales, is treated. Therefore, a spectrum continuing up to $k_{\max} = 2$ is initialized with 60 A/IC waves beginning at $k_0 \approx 0.06$. It can be used to investigate how power is transferred into the dissipation range and how kinetic resonances can change the spectral slope. Each cell is filled with 400 superparticles. The initial amplitude is set to $A = 0.1$ and the plasma beta to $\beta_\mathrm{p} = 0.08$. The initial condition is by definition incompressible. The spectra at different times during the evolution are shown in Fig. VII-2.

Case B In the second case, the spectrum is initialized only up to $k_{\max} = 0.5$ to see the interesting spectral range, in which the A/IC waves can act as the source of resonant heating. The region in which their damping dominates can be found in this case. The other parameters are chosen as before. The power spectrum after the time $t = 1125$ is shown in Fig. VII-3. Also here a spectral break is clearly visible. At $k_z \approx 0.5$, the spectrum drops significantly. Up to $k_z \approx 3$, the power spectrum remains on a more or less constant level. The break point is closer to the inverse inertial length than to the inverse gyroradius, which is expected at $\ell_\mathrm{p}/r_\mathrm{p} = \sqrt{2/\beta_\mathrm{p}} = 5$. The strong break in the spectrum is in agreement with a combination of normal modes of the turbulence as it can be assumed in weak turbulence (Li *et al.*, 2001). The onset of the kinetic damping, which is natural for normal modes, leads to a distinct cutoff in the spectrum.

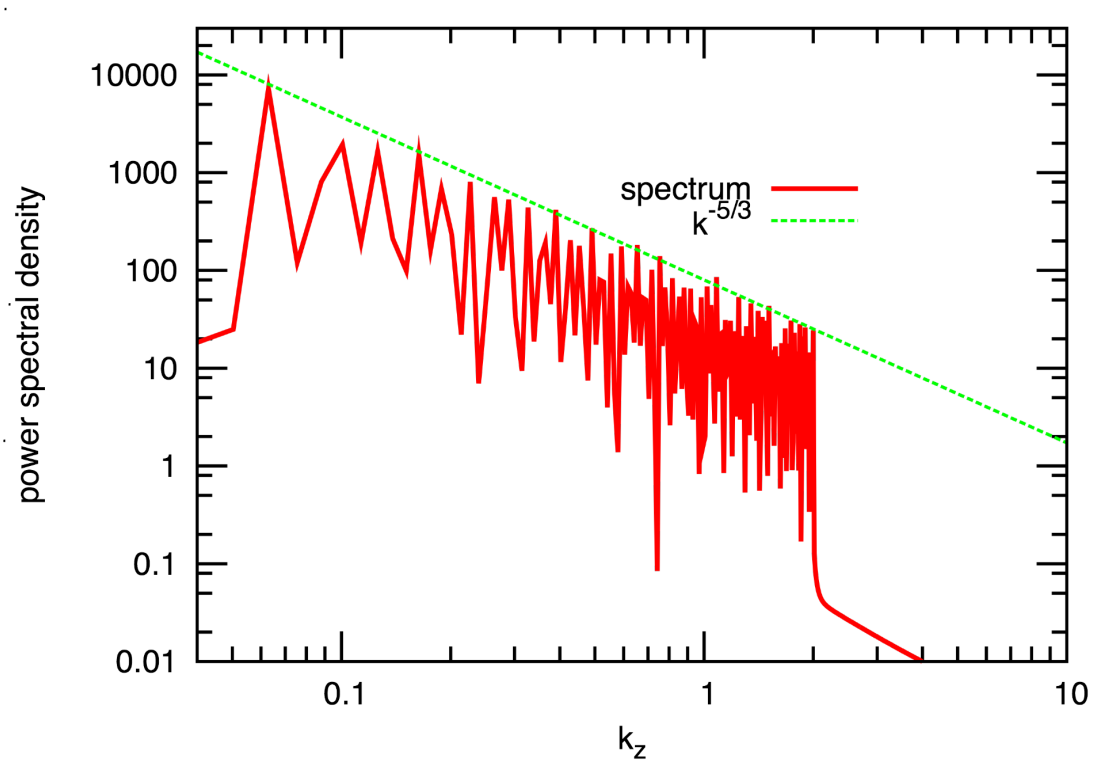

Figure VII-1: Initial spectrum of A/IC waves. The transversal power is shown depending on wavenumber k_z. It consists of a superposition of 60 waves at equidistant spectral positions between $k_0 = 0.06$ and $k_{\max} = 2$. The intensities of the single constituents follow a power-law with the Kolmogorov power index of $-5/3$. At low k-values, the single modes become apparent due to the logarithmic plotting.

In order to determine the nature of the higher-frequency part in detail, a dispersion analysis has to be applied. A typical dispersion diagram after a sufficient time of evolution is shown in Fig. VII-4, taken with $N_t = 400$ and $\Delta t = 10$.

Two dispersion branches occur with small widths. One branch ends at $k \approx 0.8$; the other one continues almost with a quadratic dependence of ω on k_z at higher wavenumbers and frequencies. For the later discussion, the red curve in Fig. VII-4 shows the R-mode or fast/whistler mode dispersion including some further corrections for ionic influences at low wavenumbers additionally to the quadratic behavior of the whistler wave. This dispersion relation has been discussed already in Chapt. V. It is given by

$$\omega = \frac{k^2}{2}\left[1 + \sqrt{1 + \frac{4}{k^2}}\right] \qquad \text{(VII-2.12)}$$

in this normalization.

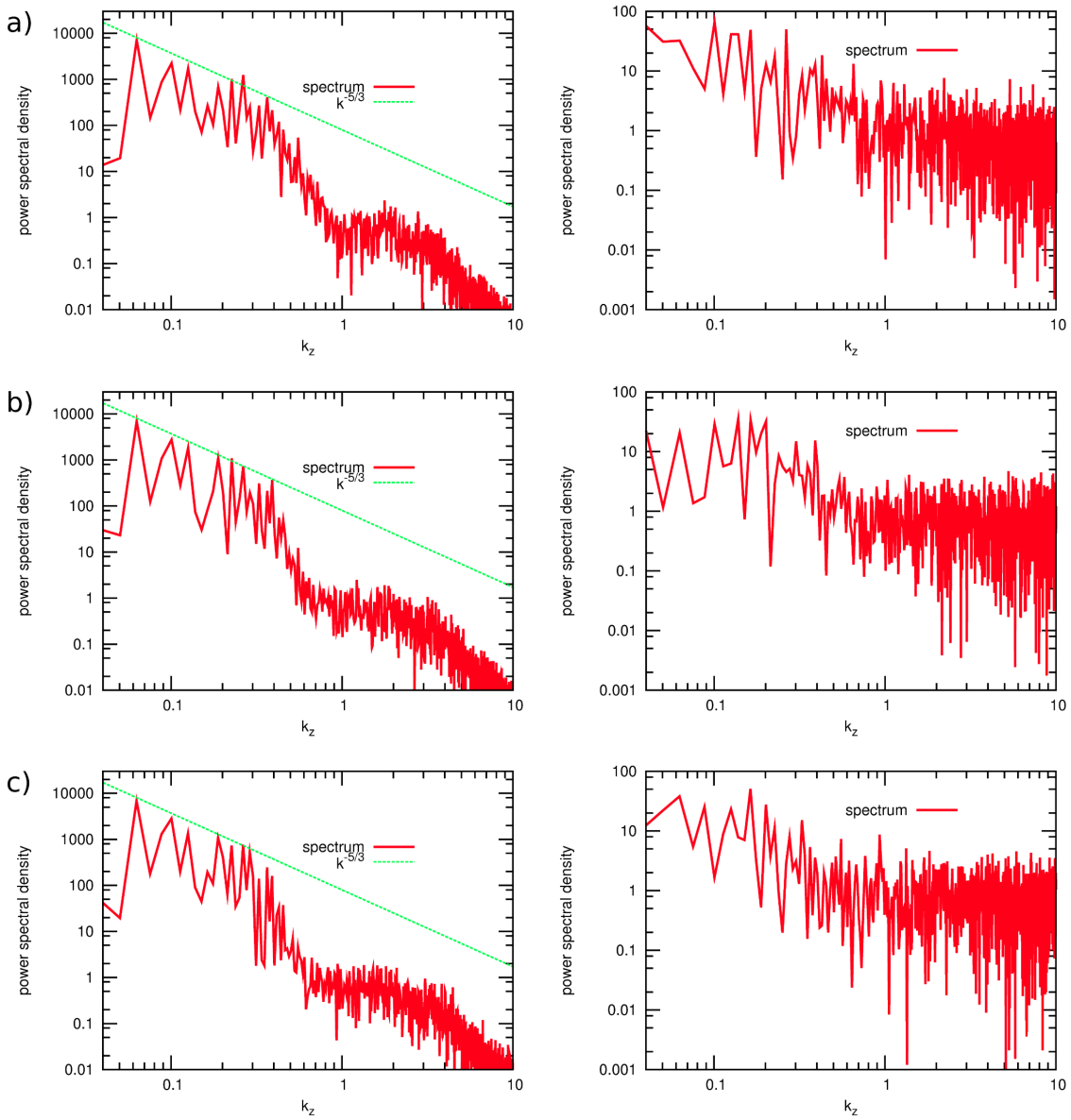

Figure VII-2: The left panels show the power spectral density of transversal magnetic field fluctuations, the right panels show the power spectral density of density fluctuations for Case A in arbitrary units. The line for the Kolmogorov spectrum with power-index $-5/3$ has in all cases the same amplitude as in Fig. VII-1 to make the transfer comparable. a) $t = 630$, b) $t = 1000$, c) $t = 1500$.

VII.3 Two-dimensional analysis

VII.3.1 Numerical setup

The width of the Maxwellian distribution is determined by the species' beta, which represents the ratio of thermal to magnetic energy density and is set to $\beta_\mathrm{p} = 0.05$ for the protons. The electron beta is fixed at $\beta_\mathrm{e} = 0.5$. In this beta regime, even low amplitudes

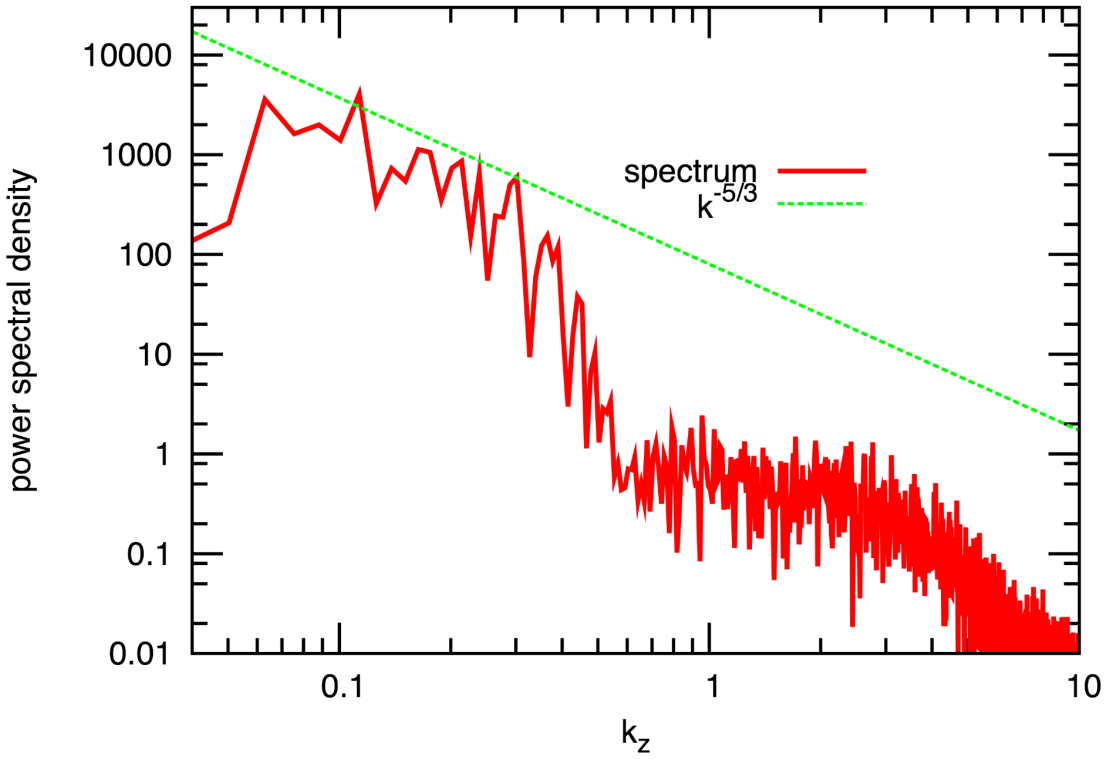

Figure VII-3: Power spectral density of the transversal magnetic field fluctuations at t = 1125 in arbitrary units for Case B.

of magnetic fluctuations will have a strong influence on the motion of the particles due to their high magnetization. In the known normalization, the two-dimensional integration box has a size of 250 × 250, which is covered by 2 × 1024 × 1024 cells, each of which filled with 500 superparticles representing the real number density of protons. A divergence-cleaning algorithm is applied to guarantee numerical stability.

The initial magnetic field is given as a superposition of linear Alfvén waves according to

$$\delta B_x = \sum_{m=1}^{m_{\max}} \sum_{n=1}^{n_{\max}} b_n \cos(k_n y \sin \vartheta_m + k_n z \cos \vartheta_m + p_{n,m}), \tag{VII-3.13}$$

where a constant background field $\boldsymbol{B}_0$ is aligned along the z-axis. A random phase shift $p_{n,m}$ is applied to each wave. The amplitudes b_n are fixed in such a way that the power spectrum follows a Kolmogorov power-law (Kolmogorov, 1941) in wavenumber with the scaling $\propto k^{-5/3}$, and the total power of the composed wave field is made equal to the power of a monochromatic wave with $\delta B = 0.01 B_0$. The angles ϑ_m cover 360° of propagation directions by $m_{\max} = 50$ discrete values, and the spectrum ranging between $k_0 = 0.05$ and $k_{\max} = 0.2$ is covered by $n_{\max} = 20$ waves. The upper limit $k_{\max}$ is quite high compared to typical MHD scales but still in the dispersion-less range in first order. The initial velocity

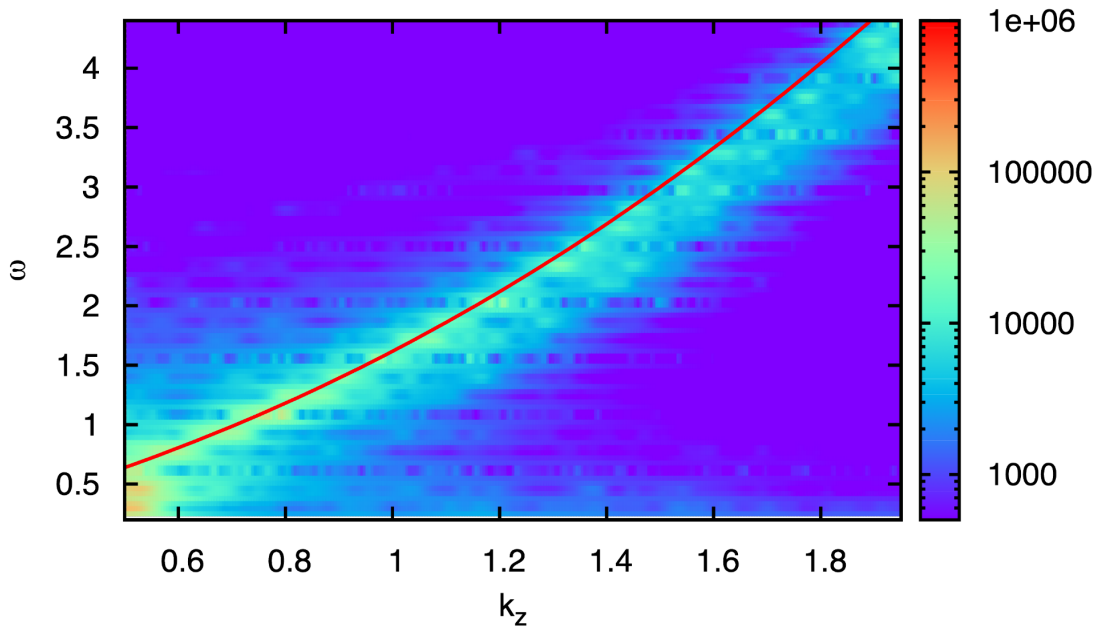

Figure VII-4: Dispersion relation at $t \approx 1125$ in Case B. The color indicates the power spectral density in arbitrary units. The red line shows the cold dispersion relation for fast/whistler waves with ion corrections at low wavenumbers.

is obtained from the Alfvénic polarization relation

$$\frac{\delta \boldsymbol{V}}{V_\mathrm{A}} = \mp \frac{\delta \boldsymbol{B}}{B_0} \tag{VII-3.14}$$

with the Alfvén speed $V_\mathrm{A} = \ell_\mathrm{p}\Omega_\mathrm{p}$.

VII.3.2 Results

In this section, some results of the numerical simulation runs are shown. The code ran for a sufficiently long time so that an evolved nonlinear dynamic plasma state could be expected. This was typically the case after an evolution time of about 500 gyroperiods, at which time the system was analyzed. For this purpose, Fourier transformations in two dimensions were applied subsequently to the magnetic field data and the density data. The power spectral density was then calculated and could be shown to depend on the wavenumbers k_z for the direction parallel to the background field and k_y perpendicular to it. The resulting magnetic field power spectral density is shown in Fig. VII-5, and the power spectral density of the compressive fluctuations is shown in Fig. VII-6. For comparison, the initial power spectral density of magnetic field fluctuations is presented in Fig. VII-7.

Apparently the magnetic field fluctuations show a preferred alignment with the direction perpendicular to the background magnetic field. Especially, turbulence energy is spreading in this direction to much higher wavenumbers than in the parallel direction. But also the parallel fluctuations at wavenumbers beyond the initialized range are excited and

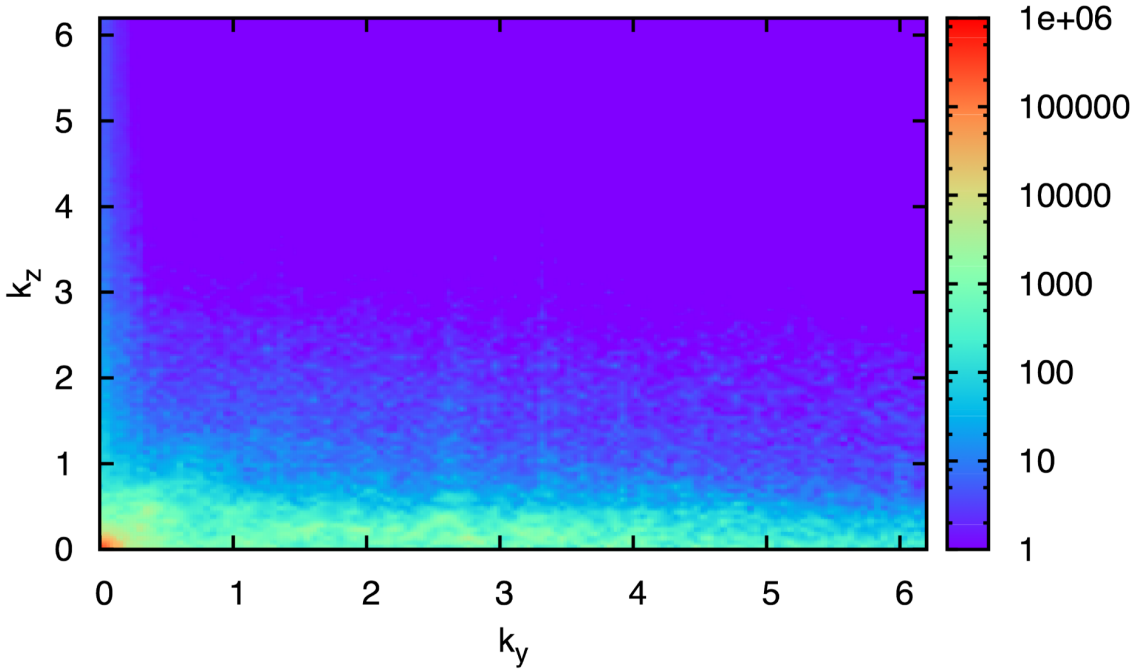

Figure VII-5: Two-dimensional power spectral density of magnetic field fluctuations in arbitrary units. The background magnetic field is oriented along the k_z-axis. The cascade of energy into the high-wavenumber ranges occurs preferentially in the perpendicular direction.

gain energy. The compressive density fluctuations, however, are mainly aligned perpendicularly to the background field and have almost no components parallel to $\boldsymbol{B}_0$.

Cuts through the two-dimensional spectra along the perpendicular direction are shown in Fig. VII-8.

The power spectral density of the compressive fluctuations in the proton number density is enhanced for $k_y \gtrsim 1$ and follows mainly a power-law with a slightly steeper index than $k^{-5/3}$ in this range. The magnetic field spectrum is flatter in the dispersive range.

To study the nature of these fluctuations, a Fourier transformation can also be used, but here it is applied in the time domain leading to the corresponding dispersion diagrams. Therefore, first the two-dimensional spatial Fourier transformation is applied, and the result is taken in one dimension only (parallel or perpendicular to $\boldsymbol{B}_0$). Then the data are yet again Fourier transformed, now with respect to time. The result for the parallel magnetic field dispersion is shown in Fig. VII-9. Two sharp branches can clearly be seen beyond the initial wavenumber limit at $k_{\max} = 0.2$. For an easier identification of them, the cold-plasma dispersions for the left-handed A/IC waves and for the right-handed F/W waves are additionally shown in the parallel dispersion diagram (Stix, 1992). The observed parallel dispersion agrees well with that of the linear normal modes. The A/IC branch ends at a wavenumber value below 1, whereas the right-handed branch continues to higher wavenumbers and frequencies.

The perpendicular magnetic field dispersion is depicted in Fig. VII-10. Since the density fluctuations are mainly perpendicularly oriented, their parallel dispersion diagram

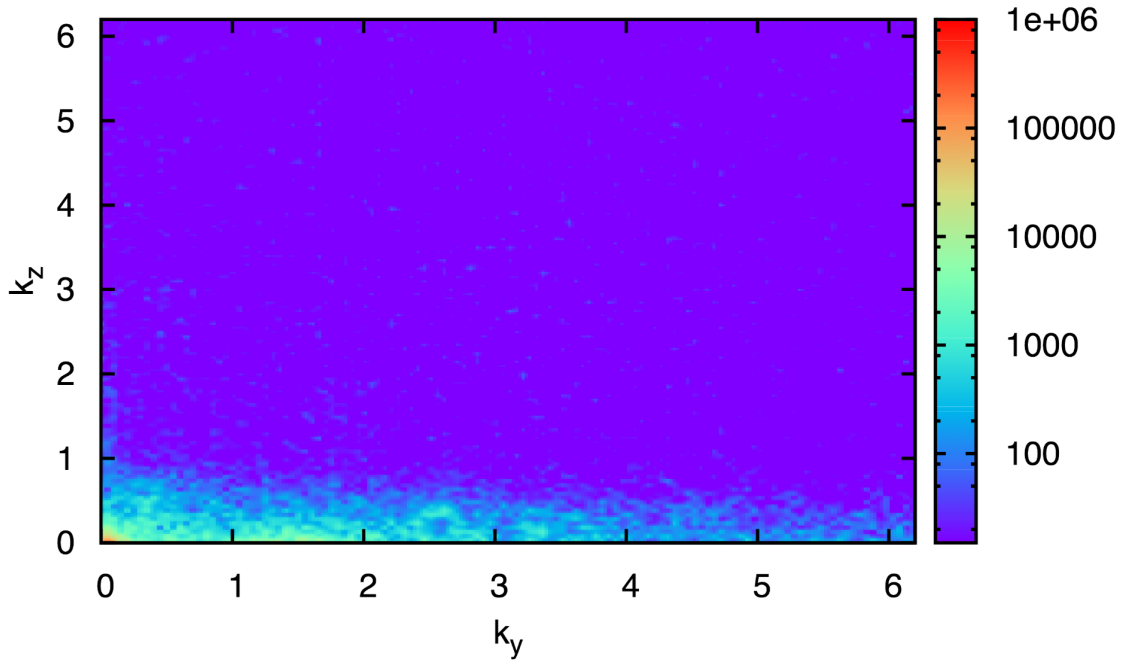

Figure VII-6: Power spectral density of compressive fluctuations in the proton number density in arbitrary units. The spatial variation of the fluctuations occurs mainly perpendicularly to the background magnetic field.

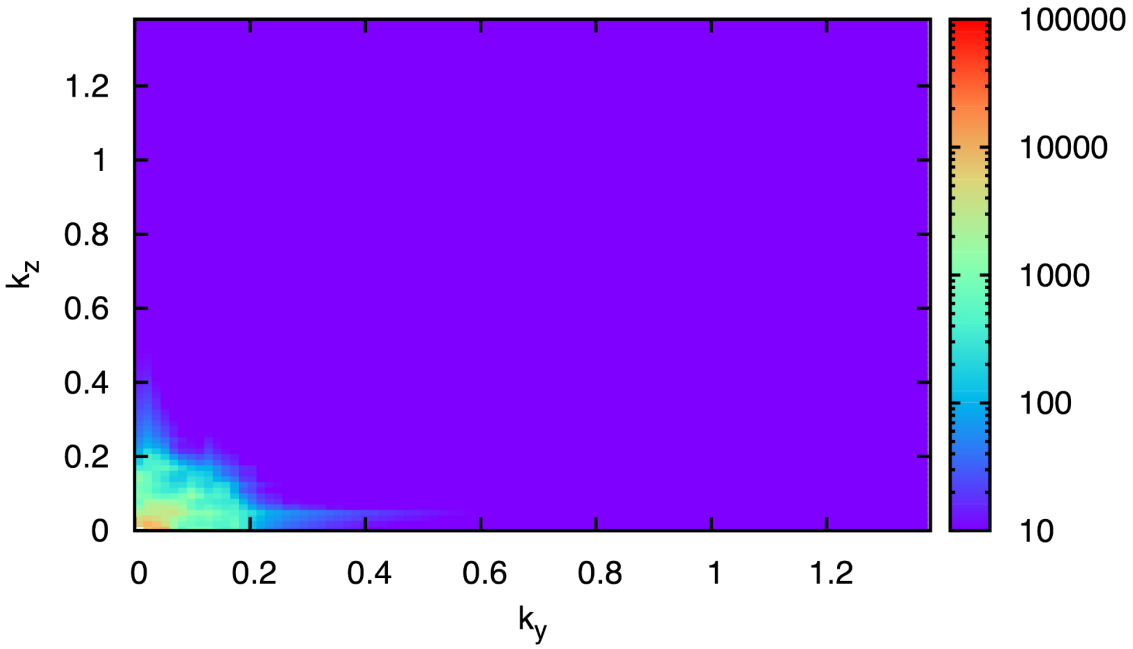

Figure VII-7: Initial power spectral density of magnetic field fluctuations in arbitrary units at $t = 0$.

is not shown here. But the perpendicular dispersion diagram is illustrated in Fig. VII-11.

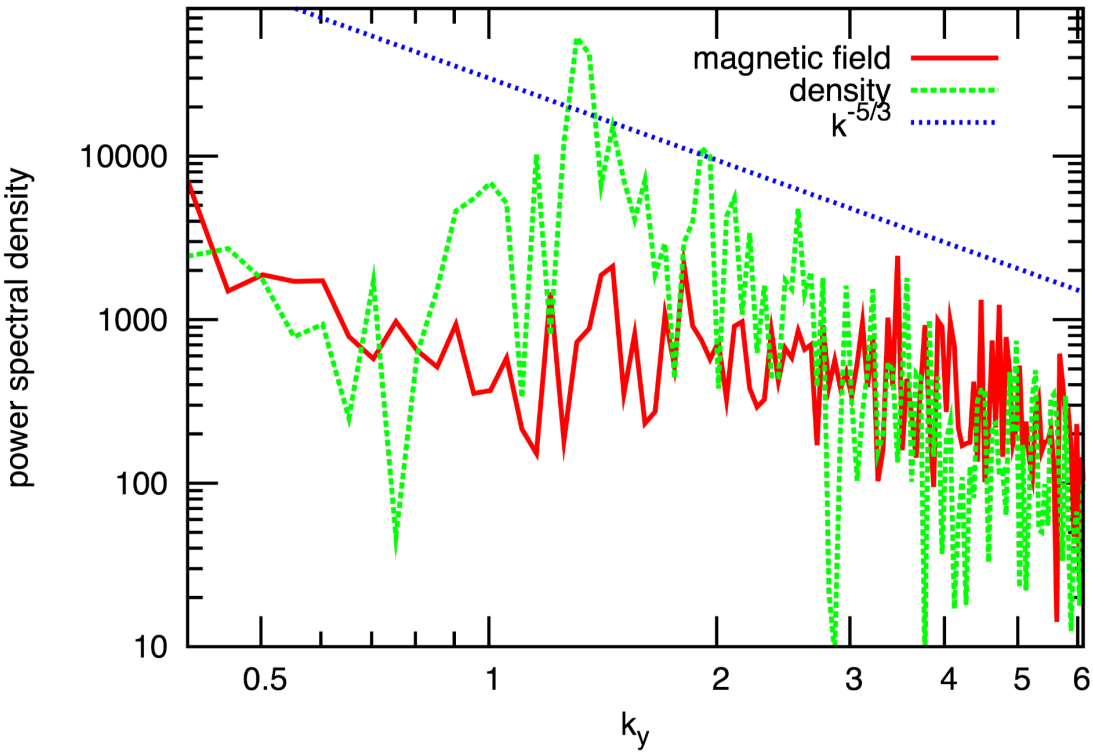

Figure VII-8: Power spectral density of fluctuations in the magnetic field and density at $t = 500$ along the perpendicular direction. A power-law with power-index $-5/3$ is shown additionally to estimate the slope of the spectrum.

These two dispersion diagrams show a common structure in the fluctuations in the form of a band signature of the intensity near the gyrofrequency and at higher harmonics in the magnetic and compressive dispersion. This is a typical indication for the occurrence of ion-Bernstein waves (Stix, 1992; Brambilla, 1998; Swanson, 2003). A linear branch with weak power is observed at $\omega/k = 1$ in the perpendicular dispersion plots of the magnetic field and density fluctuations. It corresponds to the linear fast-mode wave in a low-beta plasma. A linear Alfvén wave does not propagate perpendicularly to the background magnetic field and therefore can be excluded from the interpretation of this branch. A coupling between it and the ion-Bernstein modes is not observed and can presumably not be detectable, given the spectral resolution of the numerical analysis applied.

There is further power distributed in compressive and magnetic structures at $\omega \approx 0$. These signatures cannot be explained as ion-Bernstein waves because they do not have the minimum frequency of Ω_p and are merely spatial structures constant over time. To analyze their nature, the possible correlation between the magnetic pressure $P_B = \delta \boldsymbol{B}^2/(8\pi)$ and the density fluctuations δn can be applied. It is defined as

$$C \equiv \frac{\langle \delta n \, \delta |\boldsymbol{B}|^2 \rangle}{\sqrt{\langle \delta n^2 \rangle \langle \delta |\boldsymbol{B}|^4 \rangle}}, \tag{VII-3.15}$$

where the brackets indicate a certain way of averaging. This averaging is here done only perpendicularly to the magnetic field and in the time domain. Averaging over a long time

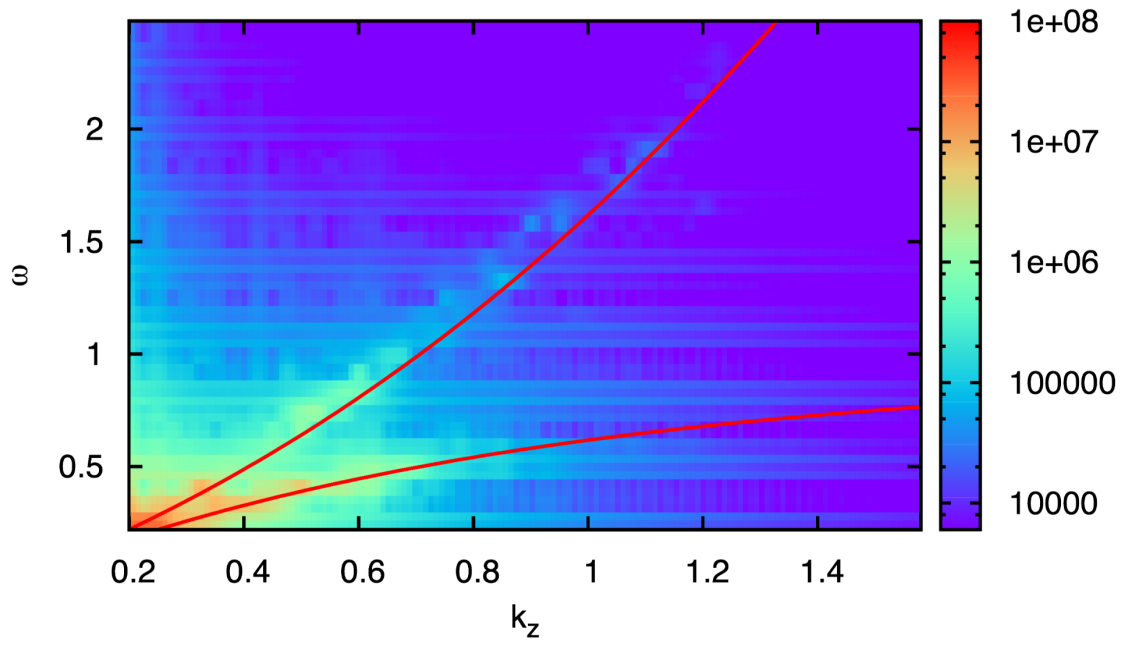

Figure VII-9: Dispersion relation of magnetic field fluctuations parallel to the background magnetic field at $t \approx 500$. The red lines indicate the F/W (upper line) and A/IC (lower line) cold dispersion relation.

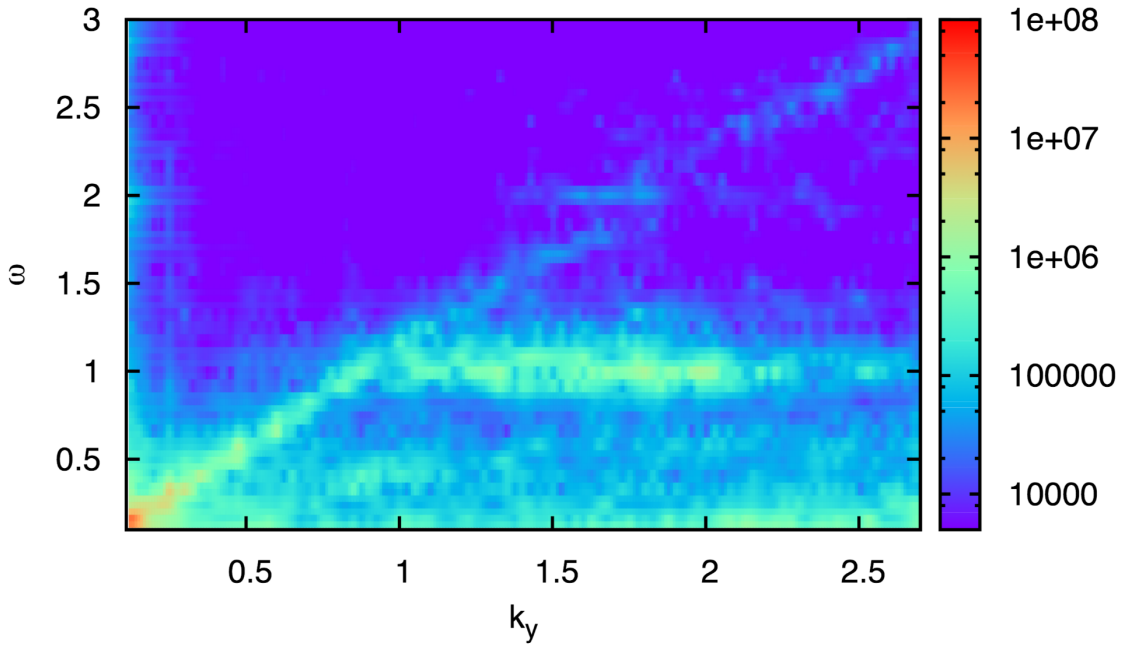

Figure VII-10: Dispersion relation of magnetic field fluctuations perpendicular to the background magnetic field at $t \approx 500$.

scale corresponds to structures with low frequency, and averaging over short time scales corresponds to higher frequencies. The same is true in the spatial domain.

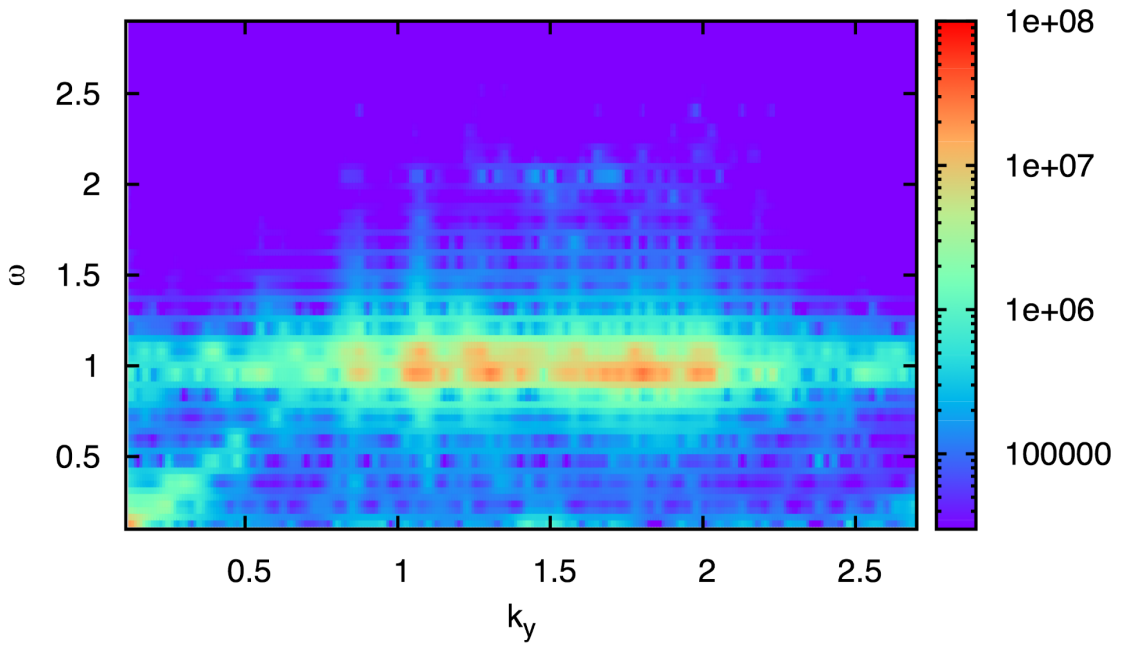

Figure VII-11: Dispersion relation of magnetic field fluctuations perpendicular to the background magnetic field at $t \approx 500$. The fluctuations coincide well with the magnetic fluctuations.

The result of this calculation is shown in Fig. VII-12. At high values for the time averaging and at low values for the spatial averaging, a strong anti-correlation between P_B and δn is found. This indicates the existence of pressure-balanced structures (PBSs), which correspond to steepened-up slow-mode waves in the perpendicular direction (Tu and Marsch, 1994). The classical slow-mode wave does not propagate at 90 degrees but in this direction transforms into a tangential discontinuity, which some of the numerical structures may represent. Therefore, it seems useful to analyze the perpendicular correlation only since a parallel slow-mode component is not expected to survive but to undergo strong Landau damping. However, it is also important to state that the simulation results cannot be unequivocal on this issue because at other positions and different time intervals the anti-correlation is not always pronounced, and some cases even show a positive correlation. These findings should be understood just as an indication for the presence of PBSs. In this special case, the correlation remains positive for only a few averaging steps in time.

VII.4 Discussion

The one-dimensional analysis provides a first insight into the spectral transfer. Due to the lower numerical needs, a longer integration time can be covered. However, the properties of the waves are quite limited in this geometry. The typical parallel normal modes are generated. The lower dispersion branch ending at about $k \approx 0.8$ corresponds to A/IC waves. This branch approaches the gyrofrequency asymptotically. The A/IC waves are

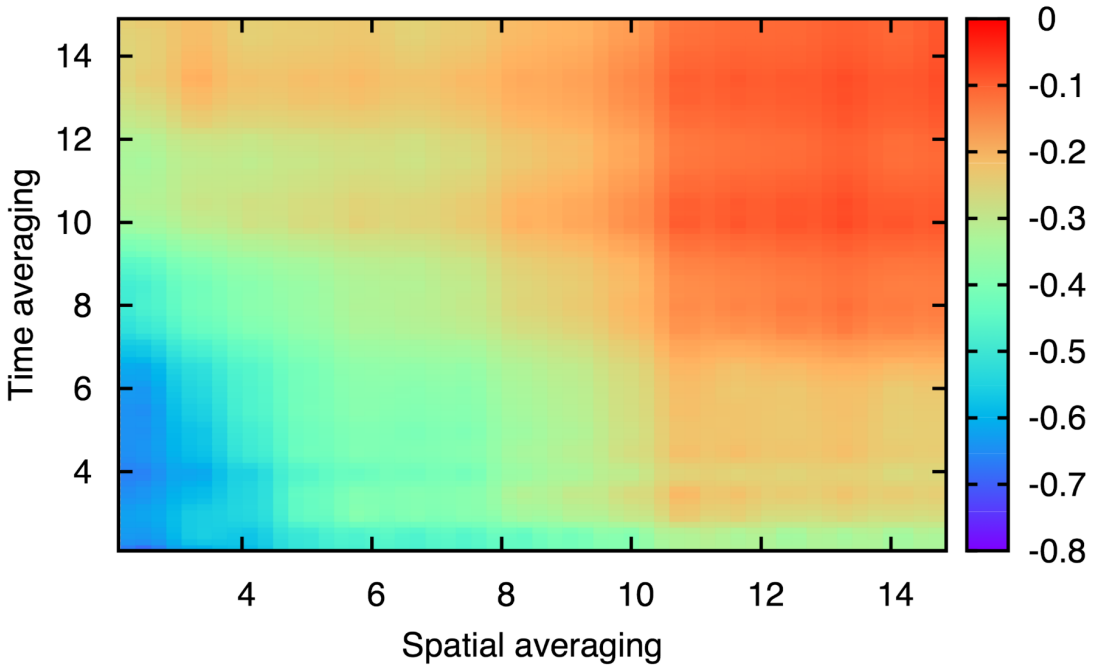

Figure VII-12: Correlation coefficient C between fluctuations of magnetic pressure and density depending on the averaging in space and time. The range for the spatial averaging is given in units of the proton inertial length and the time interval for the temporal averaging in units of the inverse proton gyration frequency. A strong anti-correlation is found up to long averaging times, which correspond to low frequencies in the dispersion diagrams. This is an indication for the existence of PBSs.

damped at around $k \gtrsim 0.8$ as it has been also found in other numerical treatments (Ofman *et al.*, 2005). This shows that the part of higher frequency fluctuations is mainly dominated by weak and undamped fast/whistler turbulence. So the polarization of the waves has changed from the left-handed A/IC waves to right-handed F/W waves. The system is distorted in such a non-trivial way by the initial conditions that the initial polarization is not important for the later nonlinear evolution. This effect is also seen in the simulations with two dimensions. The turbulence consists of fast/whistler normal modes and is thus a representation of weak turbulence.

The two-dimensional simulations show that the turbulent power cascades preferentially into directions perpendicular to the background magnetic field, which is consistent with the recent results of other numerical simulations (MacBride *et al.*, 2008; Jiang *et al.*, 2009; Markovskii *et al.*, 2010) and observations (Chen *et al.*, 2010; Sahraoui *et al.*, 2010; Narita *et al.*, 2011). However, there is also a parallel cascade present, and the nature of all the fluctuations shall be discussed depending on the direction of propagation.

The parallel fluctuations again seem to be well described as a superposition of normal modes. In the range above the ion-cyclotron scales, they are mainly F/W waves as it has been suggested before by many authors (Matthaeus *et al.*, 1990; Stawicki *et al.*, 2001; Gary *et al.*, 2008). This finding is in agreement with observations in the solar wind, indicating that left- and right-handed normal modes coexist until a wavelength of the order of $1/\ell_\mathrm{p}$, where the left-handed waves undergo resonant wave–particle interactions (Goldstein

et al., 1994) with cyclotron absorption. At higher wavenumbers, only right-handed waves can survive the transition into the intermediate dissipative range of solar wind turbulence (He *et al.*, 2011a). Linear wave damping seems to dominate the dissipation compared to nonlinear damping effects as it has been discussed before in the context of interstellar medium heating (Spangler, 1991).

Parallel A/IC waves are the most prominent of the left-handed waves that are known to undergo strong ion-cyclotron damping under certain conditions (Marsch, 2006). The observed perpendicular solar wind heating (Marsch *et al.*, 2004) can, thus, be largely explained by absorption of this left-handed normal mode, which is mostly observed in parallel propagation. Quasi-perpendicular ion-Bernstein waves may also be able to heat the plasma due to cyclotron-resonance effects. Therefore, also the here identified ion-Bernstein modes could provide a heat source for the ions. The efficiency of the dissipation of ion-Bernstein waves strongly depends on beta and is higher for larger beta values. This effect is also discussed by Markovskii *et al.* (2010) in the context of a cascade of F/W waves.

Fast waves themselves can of course also be dissipated by ions if they propagate obliquely (Marsch, 2006). This effect may, however, be slow when compared to the cyclotron-resonant absorption of A/IC waves and needs to be accumulated over a longer solar wind travel time to become significant. The intensity of the ion-Bernstein bands is more pronounced for higher electron betas, which is an indication for the electrostatic character of these wave structures. A kinetic micro-instability, which is able to excite ion-Bernstein waves in a way consistent with the wave structures observed in magnetospheres, has recently been treated in detail with particle-in-cell simulations (Liu *et al.*, 2011).

The nature of the perpendicular low-frequency fluctuations cannot be uniquely identified. There is evidence for the existence of pressure-balanced structures (PBSs), which show the typical anti-correlation between δP_B and δn. It is observed in the solar wind that this anti-correlation dominates on shorter time averaging (Tu and Marsch, 1995). A positive correlation dominates on longer time-scales, which is interpreted as the indication for co-rotating interaction regions as a result of interactions between different solar wind streams with high and low outflow speeds. The correlation shows a typical spatial dependence on large scales in the solar wind. A positive correlation is built up inside 0.7 to 0.8 AU, whereas the anti-correlation is already observed closer to the Sun prevailing over a large distance range (Roberts *et al.*, 1987a). Cluster observations also show PBSs on smaller scales than the typical low-frequency MHD range (Yao *et al.*, 2011). The origin of these structures, however, is unclear. Part of these structures may be generated by a nonlinear cascade of the turbulence into the intermediate wavenumber range as it is revealed by the simulations. Other possible non-propagating perpendicular wave structures are mirror modes or Weibel modes.

The MHD modes with low wavenumbers mainly keep their amplitude level over their temporal evolution and stay mostly isotropic. A longer integration time might also show a preferred direction of the cascade at lower wavenumbers as it was observed by other authors (Wicks *et al.*, 2010). Waves with higher wavenumbers, however, may hand over their energy more easily. This underlines that the spectral transfer occurs also in this case locally in wavenumber space as it seems typical for a turbulent cascade (Coleman, 1968). This effect is also incorporated in models concerning the coronal heating problem, where a

nonlinear local cascade is often effectively described as an advection and diffusion process in wavenumber space (Zhou and Matthaeus, 1990; Cranmer and van Ballegooijen, 2003).

Normal modes can also be directly excited from the ubiquitous thermal fluctuations in a plasma (Araneda *et al.*, 2011). However, their amplitudes usually stay on a very low level, and they do not increase with time at the expense of energy drawn from lower wavenumbers as it is observed in the here analyzed simulations. Therefore, it is reasonable to interpret the observed wave structures at higher frequencies as being the products of processes driven from the low-frequency side in the sense of a nonlinear mechanism, instead of being of purely thermal origin with a typical energy content of the order $k_\mathrm{B}T$.

If the wave power in the inertial range is much higher than assumed here, other nonlinear couplings might also play a role in the kinetic regime. This can possibly destroy the normal mode superposition even above $k = 1$ and then lead to a completely different picture with respect to both the spectral transfer to higher wavenumbers and the dispersion structure in the dispersive spectral range.

Finally, the treated simulation box is small compared to all global structures in the solar wind, and the numerical conditions are hence homogeneous in the above considerations. There are, however, recent indications that inhomogeneities foster the thermalization of wave energy (Ofman *et al.*, 2011). This effect may play also a role for the global evolution of the solar wind.

VIII Conclusions and outlook

This thesis has approached the problem of convected wave structures and spectral transfer in space plasmas in three different ways. A kinetic study has shown how the presence of a plasma wave (or even a wave field) modifies the structure of the velocity distribution function. The particles have to participate in the wave and follow the wave fields coherently. It has been shown that measurements of these moving particle distributions can lead to apparent temperature anisotropies due to a finite sampling effect. This smearing out could be even stronger for future missions, such as Solar Orbiter or Solar Probe+, because of the higher wave activity at close distances to the Sun compared to the orbits of Helios and due to the high aberration as a consequence of the special orbital configuration of these spacecraft. However, the better technical possibilities of modern instruments permit a lower sampling time, which is, nevertheless, limited by the finite counting rates in dilute plasmas.

The classical circularly polarized Alfvén/ion-cyclotron wave, which is believed to be an important component of space plasma turbulence, has been studied in Chapts. IV and V. Only a simplified case (monochromatic, parallel, fully-circularly polarized) allows one to apply the classical incompressible description. As soon as one of these conditions is broken, the wave obtains a compressive electrostatic component, and density fluctuations of the ion-acoustic type are driven by ponderomotive forces. A multi-fluid description allows one to take finite scale effects at the important kinetic plasma scales and frequencies into account. Furthermore, the finite compressive effects change the mode structure of the plasma significantly if a purely electromagnetic wave is present. Under certain reasonable solar wind conditions, the large-amplitude wave can even provide free energy for an instability of waves with a high wavenumber in the range of the inverse ion inertial length. These waves are good candidates for resonant plasma heating. Thus, a new spectral transfer mechanism has been found, which generates waves due to weakly-compressive effects in the presence of a low-frequency wave. These high-frequency waves are able to interact with particles resonantly. This mechanism is similar to the classical parametric decay, but the shown derivation reveals the role of compressibility in a different, somewhat more comprehensible way.

Another complication in real plasmas is the possibility of oblique propagation. The study of parametric instabilities of oblique waves is still incomplete because of previous computational limitations. The study in this work has shown that the decay of a circularly polarized wave favors daughter waves in the same direction of propagation and with the same polarization as the pump wave. The pump wave is already intrinsically compressive, and so are the daughter waves.

A two-dimensional hybrid analysis of the turbulence spectrum beyond the MHD-inertial range has shown that the parallel component favors the known normal modes

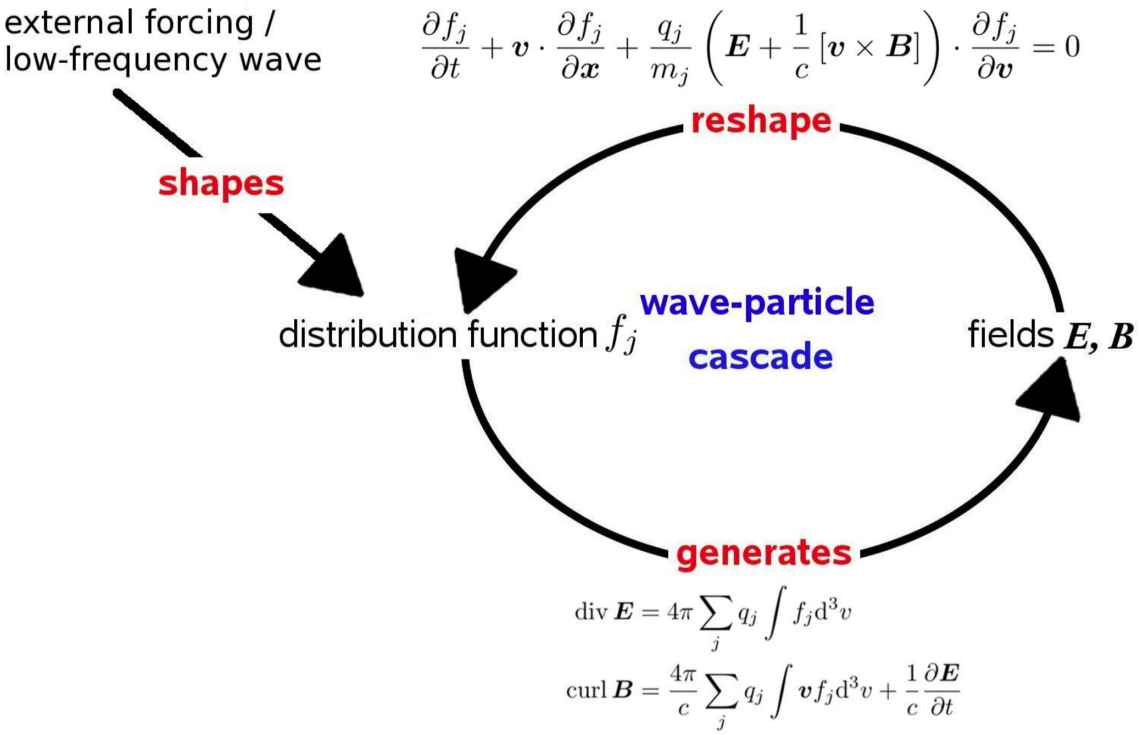

Figure VIII-1: Consistent picture of the wave–particle cascade. The interplay of the particles (represented by the distribution function) and the electromagnetic fields (according to Maxwell's equations) is the crucial reason for spectral transfer in a collisionless plasma.

(Alfvén/ion-cyclotron and fast/whistler wave) for weak turbulence. The perpendicular component shows signatures of a broad turbulent spectrum, which can be partly interpreted as pressure-balanced structures on small scales together with evidence for ion-Bernstein waves.

Still, the nature of space plasma turbulence has not been fully understood. Once this is achieved satisfactorily, these considerations should be integrated into the kinetic and fluid models for the turbulence dissipation self-consistently. This additional aspect is, however, far beyond the focus of this work.

It has become clear that the interplay between waves and particles plays an important role in the framework of the cascade of energy. The consistent picture is shown in Fig. VIII-1. Energy is introduced to the system on large scales. It may be interpreted as a low-frequency forcing of the plasma, which is by nature a deformation of the distribution function similar to the description that has been found in Chapt. III. The distribution functions of particular plasma species modify the electromagnetic fields according to Maxwell's equations. These fields in turn shape the distribution function according to the Vlasov equation. A self-consistent solution for this circle is an appropriate description of the cascade mechanism. As described in Chapt. III, properties of the solar wind velocity distribution function are in many cases limited by micro-physical thresholds for instabilities. Waves can, for example, shape the distribution function by pitch-angle scattering and lead to a temperature anisotropy. If this anisotropy exceeds a certain threshold, the distribution function becomes unstable and radiates waves with different wavenum-

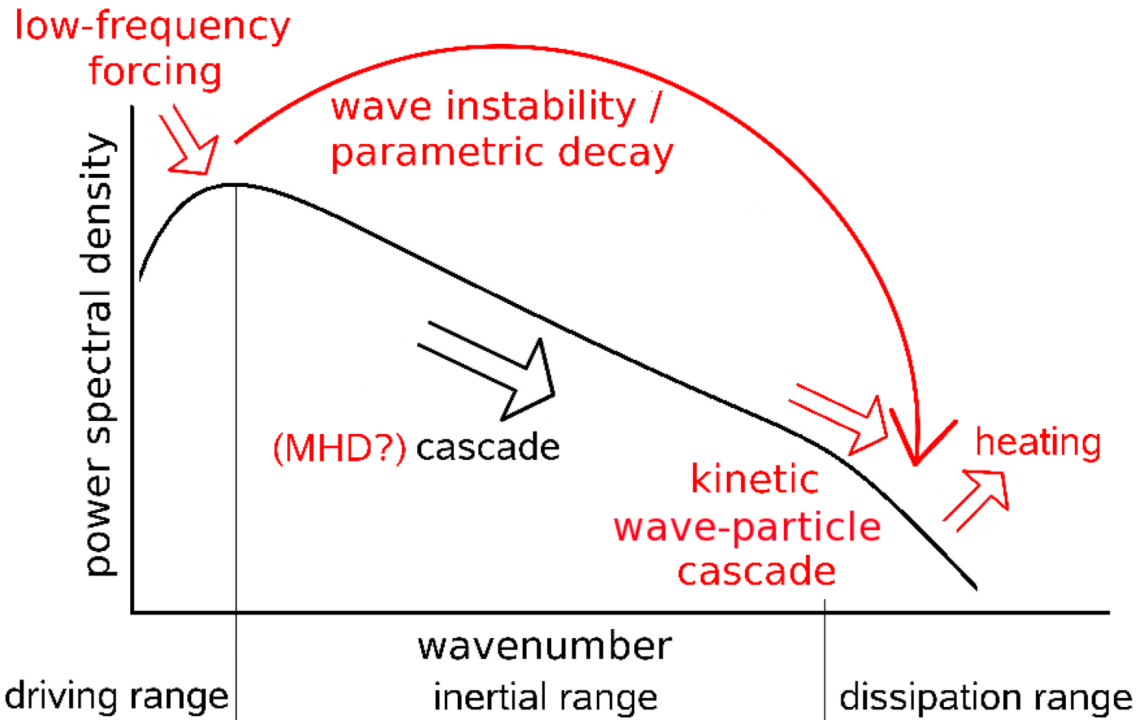

Figure VIII-2: Qualitative picture of a turbulent power spectrum. The red informations summarize conclusions of this work.

bers/frequencies. This emission and absorption can occur until an equilibrium is reached. A low-frequency wave itself can be the source of free energy, which generates high-frequency waves as shown in Chapt. V. In all cases, the wave–particle nature of plasma turbulence has to be taken into account.

The idea of spectral transport after the considerations of this thesis is depicted in Fig. VIII-2, revisiting Fig. I-5 from the Introduction. Energy is injected to the system at low wavenumbers. These waves can directly generate waves in the dispersive/dissipative wavenumber ranges due to parametric decay or other instabilities. In the classical inertial range, energy is transported from lower to higher wavenumbers following the typical cascade, which is well confirmed by plenty of observations. The cascade may be described by the methods of magnetohydrodynamics, or maybe even by hydrodynamics, consistently with the observed spectral indices in this range. However, other processes are needed to explain the transport of energy to higher wavenumbers in the dissipation range. Nonlinear wave–wave interactions in the sense of the above described wave–particle cascade are such mechanisms. These effects are well modeled by numerical simulations. Anisotropy and oblique propagation play major roles there. Under weakly-turbulent conditions, the turbulence is well represented by a superposition of normal modes. Starting from the inverse proton inertial length scale, their energy is dissipated by the cyclotron resonance of protons, and only the non-resonant modes survive. Up to the electron inertial length scale, a cascade of mainly R-mode or whistler turbulence, respectively, is expected.

To summarize the conclusions of this work, the six open questions from the Introduction are revisited, and the possible answers after the analyses of this thesis are given:

- How can coherent motions due to waves be described, and how can they influence particle measurements from space probes?

  → A plasma wave leads to a coherent variation in the velocity distribution function of the particles. Sampling over time can lead to a smearing effect and hence to apparent temperature anisotropies in the measured distribution function.

- What is the nature of fluctuations below the ion scales?

  → At wavenumbers higher than the inverse inertial length of the solar wind protons, only right-handed waves are possible propagating normal modes for parallel propagation. Fast/whistler waves are good candidates in this case. The perpendicular direction mainly shows a broad spectrum for density fluctuations with signatures of ion-Bernstein modes and small-scale pressure-balanced structures.

- How are these waves associated with electric fields that can accelerate/thermalize particles?

  → Already a non-constant transversal amplitude of a parallel circularly polarized wave drives electrostatic fluctuations due to a non-vanishing ponderomotive field. Landau- and cyclotron-resonant wave fields are generated already as a direct consequence of the parametric decay and other spectral transfer processes.

- What is the role of compressive effects in solar wind turbulence?

  → As soon as waves leave the simplified special case of circularly polarized monochromatic parallel normal modes, they become compressive by nature with an associated electric field. Also simulations show that compressive fluctuations are always growing during the evolution of the system.

- Are the solar wind fluctuations (at least partly) a non-interacting superposition of waves?

  → If the amplitudes of the fluctuations are not too high, the parallel component is well represented by a superposition of normal modes. Also the perpendicular component shows this property, but additional higher-order effects seem to play an important role for them.

- How does the (anisotropic) spectral transfer work?

  → Daughter-wave products of the parametric decay of a monochromatic oblique wave seem to favor the initial direction of the pump wave with respect to the background magnetic field and its polarization. A broad isotropic inertial-range spectrum evolves into different fluctuating structures depending on the direction with a preferentially perpendicular orientation.

The observational confirmation of some of the above predictions is still unsettled. A wave telescope in the free solar wind would be desirable, which is able to determine the polarization and dispersion of the solar wind fluctuations directly. The Cluster spacecraft can deliver these measurements in times, when the spacecraft have an appropriate geometry and are outside the Earth's magnetosphere in the free solar wind (Narita *et al.*, 2010; Sahraoui *et al.*, 2010). If a system of several (minimum four) spacecraft was available

in the unperturbed solar wind measuring the fluctuation properties in the convected solar wind reference frame due to a certain orbital configuration, the still undiscovered properties of solar wind turbulence could be revealed. However, such a mission would most probably be foredoomed due to the high efforts so that further turbulence studies will be likely achieved as side-effect results from other missions. Even the highly-elliptic orbits of the Helios space probes reached a radial spacecraft velocity of only about 30 km/s, which is still too low to be co-moving in the solar wind outflow. For the solar corona, no in-situ measurements will be possible in the medium term. The remote observations will improve and provide a better spatial and temporal resolution in future. Also the extrapolation from close orbiters, such as Solar Orbiter or Solar Probe+, will have to provide the empirical background.

From the numerical point of view, full particle-in-cell simulations can deliver promising access to yet unsolved questions because the high-frequency processes and effects due to finite space charge densities can be treated with them. Also strong turbulence should be approached with this strategy. Maybe one day the computational systems permit a multi-dimensional treatment of space plasma turbulence on the many relevant scales. The global evolution of the solar wind, including all observed particle species (protons, electrons, other ions, neutrals, pick-up ions, cosmic rays, and so on), could then perhaps be modeled based on the underlying micro-physical mechanisms. Analytical studies (especially in the focus of the yet open question about the role of compressibility and oblique propagation) shall deliver, until then and beyond that time, an intuitive and comprehensible access to the problem of the nature of space plasma turbulence.

Bibliography

Abramowitz, M. and I. A. Stegun: *Handbook of Mathematical Functions*, Dover Publ., New York, USA, 1972

Akhiezer, A. I., I. A. Akhiezer, R. V. Polovin, A. G. Sitenko, and K. N. Stepanov: *Plasma electrodynamics - Vol.1: Linear theory*, Pergamon Press, Oxford, UK, 1975

Alexandrova, O., V. Carbone, P. Veltri, and L. Sorriso-Valvo: *Small-Scale Energy Cascade of the Solar Wind Turbulence*, Astrophys. J. **674**, 1153, 2008a

Alexandrova, O., C. Lacombe, and A. Mangeney: *Spectra and anisotropy of magnetic fluctuations in the Earth's magnetosheath: Cluster observations*, Ann. Geophys. **26**, 3585, 2008b

Alexandrova, O., J. Saur, C. Lacombe, A. Mangeney, J. Mitchell, S. J. Schwartz, and P. Robert: *Universality of Solar-Wind Turbulent Spectrum from MHD to Electron Scales*, Phys. Rev. Lett. **103**, 165 003, 2009

Antonucci, E., M. A. Dodero, and S. Giordano: *Fast Solar Wind Velocity in a Polar Coronal Hole during Solar Minimum*, Solar Phys. **197**, 115, 2000

Appleton, E. V.: *Wireless Studies of the Ionosphere*, Journal of the Institution of Electrical Engineers **71**, 642, 1932

Araneda, J. A.: *Parametric Instabilities of Parallel-Propagating Alfvén Waves: Kinetic Effects in the MHD-Model*, Phys. Scripta T **75**, 164, 1998

Araneda, J. A., E. Marsch, and A. F. Viñas: *Collisionless damping of parametrically unstable Alfvén waves*, J. Geophys. Res. **112**, 4104, 2007

Araneda, J. A., E. Marsch, and A. F.-Viñas: *Proton Core Heating and Beam Formation via Parametrically Unstable Alfvén-Cyclotron Waves*, Phys. Rev. Lett. **100**, 125 003, 2008

Araneda, J. A., Y. Maneva, and E. Marsch: *Preferential Heating and Acceleration of α Particles by Alfvén-Cyclotron Waves*, Phys. Rev. Lett. **102**, 175 001, 2009

Araneda, J. A., H. Astudillo, and E. Marsch: *Interactions of Alfvén-Cyclotron Waves with Ions in the Solar Wind*, Space Sci. Rev. **online**, doi:10.1007/s11 214–011–9773–0, 2011

Aschwanden, M. J.: *Physics of the Solar Corona. An Introduction with Problems and Solutions, 2nd Edition*, Springer-Verlag, Berlin, Germany, 2005

Båth, M.: *Spectral analysis in geophysics*, Elsevier Science Ltd., Amsterdam, Netherlands, 1974

Bagdonat, T.: *Hybrid Simulation of Weak Comets*, PhD thesis, TU Braunschweig, Germany, 2005

Bagdonat, T. and U. Motschmann: *3D Hybrid Simulation Code Using Curvilinear Coordinates*, J. Comput. Phys. **183**, 470, 2002

Bale, S. D., P. J. Kellogg, F. S. Mozer, T. S. Horbury, and H. Reme: *Measurement of the Electric Fluctuation Spectrum of Magnetohydrodynamic Turbulence*, Phys. Rev. Lett. **94**, 215 002, 2005

Bale, S. D., J. C. Kasper, G. G. Howes, E. Quataert, C. Salem, and D. Sundkvist: *Magnetic Fluctuation Power Near Proton Temperature Anisotropy Instability Thresholds in the Solar Wind*, Phys. Rev. Lett. **103**, 211 101, 2009

Baumjohann, W. and R. A. Treumann: *Basic space plasma physics*, Imperial College Press, London, UK, 1996

Bavassano, B., R. Bruno, and H. Rosenbauer: *Compressive fluctuations in the solar wind and their polytropic index*, Ann. Geophys. **14**, 510, 1996

Belcher, J. W. and L. Davis, Jr.: *Large-amplitude Alfvén waves in the interplanetary medium, 2.*, J. Geophys. Res. **76**, 3534, 1971

Bhattacharjee, A., C. S. Ng, S. Ghosh, and M. L. Goldstein: *A comparative study of four-field and fully compressible magnetohydrodynamic turbulence in the solar wind*, J. Geophys. Res. **104**, 24 835, 1999

Bian, N. H. and E. P. Kontar: *A gyrofluid description of Alfvénic turbulence and its parallel electric field*, Phys. Plasmas **17**, 062 308, 2010

Bieber, J. W., W. Wanner, and W. H. Matthaeus: *Dominant two-dimensional solar wind turbulence with implications for cosmic ray transport*, J. Geophys. Res. **101**, 2511, 1996

Biermann, L.: *Kometenschweife und solare Korpuskularstrahlung*, Z. Astrophys. **29**, 274, 1951

Bingert, S., P. Zacharias, H. Peter, and B. V. Gudiksen: *On the nature of coronal loops above the quiet sun network*, Adv. Space Res. **45**, 310, 2010

Borovsky, J. E. and S. P. Gary: *Electron-ion Coulomb scattering and the electron Landau damping of Alfvén waves in the solar wind*, J. Geophys. Res. **116**, A07 101, 2011

Bourouaine, S., E. Marsch, and C. Vocks: *On the Efficiency of Nonresonant Ion Heating by Coronal Alfvén Waves*, Astrophys. J. Lett. **684**, L119, 2008

Bourouaine, S., E. Marsch, and F. M. Neubauer: *Correlations between the proton temperature anisotropy and transverse high-frequency waves in the solar wind*, Geophys. Res. Lett. **37**, 14 104, 2010

Brambilla, M.: *Kinetic theory of plasma waves: homogeneous plasmas*, Clarendon Press, Oxford, UK, 1998

Brodin, G. and L. Stenflo: *Parametric instabilities of finite amplitude Alfven waves*, Phys. Scripta **37**, 89, 1988

Brodin, G., P. K. Shukla, and L. Stenflo: *A new decay channel for compressional Alfvén waves in plasmas*, J. Plasma Phys. **74**, 99, 2008

Bruno, R. and V. Carbone: *The Solar Wind as a Turbulence Laboratory*, Living Rev. Sol. Phys. **2**, 4, 2005

Chandran, B. D. G.: *Weak Compressible Magnetohydrodynamic Turbulence in the Solar Corona*, Phys. Rev. Lett. **95**, 265 004, 2005

Chandran, B. D. G., E. Quataert, G. G. Howes, Q. Xia, and P. Pongkitiwanichakul: *Constraining Low-Frequency Alfvénic Turbulence in the Solar Wind Using Density-Fluctuation Measurements*, Astrophys. J. **707**, 1668, 2009

Chandran, B. D. G., B. Li, B. N. Rogers, E. Quataert, and K. Germaschewski: *Perpendicular Ion Heating by Low-frequency Alfvén-wave Turbulence in the Solar Wind*, Astrophys. J. **720**, 503, 2010a

Chandran, B. D. G., P. Pongkitiwanichakul, P. A. Isenberg, M. A. Lee, S. A. Markovskii, J. V. Hollweg, and B. J. Vasquez: *Resonant Interactions Between Protons and Oblique Alfvén/Ion-cyclotron Waves in the Solar Corona and Solar Flares*, Astrophys. J. **722**, 710, 2010b

Chen, C. H. K., T. S. Horbury, A. A. Schekochihin, R. T. Wicks, O. Alexandrova, and J. Mitchell: *Anisotropy of Solar Wind Turbulence between Ion and Electron Scales*, Phys. Rev. Lett. **104**, 255 002, 2010

Chen, F. F.: *Introduction to Plasma Physics and Controlled Fusion*, Plenum Press, New York, USA, 1985

Cohen, R. H.: *Mode decay and evolution of the solar wind Alfven wave spectrum*, J. Geophys. Res. **80**, 3678, 1975

Coleman, Jr., P. J.: *Turbulence, Viscosity, and Dissipation in the Solar-Wind Plasma*, Astrophys. J. **153**, 371, 1968

Cranmer, S. R.: *Coronal Holes*, Living Rev. Sol. Phys. **6**, 3, 2009

Cranmer, S. R. and A. A. van Ballegooijen: *Alfvénic Turbulence in the Extended Solar Corona: Kinetic Effects and Proton Heating*, Astrophys. J. **594**, 573, 2003

Cranmer, S. R., W. H. Matthaeus, B. A. Breech, and J. C. Kasper: *Empirical Constraints on Proton and Electron Heating in the Fast Solar Wind*, Astrophys. J. **702**, 1604, 2009

Davidson, R. C.: *Methods in nonlinear plasma theory*, Academic Press, New York, USA, 1972

Davidson, R. C.: *Kinetic waves and instabilities in a uniform plasma*, in *Basic Plasma Physics: Handbook of Plasma Physics, Volume 1*, edited by A. A. Galeev & R. N. Sudan, p. 229, 1983

De Pontieu, B., S. W. McIntosh, M. Carlsson, V. H. Hansteen, T. D. Tarbell, C. J. Schrijver, A. M. Title, R. A. Shine, S. Tsuneta, Y. Katsukawa, K. Ichimoto, Y. Suematsu, T. Shimizu, and S. Nagata: *Chromospheric Alfvénic Waves Strong Enough to Power the Solar Wind*, Science **318**, 1574, 2007

Derby, Jr., N. F.: *Modulational instability of finite-amplitude, circularly polarized Alfven waves*, Astrophys. J. **224**, 1013, 1978

Elskens, Y. and D. Escande: *Microscopic Dynamics of Plasmas and Chaos*, Institute of Physics Publishing, Bristol, UK, 2003

Eriksson, A. I.: *Spectral Analysis*, in *Analysis Methods for Multi-Spacecraft Data, ISSI Scientific Reports Series 1, ESA/ISSI*, edited by G. Paschmann & P. W. Daly, p. 5, 1998

Fahr, H. J. and I. V. Chashei: *On the thermodynamics of MHD wave-heated solar wind protons*, Astron. Astrophys. **395**, 991, 2002

Galeev, A. A. and V. N. Oraevskii: *The Stability of Alfvén Waves*, Sov. Phys. Doklady **7**, 988, 1963

Gary, G. A.: *Plasma Beta above a Solar Active Region: Rethinking the Paradigm*, Solar Phys. **203**, 71, 2001

Gary, S. P.: *Theory of Space Plasma Microinstabilities*, Cambridge University Press, Cambridge, UK, 1993

Gary, S. P., L. Yin, and D. Winske: *Electromagnetic proton cyclotron anisotropy instability: Wave-particle scattering rate*, Geophys. Res. Lett. **27**, 2457, 2000

Gary, S. P., R. M. Skoug, J. T. Steinberg, and C. W. Smith: *Proton temperature anisotropy constraint in the solar wind: ACE observations*, Geophys. Res. Lett. **28**, 2759, 2001

Gary, S. P., R. M. Skoug, and C. W. Smith: *Learning about coronal heating from solar wind observations*, Phys. Plasmas **12**, 056 501, 2005a

Gary, S. P., C. W. Smith, and R. M. Skoug: *Signatures of Alfvén-cyclotron wave-ion scattering: Advanced Composition Explorer (ACE) solar wind observations*, J. Geophys. Res. **110**, 7108, 2005b

Gary, S. P., S. Saito, and H. Li: *Cascade of whistler turbulence: Particle-in-cell simulations*, Geophys. Res. Lett. **35**, L02 104, 2008

Goldreich, P. and S. Sridhar: *Toward a theory of interstellar turbulence. 2: Strong alfvenic turbulence*, Astrophys. J. **438**, 763, 1995

Goldstein, M. L.: *An instability of finite amplitude circularly polarized Alfven waves*, Astrophys. J. **219**, 700, 1978

Goldstein, M. L., D. A. Roberts, and C. A. Fitch: *Properties of the fluctuating magnetic helicity in the inertial and dissipation ranges of solar wind turbulence*, J. Geophys. Res. **99**, 11 519, 1994

Goossens, M.: *An introduction to plasma astrophysics and magnetohydrodynamics*, Kluwer Academic Publishers, Dordrecht, Netherlands, 2003

Grappin, R., M. Velli, and A. Mangeney: *'Alfvenic' versus 'standard' turbulence in the solar wind*, Ann. Geophys. **9**, 416, 1991

Gurnett, D. A. and A. Bhattacharjee: *Introduction to Plasma Physics*, Cambridge University Press, Cambridge, UK, 2005

Hackenberg, P., G. Mann, and E. Marsch: *Solitons in multi-ion plasmas*, J. Plasma Phys. **60**, 845, 1998

Hamza, A. M., K. Meziane, and C. Mazelle: *Oblique propagation and nonlinear wave particle processes*, J. Geophys. Res. **111**, 4104, 2006

He, J.-S., E. Marsch, C.-Y. Tu, S. Yao, and H. Tian: *Possible Evidence of Alfvén-cyclotron Waves in the Angle Distribution of Magnetic Helicity of Solar Wind Turbulence*, Astrophys. J. **731**, 85, 2011a

He, J.-S., E. Marsch, C.-Y. Tu, Q.-G. Zong, S. Yao, and H. Tian: *Two-dimensional correlation functions for density and magnetic field fluctuations in magnetosheath turbulence measured by the Cluster spacecraft*, J. Geophys. Res. **116**, A06 207, 2011b

Heuer, M. and E. Marsch: *Diffusion plateaus in the velocity distributions of fast solar wind protons*, J. Geophys. Res. **112**, 3102, 2007

Hizanidis, K., Y. Kominis, and A. K. Ram: *Quasilinear theory revisited: general kinetic formulation of wave-particle interactions in plasmas*, Plasma Phys. Contr. F. **52**, 124 022, 2010

Hollweg, J. V.: *Beat, modulational, and decay instabilities of a circularly polarized Alfven wave*, J. Geophys. Res. **99**, 23 431, 1994

Hollweg, J. V.: *Kinetic Alfvén wave revisited*, J. Geophys. Res. **104**, 14 811, 1999

Hollweg, J. V. and P. A. Isenberg: *Generation of the fast solar wind: A review with emphasis on the resonant cyclotron interaction*, J. Geophys. Res. **107**, 1147, 2002

Hollweg, J. V., R. Esser, and V. Jayanti: *Modulational and decay instabilities of Alfven waves - Effects of streaming He^{++}*, J. Geophys. Res. **98**, 3491, 1993

Horbury, T. S., M. A. Forman, and S. Oughton: *Spacecraft observations of solar wind turbulence: an overview*, Plasma Phys. Contr. F. **47**, B703, 2005

Howes, G. G.: *Inertial range turbulence in kinetic plasmas*, Phys. Plasmas **15**, 055 904, 2008

Inhester, B.: *A drift-kinetic treatment of the parametric decay of large-amplitude Alfven waves*, J. Geophys. Res. **95**, 10 525, 1990

Iroshnikov, P. S.: *Turbulence of a Conducting Fluid in a Strong Magnetic Field*, Astron. Zh. **40**, 742, 1963

Isenberg, P. A. and M. A. Lee: *A dispersive analysis of bispherical pickup ion distributions*, J. Geophys. Res. **101**, 11 055, 1996

Jian, L. K., C. T. Russell, J. G. Luhmann, R. J. Strangeway, J. S. Leisner, and A. B. Galvin: *Ion Cyclotron Waves in the Solar Wind Observed by STEREO Near 1 AU*, Astrophys. J. **701**, L105, 2009

Jian, L. K., P. Russell, C. T. Isenberg, J. G. Luhmann, B. J. Anderson, S. A. Boardsen, R. J. Strangeway, M. M. Cowee, and A. Wennmacher: *Observations of ion cyclotron waves in the solar wind near 0.3 AU*, J. Geophys. Res. **115**, A12 115, 2010

Jiang, Y. W., S. Liu, and V. Petrosian: *Cascade and Damping of Alfvén-Cyclotron Fluctuations: Application to Solar Wind Turbulence*, Astrophys. J. **698**, 163, 2009

Kadomtsev, B. B.: *Plasma turbulence*, Academic Press, New York, USA, 1965

Kasper, J. C., A. J. Lazarus, and S. P. Gary: *Hot Solar-Wind Helium: Direct Evidence for Local Heating by Alfvén-Cyclotron Dissipation*, Phys. Rev. Lett. **101**, 261 103, 2008

Kellogg, P. J. and T. S. Horbury: *Rapid density fluctuations in the solar wind*, Ann. Geophys. **23**, 3765, 2005

Kellogg, P. J., S. D. Bale, F. S. Mozer, T. S. Horbury, and H. Reme: *Solar Wind Electric Fields in the Ion Cyclotron Frequency Range*, Astrophys. J. **645**, 704, 2006

Kohl, J. L., G. Noci, S. R. Cranmer, and J. C. Raymond: *Ultraviolet spectroscopy of the extended solar corona*, Astron. Astrophys. Rev. **13**, 31, 2006

Kolmogorov, A.: *The Local Structure of Turbulence in Incompressible Viscous Fluid for Very Large Reynolds' Numbers*, Dokl. Akad. Nauk SSSR **30**, 301, 1941

Kraichnan, R. H.: *Inertial-Range Spectrum of Hydromagnetic Turbulence*, Phys. Fluids **8**, 1385, 1965

Krauss-Varban, D., N. Omidi, and K. B. Quest: *Mode properties of low-frequency waves: Kinetic theory versus Hall-MHD*, J. Geophys. Res. **99**, 5987, 1994

Landau, L. D. and E. M. Lifshitz: *Statistical physics. Pts. 1 and 2*, Pergamon Press, Oxford, UK, 1980

Lashmore-Davies, C. N. and L. Stenflo: *On the MHD stability of a helical magnetic field of arbitrary amplitude*, Plasma Phys. **21**, 735, 1979

Lehe, R., I. J. Parrish, and E. Quataert: *The Heating of Test Particles in Numerical Simulations of Alfvénic Turbulence*, Astrophys. J. **707**, 404, 2009

Leslie, D. C.: *Developments in the theory of turbulence*, Clarendon Press, Oxford, UK, 1973

Li, H., S. P. Gary, and O. Stawicki: *On the dissipation of magnetic fluctuations in the solar wind*, Geophys. Res. Lett. **28**, 1347, 2001

Li, X. and S. R. Habbal: *Hybrid simulation of ion cyclotron resonance in the solar wind: Evolution of velocity distribution functions*, J. Geophys. Res. **110**, A10 109, 2005

Li, X., Q. Lu, and B. Li: *Ion Pickup by Finite Amplitude Parallel Propagating Alfvén Waves*, Astrophys. J. **661**, L105, 2007

Lifshitz, E. M. and L. P. Pitaevskii: *Physical kinetics*, Pergamon Press, Oxford, UK, 1981

Liu, K., S. P. Gary, and D. Winske: *Excitation of magnetosonic waves in the terrestrial magnetosphere: Particle-in-cell simulations*, J. Geophys. Res. **116**, A07 212, 2011

Longtin, M. and B. U. Ö.. Sonnerup: *Modulation instability of circularly polarized Alfven waves*, J. Geophys. Res. **91**, 6816, 1986

Lu, Q. and L. Chen: *Ion Heating by a Spectrum of Obliquely Propagating Low-frequency Alfvén Waves*, Astrophys. J. **704**, 743, 2009

Lu, Q. and X. Li: *Heating of ions by low-frequency Alfven waves*, Phys. Plasmas **14**, 042 303, 2007

MacBride, B. T., C. W. Smith, and M. A. Forman: *The Turbulent Cascade at 1 AU: Energy Transfer and the Third-Order Scaling for MHD*, Astrophys. J. **679**, 1644, 2008

Maneva, Y., J. A. Araneda, and E. Marsch: *Ion distributions in coronal holes and fast solar wind*, Twelfth International Solar Wind Conference **1216**, 227, 2010

Mann, G., P. Hackenberg, and E. Marsch: *Linear mode analysis in multi-ion plasmas*, J. Plasma Phys. **58**, 205, 1997

Markovskii, S. A., B. J. Vasquez, and J. V. Hollweg: *Proton Heating by Nonlinear Field-Aligned Alfvén Waves in Solar Coronal Holes*, Astrophys. J. **695**, 1413, 2009

Markovskii, S. A., B. J. Vasquez, and B. D. G. Chandran: *Perpendicular Proton Heating Due to Energy Cascade of Fast Magnetosonic Waves in the Solar Corona*, Astrophys. J. **709**, 1003, 2010

Marsch, E.: *Kinetic Physics of the Solar Corona and Solar Wind*, Living Rev. Sol. Phys. **3**, 1, 2006

Marsch, E. and C.-Y. Tu: *Evidence for pitch angle diffusion of solar wind protons in resonance with cyclotron waves*, J. Geophys. Res. **106**, 8357, 2001

Marsch, E. and D. Verscharen: *On nonlinear Alfvén-cyclotron waves in multi-species plasma*, J. Plasma Phys. **77**, 385, 2011

Marsch, E., H. Rosenbauer, R. Schwenn, K. Muehlhaeuser, and K. U. Denskat: *Pronounced proton core temperature anisotropy, ion differential speed, and simultaneous Alfven wave activity in slow solar wind at 0.3 AU*, J. Geophys. Res. **86**, 9199, 1981

Marsch, E., X.-Z. Ao, and C.-Y. Tu: *On the temperature anisotropy of the core part of the proton velocity distribution function in the solar wind*, J. Geophys. Res. **109**, 4102, 2004

Marsch, E., L. Zhao, and C.-Y. Tu: *Limits on the core temperature anisotropy of solar wind protons*, Ann. Geophys. **24**, 2057, 2006

Marsch, E., S. Yao, and C.-Y. Tu: *Proton beam velocity distributions in an interplanetary coronal mass ejection*, Ann. Geophys. **27**, 869, 2009

Matsumoto, H.: *Nonlinear whistler-mode interaction and triggered emission in the magnetosphere - A review*, in *Wave instabilities in space plasmas; Proceedings of the Symposium, Helsinki, Finland, July 31-August 8, 1978. (A80-21196 07-46)*, edited by P. J. Palmadesso & K. Papadopoulos, p. 163, D. Reidel Publishing Co., Dordrecht, Netherlands, 1979

Matteini, L., S. Landi, L. Del Zanna, M. Velli, and P. Hellinger: *Parametric decay of linearly polarized shear Alfvén waves in oblique propagation: One and two-dimensional hybrid simulations*, Geophys. Res. Lett. **37**, L20 101, 2010

Matthaeus, W. H., M. L. Goldstein, and D. A. Roberts: *Evidence for the presence of quasi-two-dimensional nearly incompressible fluctuations in the solar wind*, J. Geophys. Res. **95**, 20 673, 1990

McComb, W. D.: *The physics of fluid turbulence*, Oxford University Press, Oxford, UK, 1990

McIntosh, S. W., B. De Pontieu, M. Carlsson, V. Hansteen, P. Boerner, and M. Goossens: *Alfvénic waves with sufficient energy to power the quiet solar corona and fast solar wind*, Nature **475**, 477, 2011

McKenzie, J. F., E. Marsch, K. Baumgaertel, and K. Sauer: *Wave and stability properties of multi-ion plasmas with applications to winds and flows*, Ann. Geophys. **11**, 341, 1993

Medvedev, M. V., P. H. Diamond, V. I. Shevchenko, and V. L. Galinsky: *Dissipative Dynamics of Collisionless Nonlinear Alfvén Wave Trains*, Phys. Rev. Lett. **78**, 4934, 1997

Melrose, D. B. and R. C. McPhedran: *Electromagnetic Processes in Dispersive Media*, Cambridge University Press, Cambridge, UK, 2005

Montgomery, D. and L. Turner: *Anisotropic magnetohydrodynamic turbulence in a strong external magnetic field*, Phys. Fluids **24**, 825, 1981

Müller, J., S. Simon, U. Motschmann, J. Schüle, K.-H. Glassmeier, and G. J. Pringle: *A.I.K.E.F.: Adaptive hybrid model for space plasma simulations*, Comput. Phys. Commun. **182**, 946, 2011

Murtaza, G. and P. K. Shukla: *Nonlinear generation of electromagnetic waves in a magnetoplasma*, J. Plasma Phys. **31**, 423, 1984

Narita, Y., F. Sahraoui, M. L. Goldstein, and K.-H. Glassmeier: *Magnetic energy distribution in the four-dimensional frequency and wave vector domain in the solar wind*, J. Geophys. Res. **115**, A04 101, 2010

Narita, Y., S. P. Gary, S. Saito, K. Glassmeier, and U. Motschmann: *Dispersion relation analysis of solar wind turbulence*, Geophys. Res. Lett. **38**, L05 101, 2011

Nariyuki, Y.: *On entropy-maximized velocity distributions in circularly polarized finite amplitude Alfvén waves*, Phys. Plasmas **18**, 052 112, 2011a

Nariyuki, Y.: *Equilibrium velocity distributions in parallel propagating low-frequency Alfvénic turbulence* , Phys. Plasmas **18**, 092 118, 2011b

NRL: *Plasma Formulary, revised*, Naval Research Laboratory, Washington DC, USA, 2009

O'Brien, M. R. and D. C. Robinson: *Tokamak experiments*, in *Plasma Physics: an Introductory Course*, edited by R. Dendy, p. 189, 1993

Ofman, L., J. M. Davila, V. M. Nakariakov, and A. Viñas: *High-frequency Alfvén waves in multi-ion coronal plasma: Observational implications*, J. Geophys. Res. **110**, 9102, 2005

Ofman, L., A.-F. Viñas, and P. S. Moya: *Hybrid models of solar wind plasma heating*, Ann. Geophys. **29**, 1071, 2011

Oughton, S., W. H. Matthaeus, and S. Ghosh: *Scaling of spectral anisotropy with magnetic field strength in decaying magnetohydrodynamic turbulence*, Phys. Plasmas **5**, 4235, 1998

Parker, E. N.: *Dynamics of the Interplanetary Gas and Magnetic Fields*, Astrophys. J. **128**, 664, 1958

Perri, S., V. Carbone, and P. Veltri: *Where Does Fluid-like Turbulence Break Down in the Solar Wind?*, Astrophys. J. Lett. **725**, L52, 2010

Podesta, J. J.: *Spatial scales and temporal scales in the theory of magnetohydrodynamic turbulence*, Phys. Plasmas **18**, 012 906, 2011

Podesta, J. J., J. E. Borovsky, and S. P. Gary: *A Kinetic Alfvén Wave Cascade Subject to Collisionless Damping Cannot Reach Electron Scales in the Solar Wind at 1 AU*, Astrophys. J. **712**, 685, 2010

Press, W. H., S. A. Teukolsky, W. T. Vetterling, and B. P. Flannery: *Numerical recipes in FORTRAN. The art of scientific computing*, Cambridge University Press, Cambridge, UK, 1992

Richardson, J. D., K. I. Paularena, A. J. Lazarus, and J. W. Belcher: *Radial evolution of the solar wind from IMP 8 to Voyager 2*, Geophys. Res. Lett. **22**, 325, 1995

Roberts, D. A., M. L. Goldstein, L. W. Klein, and W. H. Matthaeus: *Origin and evolution of fluctuations in the solar wind - HELIOS observations and Helios-Voyager comparisons*, J. Geophys. Res. **92**, 12 023, 1987a

Roberts, D. A., L. W. Klein, M. L. Goldstein, and W. H. Matthaeus: *The nature and evolution of magnetohydrodynamic fluctuations in the solar wind - Voyager observations*, J. Geophys. Res **92**, 11 021, 1987b

Ruderman, M. S. and D. Simpson: *The stability of parallel-propagating circularly polarized Alfvén waves revisited*, J. Plasma Phys. **70**, 143, 2004

Sahraoui, F., M. L. Goldstein, G. Belmont, P. Canu, and L. Rezeau: *Three Dimensional Anisotropic k Spectra of Turbulence at Subproton Scales in the Solar Wind*, Phys. Rev. Lett. **105**, 131 101, 2010

Schekochihin, A. A., S. C. Cowley, W. Dorland, G. W. Hammett, G. G. Howes, G. G. Plunk, E. Quataert, and T. Tatsuno: *Gyrokinetic turbulence: a nonlinear route to dissipation through phase space*, Plasma Phys. Contr. F. **50**, 124 024, 2008

Schindler, K.: *Physics of Space Plasma Activity*, Cambridge University Press, Cambridge, UK, 2006

Schwenn, R. and E. Marsch: *Physics of the Inner Heliosphere II. Particles, Waves and Turbulence*, Springer-Verlag, Berlin, Germany, 1991

Shaikh, D. and G. P. Zank: *The turbulent density spectrum in the solar wind plasma*, Mon. Not. R. Astron. Soc. **402**, 362, 2010

Sharma, R. P. and P. K. Shukla: *Nonlinear effects at the upper-hybrid layer*, Phys. Fluids **26**, 87, 1983

Silin, I., J. Büchner, and A. Vaivads: *Anomalous resistivity due to nonlinear lower-hybrid drift waves*, Phys. Plasmas **12**, 062 902, 2005

Smith, C. W., P. A. Isenberg, W. H. Matthaeus, and J. D. Richardson: *Turbulent Heating of the Solar Wind by Newborn Interstellar Pickup Protons*, Astrophys. J. **638**, 508, 2006

Sonnerup, B. U. Ö. and S.-Y. Su: *Large Amplitude Whistler Waves in a Hot Collision-Free Plasma*, Phys. Fluids **10**, 462, 1967

Spangler, S. R.: *Kinetic effects of Alfven wave nonlinearity. I - Ponderomotive density fluctuations*, Phys. Fluids B **1**, 1738, 1989

Spangler, S. R.: *The dissipation of magnetohydrodynamic turbulence responsible for interstellar scintillation and the heating of the interstellar medium*, Astrophys. J. **376**, 540, 1991

Spangler, S. R. and L. G. Spitler: *An empirical investigation of compressibility in magnetohydrodynamic turbulence*, Phys. Plasmas **11**, 1969, 2004

Srivastava, N. and R. Schwenn: *The origin of the solar wind: an overview*, in *The Outer Heliosphere: Beyond the Planets*, edited by K. Scherer, H. Fichtner, & E. Marsch, p. 13, 2000

Stawicki, O., S. P. Gary, and H. Li: *Solar wind magnetic fluctuation spectra: Dispersion versus damping*, J. Geophys. Res. **106**, 8273, 2001

Stenflo, L.: *Influence of a circularly polarized electromagnetic wave on a magnetized plasma*, Phys. Scripta **14**, 320, 1976

Stenflo, L. and P. K. Shukla: *Theory of stimulated scattering of large-amplitude waves*, J. Plasma Phys **64**, 353, 2000

Stenflo, L. and P. K. Shukla: *Nonlinear Processes in Space Plasmas*, in *Handbook of the Solar-Terrestrial Environment*, edited by Y. Kamide & A. C.-L. Chian, p. 311, 2007

Stix, T. H.: *Waves in plasmas*, American Institute of Physics, New York, USA, 1992

Swanson, D. G.: *Plasma waves, 2nd Edition*, Institute of Physics Publishing, Bristol, UK, 2003

Totten, T. L., J. W. Freeman, and S. Arya: *An empirical determination of the polytropic index for the free-streaming solar wind using HELIOS 1 data*, J. Geophys. Res. **100**, 13, 1995

Tu, C.-Y. and E. Marsch: *On the nature of compressive fluctuations in the solar wind*, J. Geophys. Res. **99**, 21 481, 1994

Tu, C.-Y. and E. Marsch: *MHD structures, waves and turbulence in the solar wind: Observations and theories*, Space Sci. Rev. **73**, 1, 1995

Ulmschneider, P. and W. Kalkofen: *Heating of the solar chromosphere*, in *Dynamic Sun*, edited by B. N. Dwivedi, p. 181, 2003

Valentini, F. and P. Veltri: *Electrostatic Short-Scale Termination of Solar-Wind Turbulence*, Phys. Rev. Lett. **102**, 225 001, 2009

Valentini, F., P. Veltri, F. Califano, and A. Mangeney: *Cross-Scale Effects in Solar-Wind Turbulence*, Phys. Rev. Lett. **101**, 025 006, 2008

Vedenov, A. A.: *Quasi-linear plasma theory (theory of a weakly turbulent plasma)*, J. Nucl. Energy **5**, 169, 1963

Vedenov, A. A.: *Theory of Turbulent Plasma*, Iliffe Books Ltd., London, UK, 1968

Verdini, A., M. Velli, W. H. Matthaeus, S. Oughton, and P. Dmitruk: *A Turbulence-Driven Model for Heating and Acceleration of the Fast Wind in Coronal Holes*, Astrophys. J. Lett. **708**, L116, 2010

Verscharen, D. and E. Marsch: *Compressive high-frequency waves riding on an Alfvén/ion-cyclotron wave in a multi-fluid plasma*, J. Plasma Phys. **77**, 693, 2011a

Verscharen, D. and E. Marsch: *Apparent temperature anisotropies due to wave activity in the solar wind*, Ann. Geophys. **29**, 909, 2011b

Verscharen, D., E. Marsch, U. Motschmann, and J. Müller: *Kinetic cascade beyond MHD of solar wind turbulence in two-dimensional hybrid simulations*, Phys. Plasmas, **accepted**, Jan, 2012

Viñas, A. F. and M. L. Goldstein: *Parametric instabilities of circularly polarized large-amplitude dispersive Alfvén waves: excitation of parallel-propagating electromagnetic daughter waves*, J. Plasma Phys. **46**, 107, 1991a

Viñas, A. F. and M. L. Goldstein: *Parametric instabilities of circularly polarized large-amplitude dispersive Alfvén waves: excitation of obliquely-propagating daughter and side-band waves*, J. Plasma Phys. **46**, 129, 1991b

Vocks, C., U. Motschmann, and K. Glassmeier: *A mode filter for plasma waves in the Hall-MHD approximation*, Ann. Geophys. **17**, 712, 1999

von Steiger, R.: *The solar wind throughout the solar cycle*, in *The Heliosphere through the Solar Activity Cycle*, edited by A. Balogh, L. Lanzerotti, and S. Suess, p. 41, Praxis Publishing Ltd., Chichester, UK, 2008

Wang, C. B. and C. S. Wu: *Pseudoheating of protons in the presence of Alfvénic turbulence*, Phys. Plasmas **16**, 020 703, 2009

Wang, C. B., C. S. Wu, and P. H. Yoon: *Heating of Ions by Alfvén Waves via Nonresonant Interactions*, Phys. Rev. Lett. **96**, 125 001, 2006

Wicks, R. T., T. S. Horbury, C. H. K. Chen, and A. A. Schekochihin: *Power and spectral index anisotropy of the entire inertial range of turbulence in the fast solar wind*, Mon. Not. R. Astron. Soc. **407**, L31, 2010

Wong, H. K. and M. L. Goldstein: *Parametric instabilities of the circularly polarized Alfven waves including dispersion*, J. Geophys. Res. **91**, 5617, 1986

Wu, C. S. and P. H. Yoon: *Proton Heating via Nonresonant Scattering Off Intrinsic Alfvénic Turbulence*, Phys. Rev. Lett. **99**, 075 001, 2007

Wu, C. S., P. H. Yoon, and C. B. Wang: *On nonresonant proton heating via intrinsic Alfvénic turbulence*, Phys. Plasmas **16**, 054 503, 2009

Wu, G., G. Huang, and H. Ji: *Dependence of the Anomalous Resistivity on the Induced Electric Field in Solar Flares*, Astrophys. J. **720**, 771, 2010

Yao, S., J.-S. He, E. Marsch, C.-Y. Tu, A. Pedersen, H. Rème, and J. G. Trotignon: *Multi-scale Anti-correlation Between Electron Density and Magnetic Field Strength in the Solar Wind*, Astrophys. J. **728**, 146, 2011

Yoon, P. H.: *Large-amplitude whistler waves and electron acceleration*, Geophys. Res. Lett. **38**, L12 105, 2011

Zhou, Y. and W. H. Matthaeus: *Models of inertial range spectra of interplanetary magnetohydrodynamic turbulence*, J. Geophys. Res. **95**, 14 881, 1990

Publications

Refereed publications

- Verscharen, D., Marsch, E., Motschmann, U., and Müller, J: *Kinetic cascade beyond MHD of solar wind turbulence in two-dimensional hybrid simulations*, Phys. Plasmas, accepted, 2012
- Verscharen, D. and Marsch, E.: *Apparent temperature anisotropies due to wave activity in the solar wind*, Ann. Geophys. 29, 909-917, 2011, doi: 10.5194/angeo-29-909-2011
- Verscharen, D. and Marsch, E.: *Compressive high-frequency waves riding on an Alfvén/ion-cyclotron wave in a multi-fluid plasma*, J. Plasma Phys. 77, 693-707, 2011, doi: 10.1017/S0022377811000080
- Marsch, E. and Verscharen, D.: *On nonlinear Alfvén-cyclotron waves in multi-species plasma*, J. Plasma Phys. 77, 385-403, 2011, doi: 10.1017/S0022377810000541
- Fahr, H.-J., Chashei, I. V., and Verscharen, D.: *Injection to the pick-up ion regime from high energies and induced ion power-laws*, Astron. Astrophys. 505, 329-337, 2009, doi: 10.1051/0004-6361/200810755
- Fahr, H.-J. and Verscharen, D.: *Spectral intensities of Anomalous Cosmic Rays derived from the injection rate at the solar wind termination shock*, Astrophys. Space Sci. Trans. 5, 21-30, 2009, doi: 10.5194/astra-5-21-2009
- Verscharen, D. and Fahr, H.-J.: *Solar wind proton reflection and injection to the ACR regime at the parallel termination shock*, Astrophys. Space Sci. Trans. 5, 15-19, 2009, doi: 10.5194/astra-5-15-2009
- Verscharen, D. and Fahr, H.-J.: *Self-initialised Fermi-1 acceleration by pitch-angle re-scattering of solar wind ions reflected from the parallel termination shock*, Astrophys. Space Sci. Trans. 4, 51-58, 2008, doi: 10.5194/astra-4-51-2008
- Fahr, H.-J. and Verscharen, D.: *Ion reflections from the parallel MHD termination shock and a possible injection mechanism into the Fermi-1 acceleration*, Astron. Astrophys. 487, L21-L24, 2008, doi: 10.1051/0004-6361:200810217
- Verscharen, D. and Fahr, H.-J.: *A kinetic description of the dissipative quasi-parallel solar wind termination shock*, Astron. Astrophys. 487, 723-729, 2008, doi: 10.1051/0004-6361:200809950

Conference contributions

In the following list, the presenting author is indicated in bold.

- **Verscharen, D.**, Marsch, E., Motschmann, U., and Müller, J.: *Compressive wave structures on kinetic scales resulting from a two-dimensional turbulent cascade in the solar wind*, Talk, Workshop "Cosmic Rays and the Heliospheric Plasma Environment", Bochum, Germany, 12.-16.9.2011

- **Verscharen, D.** and Marsch, E.: *Apparent temperature anisotropies due to wave activity in the solar wind*, Talk, 478. W.&E.-Heraeus seminar "Fusion and Astrophysical Plasmas", Bad Honnef, Germany, 18.-20.4.2011

- **Verscharen, D.** and Marsch, E.: *Compressive high-frequency waves riding on an Alfvén-cyclotron wave in a multi-fluid plasma*, Poster, EGU General Assembly, Vienna, Austria, 3.-8.4.2011

- **Verscharen, D.** and Marsch, E.: *Compressive high-frequency waves riding on an Alfvén-cyclotron wave in a multi-fluid plasma*, Talk, 71. Jahrestagung der DGG, Cologne, Germany, 21.-24.2.2011

- **Verscharen, D.** and Marsch, E.: *Kinetics of non-Maxwellian distribution functions in the turbulent solar wind*, Talk, Workshop "New perspectives on cosmic rays in the heliosphere", Parys/Potchefstroom, South Africa, 22.-26.3.2010

- **Verscharen, D.** and Marsch, E.: *Kinetics of non-Maxwellian distribution functions in the turbulent solar wind*, Talk, DPG-Frühjahrstagung, Bonn, Germany, 15.-19.3.2010

- **Fahr, H.-J.**, Chashei, I. V., and Verscharen, D.: *Extended power laws for heliospheric keV ions due to injection from the ACR-ion population*, Talk, EGU General Assembly, Vienna, Austria, 19.-24.4.2009

- **Verscharen, D.** and Fahr, H.-J.: *Kinetics of deceleration and dissipation of the solar wind plasma at the heliospheric termination shock*, Talk, DPG-Frühjahrstagung, Greifswald, Germany, 30.3.-2.4.2009

- **Fahr, H.-J.**, Chashei, I. V., and Verscharen, D.: *An ACR-induced injection into the heliospheric keV-ion regime leading to ion power laws*, Talk, DPG-Frühjahrstagung, Greifswald, Germany, 30.3.-2.4.2009

- **Verscharen, D.** and Fahr, H.-J.: *Solar wind proton reflection and induced injection to the ACR regime at the quasi-parallel termination shock*, Talk, ISSI Workshop "2nd International Heliophysical Year Conference", Bern, Switzerland, 10.-13.11.2008

- **Verscharen, D.** and Fahr, H.-J.: *Kinetic treatment of the quasi-parallel magnetohydrodynamic solar wind termination shock*, Poster, EGU General Assembly, Vienna, Austria, 13.-18.4.2008

- **Verscharen, D.** and Fahr, H.-J.: *Kinetic treatment of the parallel magnetohydrodynamic shock*, Talk, DPG-Frühjahrstagung, Freiburg, Germany, 3.-7.3.2008

Acknowledgements

First of all, I would like to thank Professor Dr. Eckart Marsch for supervision of my thesis work and guidance in all scientific questions in this field. He created a positive and productive atmosphere with the necessary input and impulse for my work, leaving the requisite freedom. Without his deep knowledge of the field and the resulting discussions on its various aspects, this thesis would have been impossible in its present form.

The support by Professor Dr. Uwe Motschmann from the Technical University of Braunschweig is also highly appreciated. I would like to express my gratitude for accepting me as a PhD student and for introducing me to the Braunschweig A.I.K.E.F. code, which led to interesting new results for this work. I appreciate that PD Dr. Yasuhito Narita from the Technical University of Braunschweig agreed to become the third member of my thesis committee.

Professor Dr. Hans-Jörg Fahr brought me into contact with the field of space plasma physics. Without his guidance during my Diploma thesis, most probably I would not have joined the field at all, and the thesis would have been written on a completely different topic, if at all. Also Dr. Karl-Ludwig Klein pushed my interest in this field at a very early stage.

The advice by the members of our group at the Max Planck Institute, Dr. Sofiane Bourouaine and Dr. Yana Maneva, is acknowledged. The interaction with Dr. Bernd Inhester on many different fields of physics and his great knowledge on all aspects of plasma physics have been very fruitful. Also the discussions with Dr. Håkan Smith and Dr. Omar Maj from the Max Planck Institute for Plasma Physics gave rise to promising new ideas.

I express my gratitude to Hendrik Kriegel, Dr. Joachim Müller, and Christoph Koenders for their detailed help on the application of the A.I.K.E.F. code and their fast replies to my questions on efficiency, feasibility, and principal realization of my plans. The numerical studies with the A.I.K.E.F. code have been performed on the Megware Woodcrest Cluster at the Gesellschaft für wissenschaftliche Datenverarbeitung mbH Göttingen (GWDG). I appreciate the easy and fast access to the computing facilities and the very efficient support by the GWDG staff.

I received financial and academic support from the International Max Planck Research School (IMPRS) on Physical Processes in the Solar System and Beyond at the Universities of Braunschweig and Göttingen, which is appreciated. Especially the commitment of the organizer PD Dr. Dieter Schmitt for the students' needs should be highlighted.

I thank Professor Dr. Sami Solanki for his responsibility for the Solar System School at the Max Planck Institute for Solar System Research and his productive leadership of the solar group. The help of the staff at the institute is highly acknowledged, especially the computer center, the canteen, and the secretaries. The thanks to Frau Claudia Rudolph

for her friendly greetings and her always nice support in all general issues shall be emphasized.

I am grateful for the time that I spent with my fellow PhD students at the institute. Among them, I would like to highlight here the discussions with Wieland Dietrich on all topics—let them be scientific, social, political, or philosophical. The free time with Dr. Manuela Lippi was great and cheerful and cannot be adequately summarized here. I thank Dr. Julia Thalmann for the relaxing moments and her straightforwardness. I am grateful for the productive atmosphere in my office, which was mainly due to my office mate Juan Sanchez. David Bühler supported me with his excellent proficiency in the English language and several late discussions outside the institute, which I appreciate a lot. Peter Kollmann's critical questions and deep insight into physics have been very helpful and led several times to rethinking aspects that seemed to be clear before.

For their outstanding support during all the time, I want to thank my parents and my siblings cordially. This work is dedicated to my family.

Lebenslauf

Persönliche Daten:

Name:	Daniel Verscharen
Geburtsdatum:	8. Dezember 1983
Geburtsort:	Bonn
Staatsangehörigkeit:	deutsch

Schulausbildung:

1990–1994	Grundschule: *Münsterschule Bonn*
1994–2003	Gymnasium: *Beethovengymnasium Bonn*, Abitur

Universitätsausbildung:

2003–2007	Studium der Physik und Astronomie mit den Nebenfächern Mathematik und Meteorologie an der *Rheinischen Friedrich-Wilhelms-Universität Bonn*, Abschluß: Diplom, Diplomarbeit unter Betreuung durch Prof. Dr. Hans-Jörg Fahr
2007–2009	wissenschaftlicher Mitarbeiter in der Arbeitsgruppe von Prof. Dr. Hans-Jörg Fahr, DFG-Projekt *Boltzmann-Kinetic studies of MHD-plasma properties near the solar wind termination shock and the heliosheath*

Promotion:

2009–2012	Doktorand am *Max-Planck-Institut für Sonnensystemforschung*, Katlenburg-Lindau unter Betreuung durch Prof. Dr. Eckart Marsch und an der *Technischen Universität Braunschweig* unter Betreuung durch Prof. Dr. Uwe Motschmann, unterstützt durch ein Stipendium der *International Max Planck Research School (IMPRS) on Physical Processes in the Solar System and Beyond*